COMMUNAUTÉ FRANÇAISE DE BELGIQUE
UNIVERSITÉ DE LIÈGE – GEMBLOUX AGRO-BIO TECH

Crop water productivity of winter wheat at multi-scale and its improvements over the Huang-Huai-Hai Plain, China

Qin LIU

Dissertation originale présentée en vue de l'obtention du grade de docteur en sciences agronomiques et ingénierie biologique

Promoteurs : Prof. Sarah GARRE - Prof. Changrong YAN
Année académique 2017

COMMUNAUTÉ FRANÇAISE DE BELGIQUE
UNIVERSITÉ DE LIÈGE – GEMBLOUX AGRO-BIO TECH

Crop water productivity of winter wheat at multi-scale and its improvements over the Huang-Huai-Hai Plain, China

Qin LIU

Dissertation originale présentée en vue de l'obtention du grade de docteur en sciences agronomiques et ingénierie biologique

CONTENTS

Contents

Contents

Contents

Abstract

Droughts and water shortage are generally accepted to be one of the most critical problems faced by worldwide agriculture, and it is so especially in China where agricultural production and prosperity are largely dependent on the timely, adequate and proper distribution of rainfall. The analysis of water productivity is becoming very critical in light of population growth, food security and increasing pressure on water resources. However, there is limited understanding of the spatio-temporal variation of crop water productivity (CWP) from the rotation system and its key influencing factors in Huang-Huai-Hai Plain (3H Plain) in which there is an over-exploitation of groundwater region and where future warmer and drought conditions will intensify crop water demand. As the largest water user, agricultural sector is facing a challenge to produce more crops with less water. Consequently, 3H Plain faced the double threat of both making contributions of high and stable yield to government and improving CWP of winter wheat through reducing water consumption. The overall ambition of this thesis was to investigate to what extent the grain yield and crop water productivity for winter wheat can respond to climate change and drought across the 3H Plain.

In our study, a combined dataset composed of a historical 54-year time series and the RCP 8.5 scenario from 40 meteorological stations was provided by the China Meteorological Administration. Among these 40 stations we selected 12 stations with more detailed information available. The minimal data sets required for model operation include daily climatic variables, soil information and management information collected from the China Soil Scientific Database. Finally, we also used satellite data to estimate water productivity mainly involved in MODIS products including MOD11A1 (land surface temperature/surface emissivity), MOD13A2 (NDVI) and MCD43B3 (surface albedo). We used SPEI-PM method, DSSAT-CERES-Wheat model and SEBAL model to explore the characteristics in grain yield and crop water productivity for winter wheat in response to climate change and drought associated with their improvements across the 3H Plain.

Our work demonstrated the investigation that an increase of ET_0 was predicted leading to subsequent drought rise in frequency, duration, severity and intensity under the RCP 8.5 scenario. The cumulative probability of the simulated yield reduction was detected to be higher during jointing to heading stage in northern than southern region due to water stress and changes in the management inputs. The lower CWP was mainly situated in the low plain-hydropenia irrigable land and dry land (zone2) and the hill-wet hot paddy field (zone6), which suggests that it is an important issue and opportunity for improving agricultural water management in the water-scarce 3H Plain. The spatial increase of yield principally controlled increase of water productivity in north agricultural sub-regions and the spatial increase of water productivity was more governed by

increment of yield than the reduction of ET_a in other agricultural sub-regions. It will be adopted to develop feasible straw mulching, regulated deficit irrigation, and soil water storage and preservation to reduce pressure on groundwater over-exploitation, especially for winter wheat in the 3H Plain.

In our work, major agronomic consequences have been drawn regarding the reform of the common agricultural policy in Huang-Huai-Hai Plain, China. Researchers are encouraged to further investigations into how to implement these practices with emphasis of improving the sustainability of these agro-ecosystems.

Acknowledgments

Time passes very quickly, often so quickly that we are surprised. Before concluding this thesis, I would like to take the precious opportunity to extend my whole hearted gratitude to all that have helped me in countless ways throughout my doctoral research and compile this paper.

I wish to express my sincere gratitude to my thesis committee: Prof. Sarah Garre, Prof. Changrong Yan, Prof. Bernard Tychon, Prof. Aurore Degre, A.P. Benoît Mercatoris, Prof. Rongle Liu, and Prof. Minggang Xu, for insightful comments and encouragement, and also for the hard questions which prompted me to broaden my research to encompass various perspectives.

I would like to express my immense gratitude to my supervisor Prof. Sarah Garre for her valuable advice, encouragement, support and patience all through this research and writing up process.

I also wish to thank my co-supervisor Prof. Changrong Yan for continuously supporting my PhD study and related research, for his motivation, constant encouragement and guidance in my doctoral research and accomplishment of this paper.

I am extremely grateful to Prof. Xurong Mei, Prof. Yanqing Zhang, Prof. Zhiqiang, Hao, Prof. Xianwu Liu and Prof. Weiping Hao for their support and for providing exceptional inspiration.

I also would like to thank my office mates, Prof. Hui Ju, Prof. Wenqing He, Prof. Enke Liu, A.P. Chunhong Qu, A.P. Junhong Ji, A.P. Yukun Liu, Dr. Dongbao Sun, Dr. Wenying Zhang, Dr. Zhen Li, Dr. Wenyi Dong, Haoru Li who have supported me from the material and psychological aspect, guided me in collection of abundant materials.

I also wish offer my special thanks to Dr. Jianying Yang, Mr Xiangxiang Li, Mis Xiaochen Qin and Mis Wenru Liu who worked with me together in process of my doctoral research.

I am also especially thankful to Prof. Vinay Nangia for his English help from International Center for Agricultural Research in the Dry Areas (ICARDA) and Prof. Canran Liu for his R program support from Arthur Rylah Institute for Environmental Research, Australia.

I want to express my immense gratitude to the University of Liège-Gembloux Agro-Bio Tech and more specifically the research platform AgricultureIsLife for the funding of the scientific stay in Belgium and Graduate School of Chinese Academy of Agricultural Sciences for giving me precious opportunity to conduct my doctoral research in University of Liège-Gembloux Agro-Bio Tech.

A special thanks to support from Chinese Academy of Agricultural Sciences scientific and technological innovation project, the National Basic Research Program of China (973 Program) (2012CB955904), the 12th five-year plan of the National Key Technologies R&D Program (2012BAD09B01) and the National Science Foundation for Young Scientists of China (41401510).

Finally, my last words of gratitude go to my family.

List of figures

List of figures

List of tables

List of abbreviations

3H Plain:	Huang-Huai-Hai Plain
ADAP:	Anthesis days
CMA:	China Meteorological Administration
CWP:	Crop water productivity
DSSAT model:	Decision Support System for Agrotechnology Transfer model
ET_0:	Potential evapotranspiration
ET_a:	Actual evapotranspiration
ET_c:	the water requirement for crops
ISODATA:	Iterative Self-Organizing Data Analysis Technique
LST:	the land surface temperature
MDAP:	Maturity days
M-K test:	Mann-Kendall test
MODIS:	Moderate-resolution imaging spectroradiometer
NDVI:	Normalized difference vegetation index
P-M:	Penman–Monteith equation
RCP:	Representative Concentration Pathway
SEBAL:	the Surface Energy Balance Algorithm for Land model
SPEI:	the Standardized Precipitation Evapotranspiration Index

Scientific publications and communications

PUBLICATIONS

FIRST AUTHOR OR CORRESPONDING AUTHOR

- Yang Jianying, **Liu Qin***, Mei Xurong, Yan Changrong, Ju Hui, Xu Jianwen. Spatiotemporal characteristics of reference evapotranspiration and its sensitivity coefficients to climate factors in Huang-Huai-Hai Plain, China. *Journal of Integrative Agriculture*, 2013,12(12):2280—2291.
- Yang Jianying, Mei Xurong, Huo Zhiguo, Yan Changrong, Ju Hui, Zhao fenghua, **Liu Qin***. Water consumption in summer maize and winter wheat cropping system based on SEBAL model in Huang-Huai-Hai Plain, China. *Journal of Integrative Agriculture*, 2015,14(10)：2065—2076.
- **Qin Liu**, Changrong Yan, Hui Ju, Sarah Garré. Impact of climate change on potential evapotranspiration under a historical and future climate scenario in the Huang-Huai-Hai Plain, China. *Theoretical and Applied Climatology*, 2017. Doi: 10.1007/s00704-017-2060-6
- LI Xiangxiang, JU Hui, Sarah Garré, YAN Changrong, William D. Batchelor, **Liu Qin***. Spatiotemporal variation of drought characteristics in the context of climate change in the Huang- Huai- Hai Plain, China. *Journal of Integrative Agriculture*, 2017, Doi: 10.1016/S2095-3119(16)61545-9
- **Qin Liu**, Changrong Yan, Jianying Yang, et al. Impacts of Climate Change on Crop Water Requirements in Huang-Huai-Hai Plain, China. Chapter 5 of Climate Change and Agricultural Water Management in Developing Countries, CABI-IWMI,2015 (ISBN-13: 978 1 78064 366 3)
- **Liu Qin**, Mei Xurong, Yan Changrong, Ju Hui, Yang Jianying. Dynamic variation of water deficit of winter wheat and its possible climatic factors in Northern China. Acta Ecologica Sinica 2013, 33:6643—6651
- Xu Jianwen, Xu Hui, **Liu Qin***, Yang Jianying. Variation of drought and regional response to climate change in Huang-Huai-Hai Plain. *Acta Ecologica Sinica*, 2014, 34(2): 460—470. (in Chinese)
- Xu Jianwen, Mei X R, Xu Hui, Li Y C, **Liu Qin***, Yang Jianying. Simulation of winter wheat yield in response to irrigation level at critical growing stages in the Huang-Huai-Hai Plain. *Acta Agronomica Sinica*, 2014, 40 (8):1485—1492. (in Chinese)
- **Liu Qin**, Yan Changrong, Zhao Caixia, Yang Jianying, Zhen Wenchao. Changes of daily potential evapotranspiration and analysis of its sensitivity coefficients to key climatic variables in Yellow River Basin. *Transactions of the Chinese Society of Agricultural Engineering*, 2014, 30 (17): 157—166. (in Chinese)
- Li Xiangxiang, Xu Hui, Yan Changrong, **Liu Qin***, Li Yingchun. Spatio-temporal variability of water deficit in Huang-Huai-Hai Plain during 1961—2013. *Chinese Journal of Agrometeorology*, 2015, 36(3): 254—262. (in Chinese)
- Zhao Caixia, Mei Xurong, Xu Hui, **Liu Qin***, Zhen Wenchao. Variation in potential evapotranspiration

and its sensitivity coefficients to climatic factors in the Huang-Huai-Hai Plain. *Chinese Journal of Agrometeorology*, 2015, 36(5): 570—577. (in Chinese)

- Yan Changrong, He Wenqing, Liu Enke, Lin Tao, Pasquale M, Liu Shuang, **Liu Qin***. Concept and estimation of crop safety period of plastic film mulching. *Transactions of the Chinese Society of Agricultural Engineering*, 2015, 31(9): 1—4. (in Chinese)
- Yan Changrong, He Wenqing, Xue Yinghao, Liu Enke, **Liu Qin***. Application of biodegradable plastic film to reduce plastic film residual pollution in Chinese agriculture. Chin J Biotech, 2016, 32(6): 1–13 (in Chinese)
- **Liu Qin**, Yan Changrong. Drought variation and its sensitivity coefficients to climatic factors in the Yellow River Basin. Chinese *Journal of Agrometeorology*, 2016, 37(6): 623—632. (in Chinese)
- Yang Jianying, Huo Zhiguo, Wu Dingrong, Wang Peijuan, **Liu Qin***. Investigation on Water Productivity of Winter Wheat Based on MODIS and SEBAL in the Huang-Huai-Hai Plain, China. Chinese *Journal of Agrometeorology*, 2017. (in Chinese)
- Yan Changrong, Yang Xiaoguang, **Liu Qin** (the third principal author). (2015). China's agricultural climate resources atlas (Special issue for water). Zhejiang Science and Technology Press. ISBN 978-7-5341-6873-4.
- Mei Xurong, **Liu Qin** (the secord principal author), Yan Changrong. (2016). Atlas of China's major crop growth period. Zhejiang Science and Technology Press. ISBN 978-7-5341-7290-8.
- Ju Hui, **Liu Qin** (the secord principal author), Yan Changrong, Yang Jianying. (2016) Potential effect of climate drought on the yield and water productivity of winter wheat over the Huang-Huai-Hai Plain. Science Press. ISBN 978-7-03-051063-1.

IN PREPARTION

- **Qin Liu**, Changrong Yan, Sarah Garré, Xiangxiang Li. Potential effect of drought on winter wheat yield using CERES-Wheat model over the Huang-Huai-Hai Plain. (submitted in *Journal of Integrative Agriculture)*
- **Qin Liu**, Xiangxiang Li, Changrong Yan, Sarah Garré. Investigation of the impact of climatic shifts in wheat yield using CERES-Wheat model over the Huang-Huai-Hai Plain of China. (submitted in *Theoretical and Applied Climatology*)
- **Qin Liu**, Changrong Yan, Jianying Yang, Sarah Garré. An assessment of water consumption, grain yield and water productivity of winter wheat in agricultural sub-regions of Huang-Huai-Hai Plain, China. (to be submitted)

CO-AUTHOR

- Liu Shuang, Yan Changrong, He Wenqing, Chen Baoqing, Zhang Yanqing, **Liu Qin**, & Liu Enke. Effects of different tillage practices on soil water-stable aggregation and organic carbon distribution in dryland farming in Northern China. Acta Ecologica Sinica, 2015, 35(4), 65—69.
- Li Xiangxiang, Ju Hui, **Liu Qin**, Li Yingchun. Characteristic analysis of drought detected by Penman-Monteith based SPEI in the Huang-Huai-Hai Plain. Acta Ecologica Sinica, 2017
- Enke Liu, Jianbo Wang, Yanqing Zhang, Denis A. Angers, Changrong Yan, **Qin Liu**. Priming effect of 13C-labelled wheat straw in no-tillage soil under drying and wetting cycles in the Loess Plateau of China. Scientific Reports, 2015, 5:13826.

ORAL COMMUNICATIONS

NATIONAL CONFERRENCE

- 《2016 academic annual conference of agricultural meteorological》 Chongqing province, 22/10/2016.

MEETING PRESENTATIONS

- 《Impact of climate change on potential evapotranspiration under a historical and future climate scenario in the Huang-Huai-Hai Plain, China》 Gembloux ART (BE), 22/8/2015.
- 《Drought variation and its sensitivity coefficients to climatic factors in the Yellow River Basin》 Tibet, Lhasa (China), 25/12/2016.

INTERNATIONAL CONFERRENCE

- 《Climate Change and International Dryland Agricultural Development》 Beijing, China 20—22/11/2015.
- 《Improving Water Productivity in Agricultural Systems with Emphasis on rainfed Agriculture》 Amman Jordan 2—17/10/2014
- 《Land System Science: Understanding Realities and Developing Solutions》 Global Land Project 3rd Open Science Meeting, Beijing China, 24—27/10/2016

Chapter Ⅰ. General Introduction

1. General content

Climate change and agricultural production

A global change in the main meteorological variables is observed in the last decades. According to the IPCC report, the global temperature has raised by 0.74 ℃ in recent 100 years (1906—2005), and it is likely to continue in the 21st century, causing changes in the hydrological cycle by affecting precipitation and evaporation (IPCC, 2013). By the end of this century, the global mean temperature could be 1.8° to 4.0°C warmer than at the end of the previous century (Solomon et al., 2007). Warming will not be even across the globe and is likely to be greater over land compared with oceans, toward the poles, and in arid regions (Solomon et al., 2007). Recent weather records also show that land surface temperatures are increasing more slowly than expected from climate models, potentially because of a higher level of absorption of CO_2 by deep oceans (Balmaseda et al., 2013). Similar to the global trend, China also experienced warming trend, the average annual temperature rose by 0.5 to 0.8°C during the 20th century, and most of the temperature increase took place over the past 50 years (Wu et al., 2016). Furthermore, dry areas in the northern China are warming faster than wet areas in the southern China (Ding et al., 2007; Piao et al., 2010). At the global scale, precipitation tended to increase in the high latitude regions of the Northern Hemisphere and in the tropical regions; while in the semi-tropical regions, the precipitation decreased over the past several decades (IPCC, 2013). In China, the decrease in annual precipitation was significant in most of northern China and the eastern part of northwest China (Bai et al., 2007).

Although there are many impacts expected from global climate change, one of the largest impacts is expected to be on agriculture (Cline, 2007; Pearce et al., 1996; Piao et al., 2010; Wang et al., 2013b). Climate change, especially the increasing risk of extreme weather events and indirect impacts on freshwater resources, threatens agricultural systems and food security (Barros et al., 2014; Field, 2012; Hertel et al., 2010; Wheeler and Von Braun, 2013). Climate change will have important implications in regions with limited water supplies, such as Huang-Huai-Hai (3H) Plain of China, where expected warmer and drier conditions will augment crop water demand. The Huang-Huai-Hai Plain, one of the largest plains in China, is located in the north of China. Water shortage in this region has become a serious concern in recent decades (Brown and Rosenberg, 1997). Excessive exploitation of groundwater resources has resulted in a declining water table depth at a rate of 1 $m \cdot y^{-1}$ and severe groundwater depression in the past 20 years (Zhang et al., 2015). An expected reduction of annual precipitation and aggravated drought risk will bring negative effect to agricultural production and food security in coming decades over the Huang-Huai-Hai Plain. A more detailed review of climate change impacts on drought and subsequent crop yields is presented in the following sections.

The potential evapotranspiration and drought

Based on observed and modeling data, numerous studies have demonstrated an increase in the frequency and intensity of droughts (Dai, 2013), which implies a growing threat to food security. Drought conditions will be aggravated due to climate change by increasing potential evapotranspiration and augmenting crop water consumption in water-limited regions (Goyal, 2004; Maracchi et al., 2005; Thomas, 2008).

Potential evapotranspiration (ET_0) is defined as the amount of water that can potentially evaporate and transpire from a vegetated surface with no restrictions other than the atmospheric demand (Lu et al., 2005), and widely acknowledged as a key hydrological variable representing an important water loss from catchments. According to the predictions of climate change models, ET_0 is expected to increase over the coming years due to an expected temperature rise (Goyal, 2004; McNulty et al., 1997). However, decreasing trends of ET_0 have been detected in some regions of China (Chen et al., 2006; Thomas, 2000; Wang et al., 2007), the United States (Irmak et al., 2012), and Australia (Roderick and Farquhar, 2004). Therefore, global atmospheric temperatures rise will not necessarily give rise to ET_0 in all cases. For example, an reduction in solar radiation can compensate for the impact of temperatures on ET_0 as obseved in many places (Stanhill and Cohen, 2001; Wild, 2014). Conventionally, aridity is usually expressed as a generalized function of precipitation, temperature, and ET_0 reflecting the degree of meteorological drought. Over last decades, the aridity index (which is defined as the ratio of ET_0 to precipitation) is expected to have different trends in different regions. Su et al (2015) found that drought index had a bigger decreasing trend (at a rate of -0.313/y) in winter than others in 1961-2012 according to 11 meteorological stations in and around the Shiyang River basin. Liu et al (2013) also witnessed that annual aridity index decreased significantly by 0.048 y^{-1} and was primarily governed by increasing precipitation according to 80 national meteorological stations in Northwest China from 1960 to 2010.

Given that agriculture in China feeds about 22% of the world's population, depending only on 7%—8% of its arable land, food security in China is an urgent issue in the context of climate change (Wang et al., 2016). Over China, droughts have become more frequent and intense during the last decades, which presents a direct threat to crop growth in vast areas across the country (Dalin et al., 2015; Piao et al., 2010). Over the past six decades, very severe droughts hit China in the 1960s, in the late 1970s and early 1980s, and in the late 1990s (Guan et al., 2015; Zhai and Zou, 2005). Accordingly, there is an urgent demand for effective monitoring of drought stress, especially in areas of limited water resources. Several techniques have been developed to quantitatively analyze drought characteristics (Heim, 2002). Some of these are the physically based indices, such as Palmer drought severity index(PDSI) along with its derivative, and statistically based indices, such as Standardized Precipitation Index (SPI) and the Standardized Precipitation Evapotranspiration Index (SPEI) (Vicente-Serrano et al., 2011). These indices have been widely used in detecting long-term drought trends under climate change at several locations around the world. The general recognition is that drought severity and duration have been intensifying around the world due to global warming in the past

decades (Allen et al., 2010; Dai, 2013). However, it has been difficult to understand how droughts have changed in China, because the findings based on the potential evapotranspiration equations vary among studies (Sheffield et al., 2012; Trenberth et al., 2014; Xu et al., 2015). Significant drying trends were detected in northern and southwestern China during the past decades, when ET_0 was estimated by temperature only (Wang et al., 2015a; Yu et al., 2014a). However, when aridity index was calculated by the Penman-Monteith equation taking more climatic variables into account, no evidence of an increase in drought severity was found across China (Wang et al., 2015b), and even more wetting areas than drying areas were observed in Northeast China Plain(Xu et al., 2015).

As a major crop production area in China, the Huang-Huai-Hai Plain has experienced serious droughts and water scarcity problems in recent years (Yong et al., 2013), which has been the limiting factor for agricultural production (Zhang et al., 2015). Furthermore, water limitations is likely to be accentuated by increased food demand, soil quality deterioration and over-exploitation of groundwater resources (Yang et al., 2015). Climate variability, especially extreme climate events such as drought, may cause fluctuation of crop yields (Lu and Fan, 2013; Yu et al., 2014b). Thus, understanding the potential variations of drought characteristics under climate change is essential for reducing vulnerability and establishing drought adaptation strategies for agriculture in 3H Plain. Most previous studies have primarily reported the seasonal and spatial variability of water deficiency (Huang et al., 2014; Yong et al., 2013) and the long term drought evolutions, including dry trends, spatial distribution of drought frequency, drought affected areas, and drought duration for historical periods (Wang et al., 2015a; Wang et al., 2015b; Xu et al., 2015; Yu et al., 2014a). However, few studies have evaluated the performance of multi-indices (such as SPEI-PM, SPEI-TH and SPI) on estimating drought impact and assessed drought risk for future climate scenarios.

Water storage

Terrestrial water storage is a key component of the global hydrological cycle and plays a critical role in Earth's climate system (Mo et al., 2016). Natural and anthropogenic stresses such as climate change, drought, increasing water use and agricultural practices will affect both surface water and groundwater resources globally (Wang et al., 2013a). A small change in the hydrological cycle may have a significant socio-economic impact, which, for example, has recently been observed in the form of groundwater depletion in northwest India probably leading to reduction of agricultural output and shortages of potable water (Rodell et al., 2009). The GRACE (the Gravity Recovery and Climate Experiment) satellite mission has proved to be an invaluable tool in monitoring such hydrological changes with global coverage and sufficient spatial and temporal resolution (Ramillien et al., 2008; Rodell et al., 2009) and revealed trends in present-day continental water storage in many parts of the world. Chen et al (2009) combined GRACE data, hydrological models, and local in situ precipitation data to study annual variations in terrestrial water storage in the Amazon basin and noted that GRACE was capable of observing the extreme Amazon drought event of 2005. In addition, on the basis of the monthly GRACE gravity field, Leblanc et al. (2009) observed changes in surface water storage caused by severe droughts in South Australia between 2003 and 2006, and Feng et al. (2012)

used GRACE data to monitor variations in terrestrial water storage in the Amazon basin from 2002 to 2010.

Mo et al.(2016) applied GRACE Tellus products in combination with Global Land Data Assimilation System (GLDAS) simulations and data from reports, to analyze variations in terrestrial water storage (TWS) in China as a whole and eight of its basins from 2003 to 2013. As described in Figure 1, from 2003 to 2013, the southwest rivers region and Huang-Huai-Hai Plain showed significant water storage depletions, and the area of depletion was largest in spring and summer, respectively. Human activities and climate parameters should be responsible for the significant water storage depletion in China, while for Huang-Huai-Hai Plain, agricultural irrigation consumes large amounts of groundwater pumped from deep wells (Kendy et al., 2004). Usually, the farmers in 3H Plain apply 3–5 times irrigation, sometimes even 6–7 times, through flood irrigation during the winter wheat growing season to get high grain yield (Li et al., 2010).

The impact of Climate change on crop yield

Drought is a most damaging and widespread climate event, negatively affecting agricultural production, water resources, ecosystem function and human lives around the world (Dai, 2011; Dilley et al., 2005; Wilhite et al., 2007). The simulations of Rosenzweig and Parry (1994) showed that there is a large degree of spatial variation in crop yields across the globe. Both the sign and magnitude of the projected changes in crop yield varied with alternative climate models and from one country to another. In general, yields increased by 30% in Northern Europe, but decreased by around 20% across Asia, Africa and South America between 2050 and 2010 (Rosenzweig and Parry, 1994) (Figure 2). As the first example of global impacts of climate change on crop production, these simulations are remarkable.

Crop production is affected by climatic variables such as rising temperatures, changing precipitation regimes and increased atmospheric CO_2 levels, and also affected by biological variables such as the lengths of the crop growth periods and the crop cycle. A longer life cycle was one of the most widely observed biological changes in the response of crops to climatic warming across the Northern Hemisphere during the twentieth century (Steltzer and Post, 2009). Overall, the yields of wheat and maize have responded negatively to the recent warming since the 1980s at the global scale, although the yield response signals of other crops (e.g., rice) are still unclear (Lobell and Field, 2007). An extensive review of the drivers of climate change impacts on crop yields is provided by Gornall et al. (2010) and Rosenzweig and Neofotis (2013). As described in Table1, direct drivers of climate impacts on crop yields include long-term change in average temperature and precipitation conditions, and the increasing occurrence of extreme weather events such as extreme temperatures, droughts, floods and tropical storms. In addition, crop yields are sensitive to indirect effects of climate change on freshwater resources, pests and diseases, and sea level rise.

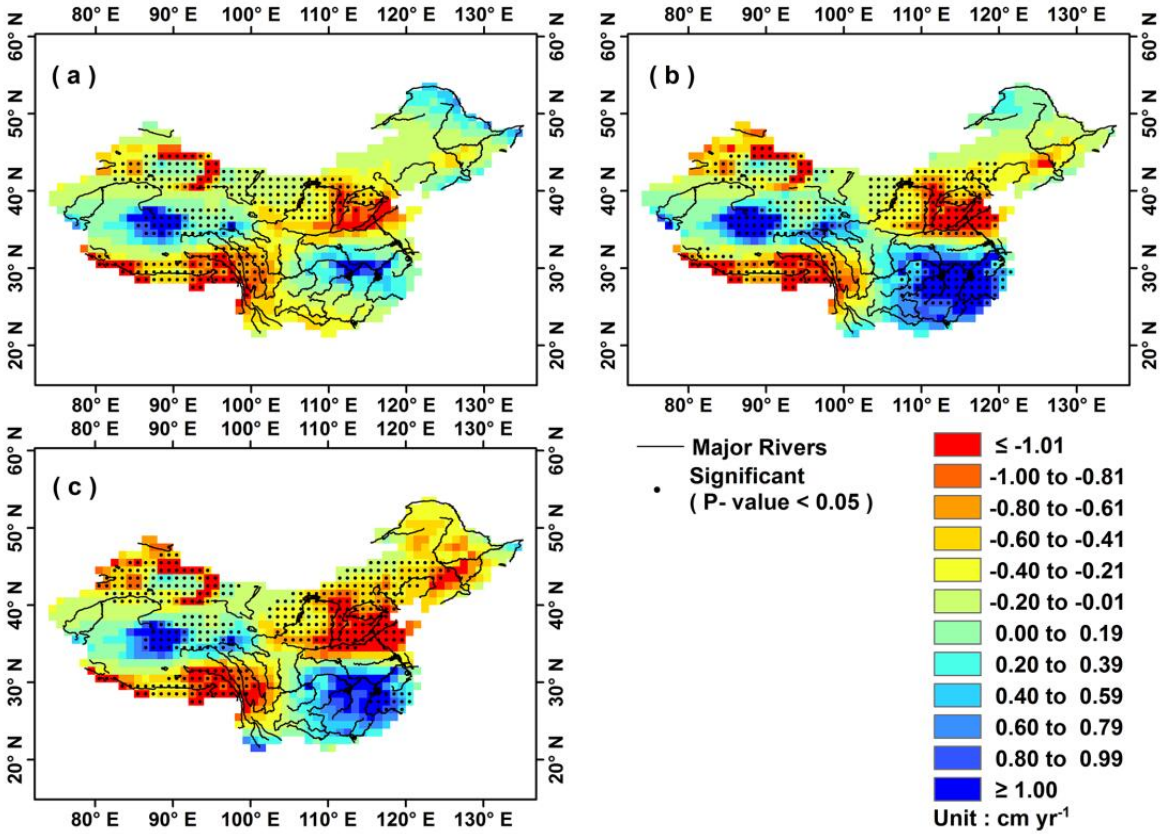

Figure 1 Spatial distribution of trends derived from linear least squares regression for seasonally averaged water storage in 2003–2013 from the scaled GRACE (the Gravity Recovery and Climate Experiment) data (unit: cm y^{-1}) (Mo et al., 2016); (a) spring (March–May); (b) summer (June–August); (c) autumn (September–November). Grids with trends significant (F test) at 95 % confidence level are marked by black dots.

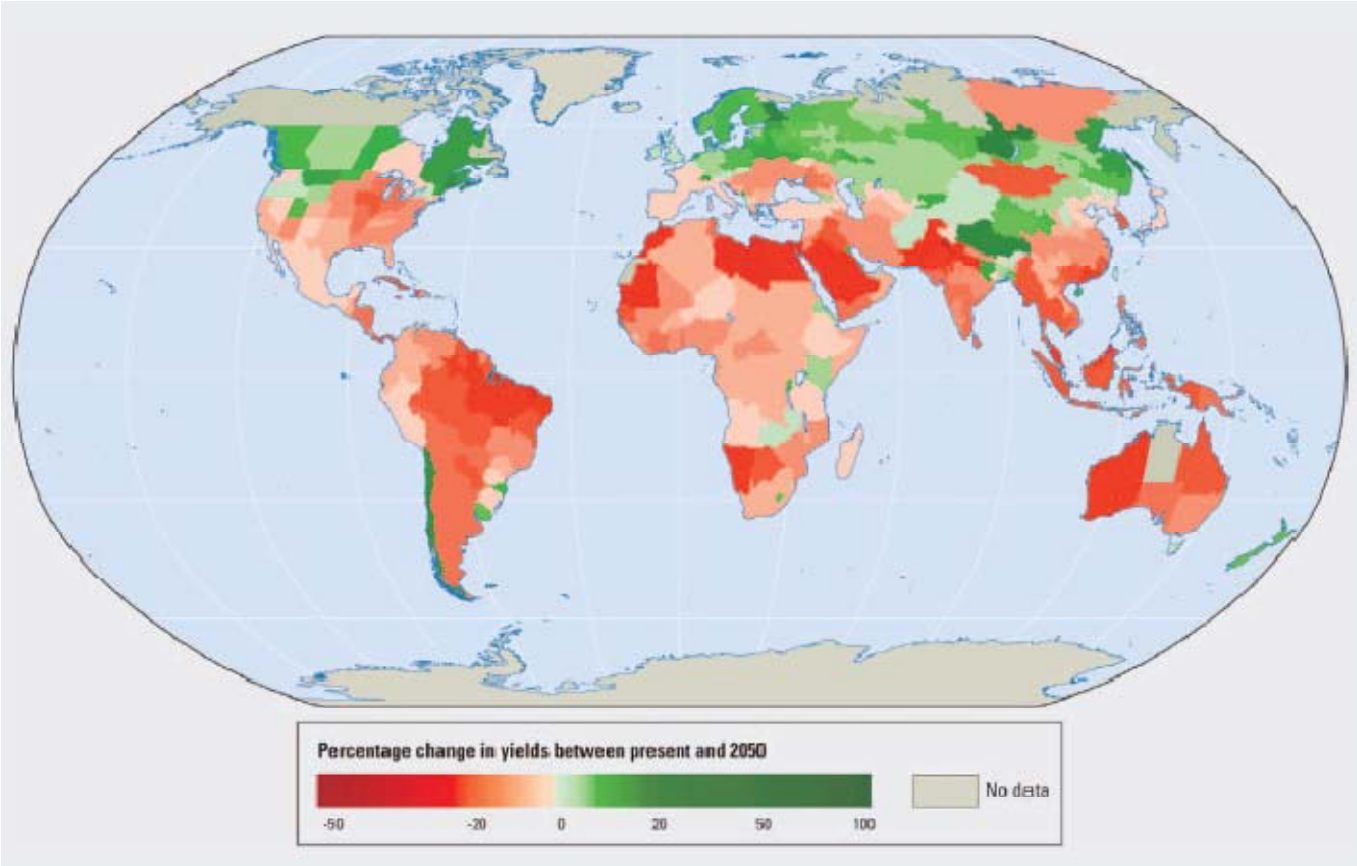

Figure 2 Global impacts of climate change on crop productivity from simulations published in 2010. The study (Mendelsohn, 2010) simulated changes in yields of 11 crops for the year 2050, averaged across three greenhouse emission scenarios and five GCMs.(Reprinted by World Publishers)

Table 1 Direct and indirect drivers of climate change impacts on crop yields according to the report by numerous researchers.

Drivers	Impacts
Mean climate change	Shift in crop growing season (Kucharik, 2008).
Extreme temperatures	Heat stress; reduce crop fertility (Semenov and Shewry, 2011).
Droughts	Water stress; crop development alteration (Li et al., 2009; Savage, 2013).
Floods	Fungal disease; crop failure (Rosenzweig et al., 2002; Schiermeier, 2011).
Tropical storms	Loss of cropland area; crop failure (Schiermeier, 2011).
Pests and diseases	Crop failure; reduce quality (Rosenzweig et al., 2001).
CO_2 increase	Enhance photosynthesis rate; reduce stomata transpiration; reduce protein content (Kimball, 2010; Myers et al., 2014; O'leary et al., 2015).

In recognizing the complex interactions between crop growth and environmental factors, numerical simulations, or crop models, have become popular research tools for researchers in agro-meteorology in recent years. Modeling techniques are involved in empirical models (Lobell and Burke, 2010), process-based crop models representing detailed biophysical process (Jones et al., 2003; Keating et al., 2003; Parry et al., 2004; Stöckle et al., 2003) and large-scale ecosystem models aiming to simulate the terrestrial carbon cycle (Deryng et al., 2011; Osborne et al., 2007). Bai et al (2016) investigated that using the Agricultural Production System Simulator (APSIM) model increase in temperature reduced wheat yield by 0.0 %–5.8 % and decrease in solar radiation reduced it by 1.5%—8.7 % in Jiangsu and Anhui province of China. Jabeen et al (2017) also observed that the rise in maximum and minimum temperature decreased the wheat yields using DSSAT and GIS across the Pothwar region, Pakistan. Deryng et al (2011) found that changes in temperature and precipitation as predicted by PEGASUS 1.0 (Predicting Ecosystem Goods And Services Using Scenarios) for the 2050s led to a global yield reduction if planting and harvesting dates remain unchanged. Wilcox and Makowski (2014) documented a meta-analysis of simulated wheat yield from 90 studies to identify the levels of temperature, precipitation and CO_2 concentration that resulted in increasing or decreasing wheat yields.

Of these models, the CERES (Crop Estimation through Resource and Environment Synthesis) cereal model simulated the growth and development of cereal crops including wheat in response to weather and management factors (Ritchie and Otter, 1985). The successful performance of CERES-Wheat in simulating wheat growth and grain yield in response to management and environmental factors has been reported under a wide range of soil and climatic conditions (Attia et al., 2016; Feng et al., 2016; Jabeen et al., 2017; Thorp et al., 2010; Timsina et al., 2008; Zheng et al., 2016). Hence, DSSAT CERES has been used for climate change and climate extreme impact assessment for rice, wheat and maize for different zones in China in historical and future scenarios (Feng et al., 2016; Liu et al., 2012; Xiong et al., 2009; Zheng et al., 2016).

Crop water productivity

Crop water productivity (CWP) is defined as the amount of yield produced per unit of water involved in the production, or the value added to water in a given circumstance (Molden et al., 1998; Sakthivadivel et al., 1999; Tuong et al., 2000), which is a quantitative term used to define the relationship between crop produced and the amount of water involved in crop production and consequently becomes a useful indicator to quantify the impact of irrigation scheduling decisions with regard to water management (Igbadun et al., 2006). The threat of climate change is affecting the important water resources (Chatterjee et al., 2012), and subsequent precipitation variability and changing evaporation rate will lead to variations in water availability and groundwater recharge (Huntington, 2006). The increased frequency of extreme weather events such as drought disaster, extreme high temperature and heavy precipitation have started creating imbalances in hydrological cycle and is resulted in large fluctuations in crop yields and water productivity in recent years.

The Huang-Huai-Hai Plain faces a serious threat of excessive exploitation of groundwater resources (Jia and Liu, 2002; Liu et al., 2010). The potential impacts of climate change are expected to reshape the patterns of demand and supply of water for agriculture, therefore the assessment of the impacts of climate change on ecological and agricultural water consumption is essential. Understanding the quantity of agricultural water consumption is a high priority in areas where water is currently scarce and over-exploited (Perry, 2011). Evapotranspiration (ET) is a useful indicator of crop water consumption; therefore, accurate estimation of regional ET is essential to achieve large scale water resources management (Rwasoka et al., 2011). Current estimates of actual evapotranspiration in China are mainly based on plot-scale experiments (Chen et al., 2002; Zhang et al., 1999; Zhang et al., 2004), from the product of soil moisture and potential ET. However, such estimates are only useful for a specific area, and cannot be expanded to large-scale areas. The level of water consumption differs significantly across regions, farming systems, canal command areas, and farms (Molden et al. 2003).

Development of remote sensing technology has made it possible to estimate land surface evapotranspiration at the regional or basin scale. Numerous remote sensing methods for modeling crop actual evapotranspiration (ET_a) have been improved in recent years (de Oliveira et al., 2009; Jia et al., 2012; Teixeira et al., 2009). Li et al (2008) estimated the ET_a for winter wheat using the SEBAL (Surface Energy Balance Algorithm for Land) model and NOAA (National Oceanic and Atmospheric Administration) data for Hebei province in the North China Plain (NCP). Liaqt et al (2015) also investigated the ET_a for the Indus Basin Irrigation System using SEBS (the Surface Energy Balance System) and MODIS (Moderate-resolution imaging spectroradiometer) products. However, observed phenological data and crop dominance map were not considered in these investigations, and specific water consumption of winter wheat and summer maize has not yet been determined in 3H Plain.

Crop water productivity is a useful indicator for quantifying the impact of irrigation management decisions (Ali and Talukder, 2008) and can be used to assess and compare the effects of water-saving

measures at different scales and under various conditions (Cui et al., 2007). Perry et al. (2009) reported in their literature review that the relationship between biomass and transpiration is essentially linear for a given crop and climate - provided nutrients are adequate. Other results, however, suggest the relationship between ET and yield is not always linear. Most of the above studies reporting on the relationship between water consumption, grain yield, and CWP obtained over a relatively short period of time, are based on data obtained in a controlled, experimental environment.

2. Context, objectives and outline of the thesis

Context

As described before, a better understanding of the impact of climate change on different weather variables and consequently ET_0 and grain yield is uttermost important to come to a sustainable agricultural production in the 3H Plain in China, which is the wheat production base of the country (Figure 3). The annual rainfall concentrates in the summer period, from July to September. However, winter and spring is strongly characterized by a lack of water for agricultural production (Yang et al., 2013a). Water shortage in this region has become a serious concern in recent decades (Brown and Rosenberg, 1997). Excessive exploitation of groundwater resources has resulted in water fallen at a rate of 1 $m \cdot y^{-1}$ and severe groundwater depression in the past 20 years (Zhang et al., 2015). Furthermore, the yield damage caused by drought tends may increase in the future, indicated by a pronounced uprising of drought events in terms of magnitude and area (Li et al., 2015). As a result, questions related to the implementation of soil conservation and alternative tillage techniques and their impact on the winter wheat yield and evapotransiration are strongly oriented to developing more sustainable agriculture.

Nevertheless, to what extent the grain yield and crop water productivity for winter wheat responds to climate change and drought together with their improvement measures across our agricultural region remains unexplored.

Numerous studies have investigated the effect of climatic drought on the grain yield and water productivity and used multi-indices to evaluate drought characteristics, but this only for historical climate scenarios (Allen et al., 2010; Dai, 2013). Crop models have been used to assess the impact of climate change and climatic extremes on rice, wheat and maize production for the whole growing season in China (Feng et al., 2016; Liu et al., 2012; Xiong et al., 2009; Zheng et al., 2016). Furthermore, most studies addressed the relationship between water consumption, grain yield, and CWP using data obtained over a relatively short period of time, or based on data obtained in a controlled, experimental environment (Perry et al., 2009), which leaves us with questions about the variability on the long term.

Therefore, the impact of climate change and drought on simulated yield and land surface evapotranspiration estimation in the Huang-Huai-Hai Plain is of primary interest in the context of improving the crop water productivity for winter wheat while minimizing water consumption in this region. This research can

contribute to the establishment of a policy to realize a more efficient use of water resources and a sustainable agricultural production in the Huang-Huai-Hai Plain, China.

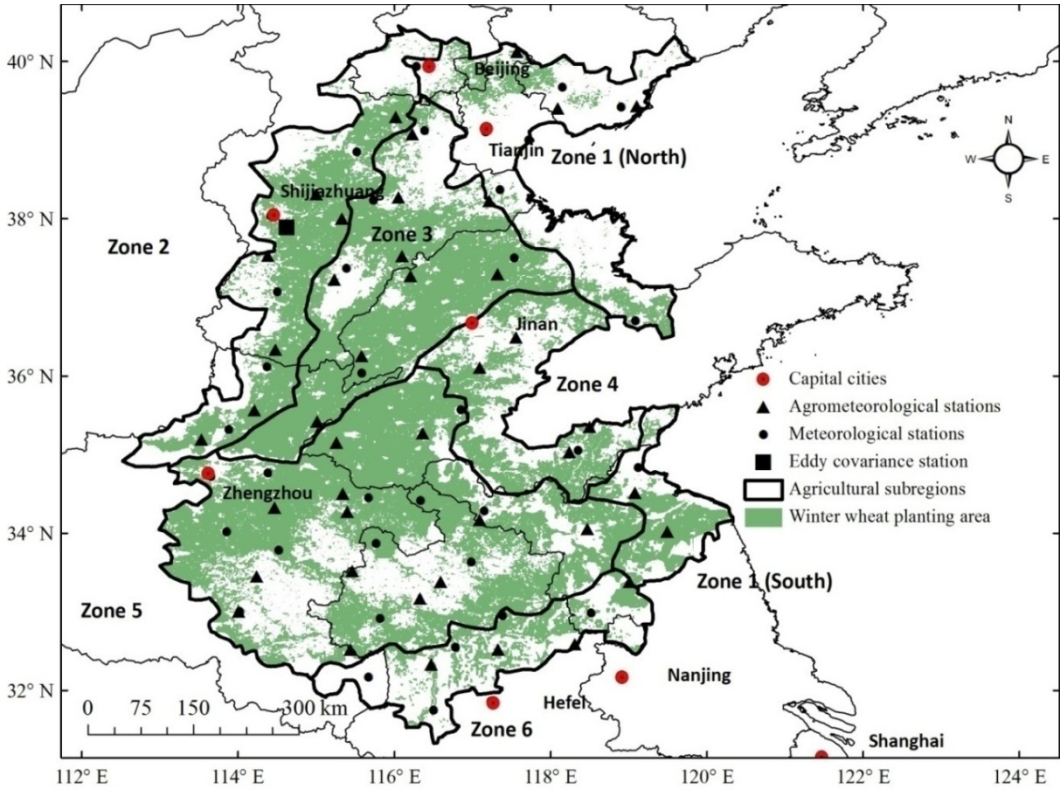

Figure 3 The crop dominance map extraction of winter wheat (the green shape) in the Huang-Huai-Hai Plain. The triangle and round black spots mean agrometeorological and meteorological stations, respectively. The round red spot means the capital cities. The black line means the boundary of agricultural sub-regions.

Objectives

In our study, we aimed (1) to identify the most sensitive and primary controlling variables to potential evapotranspiration and in subsequence projected drought characteristics under the RCP 8.5 scenario, (2) to establish the potential impact of climate change and drought on the winter wheat yield using CERES-Wheat Model over 12 selected locations, and (3) to investigate water productivity for wheat using the SEBAL model, a linear regression equation which integrated remotely sensed images and census data, and the grain yield in the Huang-Huai-Hai Plain.

To achieve these goals, we aimed to answer the following scientific questions in the context of the 3H Plain

1. What are the characteristics of ET and drought in various climate scenarios and how is it related to water consumption?

2. How is winter wheat yield affected by climate change and drought?

3. What is the averaged water productivity of winter wheat and its spatial variability in the 3H Plain?

With the projected temperature increase and change in precipitation distribution, the drought risk is expected to increase further and subsequently make crop production more uncertain through augmenting crop water consumption in study area. According to the predictions of climate change models, ET_0 is expected to increase over the coming years due to an expected temperature rise (Goyal, 2004; McNulty et al., 1997). The general recognition is that drought has been intensifying around the world due to global warming in the past decades (Allen *et al.* 2010; Dai 2013). Dynamic crop models, such as the Erosion Productivity Impact Calculator (EPIC) model (Williams et al. 1983), APSIM (Keating et al. 2003), and DSSAT-CERES (Jones et al. 1998), have been tested and used in quantifying responses to water, nitrogen and weather at scales ranging from fields to regions around the world. Jabeen et al (2017) found that the rise in maximum and minimum temperature decreased the wheat yields using DSSAT and GIS across the Pothwar region of Pakistan.

Table 2 Statement of our hypotheses in this research

Hypothesis 1	**Drought conditions will aggravate due to climate change by increasing potential evapotranspiration and augmenting crop water consumption in water-limited Huang-Huai-Hai Plain.**
Hypothesis 2	**The response of winter wheat yield to climate change and drought can be drawn available throughout the plain.**
Hypothesis 3	**The relationship between water productivity with ET and grain yield of winter wheat should be defined at the level of the sub-agricultural zone in the 3H Plain.**

Besides with the development of remote sensing technology, a number of researchers reported the crop water productivity in China, with varied spatial and temporal resolutions based on model simulation, estimation from remote sensing data and calculation from collected irrigation district data (Cao et al., 2015; Huang and Li, 2010; Liu et al., 2007; Rosengrant et al., 2002; Yan and Wu, 2014).

Climate change is widely accepted to be one of the most critical problems faced by the Huang-Huai-Hai Plain, which is an over-exploitation of groundwater region. Consequently, to answer mentioned scientific questions, we would test the following hypotheses (Table 2).

Outline

This study is a compilation of scientific papers that have been published or are being reviewed. It is structured as follows:

- **Chapter** Ⅱ **(Hypothesis 1)** investigates the spatiotemporal patterns of ET_0 and primary driving meteorological variables based on a historical period and RCP 8.5 scenario daily data set from 40 weather stations over the 3H Plain using linear regression, spline interpolation method, a partial derivative analysis and multivariate regression. ***Reference*: Qin Liu**, *Changrong Yan, Hui Ju, Sarah Garré. Impact of climate change on potential evapotranspiration under a historical and future climate scenario in the Huang-Huai-Hai Plain, China. Theoretical and Applied Climatology, 2017. Doi:10.1007/s00704- 017-2060-6*

- **Chapter** Ⅲ **(Hypothesis 1)** addresses the variations in drought characteristics (drought event frequency, duration, severity, and intensity) for the past 50 years (1961-2010) and under future scenarios (2010—2099), based on the observed meteorological data and the RCP 8.5 projection. ***Reference*:** *Xiangxiang Li, Hui Ju, Sarah Garré, Changrong Yan, William D. Batchelor, Qin Liu *. Spatiotemporal variation of drought characteristics in the context of climate change in the Huang- Huai-Hai Plain, China. Journal of Integrative Agriculture, 2017, Doi: 10.1016/S2095-3119(16)61545-9.*

- **Chapter** Ⅳ **(Hypothesis 2)** determines the potential impacts of drought on wheat yield using CERES-Wheat model at twelve stations representing different locations on the 3H Plain. The cumulative probability of the yield reduction rate during the jointing to heading stage and the filling stage will be investigated. ***Reference*:** *Qin Liu, Changrong Yan, Sarah Garré, Xiangxiang Li. Potential effect of drought on winter wheat yield using CERES-Wheat model over the Huang-Huai-Hai Plain. submitted in Journal of Integrative Agriculture (JIA), 2017.*

- **Chapter** Ⅴ **(Hypothesis 2)** describes the effects of climate change (including solar radiation, maximum temperature, minimum temperature, and precipitation) between historical records (1985—2014) and future climate projections under the RCP4.5 and RCP8.5 pathways (2021—2050) on winter wheat yield, using the CERES-Wheat model. ***Reference*:** *Qin Liu, Xiangxiang Li, Changrong Yan, Sarah Garré. Investigation of the impact of climatic shifts in wheat yield using CERES-Wheat*

model over the Huang-Huai-Hai Plain of China, submitted in Theoretical and Applied Climatology, 2017.

- **Chapter Ⅵ (Hypothesis 3)** documents an attempt to apply a regional evapotranspiration model (SEBAL) and crop information for assessment of regional crop (winter wheat and summer maize) actual evapotranspiration (ET_a) in 3H Plain. ***Reference:*** *Jianying Yang, Xurong Mei, Zhiguo Huo, Changrong Yan, Hui Ju, fenghua Zhao, Qin Liu *. Water consumption in summer maize and winter wheat cropping system based on SEBAL model in Huang-Huai-Hai Plain, China. Journal of Integrative Agriculture, 2015, 14(10): 2065—2076.*

- **Chapter Ⅶ (Hypothesis 3)** describes spatio-temporal characteristics of water productivity of winter wheat in Huang-Huai-Hai Plain and in subsequent correlation of water productivity to actual evapotranspiration and grain yield of winter wheat in sub agricultural regions over the Huang-Huai-Hai Plain, China. ***Reference:*** *Qin Liu, Changrong Yan, Jianying Yang, Sarah Garré. An assessment of water consumption, grain yield and water productivity of winter wheat in agricultural sub-regions of Huang-Huai-Hai Plain, China, will be submitted.*

Finally, in **Chapter Ⅷ** we discuss the main results and also conclude the prospects and potential improvements.

3. Study region description, data collection

Study region description

Climate change is one of the most critical problems faced by the Huang-Huai-Hai Plain, which is an over-exploitation of groundwater region and where future warmer and drought conditions will intensify crop water demand. The 3H Plain is located in the middle and lower of the Yellow River basin, the Huaihe River plain, and the Haihe River valley plain, extending over 32°00′—40°30′N and 113°00′E to the east coast (Figure 4). It is surrounded by the south foot of Yanshan Mountain to the north, north foot of Tongbai Mountain and Dabie Mountain and Jianghuai Watershed to the south, and eastern foot of Taihang Mountain and Qinling Range to the west, whereas the eastern boundary lies the Bohai Sea and Yellow Sea.

The 3H Plain belongs to the extratropical monsoon climatic region. The annual mean precipitation is 348.5 mm, while the atmospheric evaporative demand is about 1000 mm y^{-1} (Ren et al., 2008). As described in Figure 5, annual precipitation is concentrated in summer (July through September) and winter is strongly characterized by a lack of water for agricultural production. Water shortages on the 3H Plain have become of considerable concern over recent decades (Brown and Rosenberg, 1997). Increasing magnitudes of 0.003, 0.018 and 0.034 °C $year^{-1}$, respectively, were detected for maximum temperature (T_{max}), average temperature (T_a) and minimum temperature (T_{min}) in past 54 years, which only were statistically significant ($p < 0.01$) for T_a and T_{min} (Figure 6). The main cropping system is a rotation of wheat and maize with the systematic

application of irrigation water and fertilizer on the 3H Plain (Liang et al., 2011; Sun et al., 2011; Zhao et al., 2006), while for this rotation system rainfall can just meet 65% of total agricultural water demand, especially for winter wheat, from which only 25%—40% of the demand is satisfied with rainfall (Mei et al., 2013b). High irrigation is necessary to maintain high yield levels under these climatic conditions. The irrigation water is primarily pumped from groundwater. Usually, the farmers in 3H Plain apply 3–5 times irrigation, sometimes even 6–7 times, through flood irrigation during the winter wheat growing season (Li et al., 2010); this may result in a low potential irrigation water use efficiency and inefficient use of nitrogen (Wang et al., 2004). However, the groundwater level has decreased from a depth of 10m in the 1970s to 32m in 2001, and has continued to decrease at the rate of 1m per year (Zhang et al., 2015).

Figure 4 The location of Huang-Huai-Hai Plain (Green shape) in China. The Huang-Huai-Hai Plain is located in the middle and lower of the Yellow River basin, the Huaihe River plain, and the Haihe River valley plain, covering Beijing, Tianjin, Hebei, Henan, Shandong, Anhui and Jiangsu province. The upper blue line is Yellow River and the below blue one is Yangtze River.

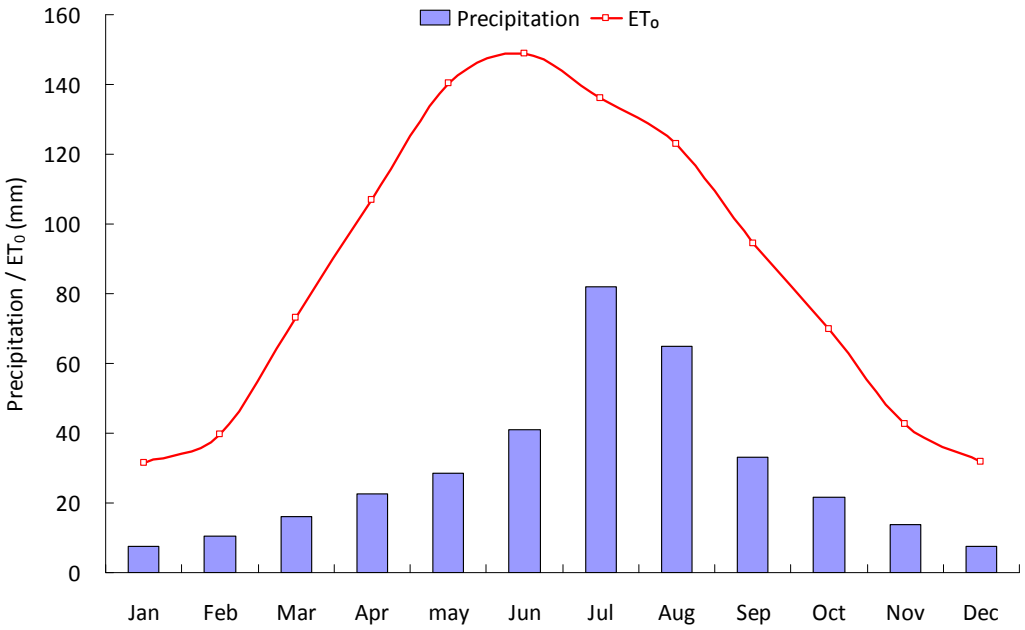

Figure 5 Comparison of monthly precipitation and ET_0 in past 54 years. The monthly area-averaged precipitation and ET_0 were obtained from 40 meteorological stations across the Huang-Huai-Hai Plain.

The plain encompasses around 18 million hectares farmland of which about 61% and 31% are dedicated to wheat and maize production respectively (Jin et al., 2009), with intensive management characterized by the application of sufficient irrigation water and fertilizers. Drought is one of the most damage and widespread climate event facing the 3H Plain, and in subsequence has been the main restriction factor for agriculture and economy development. Winter wheat is sown in early October and harvested in June of the second year, and that summer maize is then sown immediately afterwards and harvested in later September. The 3H Plain (Figure 5) is divided into six agricultural sub-regions: coastal land, a farming-fishing area (including the northern part, Zone 1, and the southern part), piedmont plain-irrigable land (Zone 2), low plain-hydropenia irrigable land and dry land (Zone 3), hill-irrigable land and dry land (Zone 4), basin- irrigable land and dry land (Zone 5) and hill-wet hot paddy field (Zone 6) in terms of climate conditions and agricultural management practices.

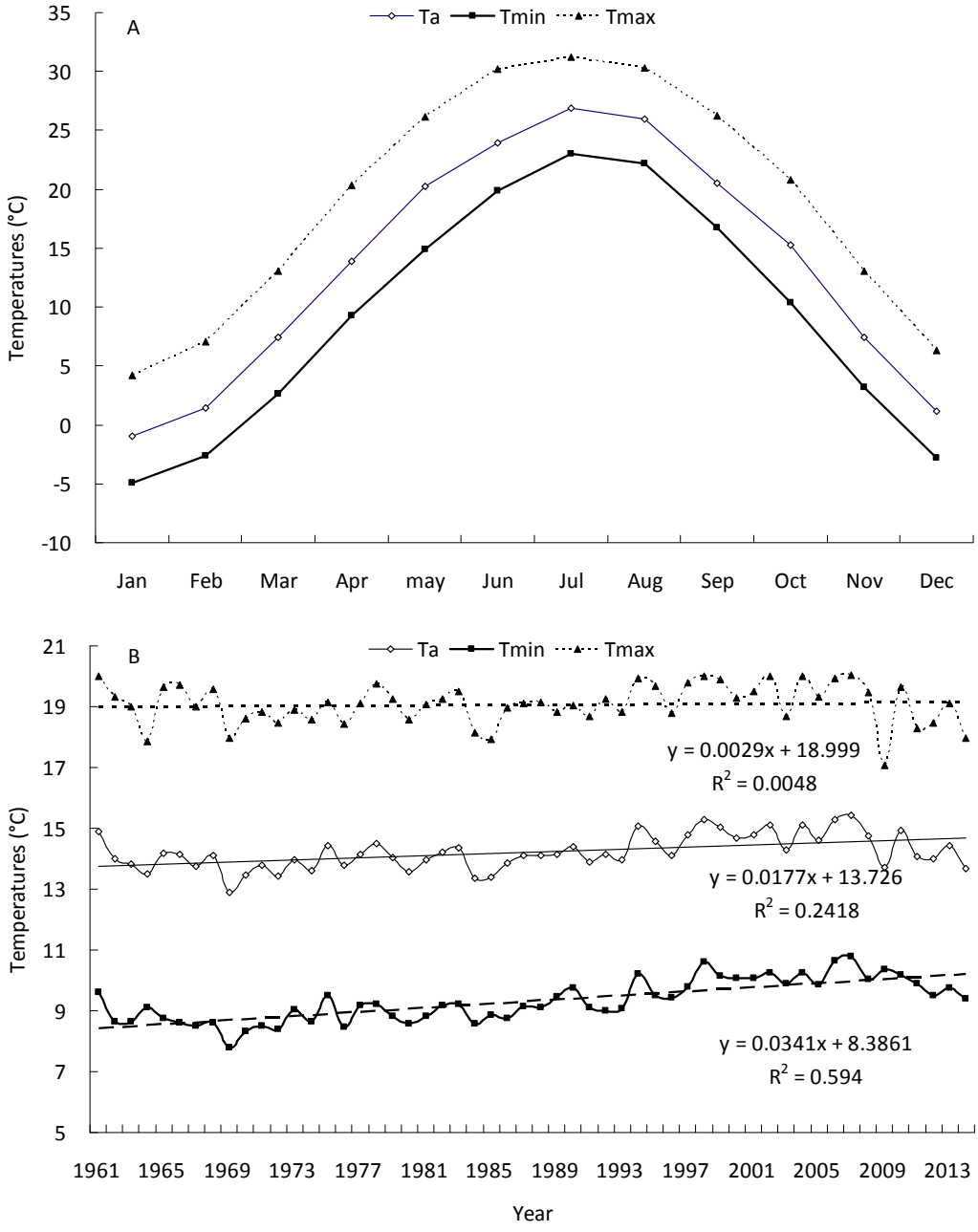

Figure 6 Comparison of monthly (A) and yearly (B) maximum (T_{max}), minimum (T_{min}) and average (T_a) temperature in past 54 years. The monthly and yearly area-averaged three temperatures were obtained from 40 meteorological stations across the Huang-Huai-Hai Plain.

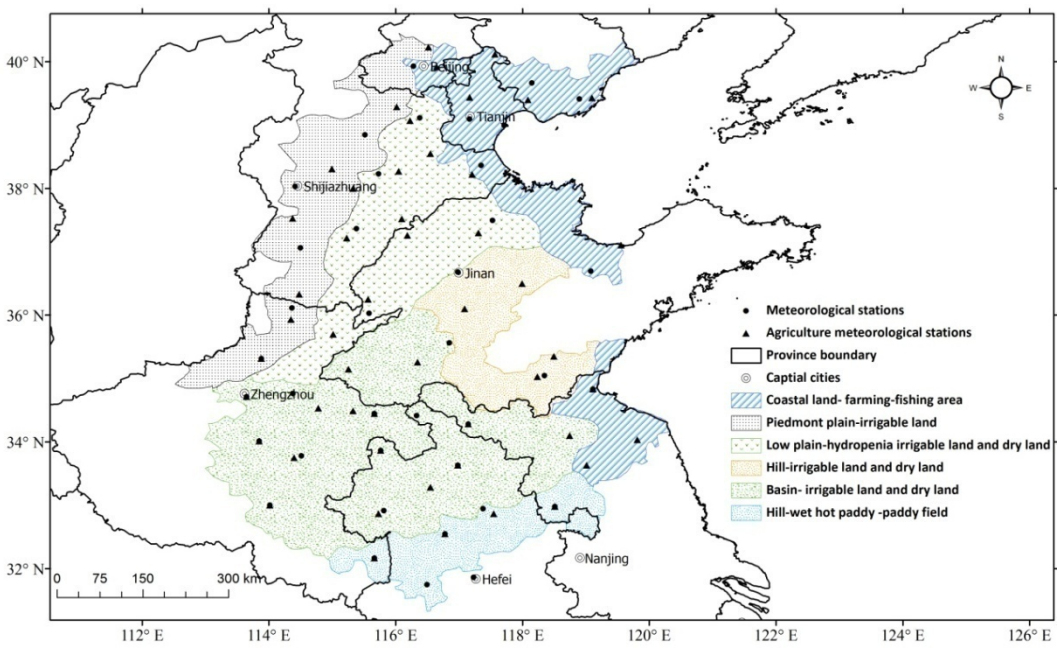

Figure 7 Location of the Huang-Huai-Hai Plain and its six agricultural sub regions (Coastal land- farming-fishing area, Piedmont plain-irrigable land, Low plain-hydropenia irrigable land and dry land, Hill-irrigable land and dry land, Basin- irrigable land and dry land and Hill-wet hot paddy field). The triangle and round black spot mean agrometeorological stations and meteorological stations respectively. The round spot means the capital cities. The black line means the province boundary.

Data collection

As mentioned in our study, the first emphasis is to identify the most sensitive and primary controlling variables of ET_0 and in subsequent projected drought characteristics under the alternative period or scenario in Chapter Ⅱ and Ⅲ. A historical dataset from 1961 to 2014, composed of data from 40 meteorological stations, was provided by the China Meteorological Administration (Figure 7). Daily maximum (T_{max}, °C), average (T_a, °C) and minimum temperature (T_{min}, °C), average relative humidity (RH, %), wind speed (WS, $m \cdot s^{-1}$) observed at 10-m height, and daily sunshine duration (SD, h) data were available.

The 0.5° × 0.5° gridded data of the 3H Plain from 2015 to 2099 simulated under the future RCP 8.5 climatic scenario and obtained from the National Climate Center, included daily average temperature (T_a, °C), daily maximum (T_{max}, °C) and minimum temperature (T_{min}, °C), daily precipitation (mm), daily average wind speed (WS, $m \cdot s^{-1}$), daily average relative humidity (RH, %), and daily net radiation (RS, $MJ \cdot m^{-2} \cdot d^{-1}$). The 0.5° × 0.5° gridded data was upscaled to 40 meteorological stations using double-linear interpolation method (Yuan et al, 2012). The RCP8.5 scenario is characterized by high concentration of greenhouse gas with stabilizing emissions post-2099 (increase by about 120 Gt CO2-eq. by 2100 compared to 2000) (Riahi et al., 2011).

Among these 40 stations we selected 12 stations with more detailed information available. The minimal data sets required for model operation include weather information (daily global solar radiation, maximum and

minimum temperature, precipitation), soil information (classification and basic profile characteristics by soil layer) and management information (e.g., cultivar, planting, irrigation and fertilization information). In this study, the soil classification and profile characteristics were collected from the China Soil Scientific Database.

Finally, we also used satellite data to estimate water productivity in the framework of this project. The data is mainly involved in MODIS products including MOD11A1 (land surface temperature/surface emissivity), MOD13A2 (NDVI) and MCD43B3 (surface albedo). The spatial resolution of the three MODIS products is 1 km. The temporal resolution of MOD11A1, MOD13A2 and MCD43B3 was 1-d, 16-d, and 8-d, respectively. For land surface temperature images, cloudy areas were eliminated by replacing the values with the average of two images in the nearest clear dates.

4. Methods

Calculation of potential evapotranspiration

Potential evapotranspiration is an integrated climate variable that gives a measure of the evaporation demand of the air. ET_0 is essentially dependent on four meteorological variables: air temperature, solar radiation, relative humidity and wind speed (Allen et al., 1998). The main advantage of the PM approach is that it takes into account the most significant variables, so that the influence of each of them can be analyzed (Blaney, 1952; Mei et al., 2013a), physically based equations requiring daily data for temperature and relative humidity of the air, solar radiation and wind speed (Allen et al., 1998). Also, it is recommended as the standard ET_0 method, within which the evapotranspiration of a hypothetical reference vegetated field is explicitly determined (Allen et al., 2006; Cai et al., 2007). Estimate the evolution of ET_0 and meteorological variables affecting ET_0 is necessary (Mínguez et al., 2007), and past trends of meteorological variables and ET_0 values is still need to establish a solid baseline for future adaptation strategies (Mearns et al., 2003).

We used the Penman–Monteith formula recommended by the Food and Agriculture Organization (FAO) of the United Nations to calculate the ET_0 for both the historical and future conditions:

$$ET_0 = \frac{0.408\Delta(R_n - G) + \gamma \frac{900}{T+273} U_2 (e_s - e_a)}{\Delta + \gamma(1 + 0.34U_2)} \qquad \text{Formula 1}$$

Where ET_0 is potential evapotranspiration (mm·d^{-1}); $\triangle$ represents the saturation vapor pressure/temperature curve (kPa·°C^{-1}); G is the soil heat flux (MJ·m^{-2}·d^{-1}); T is the average daily temperature at 2m height (°C); U_2 is the wind speed at 2m height (m·s^{-1}); e_s is the saturation vapor pressure (kPa); e_a is the actual water vapor pressure (kPa); e_s–e_a is the vapor pressure deficit (kPa); γ is the psychometric constant (kPa·°C^{-1}); R_n is the net radiation from the canopy (MJ·m^{-2}·d^{-1}), which is the difference between

net shortwave radiation (R_{ns}) and net longwave radiation (R_{nl}). R_{ns} is calculated as

$$R_{ns} = (1-\lambda)R_s \quad \text{Formula 2}$$

sWhere R_s is surface solar radiation (MJ·m^{-2}·d^{-1}) and λ (=0.23) is the albedo of reference grassland. R_s can be calculated from sunshine duration:

$$R_s = \left(a_s + b_s \frac{n}{N}\right) R_a \quad \text{Formula 3}$$

Where N is the maximum possible sunshine duration (h), n/N is the relative sunshine duration, R_a is the extraterrestrial radiation (MJ·m^{-2}·d^{-1}), and a_s and b_s are regression constants and are set to be 0.25 and 0.5 respectively. R_a is calculated as

$$R_a = \frac{24(60)}{\pi} G_{sc} dr\left(w_s \sin(\phi)\sin\xi + \cos(\phi)\cos\xi \sin w_s\right) \quad \text{Formula 4}$$

Where is the solar constant (=0.082 MJ·m^{-2}·d^{-1}), dr is inverse relative distance Earth-Sun, w_s is the sunset hour angle (rad), ϕ is the latitude (rad), ξ is the solar declination (rad).

R_{nl} is calculated as

$$R_{nl} = \sigma\left[\frac{T_{max,K}^4 + T_{min,K}^4}{2}\right](0.34 - 0.14\sqrt{e_a})\left(1.35\frac{R_s}{R_{so}} - 0.35\right) \quad \text{Formula 5}$$

Where σ is the Stefan-Bolzmann contant (=4.903$\times$ 10^{-9} MJ·k^4·m^{-2}·d^{-1}), $T_{max,K}$ is the maximum absolute temperature during the 24-h period (K= °C+273.16), $T_{min,K}$ is the minimum absolute temperature during the 24-h period (K= °C+273.16), e_a is the actual vapor pressure (kPa), and R_{so} is the clear-sky radiation (MJ·m^{-2}·d^{-1}).

DSSAT-CERES-Wheat model for yield simulation

Crop models can be used to analyse the effects of various climatic factors on crop growth and grain yield considering the interactions with edaphic, biotic and agronomic factors. One of them, DSSAT is an integrated software comprising different computer programs that can simulate crop growth and grain yield for research and decision-making. The latest version DSSAT ver. 4.6.1.0 (http://dssat.net/downloads/dssat-v46) includes Cropping System Model (CSM), the primary modules of

which are consisted by weather module, soil module, soil-plant-atmosphere module, management operation module and 27 individual plant growth modules (Figure 8). Each plant growth is a separate module to simulate phenology, biomass, growth and yield, based on the soil water and fertility supplement in response to weather and management (Jones et al., 2003).

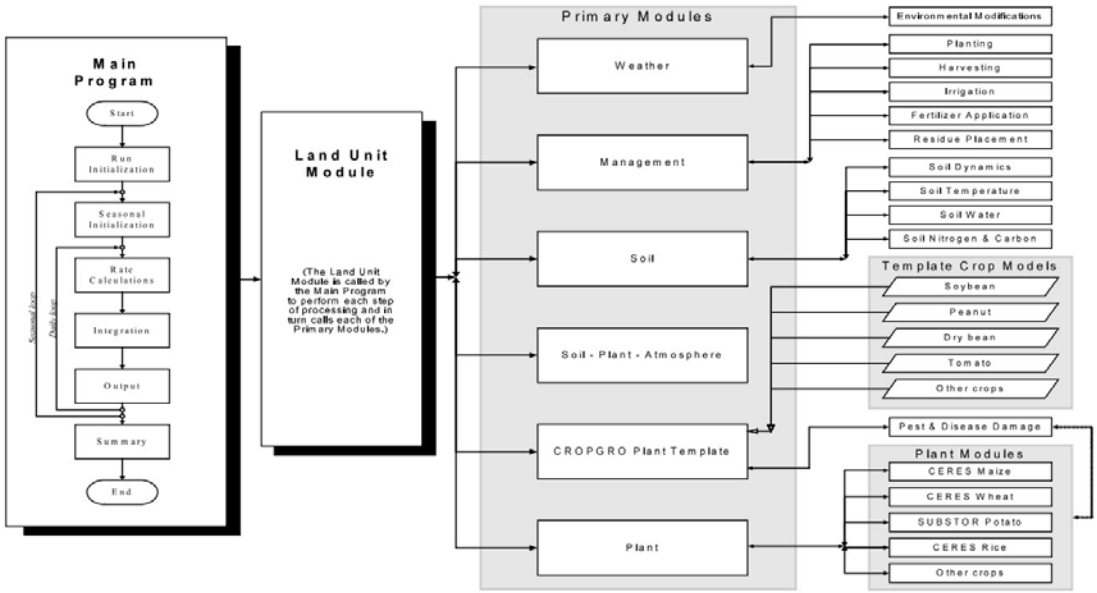

Figure 8 Overview of the components and modular structure of the DSSAT/CSM. The DSSAT-CSM has a main drive program, a land unit module, and modules for the primary components that make up a land unit in a cropping system. Each module has six operational steps, as shown in this Figure (run initialization, season initialization, rate calculations, integration, daily output, and summary output). The application driver communicates with only one module of the Land Unit module which provides the interface between the application driver (main program) and all of the components that interact in a uniform area of land. Source: Jones J.W. et al., 2003.

The minimal data sets required for DSSAT model operation consist of weather information (daily global solar radiation, maximum and minimum temperature, precipitation) (Panda et al., 2003), soil information (classification and basic profile characteristics by soil layer) and management information (e.g., cultivar, planting, irrigation and fertilization information). In the CERES-Wheat model, there are seven coefficients that control the development and growth of wheat (Ritchie et al., 1998), which must be calibrated and evaluated to meet the observed development and growth process under specific environmental conditions before being used for climate impact analyses (Hunt and Boote, 1998).

Due to its options to change the irrigation schedule to simulate plausible climatic drought effects on the crop, the DSSAT CERES-wheat model (He et al., 2013; He et al., 2012) was adopted here to simulate the wheat yield during 1981–2014 at all 12 locations. Hence, much work has been done on the impacts of climate change, irrigation scheduling and water and fertilizer conditions on the crop yield using DSSAT in China (Hui et al., 2005; Jiang et al., 2016; Yang et al., 2013b; Yang et al., 2010).

Satellite-based actual evapotranspiration estimation using the SEBAL method

In this study, the Surface Energy Balance Algorithm for Land (SEBAL) method from the meteorological stations and remote sensing data was used to compute the evapotranspiration (ET) rate for in 3H Plain in China. The SEBAL method has been used in various studies to assess ET rates in European countries, Southern Asia and China (Bastiaanssen et al., 1998a; Bastiaanssen et al., 1998b; Wang et al., 1995; Zhang et al., 2016). In addition, Bastiaanssen et al (2002) have compared predictions of ET and sensible heat flux (H) by SEBAL with measurements made by eddy covariance and scintillometer systems with the determination in confidence interval. Comparisons with fluxes measured by other methods confirm the robustness of the SEBAL procedure. A conceptual scheme of SEBAL is presented in Figure 9. Hence, various applications have demonstrated the ability of SEBAL to accurately estimate daily ET. The SEBAL algorithm can be applied with little or no ground-based weather data (Allen et al., 2001). When data such as actual measurements for solar radiation and wind speed on the day of the image are available, the predictions by the procedure are improved. The regional ET was not always available in the resolution of Landsat TM (Thematic mapper), and SEBAL should be the best way to fix it up.

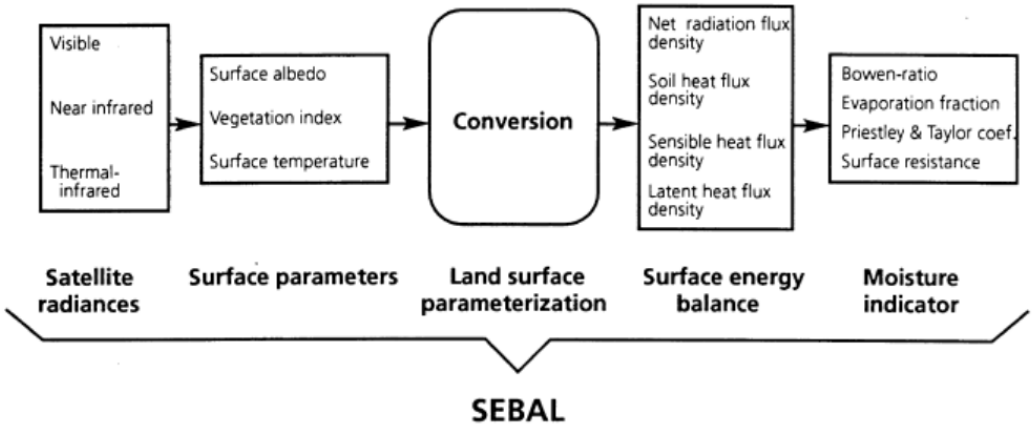

Figure 9 Principal components of the Surface Energy Balance Algorithm for Land (SEBAL) which converts remotely measured spectrally emitted and reflected radiance's into the surface energy balance and land wetness indicators (Bastiaanssen et al., 1998a).

The SEBAL procedure consists of a suite of algorithms in this case implemented with the ModelMaker module ERDAS software. The algorithms solve the complete energy balance equation:

$$R_n = G + H + \lambda ET \qquad \text{Formula 6}$$

Where, R_n (W·m^{-2}) is the net radiation; G (W m^{-2}) is the soil heat flux; H (W m^{-2}) is the sensible heat flux; and λET (W m^{-2}) is the latent heat flux associated with evapotranspiration.

The net radiation flux on the land surface, R_n (W·m^{-2}), was calculated using the following equation:

$$R_n = (1-\alpha)K_{in} + (L_{in} - L_{out}) - (1-\varepsilon)L_{in} \qquad \text{Formula 7}$$

where α is the surface albedo, K_{in} is the incoming short wave radiation (W·m^{-2}), L_{in} is the incoming long wave radiation (W·m^{-2}) , L_{out} is the outgoing long wave radiation (W·m^{-2}), and ε is the land surface emissivity.

The soil heat flux (G)is known to primarily depend on land surface characteristics and soil water content. The soil heat flux was calculated for the SEBAL model by the following equation:

$$G = \frac{T - 273.16}{\alpha}\left[(0.0032 \times \frac{\alpha}{0.9} + 0.0062 \times (\frac{\alpha}{0.9})^2\right](1 - 0.98NDVI^4)R_n \qquad \text{Formula 8}$$

The sensible heat flux (H) was calculated using the following equation:

$$H = \frac{\rho_{\text{air}} C_P dT}{r_{ah}} \qquad \text{Formula 9}$$

where ρ_{air} is the air density (kg·m^{-3}), and C_P is the air specific heat at constant pressure (J·kg^{-1}·K^{-1}).

Since the evaporative fraction Λ is constant during a day, the daily ET_{24} (mm) can be estimated using the following equations:

$$\Lambda = \frac{\lambda ET}{R_n - G} \qquad \text{Formula 10}$$

$$ET_{24} = \frac{\Lambda(R_{24} - G_{24})}{\lambda} \qquad \text{Formula 11}$$

where ET_{24} is the daily net radiation (W·m^{-2}); G_{24} is the daily soil heat flux (W·m^{-2}); and λ is the latent heat of vaporization (MJ·kg^{-1}).

5. Reference

Ali, M.H. and Talukder, M.S.U., 2008. Increasing water productivity in crop production—A synthesis. Agricultural Water Management, 95(11): 1201-1213.

Allen, C.D., Macalady, A.K., Chenchouni, H., Bachelet, D., McDowell, N., Vennetier, M., Kitzberger, T., Rigling, A., Breshears, D.D., Hogg, E.T. and Gonzalez, P., 2010. A global overview of drought and heat-induced tree mortality reveals emerging climate change risks for forests. Forest Ecology and Management, 259(4): 660-684.

Allen, R. G., Morse, A., Tasumi, M., Bastiaanssen, W., Kramber, W., & Anderson, H., 2001. Evapotranspiration from Landsat (SEBAL) for water rights management and compliance with multi-state water compacts, Geoscience and Remote Sensing Symposium, 2001. IGARSS'01. IEEE 2001 International. IEEE, pp. 830-833.

Allen, R.G., Pereira, L.S., Raes, D. and Smith, M., 1998. Crop evapotranspiration-Guidelines for computing crop water requirements-FAO Irrigation and drainage paper 56. FAO, Rome, 300(9): D05109.

Allen, R.G., Pruitt, W.O., Wright, J.L., Howell, T.A., Ventura, F., Snyder, R., Itenfisu, D., Steduto, P., Berengena, J., Yrisarry, J.B. and Smith, M., 2006. A recommendation on standardized surface resistance for hourly calculation of reference ETo by the FAO56 Penman-Monteith method. Agricultural Water Management, 81(1): 1-22.

Attia, A., Rajan, N., Xue, Q., Nair, S., Ibrahim, A. and Hays, D., 2016. Application of DSSAT-CERES-Wheat model to simulate winter wheat response to irrigation management in the Texas High Plains. Agricultural Water Management, 165: 50-60.

Bai, A., Zhai, P. and Liu, X., 2007. Climatology and trends of wet spells in China. Theoretical and Applied Climatology, 88, 139-148.

Bai, H., Tao, F., Xiao, D., Liu, F. and Zhang, H., 2016. Attribution of yield change for rice-wheat rotation system in China to climate change, cultivars and agronomic management in the past three decades. Climatic Change, 135(3-4): 539-553.

Balmaseda, M.A., Trenberth, K.E. and Källén, E., 2013. Distinctive climate signals in reanalysis of global ocean heat content. Geophysical Research Letters, 40(9): 1754-1759.

Barros, V.R., Field, C.B., Dokke, D.J., Mastrandrea, M.D., Mach, K.J., Bilir, T.E., Chatterjee, M., Ebi, K.L., Estrada, Y.O., Genova, R.C. and Girma, B. , 2014. Climate change 2014: impacts, adaptation, and vulnerability. Part B: regional aspects. Contribution of Working Group II to the fifth assessment report of the Intergovernmental Panel on Climate Change.

Bastiaanssen, W., Menenti, M., Feddes, R. and Holtslag, A., 1998a. A remote sensing surface energy balance algorithm for land (SEBAL). 1. Formulation. Journal of hydrology, 212: 198-212.

Bastiaanssen, W.G., Pelgrum, H., Wang, J., Ma, Y., Moreno, J.F., Roerink, G.J. and Van der Wal, T., 1998b. A remote sensing surface energy balance algorithm for land (SEBAL).: Part 2: Validation. Journal of hydrology, 212: 213-229.

Bastiaanssen, W.G., Ahmad, M.u.D. and Chemin, Y., 2002. Satellite surveillance of evaporative depletion across the Indus Basin. Water Resources Research, 38(12).

Blaney, H.F., 1952. Determining water requirements in irrigated areas from climatological and irrigation data.

Brown, R.A. and Rosenberg, N.J., 1997. Sensitivity of crop yield and water use to change in a range of climatic factors

and CO2 concentrations: a simulation study applying EPIC to the central USA. Agricultural and Forest Meteorology, 83(3-4): 171-203.

Cai, J., Liu, Y., Lei, T. and Pereira, L.S., 2007. Estimating reference evapotranspiration with the FAO Penman–Monteith equation using daily weather forecast messages. Agricultural and Forest Meteorology, 145(1–2): 22-35.

Cao, X., Wang, Y., Wu, P. and Zhao, X., 2015. Water productivity evaluation for grain crops in irrigated regions of China. Ecological Indicators, 55: 107-117.

Chatterjee, S.K., Banerjee, S. and Bose, M., 2012. Climate Change Impact on Crop Water Requirement in Ganga River Basin, West Bengal, India, Third International Conference on Biology, Environment and Chemistry IPCBEE, pp. 17-20.

Chen, J.-H., Kan, C.-E., Tan, C.-H. and Shih, S.-F., 2002. Use of spectral information for wetland evapotranspiration assessment. Agricultural Water Management, 55(3): 239-248.

Chen, J., Wilson, C., Tapley, B., Yang, Z. and Niu, G., 2009. 2005 drought event in the Amazon River basin as measured by GRACE and estimated by climate models. Journal of Geophysical Research: Solid Earth, 114(B5).

Chen, S., Liu, Y. and Thomas, A., 2006. Climatic change on the Tibetan Plateau: potential evapotranspiration trends from 1961–2000. Climatic Change, 76(3-4): 291-319.

Cline, W., 2007. Global warming and agriculture: Impact estimates by country. Columbia University Press.

Cui, Y., Dong, B., Li, Y. and Cai, X., 2007. Assessment indicators and scales of water saving in agricultural irrigation. Nongye Gongcheng Xuebao/Transactions of the Chinese Society of Agricultural Engineering, 23(7): 1-7.

Dai, A., 2011. Drought under global warming: a review. Wiley Interdisciplinary Reviews Climate Change, 2(1): 45-65.

Dai, A., 2013. Increasing drought under global warming in observations and models. Nature Climate Change, 3(1): 52-58.

Dalin, C., Qiu, H., Hanasaki, N., Mauzerall, D.L. and Rodriguez-Iturbe, I., 2015. Balancing water resource conservation and food security in China. Proceedings of the National Academy of Sciences, 112(15): 4588-4593.

de Oliveira, A.S., Trezza, R., Holzapfel, E.A., Lorite, I. and Paz, V.P.S., 2009. Irrigation water management in Latin America. Chilean journal of agricultural research, 69(Suppl 1): 7-16.

Deryng, D., Sacks, W., Barford, C. and Ramankutty, N., 2011. Simulating the effects of climate and agricultural management practices on global crop yield. Global biogeochemical cycles, 25(2).

Dilley, M., Chen, R.S., Deichmann, U., Lerner Lam, A.L. and Arnold, M., 2005. Natural disaster hotspots: a global risk analysis. Uwe Deichmann: 1-145.

Ding, Y., Ren, G., Zhao, Z., Xu, Y., Luo, Y., Li, Q. and Zhang, J., 2007. Detection, causes and projection of climate change over China: an overview of recent progress. Advances in Atmospheric Sciences, 24(6): 954-971.

ECSNCCA, 2011. Second National Climate Change Assessment Report. Science Press, Beijing.

Feng, H., Li, Z., He, P., Jin, X., Yang, G., Yu, H. and Yang, F. , 2016. Simulation of Winter Wheat Phenology in Beijing Area with DSSAT-CERES Model, Computer and Computing Technologies in Agriculture IX: 9th IFIP WG 5.14 International Conference, CCTA 2015, Beijing, China, September 27-30, 2015, Revised Selected Papers, Part II 9. Springer, pp. 259-268.

Feng, W., Lemoine, J.M., Zhong, M. and Tou-Tse, H., 2012. Terrestrial water storage changes in the Amazon basin measured by GRACE during 2002—2010. Chinese Journal of Geophysics, 55(3): 814-821.

Field, C.B., 2012. Managing the risks of extreme events and disasters to advance climate change adaptation: special report of the intergovernmental panel on climate change. Cambridge University Press.

Gornall, J., Betts, R., Burke, E., Clark, R., Camp, J., Willett, K. and Wiltshire, A. , 2010. Implications of climate change for agricultural productivity in the early twenty-first century. Philosophical Transactions of the Royal Society of London B: Biological Sciences, 365(1554): 2973-2989.

Goyal, R., 2004. Sensitivity of evapotranspiration to global warming: a case study of arid zone of Rajasthan (India). Agricultural Water Management, 69(1): 1-11.

Guan, Y., Zheng, F., Zhang, P. and Qin, C., 2015. Spatial and temporal changes of meteorological disasters in China during 1950–2013. Natural Hazards, 75(3): 2607-2623.

He, J., Cai, H. and Bai, J., 2013. Irrigation scheduling based on CERES-Wheat model for spring wheat production in the Minqin Oasis in Northwest China. Agricultural Water Management, 128(10): 19-31.

He, J., Dukes, M.D., Hochmuth, G.J., Jones, J.W. and Graham, W.D., 2012. Identifying irrigation and nitrogen best management practices for sweet corn production on sandy soils using CERES-Maize model. Agricultural Water Management, 109(9): 61-70.

Heim, R.R., 2002. A Review of Twentieth-Century Drought Indices Used in the United States. Bulletin of the American Meteorological Society, 83(8): 1149-1165.

Hertel, T.W., Burke, M.B. and Lobell, D.B., 2010. The poverty implications of climate-induced crop yield changes by 2030. Global Environmental Change, 20(4): 577-585.

Huang, F. and Li, B., 2010. Assessing grain crop water productivity of China using a hydro-model-coupled-statistics approach. Part II: Application in breadbasket basins of China. Agricultural water management, 97(9): 1259-1268.

Huang, Y. et al., 2014. Surface water deficiency zoning of China based on surface water deficit index (SWDI). Water Resources, 41(4): 372-378.

Hui, J.U., Wei, X., Long, X.Y. and Lin, E.D., 2005. Impacts of Climate Change on Wheat Yield in China. Acta Agronomica Sinica.

Hunt, L.A. and Boote, K.J., 1998. Data for model operation, calibration, and evaluation. In: G.Y. Tsuji, G. Hoogenboom and P.K. Thornton (Editors), Understanding Options for Agricultural Production. Springer Netherlands, Dordrecht, pp. 9-39.

Huntington, T.G., 2006. Evidence for intensification of the global water cycle: review and synthesis. Journal of Hydrology, 319(1): 83-95.

Igbadun, H.E., Mahoo, H.F., Tarimo, A.K. and Salim, B.A., 2006. Crop water productivity of an irrigated maize crop in Mkoji sub-catchment of the Great Ruaha River Basin, Tanzania. Agricultural Water Management, 85(1): 141-150.

IPCC, 2013. The physical science basis. Contribution of working group I to the fifth assessment report of the intergovernmental panel on climate change. USA: Cambridge University Press.

Irmak, S., Kabenge, I., Skaggs, K.E. and Mutiibwa, D., 2012. Trend and magnitude of changes in climate variables and reference evapotranspiration over 116-yr period in the Platte River Basin, central Nebraska–USA. Journal of Hydrology, s 420–421(4): 228–244.

Jabeen, M., Gabriel, H.F., Ahmed, M., Mahboob, M.A. and Iqbal, J., 2017. Studying Impact of Climate Change on Wheat Yield by Using DSSAT and GIS: A Case Study of Pothwar Region, Quantification of Climate Variability, Adaptation and Mitigation for Agricultural Sustainability. Springer, pp. 387-411.

Jia, J.-s. and Liu, C.-m., 2002. Groundwater dynamic drift and response to different exploitation in the North China Plain: A case study of Luancheng County, Hebei Province. ACTA GEOGRAPHICA SINICA-CHINESE EDITION-, 57(2):

201-209.

Jia, Z., Liu, S., Xu, Z., Chen, Y. and Zhu, M., 2012. Validation of remotely sensed evapotranspiration over the Hai River Basin, China. Journal of Geophysical Research: Atmospheres, 117(D13).

Jiang, Y., Zhang, L., Zhang, B., He, C., Jin, X. and Bai, X. , 2016. Modeling irrigation management for water conservation by DSSAT-maize model in arid northwestern China. Agricultural Water Management, 177: 37-45.

Jin, H., Qingjie, W., Hongwen, L., Lijin, L. and Huanwen, G., 2009. Effect of alternative tillage and residue cover on yield and water use efficiency in annual double cropping system in North China Plain. Soil and Tillage Research, 104(1): 198-205.

Jones, J.W., Tsuji, G.Y., Hoogenboom, G., Hunt, L.A., Thornton, P.K., Wilkens, P.W., Imamura, D.T., Bowen, W.T., Singh, U., 1998. Decision support system for agrotechnology transfer: DSSAT v3. In: Tsuji GY, Hoogenboom G, Thornton PK (eds) Understanding Options for Agricultural Production. Springer Netherlands, Dordrecht, pp 157-177

Jones, J.W., Hoogenboom, G., Porter, C.H., Boote, K.J., Batchelor, W.D., Hunt, L.A., Wilkens, P.W., Singh, U., Gijsman, A.J. and Ritchie, J.T., 2003. The DSSAT cropping system model. European journal of agronomy, 18(3): 235-265.

Keating, B.A., Carberry, P.S., Hammer, G.L., Probert, M.E., Robertson, M.J., Holzworth, D., Huth, N.I., Hargreaves, J.N., Meinke, H., Hochman, Z. and McLean, G. , 2003. An overview of APSIM, a model designed for farming systems simulation. European journal of agronomy, 18(3): 267-288.

Kendy, E., Zhang, Y., Liu, C., Wang, J. and Steenhuis, T., 2004. Groundwater recharge from irrigated cropland in the North China Plain: case study of Luancheng County, Hebei Province, 1949–2000. Hydrological Processes, 18(12): 2289-2302.

Kimball, B.A., 2010. Lessons from FACE: CO2 effects and interactions with water, nitrogen, and temperature. Handbook of climate change and agroecosystems: Impacts, adaptation, and mitigation. Imperial College Press, London UK: 87-107.

Kucharik, C.J., 2008. Contribution of planting date trends to increased maize yields in the central United States. Agronomy Journal, 100(2): 328-336.

Leblanc, M.J., Tregoning, P., Ramillien, G., Tweed, S.O. and Fakes, A., 2009. Basin‐scale, integrated observations of the early 21st century multiyear drought in southeast Australia. Water resources research, 45(4).

Li, H., Zheng, L., Lei, Y., Li, C., Liu, Z. and Zhang, S. , 2008. Estimation of water consumption and crop water productivity of winter wheat in North China Plain using remote sensing technology. Agricultural Water Management, 95(11): 1271-1278.

Liu, J., Wiberg, D., Zehnder, A.J. and Yang, H., 2007. Modeling the role of irrigation in winter wheat yield, crop water productivity, and production in China. Irrigation Science, 26(1): 21-33.

Li, Q., Dong, B., Qiao, Y., Liu, M. and Zhang, J., 2010. Root growth, available soil water, and water-use efficiency of winter wheat under different irrigation regimes applied at different growth stages in North China. Agricultural Water Management, 97(10): 1676-1682.

Li, Y., Huang, H., Ju, H., Lin, E., Xiong, W., Han, X., Wang, H., Peng, Z., Wang, Y., Xu, J. and Cao, Y., 2015. Assessing vulnerability and adaptive capacity to potential drought for winter-wheat under the RCP 8.5 scenario in the Huang-Huai-Hai Plain. Agriculture, Ecosystems & Environment, 209: 125-131.

Li, Y., Ye, W., Wang, M. and Yan, X., 2009. Climate change and drought: a risk assessment of crop-yield impacts. Climate Research, 39(1): 31-46.

Liang, W.L., Carberry, P., Wang, G.Y., Lü, R.H., Lü, H.Z. and Xia, A.P. , 2011. Quantifying the yield gap in wheat–maize cropping systems of the Hebei Plain, China. Field Crops Research, 124(2): 180-185.

Liaqat, U.W., Choi, M. and Awan, U.K., 2015. Spatio‐temporal distribution of actual evapotranspiration in the Indus Basin Irrigation System. Hydrological Processes, 29(11): 2613-2627.

LIU, H.L., YANG, J.Y., Ping, H., BAI, Y.L., JIN, J.Y., Drury, C.F., ZHU, Y.P., YANG, X.M., LI, W.J., XIE, J.G. and YANG, J.M., 2012. Optimizing parameters of CSM-CERES-Maize model to improve simulation performance of maize growth and nitrogen uptake in northeast China. Journal of Integrative Agriculture, 11(11): 1898-1913.

Liu, S., Mo, X., Lin, Z., Xu, Y., Ji, J., Wen, G. and Richey, J. , 2010. Crop yield responses to climate change in the Huang-Huai-Hai Plain of China. Agricultural water management, 97(8): 1195-1209.

Liu, X., Zhang, D., Luo, Y. and Liu, C., 2013. Spatial and temporal changes in aridity index in northwest China: 1960 to 2010. Theoretical and Applied Climatology, 112(1): 307-316.

Lobell, D.B. and Burke, M.B., 2010. On the use of statistical models to predict crop yield responses to climate change. Agricultural and Forest Meteorology, 150(11): 1443-1452.

Lobell, D.B. and Field, C.B., 2007. Global scale climate–crop yield relationships and the impacts of recent warming. Environmental research letters, 2(1): 014002.

Lu, C. and Fan, L., 2013. Winter wheat yield potentials and yield gaps in the North China Plain. Field Crops Research, 143: 98-105.

Lu, J., Sun, G., Mcnulty, S.G. and Amatya, D.M., 2005. A Comparison of six potential evapotranspiration methods for regional use in the Southwestern United States. Jawra Journal of the American Water Resources Association, 41(3): 621–633.

Mínguez, M.I., Ruiz-Ramos, M., Díaz-Ambrona, C.H., Quemada, M. and Sau, F., 2007. First-order impacts on winter and summer crops assessed with various high-resolution climate models in the Iberian Peninsula. Climatic Change, 81: 343-355.

Maracchi, G., Sirotenko, O. and Bindi, M., 2005. Impacts of present and future climate variability on agriculture and forestry in the temperate regions: Europe. Climatic Change, 70(1-2): 117-135.

McNulty, S.G., Vose, J.M. and Swank, W.T., 1997. R egional hydrologic response of loblolly pine and air temperature and precipitation. Journal of the American Water Resources Association, 33(5): 1011-1022.

Mearns, L., Giorgi, F., McDaniel, L. and Shields, C., 2003. Climate scenarios for the southeastern US based on GCM and regional model simulations, Issues in the Impacts of Climate Variability and Change on Agriculture. Springer, pp. 7-35.

Mei, X.R., Zhong, X.L., Vincent, V. and LIU, X.Y., 2013a. Improving water use efficiency of wheat crop varieties in the North China Plain: Review and Analysis. Journal of Integrative Agriculture, 12(7): 1243-1250.

Mei, X.R., Kang, S.Z., Yu, Q., Huang, Y.F., Zhong, X.L., Gong, D.Z., Huo, Z.L. and Liu, E.K., 2013b. Pathways to synchronously improving crop productivity and field water use efficiency in the North China Plain. Scientia Agricultura Sinica, 46(6): 1149-1157.

Mendelsohn, R., 2010. World Development Report 2010: Development and Climate Change World Bank. Journal of Economic Literature, 48(48): 786-788.

Mo, X., Wu, J., Wang, Q. and Zhou, H., 2016. Variations in water storage in China over recent decades from GRACE observations and GLDAS. Natural Hazards and Earth System Sciences, 16(2): 469-482.

Molden, D.J., Sakthivadivel, R., Perry, C.J. and De Fraiture, C., 1998. Indicators for comparing performance of irrigated agricultural systems, 20. IWMI.

Myers, S.S., Zanobetti, A., Kloog, I., Huybers, P., Leakey, A.D., Bloom, A.J., Carlisle, E., Dietterich, L.H., Fitzgerald, G., Hasegawa, T. and Holbrook, N.M, 2014. Increasing CO2 threatens human nutrition. Nature, 510(7503): 139-142.

O'leary, G.J., Christy, B., Nuttall, J., Huth, N., Cammarano, D., Stöckle, C., Basso, B., Shcherbak, I., Fitzgerald, G., Luo, Q. and Farre‐Codina, I. , 2015. Response of wheat growth, grain yield and water use to elevated CO2 under a free‐air CO2 enrichment (FACE) experiment and modelling in a semi‐arid environment. Global change biology, 21(7): 2670-2686.

Osborne, T.M., Lawrence, D.M., Challinor, A.J., Slingo, J.M. and Wheeler, T.R., 2007. Development and assessment of a coupled crop–climate model. Global Change Biology, 13(1): 169-183.

Panda, R., Behera, S. and Kashyap, P., 2003. Effective management of irrigation water for wheat under stressed conditions. Agricultural water management, 63(1): 37-56.

Parry, M.L., Rosenzweig, C., Iglesias, A., Livermore, M. and Fischer, G., 2004. Effects of climate change on global food production under SRES emissions and socio-economic scenarios. Global Environmental Change, 14(1): 53-67.

Pearce, D.W., Cline, W.R., Achanta, A.N., Fankhauser, S., Pachauri, R.K., Tol, R.S. and Vellinga, P., 1996. The social costs of climate change: greenhouse damage and the benefits of control. Climate change 1995: Economic and social dimensions of climate change: 179-224.

Perry, C., 2011. Accounting for water use: Terminology and implications for saving water and increasing production. Agricultural Water Management, 98(12): 1840-1846.

Perry, C., Steduto, P., Allen, R.G. and Burt, C.M., 2009. Increasing productivity in irrigated agriculture: agronomic constraints and hydrological realities. Agricultural Water Management, 96(11): 1517-1524.

Piao, S., Ciais, P., Huang, Y., Shen, Z., Peng, S., Li, J., Zhou, L., Liu, H., Ma, Y., Ding, Y. and Friedlingstein, P. , 2010. The impacts of climate change on water resources and agriculture in China. Nature, 467(7311): 43-51.

Ramillien, G., Famiglietti, J.S. and Wahr, J., 2008. Detection of continental hydrology and glaciology signals from GRACE: a review. Surveys in Geophysics, 29(4-5): 361-374.

Ren, J., Chen, Z., Zhou, Q. and Tang, H., 2008. Regional yield estimation for winter wheat with MODIS-NDVI data in Shandong, China. International Journal of Applied Earth Observation and Geoinformation, 10(4): 403-413.

Riahi, K., Rao, S., Krey, V., Cho, C., Chirkov, V., Fischer, G., Kindermann, G., Nakicenovic, N. and Rafaj, P. , 2011. RCP 8.5—A scenario of comparatively high greenhouse gas emissions. Climatic Change, 109(1-2): 33-57.

Ritchie, J. and Otter, S., 1985. Description and performance of CERES-Wheat: a user-oriented wheat yield model. ARS-United States Department of Agriculture, Agricultural Research Service (USA).

Ritchie, J.T., Singh, U., Godwin, D.C. and Bowen, W.T., 1998. Cereal growth, development and yield. In: G.Y. Tsuji, G. Hoogenboom and P.K. Thornton (Editors), Understanding Options for Agricultural Production. Springer Netherlands, Dordrecht, pp. 79-98.

Rodell, M., Velicogna, I. and Famiglietti, J.S., 2009. Satellite-based estimates of groundwater depletion in India. Nature, 460(7258): 999-1002.

Roderick, M.L. and Farquhar, G.D., 2004. Changes in Australian pan evaporation from 1970 to 2002. International Journal of Climatology, 24(9): 1077-1090.

Rosenzweig, C., Iglesias, A., Yang, X., Epstein, P.R. and Chivian, E., 2001. Climate change and extreme weather events;

implications for food production, plant diseases, and pests. Global change and human health, 2(2): 90-104.

Rosenzweig, C., Jones, J.W., Hatfield, J.L., Ruane, A.C., Boote, K.J., Thorburn, P., Antle, J.M., Nelson, G.C., Porter, C., Janssen, S. and Asseng, S. , 2013. The agricultural model intercomparison and improvement project (AgMIP): protocols and pilot studies. Agricultural and Forest Meteorology, 170: 166-182.

Rosenzweig, C. and Parry, M.L., 1994. Potential impact of climate change on world food supply. Nature, 367(6459): 133-138.

Rosenzweig, C., Tubiello, F.N., Goldberg, R., Mills, E. and Bloomfield, J., 2002. Increased crop damage in the US from excess precipitation under climate change. Global Environmental Change, 12(3): 197-202.

Rwasoka, D., Gumindoga, W. and Gwenzi, J., 2011. Estimation of actual evapotranspiration using the Surface Energy Balance System (SEBS) algorithm in the Upper Manyame catchment in Zimbabwe. Physics and Chemistry of the Earth, Parts A/B/C, 36(14): 736-746.

Rosengrant, M., Cai, X. and Cline, S.A., 2002. World water and food to 2025. International Food Policy Research Institute, Washington, DC.

Sakthivadivel, R., De Fraiture, C., Molden, D.J., Perry, C. and Kloezen, W., 1999. Indicators of land and water productivity in irrigated agriculture. International Journal of Water Resources Development, 15(1-2): 161-179.

Savage, N., 2013. Modelling: predictive yield. Nature, 501(7468): S10-S11.

Schiermeier, Q., 2011. Extreme measures. Nature, 477(7363): 148.

Semenov, M.A. and Shewry, P.R., 2011. Modelling predicts that heat stress, not drought, will increase vulnerability of wheat in Europe. Scientific Reports, 1.

Sheffield, J., Wood, E.F. and Roderick, M.L., 2012. Little change in global drought over the past 60 years. Nature, 491(7424): 435-438.

Shi, W., Tao, F. and Zhang, Z., 2013. A review on statistical models for identifying climate contributions to crop yields. Journal of Geographical Sciences, 23(3): 567-576.

Solomon, S., Qin, D., Manning, M., Chen, Z., Marquis, M., Averyt, K.B., Tignor, M. and Miller, H. , 2007. Summary for Policymakers. In: Climate Change 2007: The Physical Science Basis. Contribution of Working Group I to the Fourth Assessment Report of the Intergovernmental Panel on Climate Change. 2007(2): 1-21.

Stöckle, C.O., Donatelli, M. and Nelson, R., 2003. CropSyst, a cropping systems simulation model. European journal of agronomy, 18(3): 289-307.

Stanhill, G. and Cohen, S., 2001. Global dimming: a review of the evidence for a widespread and significant reduction in global radiation with discussion of its probable causes and possible agricultural consequences. Agricultural and forest meteorology, 107(4): 255-278.

Steltzer, H. and Post, E., 2009. Seasons and life cycles. Science, 324(5929): 886-887.

Su, X., Singh, V.P., Niu, J. and Hao, L., 2015. Spatiotemporal trends of aridity index in Shiyang River basin of northwest China. Stochastic Environmental Research and Risk Assessment, 29(6): 1571-1582.

Sun, Q., Kröbel, R., Müller, T., Römheld, V., Cui, Z., Zhang, F. and Chen, X., 2011. Optimization of yield and water-use of different cropping systems for sustainable groundwater use in North China Plain. Agricultural Water Management, 98(5): 808-814.

Teixeira, A.d.C., Bastiaanssen, W., Ahmad, M.-u.-D. and Bos, M., 2009. Reviewing SEBAL input parameters for assessing evapotranspiration and water productivity for the Low-Middle Sao Francisco River basin, Brazil: Part A:

Calibration and validation. agricultural and forest meteorology, 149(3): 462-476.

Thomas, A., 2000. Spatial and temporal characteristics of potential evapotranspiration trends over China. International Journal of Climatology, 20(4): 381-396.

Thomas, A., 2008. Agricultural irrigation demand under present and future climate scenarios in China. Global and Planetary Change, 60(3): 306-326.

Thorp, K.R., Hunsaker, D.J., French, A.N., White, J.W., Clarke, T.R. and Pinter Jr, P.J. , 2010. Evaluation of the CSM-CROPSIM-CERES-Wheat model as a tool for crop water management. Transactions of the ASAE (American Society of Agricultural Engineers), 53(1): 87.

Timsina, J., Godwin, D., Humphreys, E., Kukal, S. and Smith, D., 2008. Evaluation of options for increasing yield and water productivity of wheat in Punjab, India using the DSSAT-CSM-CERES-Wheat model. Agricultural Water Management, 95(9): 1099-1110.

Trenberth, K.E., Dai, A., Van Der Schrier, G., Jones, P.D., Barichivich, J., Briffa, K.R. and Sheffield, J., 2014. Global warming and changes in drought. Nature Climate Change, 4(1): 17-22.

Tuong, T., Pablico, P., Yamauchi, M., Confesor, R. and Moody, K., 2000. Increasing water productivity and weed suppression of wet seeded rice: effect of water management and rice genotypes. Experimental Agriculture, 36(01): 71-89.

Vicente-Serrano, S.M., Begueria, S. and Lopez-Moreno, J.I., 2011. Comment on "Characteristics and trends in various forms of the Palmer Drought Severity Index (PDSI) during 1900-2008" by Aiguo Dai. Journal of Geophysical Research-Atmospheres, 116: D19112.

Wang, F., Wang, X. and Ken, S., 2004. Comparison of conventional, flood irrigated, flat planting with furrow irrigated, raised bed planting for winter wheat in China. Field Crops Research, 87(1): 35-42.

Wang, H., Chen, A., Wang, Q. and He, B., 2015a. Drought dynamics and impacts on vegetation in China from 1982 to 2011. Ecological Engineering, 75: 303-307.

Wang, H., Jia, L., Steffen, H., Wu, P., Jiang, L., Hsu, H., Xiang, L., Wang, Z. and Hu, B. , 2013a. Increased water storage in North America and Scandinavia from GRACE gravity data. Nature Geoscience, 6(1): 38-42.

Wang, H., Vicente-serrano, S.M., Tao, F., Zhang, X., Wang, P., Zhang, C., Chen, Y., Zhu, D. and El Kenawy, A., 2016. Monitoring winter wheat drought threat in Northern China using multiple climate-based drought indices and soil moisture during 2000–2013. Agricultural and Forest Meteorology, 228: 1-12.

Wang, J.X., Huang, J.K. and Yan, T.T., 2013b. Impacts of climate change on water and agricultural production in ten large river basins in China. Journal of Integrative Agriculture, 12(7): 1267-1278.

Wang, J., Ma, Y., Menenti, M., Bastiaanssen, W. and Mitsuta, Y., 1995. The scaling-up of processes in the heterogeneous landscape of HEIFE with the aid of satellite remote sensing. Journal of the Meteorological Society of Japan. Ser. II, 73(6): 1235-1244.

Wang, W., Zhu, Y., Xu, R. and Liu, J., 2015b. Drought severity change in China during 1961–2012 indicated by SPI and SPEI. Natural Hazards, 75(3): 2437-2451.

Wang, Y., Jiang, T., Bothe, O. and Fraedrich, K., 2007. Changes of pan evaporation and reference evapotranspiration in the Yangtze River basin. Theoretical and applied climatology, 90(1-2): 13-23.

Wheeler, T. and Von Braun, J., 2013. Climate change impacts on global food security. Science, 341(6145): 508-513.

Wilcox, J. and Makowski, D., 2014. A meta-analysis of the predicted effects of climate change on wheat yields using

simulation studies. Field Crops Research, 156: 180-190.

Wild, M., 2014. Global Dimming and Brightening. Global Environmental Change: 39-47.

Wilhite, D.A., Svoboda, M.D. and Hayes, M.J., 2007. Understanding the complex impacts of drought: A key to enhancing drought mitigation and preparedness. Water Resources Management, 21(5): 763-774.

Williams, J.R., Renard, K.G., Dyke, P.T., 1983. EPIC: A new method for assessing erosion's effect on soil productivity. Journal of Soil and Water Conservation 38:381-383

Xiong, W., Conway, D., Lin, E. and Holman, I., 2009. Potential impacts of climate change and climate variability on China's rice yield and production. Climate Research, 40(1): 23-35.

Xu, K., Yang, D., Yang, H., Li, Z., Qin, Y. and Shen, Y., 2015. Spatio-temporal variation of drought in China during 1961–2012: A climatic perspective. Journal of Hydrology, 526: 253-264.

Yan, N. and Wu, B., 2014. Integrated spatial–temporal analysis of crop water productivity of winter wheat in Hai Basin. Agricultural Water Management, 133: 24-33.

Yang, J. et al., 2015. Water consumption in summer maize and winter wheat cropping system based on SEBAL model in Huang-Huai-Hai Plain, China. Journal of Integrative Agriculture, 14(10): 2065-2076.

Yang, J.Y., Qin, L., Mei, X.R., Yan, C.R., Hui, J.U. and Xu, J.W., 2013a. Spatiotemporal characteristics of reference evapotranspiration and its sensitivity coefficients to climate factors in Huang-Huai-Hai Plain, China. Journal of Integrative Agriculture, 12(12): 2280-2291.

Yang, J.M., Yang, J.Y., Dou, S., Yang, X.M. and Hoogenboom, G., 2013b. Simulating the effect of long-term fertilization on maize yield and soil C/N dynamics in northeastern China using DSSAT and CENTURY-based soil model. Nutrient Cycling in Agroecosystems, 95(3): 287-303.

Yang, Y., Yang, Y., Moiwo, J.P. and Hu, Y., 2010. Estimation of irrigation requirement for sustainable water resources reallocation in North China. Agricultural Water Management, 97(11): 1711-1721.

Yong, B., Ren, L., Hong, Y., Gourley, J.J., Chen, X., Dong, J., Wang, W., Shen, Y. and Hardy, J. , 2013. Spatial–Temporal Changes of Water Resources in a Typical Semiarid Basin of North China over the Past 50 Years and Assessment of Possible Natural and Socioeconomic Causes. Journal of Hydrometeorology, 14(4): 1009-1034.

Yu, M., Li, Q., Hayes, M.J., Svoboda, M.D. and Heim, R.R., 2014a. Are droughts becoming more frequent or severe in China based on the Standardized Precipitation Evapotranspiration Index: 1951-2010? International Journal of Climatology, 34(3): 545-558.

Yu, Q., Li, L., Luo, Q., Eamus, D., Xu, S., Chen, C., Wang, E., Liu, J. and Nielsen, D.C., 2014b. Year patterns of climate impact on wheat yields. International Journal of Climatology, 34(2): 518-528.

Yuan, B., Gou, J.P., Ye, M.Z. and Zhao, J.F., 2012. Variety distribution pattern and climatic potential productivity of spring maize in Northeast China under climate change. Atmospheric Science, 57(14):1252-1262.

Zhai, P. and Zou, X., 2005. Changesoftemperatureandprecipitation andtheireffects on drought in China during 1951-2003. Advances in Climate Chang Research, 1(1): 16-18.

Zhang, H.L., Zhao, X., Yin, X.G., Liu, S.L., Xue, J.F., Wang, M., Pu, C., Lal, R. and Chen, F. , 2015. Challenges and adaptations of farming to climate change in the North China Plain. Climatic Change, 129(1-2): 213-224.

Zhang, H., Wang, X., You, M. and Liu, C., 1999. Water-yield relations and water-use efficiency of winter wheat in the North China Plain. Irrigation Science, 19(1): 37-45.

Zhang, K., Kimball, J.S. and Running, S.W., 2016. A review of remote sensing based actual evapotranspiration estimation.

Wiley Interdisciplinary Reviews: Water, 3(6): 834-853.

Zhang, Y., Yu, Q., Liu, C., Jiang, J. and Zhang, X., 2004. Estimation of winter wheat evapotranspiration under water stress with two semiempirical approaches. Agronomy Journal, 96(1): 159-168.

Zhao, R.F., Chen, X.P., Zhang, F.S., Zhang, H., Schroder, J. and Römheld, V. , 2006. Fertilization and nitrogen balance in a wheat–maize rotation system in North China. Agronomy Journal, 98(4): 938-945.

Zheng, Z., Cai, H., Yu, L. and Hoogenboom, G., 2016. Application of the CSM–CERES–Wheat Model for Yield Prediction and Planting Date Evaluation at Guanzhong Plain in Northwest China. Agronomy Journal.

Chapter Ⅱ. Impact of climate change on ET_0 under a historical period and future climate scenario

Impact of climate change on potential evapotranspiration (ET_0) under a historical period and future climate scenario in the Huang-Huai-Hai Plain, China

Published in Theoretical and Applied Climatology, 14, March 2017

Qin Liu, Changrong Yan, Hui Ju, Sarah Garré*

** Corresponding author*

outline

As one of the important parameters of the hydrologic cycle, potential evapotranspiration (ET_0) plays a key role in understanding the energy balance of terrestrial systems and in estimating crop evapotranspiration, water management, establishing irrigation scheme and other practice of agricultural production. The research presented in this paper had the following objectives: (1) To quantify the characteristics of the meteorological variables and ET_0 on seasonal and annual scales on the 3H Plain under a historical (1961—2014) period and the RCP 8.5 scenario (2) To conduct a sensitivity analysis of ET_0 on seasonal and annual scales; and (3) To identify the primary variables controlling changes in ET_0 changes within the context of climate change.

1. Abstract

Climate change is widely accepted to be one of the most critical problems faced by the Huang-Huai-Hai Plain (3H Plain), which is a region in which there is an over-exploitation of groundwater region and where future warmer and drought conditions might intensify crop water demand. In this study, the spatiotemporal patterns of ET_0 and primary driving meteorological variables were investigated based on a historical period and RCP 8.5 scenario daily data set from 40 weather stations over the 3H Plain using linear regression, spline interpolation method, a partial derivative analysis and multivariate regression. The results indicated a negative trend in all the analysis periods (except spring) of the past 54 years of which only summer and the entire year were statistically significant ($p < 0.01$) with slopes of -1.09 and -1.29 $mm \cdot y^{-1}$ respectively. In contrast, a positive trend was observed in all four seasons and the entire year under the RCP 8.5 scenario, with the biggest increment equal to 1.36 $mm \cdot y^{-1}$ in summer and an annual increment of 3.37 $mm \cdot y^{-1}$. The spatial patterns of the seasonal and annual ET_0 exhibited the lowest values in southeastern regions and the highest values in northeastern parts of Shandong Province, probably because of the combined effects of various meteorological variables over the past 54 years. Relative humidity (RH) together with solar radiation (RS) were detected to be the main climatic factors controlling the reduction of ET_0 in summer, autumn, and the entire year on the 3H Plain. ET_0 in spring was mainly sensitive to changes in RS and RH, whereas ET_0 in winter was most sensitive to changes in wind speed (WS) and decreased due to declining RH. Under the future RCP 8.5 scenario, the annual ET_0 distribution displays a rich spatial structure with a clear northeast-west gradient and an area with low values in the southern regions, which is similarly detected in spring and summer. The most sensitive and primary controlling variables with respect to the increment of future ET_0 are in the first place RS and then mean temperature in spring, while turn to be mean temperature and then RS in summer. In autumn, future ET_0 is most sensitive to RH changes. WS and RH are the controlling variables for ET_0 in winter. Annual future ET_0 is most sensitive to RH changes and accordingly RS is responsible for the predicted increment of the annual ET_0. Better understanding of current and future spatiotemporal patterns of ET_0 and of the regional response of ET_0 to climate change can contribute to the establishment of a policy to realize a more efficient use of water resources and a sustainable agricultural production in the 3H Plain.

Keywords

Potential evapotranspiration; RCP 8.5 scenario; Spatiotemporal trends; Sensitivity analysis; Controlling variable; Huang-Huai-Hai Plain

2. Introduction

Potential evapotranspiration (ET_0) is widely acknowledged as a key hydrological variable representing an important water loss from catchments. It is closely related to groundwater recharge, runoff generation, and soil water movements, some important terms of hydrological processes (Xu and Singh, 2005; Zhang et al., 2011a), and with which it can be used to estimate actual evapotranspiration (ET_a), schedule irrigation and other agricultural management practices (Dyck, 1985; Hobbins et al., 2001; Xu and Li, 2003). Drought conditions is anticipated to be aggravated due to climate change by increasing potential evapotranspiration and augmenting crop water consumption in water-limited regions (Goyal, 2004; Maracchi et al., 2005; Thomas, 2008). It is recognized to be essential for efficient water resources management and water productivity assessment to in depth understand the spatiotemporal pattern of evapotranspiration and accurately estimate its response to climate change (Chen et al., 2007a; Drogue et al., 2004; Han et al., 2014; Yang et al., 2015).

According to the predictions of climate change models, ET_0 is expected to increase over the coming years due to an expected temperature rise (Goyal, 2004; McNulty et al., 1997). However, decreasing trends of ET_0 have been detected in some regions of China (Chen et al., 2006; Thomas, 2000; Wang et al., 2007), Korea (Song et al. 2014), the United States (Irmak et al., 2012), and Australia (Roderick and Farquhar, 2004). Therefore, global atmospheric temperatures rise might not necessarily give rise to ET_0 in all cases. For example, the reduction in solar radiation could compensate for the impact of temperatures on ET_0 which has been depicted in many places (Stanhill and Cohen, 2001; Wild, 2014). Chen et al. (2006) concluded that the reduction of WS was the primary meteorological variable contributing to the observed decline of ET_0 rates on the Tibetan Plateau. While, Gao et al. (2006) and Wang et al. (2007) have identified reductions in WS and RS as the primary contributing factors to decreasing trends of ET_0. Atmospheric temperature is probably thought to be the most widely used marker of climatic change on both regional and global scales. According to the 2013 IPCC report, over the past 100 years (1913–2012), global temperature has risen by 0.91 °C (Stocker et al., 2014) and it is expected to continue rising throughout the 21st century, altering the hydrological cycle by affecting both or one of precipitation and evaporation (Huntington, 2006). The patterns of the spatiotemporal distribution of climatic variables in response to global warming remain a matter of active debate and the numbers of related studies are increasing worldwide (Feddema, 1999; Georgia, 2000; McNulty et al., 1997; Muhs and Maat, 1993). Consequently, analysis of the contribution of the main four climate factors to changes in the estimated ET_0 changes is essential.

A sensitivity analysis is essential to capture the importance of the meteorological variables in the Penman–Monteith formulation, the results from which are of great concern for ascertaining the effects of climate change on ET_0 (Zhang, et al., 2010). Several researches have described the sensitivity of ET_0 to meteorological factors in selected climate scenarios (Rana and Katerji, 1998; Goyal, 2004; Irmak et al., 2006). Furthermore, the most effective variables have been reported to be wind speed (Cohen et al., 2002; Todisco and Vergni, 2008; Wang et al., 2007), solar radiation (Gao et al., 2006; Wang et al., 2007) and relative

humidity (Gong et al., 2006). Song et al (2009) indicated that for entire North China plain annual ET_0 has undergone a statistically pronounced reduction of 11.9 mm decade^{-1} in past 46 years and that reductions of RS and WS have exerted a greater influence on ET_0 than the other variables. Although analyses of the sensitivity of ET_0 to climatic factors have been performed before, a focus on the ranges of variation of the variables in the historic record of the Huang-Huai-Hai Plain (3H Plain) are not necessarily all covered. In addition, few studies have focused on future changes of ET_0 (especially in the 3H plain), which limits the potential of the former studies to provide guidelines for more efficient water resources management. To predict future changes of ET_0, climate scenarios are often used to provide future climatic factors for the estimation of ET_0. A few studies have calculated ET_0 directly using climatic factors from such climate scenarios. In order to obtain information on future climate change with higher spatial and temporal resolutions, most studies have generated future ET_0 through the downscaling General Circulation Models outputs. Li et al (2012) investigated the spatiotemporal variability of ET_0 during 1961–2009 and 2011–2099 under two emission scenarios (A2 and B2) on the Loess Plateau of China. Zhou and Hong (2013) investigated the projected changes of the Palmer Drought Severity Index with ET_0 under the Representative Pathway 8.5 (RCP8.5). This RCP 8.5 scenario can be considered as a worst-case scenario, since it represents future high CO_2-emission rates (increase by about 120 Gt CO2-eq. by 2100 compared to 2000).

The Huang-Huai-Hai Plain (3H Plain) is a major crop-producing area in China that encompasses 18 million hectares of intensively farmed arable land (19% of the country's total crop producing land). Water is thought to be the main factor limiting agricultural production on the 3H Plain, because of its high consumption through crop transpiration and soil evaporation. Furthermore, water limitations will probably be accentuated by continuous food demand, soil quality deterioration and also over-exploitation of groundwater resources (Chen et al., 2003). Moreover, changes in climate have intensified with annual precipitation decreasing at an average rate of 2.92 mm·y^{-1} (Suxia et al., 2010). Thus, the regional aggravation of water scarcity has led to an increased a wareness of the importance of water as an agricultural resource for crop production in the 3H Plain.

Given this context, the research presented in this paper had the following objectives:
(1) An investigation of the characteristics of the meteorological variables and ET_0 on seasonal and annual scales over the 3H Plain under a historical (1961—2014) period and the RCP 8.5 scenario, using linear regression and spline interpolation. (2) The establishment of a sensitivity analysis for ET_0 on seasonal and annual scales using the partial derivative method. (3) To identify the primary variables controlling changes in ET_0 within the context of climate change.

3. Materials and methods

Study area

The 3H Plain (31°14′–40°25′N, 112°33′–120°17′E) is known as the largest agricultural production

region in China. The climate is temperate, sub-humid, and continental monsoon, with average annual precipitation of 348.5 mm (Ren et al., 2008). Annual precipitation is concentrated in summer (July through September) and winter is strongly characterized by a lack of water for agricultural production. Water shortages on the 3H Plain have become of considerable concern over recent decades (Brown and Rosenberg, 1997). The plain encompasses around 18 million hectares of farmland of which about 61% and 31% are dedicated to wheat and maize production, respectively (Jin et al., 2009). The main cropping system is well known as the rotation of wheat and maize with the systematic application of irrigation water and fertilizer on the 3H Plain (Liang et al., 2011; Sun et al., 2011; Zhao et al., 2006).

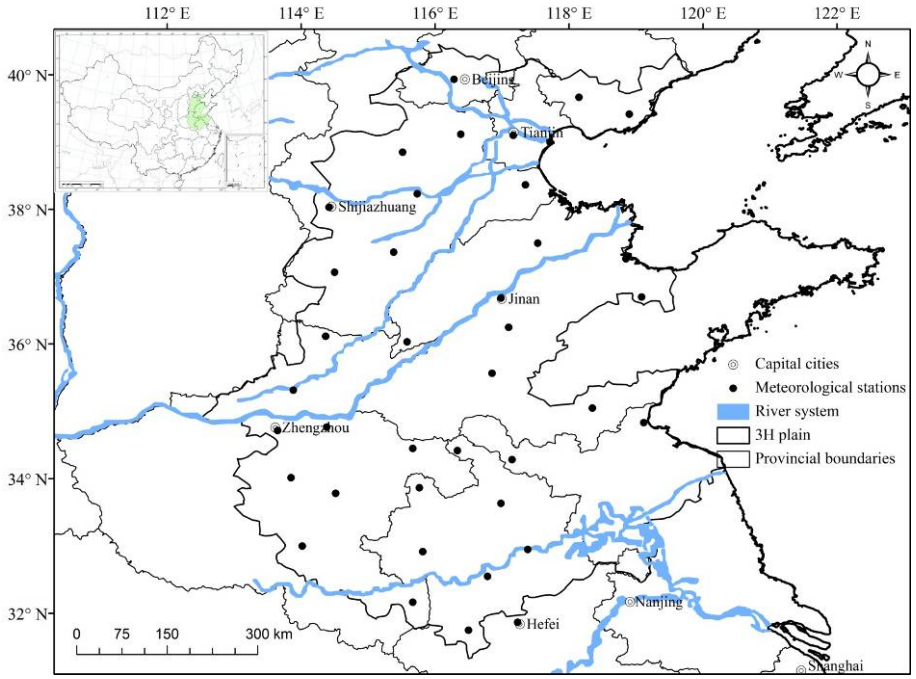

Figure 10 Location of meteorological stations on Huang-Huai-Hai Plain, China. The map on the top left corner describes the location of Huang-Huai-Hai Plain in China. The upper blue line is Hai River and the middle, below blue one is Yellow and Huai River, respectively. The round spot means the capital cities.

Meteorological data

A historical dataset from 1961 to 2014, composed of data from 40 meteorological stations, was provided by the China Meteorological Administrationto (Figure 10). Daily maximum (T_{max}, °C) and minimum temperature (T_{min}, °C), average relative humidity (RH, %), wind speed (WS, $m \cdot s^{-1}$) observed at 10-m height, and daily sunshine duration (SD, h) data were available. The 0.5° × 0.5° gridded data of the 3H Plain from 2015 to 2099 simulated under the future RCP 8.5 climatic scenario and obtained from the National Climate Center, included daily average temperature (T_a, °C), daily highest (T_{max}, °C) and lowest temperature (T_{min}, °C), daily precipitation (P, mm), daily average wind speed (WS, $m \cdot s^{-1}$), daily average relative humidity (RH, %), and daily net radiation (RS, $MJ \cdot m^{-2} \cdot d^{-1}$). The RCP8.5 scenario is

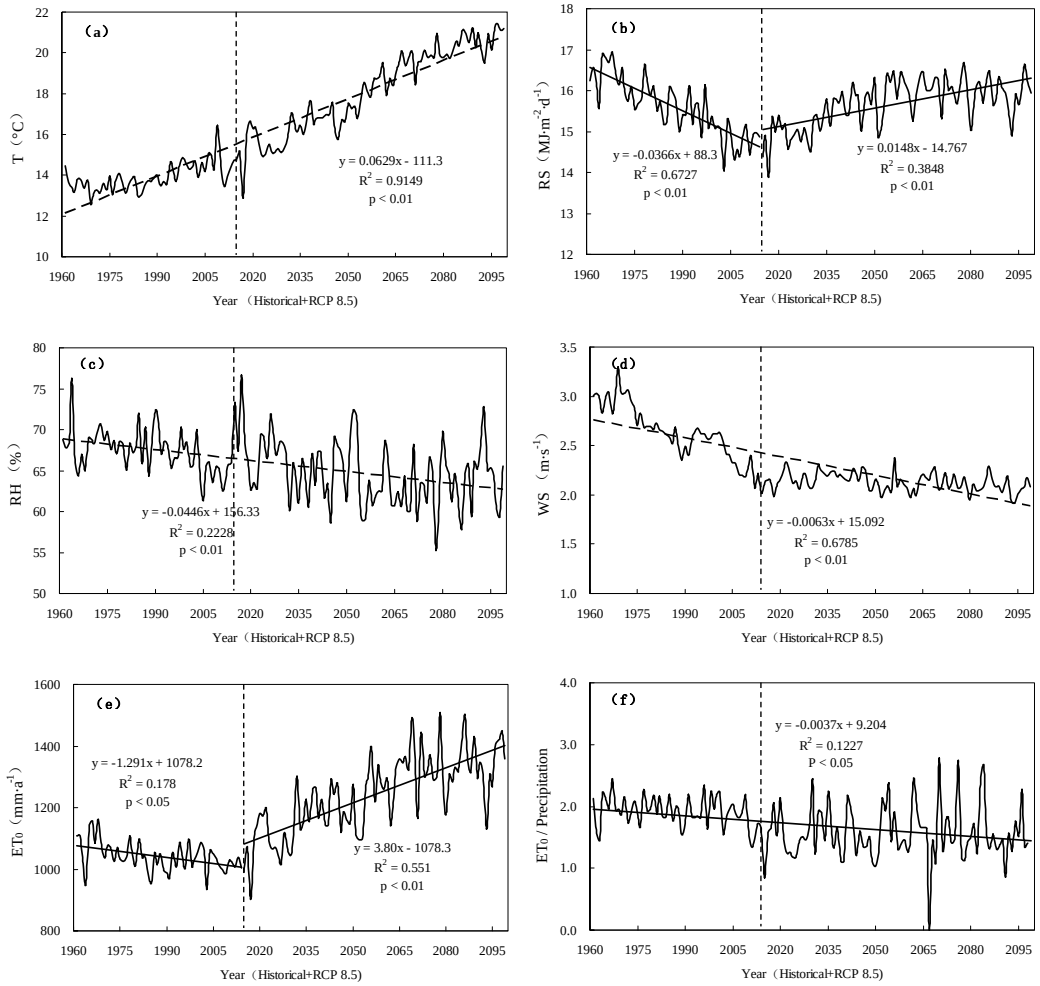

Figure 11 Annual (a) daily mean surface air temperature (Ta), (b) daily net radiation (RS), (c)daily average relative humidity (RH), (d) daily average wind speed (WS), (e) potential evapotranspiration (ET_0) and (f) ET_0/ precipitation in the historical period and under RCP 8.5 scenario. The data was obtained from area-averaged values of meteorological variables, ET_0 and ET_0 divided precipitation from 40 stations in past 54 years and future 85 years.

characterized by high concentration of greenhouse gas with stabilizing emissions post-2099 (increase by about 120 Gt CO2-eq. by 2100 compared to 2000) (Riahi et al., 2011). We used a bilinear interpolation method to interpolate the RCP 8.5 gridded data to the historical stations, and the results was then validate by the observational data during 2005—2014 (Yuan et al., 2012). The annual daily air temperature, net radiation, average relative humidity, and wind speed of the historical period and RCP 8.5 scenario are plotted in Figure 11. A remarkable positive trend with a slope of 0.63 °C decade^{-1} can be seen for T_a, whereas WS and RH have significant negative trends with slopes of -0.06 m·s^{-1}·decade^{-1} and -0.45 percent·decade^{-1}, respectively. For RS, a slope of -0.37MJ·m^{-2}·d^{-1}·decade^{-1} is observed based on the recorded dataset in the historical period, whereas a significant positive trend with a slope of 0.15 MJ·m^{-2}·d^{-1}·decade^{-1} can be seen based on predicted dataset under the RCP 8.5 scenario.

Estimation of potential evapotranspiration

The Penman–Monteith formula recommended by the Food and Agriculture Organization (FAO) of the United Nations was used to calculate the ET_0 for both the historical and future conditions:

$$ET_0 = \frac{0.408\Delta(R_n - G) + \gamma \frac{900}{T+273} U_2 (e_s - e_a)}{\Delta + \gamma(1 + 0.34U_2)} \quad \text{Formula 12}$$

Where ET_0 is in $mm \cdot d^{-1}$; $\triangle$ represents the saturation vapor pressure/temperature curve (kPa $°C^{-1}$); R_n is the net radiation from the canopy ($MJ \cdot m^{-2} \cdot d^{-1}$); G is the soil heat flux ($MJ \cdot m^{-2} \cdot d^{-1}$); T_a is the average daily temperature; U_2 is the wind velocity (ms^{-1}); e_s is the saturation vapor pressure (kPa); e_a is the actual water vapor pressure (kPa); e_s–e_a is the vapor pressure deficit (kPa); γ is the psychometric constant (kPa $°C^{-1}$). Allen et al (1998) explains how to obtain the different parameters and variables from meteorological data.

Time series analysis to quantify major trends

Both parametric and non-parametric methods have been widely used to identify trends in climatic variables. However, recent studies suggest that non-parametric tests are more suitable for non-normally distributed and censored data, which are frequently encountered in meteorological and hydrological time series. Among them, the non-parametric Mann-Kendall test (Kendall, 1975; Mann, 1945) is widely accepted to be one popular method for trend analysis in hydrological and meteorological series (Dinpashoh et al., 2011; Jhajharia et al., 2012; Kousari and Ahani, 2012; Zheng and Wang, 2014) with little influence by the presence of outliers in the data. In addition, it is highly recommended for general use by the World Meteorological Organization (Zhang et al., 2011b). Therefore, we used the Mann-Kennall test for the trend analysis of our data. Furthermore, the magnitude of the trends in the time series was estimated using the non-parametric Theil–Sen's slope (Sen, 1968; Theil, 1992), which is robust because it is resistant to the effect of outlier values in the observations (Jhajharia et al., 2015; Su et al., 2015; Xu et al., 2003; Yue et al., 2002). We refer to Jhajharia et al (2015), Su et al (2015) and Kumar et al (2009) for further details on how to apply these methods. The confidence level used in this study is 95%. In our study, we applied two Mann-kennal tests recommended in the literature (Kumar et al., 2009; Nalley et al., 2012; Zamani et al., 2016): (i) a MK test considering all the significant autocorrelation structure (MK3) and (ii) a MK test considering long-term persistence (LTP) and Hurst coefficient (MK4). The two modified Mann-Kendall test and Theil–Sen's slope estimator involved in this study were performed using R software version 3.2.4 (Team, 2011).

Sensitivity analysis and multivariate regression

McKenney and Rosenberg (1993) and Goyal (2004) have carried out sensitivity analysis for ET_0 where the relative changes of input meteorological factors were plotted against variations of output ET_0 as

sensitivity curves. Irmak et al. (2006) then reduced the sensitivity coefficients on a daily step by dividing the amount of increase/decrease in ET_0 by the increase/decrease of each meteorological factors. However, Zhang et al. (2010) highlighted that such a sensitivity coefficient is susceptible to the effects of variations in the magnitudes of ET_0 and the meteorological factors. To obtain a non-dimensional sensitivity coefficient, it can be normalized as

$$SC = \frac{\partial ET_0}{\partial V} = \frac{\Delta ET_0 / ET_0}{\Delta CV / CV} \qquad \text{Formula 13}$$

Where SC is the dimensionless sensitivity coefficient, and ET_0 and CV (air temperature, relative humidity, solar radiation and wind speed) are base values before the change.

To investigate the major controlling variables of ET_0 trends, multivariate regression is conducted over the 3H Plain, which could be treated as the controlling climate factors in the change and variation of ET_0 (Chun et al., 2012; Ma et al., 2012).

4. Results

Historical and future trends of meteorological variables

Seasonal trends of Ta, RS, RH and WS during the historical dataset of 1961–2014 and the RCP 8.5 scenario of 2015–2099 are presented in Table 3. The Mann-Kendall test of Ta is characterized by an increasing trend under both the historical period and the RCP 8.5 scenario. The trend of increase in Ta is 0.38 and 0.36 °C decade^{-1} for spring and winter, respectively, over the past 54 years. Similarly, in autumn, a significantly increasing trend of 0.25 °C decade^{-1} is detected. The increase in T_a is higher in the cooler seasons than in the warmer seasons. Furthermore, Ta increases by 0.65 and 0.84 °C decade^{-1} for spring and winter, respectively, under the future RCP 8.5 condition. Similarly, in summer and autumn, a significantly increasing trend of 0.76 and 0.77 °C decade^{-1} is also detected. Accordingly, the increase in Ta is higher under the RCP 8.5 scenario than for the historical 54 years.

For RS in the past 54 years, a significant negative trend is detected in all seasons and during the entire year, i.e., 136.3 MJ·m^{-2} decade^{-1}, whereas under the RCP 8.5 scenario, an increasing trend is observed in all analysis seasons, only one (winter) of which is not statistically significant. It is noted that RH has a significant decrease trend over the past 54 years. In spring and winter, RH reduces by -1.12 and -0.46% decade^{-1}, respectively. Similarly, it reduces by -0.47 and -1.11% decade^{-1} in summer and autumn, respectively. Under the RCP 8.5 scenario, a negative trend can be observed in all analysis seasons, only one (summer) of which is statistically significant. In all seasons, WS shows a negative trend and the amplitude of reduction can be observed to be slightly bigger over the past 54 years than under the RCP 8.5 scenario. In general, for annual RH and WS, significant declining trends of -0.77% decade^{-1} and -0.17 m·s^{-1} decade^{-1}can be found over the historical 54 year, which are slightly stronger than under the RCP 8.5 scenario. The seasonal-scale changes of

Ta over the historical 54 years and under the RCP scenario show significant increasing trends of 0.28 and 0.75 °C decade^{-1}, respectively.

Table 3 Trend analysis of meteorological variables with Mann-Kendall test and Theil–Sen's slope estimator under the historical period and RCP 8.5 scenarios**.** The values described in table were obtained from area-averaged values of meteorological variables from 40 meteorological stations using Theil–Sen's slope estimator in past 54 years and future 85 years. In this and in subsequent tables of this chapter, the positive values mean upward trends and negative values mean downward trends. No star means the significance level exceeds 0.05; * indicates a significance level of 0.05, and ** indicates a significance level of 0.01.

	Ta (°C)	RS (MJ·m^{-2})	RH (%)	WS (m/s)
Historical				
Spring	0.41*	-23.3**	-1.28*	-0.19**
Summer	0.07*	-65.7**	-0.49*	-0.12**
Autumn	0.23**	-28.9**	-1.02**	-0.16**
Winter	0.39**	-23.9*	-0.60	-0.20**
Entire year	0.28**	-139.3**	-0.73**	-0.17**
RCP 8.5				
Spring	0.64**	12.6**	-0.09	-0.021**
Summer	0.76**	21.7**	-0.81**	-0.014*
Autumn	0.77**	16.9**	-0.47	-0.022**
Winter	0.80**	1.58	-0.12	-0.012**
Entire year	0.77**	53.1**	-0.38*	-0.018**

Spatial and temporal characteristics of ET_0

Table 4 Trend analysis of ET_0 with Mann-Kendall test and Theil–Sen's slope estimator slope estimator under the historical period and RCP 8.5 scenarios. The unit of the slopes are mm·y^{-1}. The values described in table were obtained from area-averaged ET_0 from 40 meteorological stations using Theil–Sen's slope estimator in past 54 years and future 85 years.

	Spring		Summer		Autumn		Winter		Entire year	
	Value (mm)	slope	Value (mm)	slope	Value (mm)	slope	Value (mm)	slope	Value (mm)	slope
Historical	322.5	0.08	410.4	-1.08*	206.4	-0.21	102.8	-0.11	1042.4	-1.20**
RCP 8.5	388.5	0.82**	473.4	1.35**	255.1	0.85**	113.3	0.35**	1230.3	3.45**

The investigation of the trends of ET_0 and their persistence using modified Mann-Kendall test and Theil–Sen's slope estimator under the historical period and RCP 8.5 scenario gives a better insight in the

expected seasonal differences of water demand and the evolution of these demands in the future. As shown in Table 4, average ET_0 is highest in summer, accounting for 39.4% and 38.5% of the annual ET_0 under the historical period and RCP 8.5 scenario, respectively, followed in descending order by spring, autumn, and winter. Over the past 54 years, a negative trend occurs in all analysis periods (except spring), of which only summer and the entire year are statistically significant with slopes of -1.09 and -1.30 mm y^{-1}. In contrast, a positive trend can be observed in all four seasons and the entire year under the RCP 8.5 scenario; the biggest seasonal increment is 1.35 mm y^{-1} in summer and the annual increment is 3.45 mm y^{-1}. On average, the prediction of ET_0 (RCP 8.5 scenario) is larger than what was observed during the past 54 years: 1042.4mm for the historical data set and 1230.3mm for the RCP8.5 scenarios.

Seasonal and annual spatial variability of ET_0 can be observed under the historical period and RCP 8.2 scenario. In the historical dataset of 1961-2014 for the 3H Plain, the regional difference range from 652.1 to 1182.0 mm/year. The coefficient of variation for the average annual ET_0 of the 40 stations is 0.10, which signifies rather low spatial variation. Figure 12 shows the spatial pattern for the ET_0 in four seasons and the entire year on the 3H Plain for 1961–2014. The lowest ET_0 values (<950mm) are found in a small region of the southeast. The annual Ta and RH decrease from the southeast to the northwest, whereas the annual WS and RS increase from the southeast to the northwest (Liu et al., 2013a; Yang et al., 2011). Low values of Ta, WS, and RS and high values of RH are the primary cause of lowest ET_0 values in the southeastern region. The highest ET_0 values (>1000 mm) are found in the northeast region of Shandong Province and south region of Hebei Province, which can mainly be attributed to the low RH, high WS and strong RS. The ET_0 characteristics of the four seasons (except summer), follow the spatial pattern of ET_0 for the entire year. In summer, the spatial distribution turns to a different pattern in which the highest values are observed in the northeast of Shandong Province and the south part of 3H Plain.

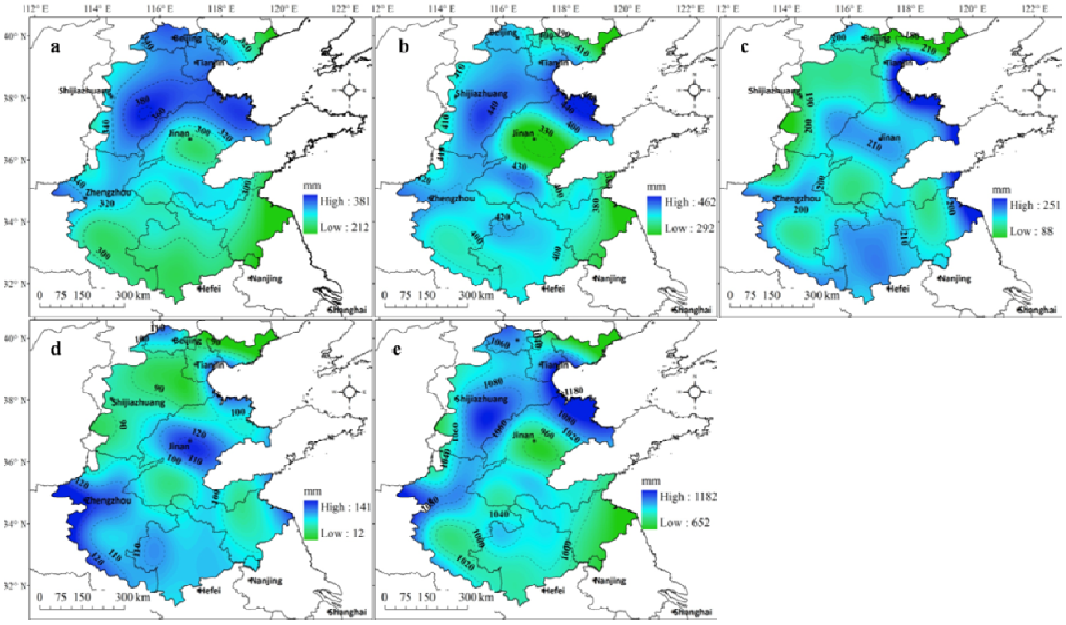

Figure 12 Spatial patterns of ET_0 for historical 54 years: (a) spring, (b) summer, (c) autumn, (d) winter and (e) the entire year. These maps were obtained using the Spline method for interpolation with Geostatistical Analysis

modual in the software ArcGIS.

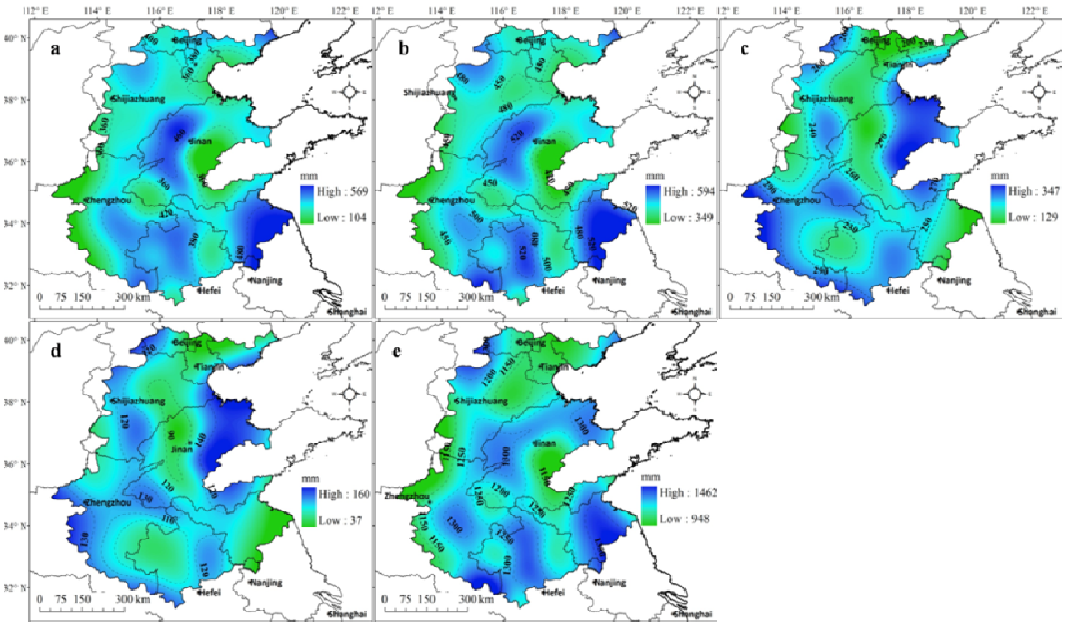

Figure 13 Spatial patterns of ET_0 under the RCP 8.5 scenario: (a) spring, (b) summer, (c) autumn, (d) winter and (e) the entire year. These maps were obtained using the Spline method for interpolation with Geostatistical Analysis modual in the software ArcGIS.

Figure 13 shows the projected (RCP8.5) spatial patterns of seasonal and annual ET_0 for the 3H Plain. The distribution of the annual averages has a heterogeneous spatial structure with a northeast-west gradient of relatively low ET_0 areas and high areas in southern region, similar patterns are found in spring and summer. A spatial comparison of RCP 8.5 predicted average ET_0 values with respect to the historical ET_0 averages reveals where the changes are expected to be largest in the 3H Plain. We observed the largest increase with respect to the past in the southwest with a change in magnitude of 25%—32%, whereas the smallest increase was located in the northeast (3%—10%). As for autumn and winter, marked areas of low values are visible in the projected pattern of ET_0 from the north to central parts of the region, whereas higher values can be found in eastern and southwestern regions.

The results from the investigation of ET_0 trends at annual time scale for the historical 54 years and the RCP 8.5 scenario are shown in Figure 14 in order to compare the results of each station according to its location in the 3H Plain. We also compared the two versions of MK test (MK3/MK4). Nearly 12.5 and 32.5 % of the stations witnessed significant decreasing trends at the 1 % level of significance using MK3 and MK4 tests, respectively, while these percentages changed to 50 and 55 % for historical 54 years. Additionally, for the RCP 8.5 scenario the percentage of significant increasing trends was 100% for both MK3 and MK4 tests. Comparing the results of the two versions of the Mann–Kendall test, the Z-statistic values of MK3 test were found to be slightly higher than those obtained from the MK4 test, indicating that the consideration of Hurst coefficient has led to a decrease in the level of significance, in accordance with the findings in streamflow

and precipitation for MK3 and MK4 tests in Iran (Zamani et al., 2016). As already mentioned, the historical data set mainly displays annual decreasing trends, whereas the RCP8.5 scenario results in increasing trends in general. As for spatial variability in ET_0 trends for the different stations, a consistent significant increase is visible all over the plain and stations with relative bigger increment were mainly located in southwest. Some stations in the North of 3H Plain also show larger increasing trends.

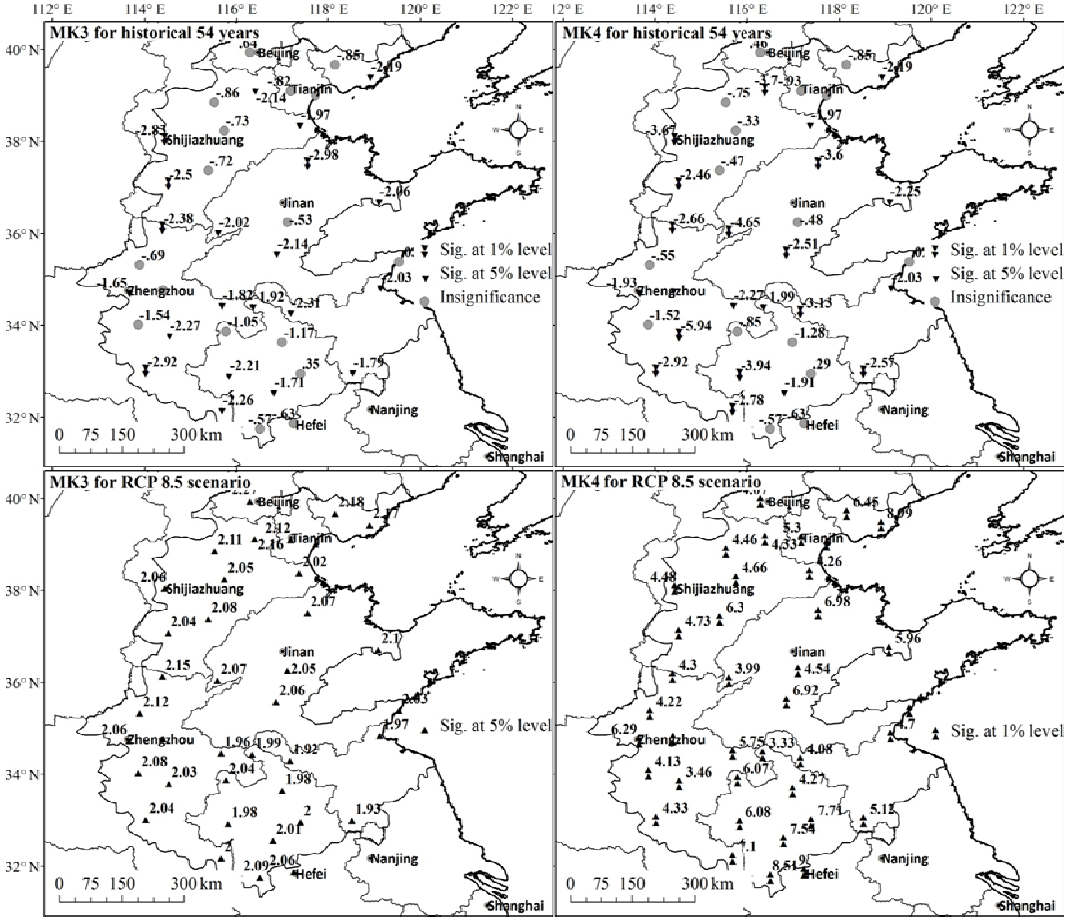

Figure 14 Z-statistic values of annual ET_0 and spatial pattern of ET_0 trends for the entire year using MK test considering all the significant autocorrelation structure (MK3) and MK test considering long-term persistence and Hurst coefficient (MK4) for historical 54 years and RCP 8.5 scenario These maps were obtained with the software ArcGIS with down arrows for descending trend and upward arrows for ascending trend.

Temporal variation of sensitivity coefficients

Table 5 lists annual and seasonal trends of sensitivity coefficients for ET_0 under historical period and RCP 8.5 scenario. They show that the most effective meteorological factor impacting ET_0 varied with season and scenario. For the historical period, ET_0 is most influenced by solar radiation (positive relationship) and relative humidity (negative relationship). Only during winter, wind speed becomes the most influencial factor. On a yearly basis, S_{RS} equals 0.4 and S_{RH} equals -0.93. The trend over time of the influence of T and RS

on ET_0 is negative (negative slope of their sensitivity coefficients over time), whereas RH and WS are of increasing importance (positive slope of their sensitivity coefficients over time). Looking at the results of the RCP8.5 scenario, we get a different view. Solar radiation is still the variable having a postive impact on potential evapotranspiration and this relationship becomes more important as we go through the future scenario. Looking at yearly averages, relative humidity has the highest absolute value of sensitivity coefficient and a negative relationship with respect to ET_0; whereas solar radiation is the most important factor positively influencing ET_0. The trends of the sensitivity coefficients of RS, RH and WS are all positive, only the influence of temperature seems to decrease with time in the future scenario.

Table 5 Trend analysis of sensitivity coefficients for ET_0 with Mann-Kendall test and Theil–Sen's slope estimator under the historical period and RCP 8.5 scenario. The unit of slopes is y^{-1}. The values described in table were obtained from area-averaged values of sensitivity coefficients for ET_0 from 40 meteorological stations using Theil–Sen's slope estimator in past 54 years and future 85 years.

	S_T		S_{Rs}		S_{RH}		S_{Ws}	
	value	slope	value	slope	value	slope	value	slope
Historical								
Spring	-0.22	-0.016**	0.45	0.000	-0.44	0.050**	0.14	0.010**
Summer	-0.62	-0.012**	0.66	-0.005**	-0.69	0.001	0.07	0.007**
Autumn	-0.27	-0.012**	0.37	-0.005**	-0.53	0.033*	0.18	0.009**
Winter	0.08	-0.013	0.12	-0.003*	-0.03	0.002**	0.27	0.007*
Entire year	-0.26	-0.014**	0.40	-0.003**	-0.93	0.006*	0.17	0.008**
RCP 8.5								
Spring	-0.36	-0.026**	0.45	0.004**	-0.44	0.042**	0.18	0.003*
Summer	-0.90	-0.048**	0.58	0.004*	-0.07	0.007**	0.18	0.005**
Autumn	-0.43	-0.033**	0.36	0.007**	-0.62	0.071**	0.23	0.003
Winter	-0.03	-0.016**	0.16	0.001	-0.04	0.006**	0.22	0.008**
Entire year	-0.43	-0.031**	0.39	0.004**	-0.65	0.002**	0.20	0.005**

As described in Table 5, the most effective meteorological factor impacting ET_0 varied with season and scenario. For the historical period, the ET_0 in spring is most sensitive to RS and in winter to WS, with sensitivity coefficients of RS (S_{RS}=0.45) and WS (S_{WS}=0.27). Trends of S_{RS} are negative in the time series analysis, indicating that the negative influence on ET_0 became weaker in the past 54 years, in combination with the positive value of S_{RS}. However, the positive influence on ET_0 strengthened in combination with the positive value of S_{WS}. The ET_0 in summer, autumn, and the entire year shows greatest sensitivity to RH, i.e., the sensitivity coefficients of RH (S_{RH}) in summer, autumn, and entire year (-0.69, -0.53, and -0.93, respectively) are larger than for the other variables. Trends of S_{RH} are positive in the time series analysis, indicating that the negative influence on ET_0 became smaller in the past 54 years, in combination with the negative value of S_{RH}.

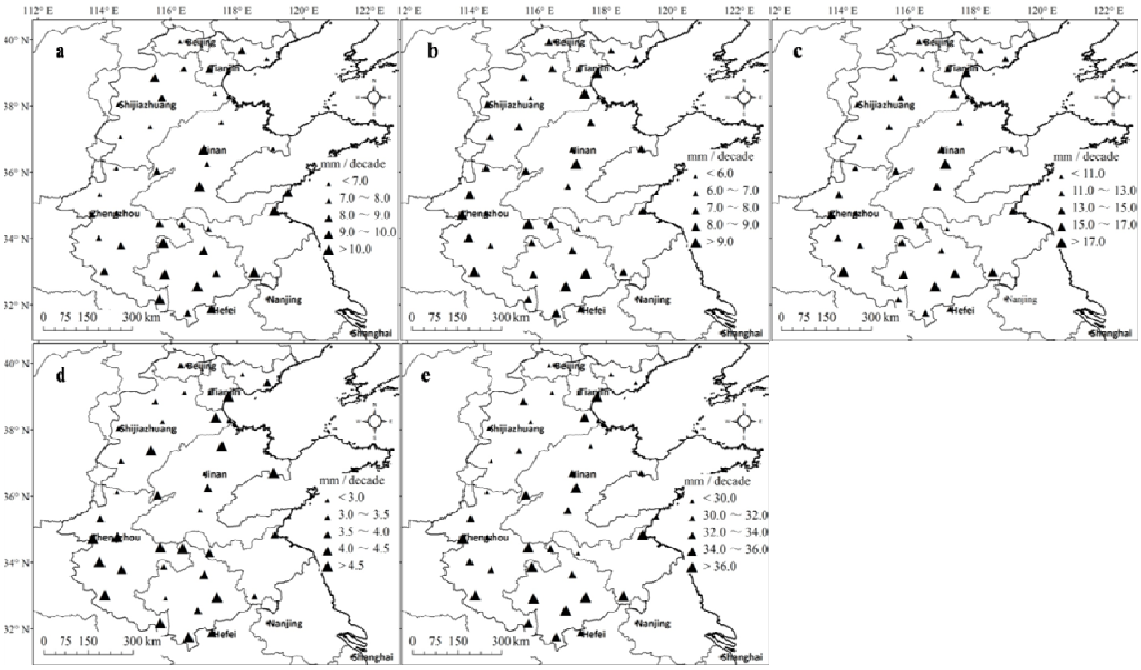

Figure 15 Spatial patterns of ET_0 trends under the RCP 8.5 scenario: (a) spring, (b) summer, (c) autumn, (d) winter, and (e) the entire year. These maps were obtained with the software ArcGIS with upward arrows for ascending trend.

Similar to the historical condition, the ET_0 in spring and winter under the RCP 8.5 scenario shows greatest sensitivity to RS (S_{RS}=0.45) and WS (S_{WS}=0.22). Trends of S_{RS} and S_{WS} are positive in the time series analysis, indicating that the positive influence on ET_0 strengthens in the future 74 years, in combination with their positive values. The ET_0 in autumn and the entire year shows greater sensitivity to RH (S_{RH}=-0.62 and -0.65, respectively) than to the other variables. Trends of S_{RH} in the time series analysis indicate that the negative influence on ET_0 become weaker. An average temperature is detected to be the most sensitive factor to ET_0 in summer (S_T=-0.90) and its negative influence on ET_0 strengthens in the future 74 years. Figure 15 shows the spatial patterns of these ET_0 trends under the RCP 8.5 scenario

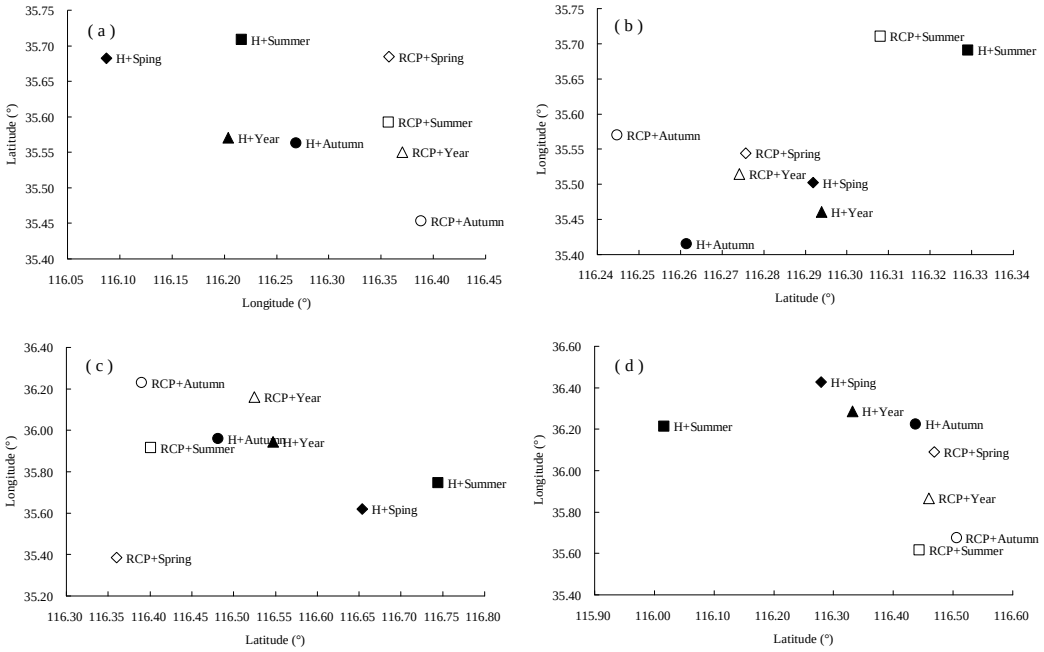

Figure 16 Sensitivity centrals of ET_0 to (a) air temperature, (b) net radiation, (c) relative humidity and (d) wind speed under the historical period and RCP 8.5 scenario. The coordinates of sensitivity centrals for ET_0 to meteorological variables were estimated using barycentric fitting method from 40 stations under the historical period and RCP 8.5 scenario. The barycentric fitting method comes from literatures reported by Xu et al.(2004), He et al (2004) and Liu et al.(2012).

In this study, sensitivity centrals of ET_0 were calculated using a gravity center analysis method, based on the data-set of sensitivity coefficients for the 40 stations under the historical and future conditions, in order to investigate better the characteristics and spatial differentiation of the sensitivity coefficients for ET_0 (Gaile, 1984). Figure 16 shows that the centrals of S_T, S_{RS}, S_{WS} and S_{RH} in the analysis seasons (except winter)for the historical 54 years are all found in Shandong Province corresponding to the winter wheat and summer maize growing seasons (Yang et al., 2013). In comparison with the historical 54 years, the centrals of S_T and S_{WS} move eastward under the RCP 8.5 scenario, whereas the centrals of S_{RS} and S_{RH} move northwestward.

ET_0 in regional response to climate change

The sensitivity of ET_0 to changes in meteorological factors was identified through sensitivity analysis during the four seasons and the entire year under the historical and future conditions; however, because of the variation and interaction of effect of the climatic variables, the factor controlling ET_0 remains difficult to pin down. Therefore, we used a second tool to get a more complete answer to this question: a multivariate regression model. The tendencies and magnitudes of the climate variables and the relationships between ET_0 and the key climatic variables in four seasons and entire year are presented in Table 6. The historical data set displays a decline of RH primarily controlling a negative trend in ET_0 in spring and over the entire year. The decline of RS primarily controls a negative trend in ET_0 in summer, autumn, and winter. Different

from the historical condition, average Ta becomes the primary controlling factor for the increment of ET_0 in spring under the RCP 8.5 scenario. As for summer and the entire year, the increase of RS is responsible for the increment of ET_0, while the primary controlling variable turned to be RH on ET_0 in autumn and in winter.

Table 6 Response of ET_0 to climate change under the historical period and RCP 8.5 scenario. The values described in table were obtained through multivariate regression analysis between ET_0 and meteorological variables (air temperature, solar radiation, relative humidity and wind speed) in past 54 years and future 85 years over the Huang-Huai-Hai Plain.

	T_a	RS	RH	WS
Historical				
Spring	0.34**	0.42**	0.77**	0.26**
Summer	0.45**	0.68**	0.52**	0.16**
Autumn	0.48**	0.63**	0.25**	0.10*
Winter	0.39**	0.94**	0.03	-0.05
Entire year	0.32**	0.56**	0.64**	0.23**
RCP 8.5				
Spring	0.52**	0.42**	-0.37**	-0.24**
Summer	0.48**	0.50**	-0.35**	-0.29**
Autumn	0.59**	0.30**	-0.71**	-0.28**
Winter	0.25**	0.47**	-0.84**	-0.21**
Entire year	0.55**	0.58**	-0.39**	-0.48**

5. Discussions

Spatio-temporal evolution of ET_0

Under the effects of climate change, declining trends in ET_0 have been detected in various regions of the world (Jhajharia et al., 2012; Roderick and Farquhar, 2004; Thomas, 2000). Mcvicar et al. (2012) reported a global declining rate of evaporative demand of 1.31mm y^{-1} by reviewing papers reporting trends in estimated ET_0 (n = 26), whereas Thomas (2000) come to a declining rate of 2.3 mm y^{-1} over China on basis of a time series from 1954 to 1993). In our study, the annual ET_0 averaged over the entire 3H Plain revealed a general and significant decreasing trend of -1.29 mm y^{-1}, which was higher than that of the Yellow River Basin ((Liu et al., 2014; Ma et al., 2012), the Yangtze River catchment (Gong et al., 2006; Xu et al., 2006), and Haihe River Basin (Bo et al., 2011b; Wang et al., 2010). These differences in declining magnitude were mainly due to higher decrement of RH over the entire 3H Plain (as the governing climatic variable for ET_0). However, Fan et al (2016) found that the annual ET_0 at 37.5% of stations exhibited positive trends. These stations are mainly located in the mountain plateau zone in China, which behaves similarly to the increasing ET_0 trends in northeastern China (Liang et al., 2010) and the Shiyang River basin of northwest China (Su et al., 2015). The

reason for this is climate warming, which turns out to be the most significant factor for increase in annual ET_0 in these places. The declining magnitude annual ET_0 over the 3H Plain was witnessed to be far lower than that of India (Jhajharia et al., 2015) and Iran (Dinpashoh et al., 2011) due to the dominant larger reduction of RH. This increment of ET_0 during spring is bad news for the wheat production in the region, since precipitation is also scarce during that period and water resources are already over-exploited. Whereas ET_0 was slightly decreasing in the historical data set, RCP 8.5 scenario predicts an increase of ET_0 in the following 74 years. Similar predictions are done for the Loess Plateau under A2 and B2 scenarios (Li et al., 2012). If this RCP scenario comes close to reality, the already elevated water demand will continue to increase, which poses serious questions to the sustainability of the current cropping practices in the 3H Plain. Accordingly, results have to be combined with information on the spatiotemporal distribution and trends of precipitation in order to highlight periods in which the water requirement of the agricultural crops cannot be met and quantify whether the groundwater resources are being used in an unsustainable way (Xu and Xu, 2012). It must also be noted that potential evapotranspiration is only a crude proxy for potential crop evapotranspiration, since it does not take into account the specific water strategy of the crops, nor their growing curve. Furthermore, change in drought condition is a consequence of climate change and aridity is usually expressed as a generalized function of precipitation, temperature, and/ or ET_0 reflecting the degree of meteorological drought. Over last decades, the aridity index (which is defined as the ratio of ET_0 to precipitation) is expected to have different trends in different regions (Liu et al., 2013b; Su et al., 2015; Wu et al., 2006). In our study, as depicted in Figure 11(f) a declining trend in aridity was witnessed under the historical period and RCP 8.5 scenario over the entire 3H Plain, which meant that the region started wetting and is thereby in accordance with the findings in North Iran (Ahani et al., 2013) and northwest China (Huo et al., 2013; Liu et al., 2013b).

Impact of meteorological variables on ET_0

Even though the variability across the plain is not very large, some areas do stand out with a more important increase of ET_0. If this is not compensated by an increase in rainfall or other management practices, it could pose problems to the water allocation. Overall, if we regard the entire year, but also summer and autumn, ET_0 is most influenced by relative humidity as also observed in the Wei River basin (Zuo et al., 2012) and the Yangtze River basin in China (Gong et al., 2006), followed by solar radiation and mean temperature. Goyal (2004) concluded that the temperature increase contributed most to the increasing trend of ET_0 over an arid zone of Rajasthan in India. Yu et al. (2002) witnessed that the increase in ET_0 was due to changes in temperature and RH in paddy fields in southern Taiwan of China. Hess (1998) also reported that increasing wind speed were responsible for the increasing trends in ET_0 in East Nigeria. Whilst, decrease in wind speed, which was termed ‘stilling’ by Roderick et al. (2007) and Mcvicar et al. (2012) was identified to govern the reduction in ET_0 in Australia (Roderick et al., 2007), the Tibetan Plateau (Chen et al., 2006) and the south of Canada (Burn and Hesch, 2007). These findings are inconsistent with our results that declining annual ET_0 was primarily governed by relative humidity in 3H Plain. Indeed the PM equation

dictates that the higher the RH, the lower should be the ET_0. Nevertheless, our time series analysis indicated that the negative influence on ET_0 became weaker with time, and this is in agreement with in Haihe River basin and Huaihe River drainage system (Liu et al., 2012). Furthermore, the decline of relative humidity primarily controlled a negative trend in ET_0 in spring and entire year. In contrast, ET_0 during spring and winter was most sensitive to changes in RS and WS, as also reported by Bo et al (2011a) and Todisco and Vergni (2008) respectively. The decline of RS, also called global dimming, resulted in a declining trend of ET_0 in the 3H Plain, as depicted for many places (Stanhill and Cohen, 2001; Wild, 2014; Yang et al., 2014). A negative trend in ET_0 is controlled by the declining of RS in summer, autumn, and winter, as similarly found in study of Yellow River Basin (Liu et al., 2014). When going from historical data to future conditions according to the RCP 8.5 scenario, ET_0 remains most sensitive to changes in RH in autumn and over the entire year. Same condition happened to RS and WS, while the increase of RS is responsible for increment of ET_0 in entire year. Average temperature greatest influences ET_0 during summer and the negative influence on ET_0 will strengthen in future 74 years.

Estimated precipitation deficit and impact on agriculture

The fluctuation of ET_0 due to climate warming is expected to have important consequences because of its association with precipitation change. Zhai and Pan (2003) showed that annual precipitation has decreased by 30 mm in North China in the recent 50 years. In this study, a crude estimation of the precipitation deficit (PD) was established by subtracting the monthly cumulative ET_0 from the monthly cumulative precipitation (P). This approach has been used previously in agro-ecological studies of the Arabian Peninsula (De Pauw, 2002) and Northern China (Liu et al., 2013a). Positive and negative values indicate an excess or deficit in crop water requirements, respectively. It should be noted that PD was estimated using the ET_0 and not the actual crop evapotranspiration (Harmsen et al., 2009), which makes it only a crude estimation. The annual variation tendency and statistics of the PD are described in Table 7 under the historical period and RCP 8.5 scenario. It can be seen that a deficit in terms of crop water requirements is detected in all four seasons (except winter) in the historical 54-year dataset. The same behavior was observed at the scale of the entire year for both scenarios, but PD is bound to become stronger under the RCP 8.5 scenario. The fact that there already is a deficit in spring and winter and that the deficit seems to be increasing, a negative influence on wheat production and water resources in the area can be expected in the future if no management changes, such as irrigation techniques, cropping pattern, mulching, etc. are adopted (Allen et al., 1998; Olesen and Bindi, 2002). From precipitation data, ET_0 estimates and accurate crop coefficients, adapted irrigation schedules could be defined and strategies could be developed optimizing water use as well as yield. The present study gives a first hint of trends to be expected and regions should be prioritized. A study in North China revealed that mean daily soil evaporation from less and additional mulching was reduced by 16% and 37% for wheat production, respectively (Chen et al., 2007b). In Spain, Döll (2002) has predicted a declining in irrigation requirements by 2020 on account of the possibility of earlier sowing under more favorable higher temperatures. It will be necessary to develop

feasible straw (film) mulching, regulated deficit irrigation, and soil water storage and preservation to reduce pressure on groundwater over-exploitation, especially for winter wheat in the 3H Plain.

Table 7 Trend analysis of precipitation deficit with Mann-Kendall test and Theil–Sen's slope estimator slope estimator under the historical period and RCP 8.5 scenario. The units of the slope are mm decade^{-1}. The values described in table were obtained from area-averaged precipitation deficit from 40 meteorological stations using Theil–Sen's slope estimator in past 54 years and future 85 years over the Huang-Huai-Hai Plain.

	Spring		Summer		Autumn		Winter		Entire year	
	Value (mm)	Slope	Value (mm)	Slope	Value (mm)	Slope	Value (mm)	Slope	Value (mm)	Slope
Historical	-252.9	2.35	-187.6	-14.1**	31.32	-0.19	-82.8	2.58	-492.5	18.3**
RCP 8.5	-221.1	-4.12*	18.9	-1.27	-166.7	-3.62	-65.5	-0.72*	-434.4	-9.73*

6. Conclusions

This study quantified the temporal evolution of meteorological variables and their influence on potential evapotranspiration as well as their spatial patterns over the Huang-Huai-Hai Plain, China using a historical data set of 54 years and a high CO_2 emission scenario RCP 8.5 with daily time step. The historical data set revealed a decrease of ET_0 over time, which was only significant in the summer and the entire year. Spring was the only season with a positive trend of ET_0. Conversely, the RCP 8.5 scenario predicted an increase of ET_0 for all seasons.

We quantified the sensitivity of ET_0 to the different key climate factors using a sensitivity analysis based on partial derivatives. The main controlling variable was not constant for all seasons. ET_0 was most sensitive to RH in summer and autumn, whereas RS and WS were more important during spring and winter. While, a negative trend in ET_0 was primarily controlled by the declining of relative humidity in both the spring and the entire year. A negative trend in ET_0 was controlled by the declining of solar radiation in summer, autumn and winter. Also under the RCP 8.5 scenario, RH remains a variable with a large influence on ET_0 during autumn and over the entire year. The impact of RS and WS is also in the same direction as in the historical data set, while the increase of RS is responsible for increment of ET_0 in entire year. Average temperature was the variable to which ET_0 was most sensitive in summer and its negative influence on ET_0 is predicted to strengthen in the future 74 years. Analysis of the spatial patterns revealed that ET_0 has been the lowest in the Southeast and the highest in the Northeast part of Shandong province. Altogether no distinct spatial structure is visible in the 3H Plain in the historical data set, but the predictions using the RCP8.5 scenario result in a northeast-west gradient with low values in the south, mainly visible in spring and summer.

The accurate estimation of ET_0 response to meteorological variables could be favorable for designing future irrigation systems and agricultural production practices in the studied region. Variations in ET_0 in regards to meteorological parameters and agricultural production practice should be given greater attention when

considering the hydrological process and water management in coming decades under the effects of global climate change, in order to avoid problems such as the over-exploitation of groundwater resources.

Acknowledgements

This research was supported by the 12th five-year plan of the National Key Technologies R&D Program (2012BAD09B01), the National Basic Research Program of China (973 Program) (2012CB955904) and the National Science Foundation for Young Scientists of China (41401510). We thank the University of Liège-Gembloux Agro-Bio Tech and more specifically the research platform AgricultureIsLife for the funding of the scientific stay in Belgium that made this paper possible. We gratefully acknowledge the anonymous reviewers for their valuable comments on the manuscript.

7. References

Ahani, H., Kherad M., Kousari M.R., Roosmalen L.V., Aryanfar R. and Hossenini S.M.,, 2013. Non-parametric trend analysis of the aridity index for three large arid and semi-arid basins in Iran. Theoretical & Applied Climatology, 112(3-4): 553-564.

Allen, R.G., Pereira, L.S., Raes, D. and Smith, M., 1998. Crop evapotranspiration-Guidelines for computing crop water requirements-FAO Irrigation and drainage paper 56. FAO, Rome, 300: 6541.

Bo, L., Qi, H., Wenpeng, W., Xiaofan, Z. and Jianqing, Z., 2011a. Variation of actual evapotranspiration and its impact on regional water resources in the Upper Reaches of the Yangtze River. Quaternary International, 244(2): 185-193.

Bo, T., Ling, T., Shaozhong, K. and Lu, Z., 2011b. Impacts of climate variability on reference evapotranspiration over 58 years in the Haihe river basin of north China. Agricultural Water Management, 98(10): 1660-1670.

Brown, R.A. and Rosenberg, N.J., 1997. Sensitivity of crop yield and water use to change in a range of climatic factors and CO_2 concentrations: a simulation study applying EPIC to the central USA. Agricultural and Forest Meteorology, 83(3): 171-203.

Burn, D.H. and Hesch, N.M., 2007. Trends in evaporation for the Canadian Prairies. Journal of Hydrology, 336(1–2): 61-73.

Chen, H., Guo, S., Xu, C. and Singh, V.P., 2007a. Historical temporal trends of hydro-climatic variables and runoff response to climate variability and their relevance in water resource management in the Hanjiang basin. Journal of hydrology, 344(3): 171-184.

Chen, J., Tang C., Shen Y., Sakura Y., Kondoh A., and Shimada J., 2003 2003. Use of water balance calculation and tritium to examine the dropdown of groundwater table in the piedmont of the North China Plain (NCP). Environmental Geology, 44(5): 564-571.

Chen, S., Liu, Y. and Thomas, A., 2006. Climatic change on the Tibetan Plateau: potential evapotranspiration trends from 1961–2000. Climatic Change, 76(3-4): 291-319.

Chen, S., Zhang, X., Pei, D., Sun, H. and Chen, S., 2007b. Effects of straw mulching on soil temperature, evaporation and yield of winter wheat: field experiments on the North China Plain. Annals of Applied Biology, 150(3): 261-268.

Chun, K., Wheater, H. and Onof, C., 2012. Projecting and hindcasting potential evaporation for the UK between 1950 and 2099. Climatic change, 113(3-4): 639-661.

Cohen, S., Ianetz, A. and Stanhill, G., 2002. Evaporative climate changes at Bet Dagan, Israel, 1964–1998. Agricultural and Forest Meteorology, 111(2): 83-91.

Döll, P., 2002. Impact of climate change and variability on irrigation requirements: a global perspective. Climatic change, 54(3): 269-293.

De Pauw, E., 2002. An agroecological exploration of the Arabian Peninsula. Icarda.

Dinpashoh, Y., Jhajharia, D., Fakheri-Fard, A., Singh, V.P. and Kahya, E., 2011. Trends in reference crop evapotranspiration over Iran. Journal of Hydrology, 399(3–4): 422-433.

Donohue, R.J., McVicar, T.R. and Roderick, M.L., 2010. Assessing the ability of potential evaporation formulations to capture the dynamics in evaporative demand within a changing climate. Journal of Hydrology, 386(1): 186-197.

Drogue, G., Pfister, L., Leviandier T., Idrissi A.E., Iffly J.F., Matgen P., Humbert, J. and Hoffmann, L., 2004. Simulating the

spatio-temporal variability of streamflow response to climate change scenarios in a mesoscale basin. Journal of Hydrology, 293(1): 255-269.

Dyck, S., 1985. Overview on the present status of the concepts of water balance models. IAHS-AISH publication(148): 3-19.

Fan, J., Wu, L., Zhang, F., Xiang, Y. and Zheng, J., 2016. Climate change effects on reference crop evapotranspiration across different climatic zones of China during 1956–2015. Journal of Hydrology.

Feddema, J.J., 1999. Future African water resources: interactions between soil degradation and global warming. Climatic Change, 42(3): 561-596.

Gaile, G.L., 1984. Measures of spatial equality, Spatial statistics and models. Springer, pp. 223-233.

Gao, G., Chen, D., Ren, G., Chen, Y. and Liao, Y., 2006. Spatial and temporal variations and controlling factors of potential evapotranspiration in China: 1956–2000. Journal of Geographical Sciences, 16(1): 3-12.

Georgia, A., 2000. The change of the hydrological cycle under the influence of global warming.

Gong, L., Xu, C., Chen, D., Halldin, S. and Chen, Y.D., 2006. Sensitivity of the Penman–Monteith reference evapotranspiration to key climatic variables in the Changjiang (Yangtze River) basin. Journal of Hydrology, 329(3): 620-629.

Goyal, R., 2004. Sensitivity of evapotranspiration to global warming: a case study of arid zone of Rajasthan (India). Agricultural Water Management, 69(1): 1-11.

Han, S., Tang, Q., Xu, D. and Wang, S., 2014. Irrigation‐induced changes in potential evaporation: more attention is needed. Hydrological Processes, 28(4): 2717-2720.

Harmsen, E.W., Miller, N.L., Schlegel, N.J. and Gonzalez, J.E., 2009. Seasonal climate change impacts on evapotranspiration, precipitation deficit and crop yield in Puerto Rico. Agricultural water management, 96(7): 1085-1095.

He, Y., Zhang, B. and Ma, C., 2004. Dynamic change of cultivated land and its impact on grain-production in Jilin Province. Resources Science, 26(4): 119-125. (in Chinese)

Hess, T.M., 1998. Trends in reference evapo-transpiration in the North East Arid Zone of Nigeria, 1961–91. Journal of Arid Environments, 38(1): 99-115.

Hobbins, M.T., Ramírez, J.A. and Brown, T.C., 2001. The complementary relationship in estimation of regional evapotranspiration: An enhanced advection‐aridity model. Water Resources Research, 37(5): 1389-1403.

Huntington, T.G., 2006. Evidence for intensification of the global water cycle: review and synthesis. Journal of Hydrology, 319(1): 83-95.

Huo, Z., Dai, X., Feng, S., Kang, S. and Huang, G., 2013. Effect of climate change on reference evapotranspiration and aridity index in arid region of China. Journal of Hydrology, 492(492): 24-34.

Irmak, S., Payero, J.O., Martin, D.L., Irmak, A. and Howell, T.A., 2006. Sensitivity analyses and sensitivity coefficients of standardized daily ASCE-Penman-Monteith equation. Journal of Irrigation and Drainage Engineering, 132(6): 564-578.

Jhajharia, D., Dinpashoh, Y., Kahya, E., Singh, V.P. and Fakheri‐Fard, A., 2012. Trends in reference evapotranspiration in the humid region of northeast India. Hydrological Processes, 26(3): 421-435.

Jhajharia, D. , Kumar R., Dabal P.P., Singh V.P. Choudhary R.R. and Dinpashoh Y., 2015. Reference evapotranspiration under changing climate overtheTharDesertinIndia. Meteorological Applications, 22(3): 425–435.

Jin, H., Qingjie, W., Hongwen, L., Lijin, L. and Huanwen, G., 2009. Effect of alternative tillage and residue cover on yield and water use efficiency in annual double cropping system in North China Plain. Soil and Tillage Research, 104(1): 198-205.

Kendall, M., 1975. Rank Correlation Methods, Charles Griffin & Company Ltd. London.

Kousari, M.R. and Ahani, H., 2012. An investigation on reference crop evapotranspiration trend from 1975 to 2005 in Iran. International Journal of Climatology, 32(15): 2387-2402.

Kumar, S., Merwade, V., Kam, J. and Thurner, K., 2009. Streamflow trends in Indiana: Effects of long term persistence, precipitation and subsurface drains. Journal of Hydrology, 374(1–2): 171-183.

Li, Z., Zheng, F.L. and Liu, W.Z., 2012. Spatiotemporal characteristics of reference evapotranspiration during 1961–2009 and its projected changes during 2011–2099 on the Loess Plateau of China. Agricultural and Forest Meteorology, 154: 147-155.

Liang, L., Li, L. and Liu, Q., 2010. Temporal variation of reference evapotranspiration during 1961–2005 in the Taoer River basin of Northeast China. Agricultural and Forest Meteorology, 150(2): 298-306.

Liang, W., Carberry P., Wang G., Lu R. Lu H. and Xia A., 2011. Quantifying the yield gap in wheat–maize cropping systems of the Hebei Plain, China. Field Crops Research, 124(2): 180-185.

Liu, C., Zhang, D., Liu, X. and Zhao, C., 2012. Spatial and temporal change in the potential evapotranspiration sensitivity to meteorological factors in China (1960–2007). Journal of Geographical Sciences, 22(1): 3-14.

Liu, Q., Mei, X., Yan, C., Ju, H. and Yang, J., 2013a. Dybamic variation of water deficit of winter wheat and its possible climatic factors in Northern China. Acta Ecologica Sinica, 33(20): 6643-6651.

Liu, Q., Yan, C., Mei, X., Zhang, Y., Yang, J. and Liang, Y., 2012. Spatial evolution of reference crop evapotranspiration in arid area of Northwest China. Chinese Journal of Agrometeorology, 33(1): 48-53. (in Chinese)

Liu, Q., Yan, C., Zhao, C., Yang, J. and Zhen, W., 2014. Changes of daily potential evapotranspiration and analysis of its sensitivity coefficients to key climatic variables in Yellow River basin. Transactions of Chinese Society of Agricultural Engineering, 30(15): 157-166.

Liu, X., Zhang, D., Luo, Y. and Liu, C., 2013b. Spatial and temporal changes in aridity index in northwest China: 1960 to 2010. Theoretical & Applied Climatology, 112(1-2): 307-316.

Ma, X., Zhang M., Li Y., Wang S., Ma Q. and Liu W., 2012. Decreasing potential evapotranspiration in the Huanghe River Watershed in climate warming during 1960–2010. Journal of Geographical Sciences, 22(6): 977-988.

Mann, H.B., 1945. Nonparametric test against trend. Econometrica, 13(3): 245-259.

Maracchi, G., Sirotenko, O. and Bindi, M., 2005. Impacts of present and future climate variability on agriculture and forestry in the temperate regions: Europe. Climatic Change, 70(1-2): 117-135.

McKenney, M.S. and Rosenberg, N.J., 1993. Sensitivity of some potential evapotranspiration estimation methods to climate change. Agricultural and Forest Meteorology, 64(1¨C2): 81-110.

McNulty, S.G., Vose, J.M. and Swank, W.T., 1997. R egional hydrologic response of loblolly pine and air temperature and precipitation. Journal of the American Water Resources Association, 33(5): 1011-1022.

Mcvicar, T.R., Roderick M.L., Donohue R.J., Li L., Niel T.G.V., Thomas A., Grieser J., Jhajharia D. Himri Y. and Mahowald N.M., 2012. Global review and synthesis of trends in observed terrestrial near-surface wind speeds: Implications for evaporation. Journal of Hydrology, s 416–417(3): 182-205.

Muhs, D. and Maat, P., 1993. The potential response of eolian sands to greenhouse warming and precipitation reduction

on the Great Plains of the USA. Journal of Arid Environments, 25(4): 351-361.

Nalley, D., Adamowski, J. and Khalil, B., 2012. Using discrete wavelet transforms to analyze trends in streamflow and precipitation in Quebec and Ontario (1954–2008). Journal of Hydrology, 475: 204-228.

Olesen, J.E. and Bindi, M., 2002. Consequences of climate change for European agricultural productivity, land use and policy. European Journal of Agronomy, 16: 239-262.

Ren, J., Chen, Z., Zhou, Q. and Tang, H., 2008. Regional yield estimation for winter wheat with MODIS-NDVI data in Shandong, China. International Journal of Applied Earth Observation and Geoinformation, 10(4): 403-413.

Riahi, K., Rao, S., Krey, V., Cho, C., Chirkow, V., Fischer, G., Kindermann, G., Nakicenovic, N. and Rafaj, P., 2011. RCP 8.5—A scenario of comparatively high greenhouse gas emissions. Climatic Change, 109(1-2): 33-57.

Roderick, M.L. and Farquhar, G.D., 2004. Changes in Australian pan evaporation from 1970 to 2002. International Journal of Climatology, 24(9): 1077-1090.

Roderick, M.L., Rotstayn, L.D., Farquhar, G.D. and Hobbins, M.T., 2007. On the attribution of changing pan evaporation. Geophysical Research Letters, 34(34): 251-270.

Sen, P.K., 1968. Estimates of the Regression Coefficient Based on Kendall's Tau. Journal of the American Statistical Association, 63(324)(324): 1379-1389.

Song, Z., Zhang, H., Snyder, R., Anderson, F. and Chen, F., 2009. Distribution and trends in reference evapotranspiration in the North China Plain. Journal of Irrigation and Drainage Engineering, 136(4): 240-247.

Stanhill, G. and Cohen, S., 2001. Global dimming: a review of the evidence for a widespread and significant reduction in global radiation with discussion of its probable causes and possible agricultural consequences. Agricultural and forest meteorology, 107(4): 255-278.

Stocker, T., Qin D., Plattner G.K., Tignor M., Allen S.K., Boschung J., Nauels A., Xia Y., Bex V. and Midgley P.M., 2014. Climate change 2013: The physical science basis. Cambridge University Press Cambridge, UK, and New York.

Su, X., Singh, V.P., Niu, J. and Hao, L., 2015. Spatiotemporal trends of aridity index in Shiyang River basin of northwest China. Stochastic Environmental Research and Risk Assessment, 29(6): 1571-1582.

Sun, Q., Krobel R., Muller T., Romheld V., Cui Z., Zhang F. and Chen X., 2011. Optimization of yield and water-use of different cropping systems for sustainable groundwater use in North China Plain. Agricultural Water Management, 98(5): 808-814.

Liu, S., Mo, X., Lin, Z., Xu, Y., Ji, J., Wen, G. and Jeff R., 2010. Crop yield responses to climate change in the Huang-Huai-Hai Plain of China. Agricultural water management, 97(8): 1195-1209.

Team, R.D.C., 2011. R: A Language and Environment for Statistical Computing. Computing, 14: 12-21.

Theil, H., 1992. A Rank Invariant Method of Linear and Polynomial Regression Analysis. Springer Netherlands, 345-381 pp.

Thomas, A., 2000. Spatial and temporal characteristics of potential evapotranspiration trends over China. International Journal of Climatology, 20(4): 381-396.

Thomas, A., 2008. Agricultural irrigation demand under present and future climate scenarios in China. Global and Planetary Change, 60(3): 306-326.

Todisco, F. and Vergni, L., 2008. Climatic changes in Central Italy and their potential effects on corn water consumption. Agricultural and Forest Meteorology, 148(1): 1-11.

Wang, W., Peng S., Yang T., Shao Q., Xu J. and Xing W.,, 2010. Spatial and temporal characteristics of reference

evapotranspiration trends in the Haihe River basin, China. Journal of Hydrologic Engineering, 16(3): 239-252.

Wang, Y., Jiang, T., Bothe, O. and Fraedrich, K., 2007. Changes of pan evaporation and reference evapotranspiration in the Yangtze River basin. Theoretical and applied climatology, 90(1-2): 13-23.

Wild, M., 2014. Global Dimming and Brightening. Global Environmental Change: 39-47.

Wu, S., Yin, Y., Zheng, D. and Yang, Q., 2006. Moisture conditions and climate trends in China during the period 1971–2000. International Journal of Climatology, 26(2): 193–206.

Xu, C., Gong, L., Jiang, T., Chen, D. and Singh, V.P., 2006. Analysis of spatial distribution and temporal trend of reference evapotranspiration and pan evaporation in Changjiang (Yangtze River) catchment. Journal of Hydrology, 327(1-2): 81-93.

Xu, C. and Singh, V., 2005. Evaluation of three complementary relationship evapotranspiration models by water balance approach to estimate actual regional evapotranspiration in different climatic regions. Journal of Hydrology, 308(1): 105-121.

Xu, C. and Xu, Y., 2012. The projection of temperature and precipitation over China under RCP scenarios using a CMIP5 multi-model ensemble. Atmospheric and Oceanic Science Letters, 5(6): 527-533.

Xu, X., Liu J., and Zhuang, D., 2004. Analysis of temporal-spatial characteristics of reference evapotranspiration based on GIS technology in Northeast China during 1991-2000. Transactions of the CSAE, 20(2): 10-14. (in Chinese)

Xu, Z. and Li, J., 2003. A distributed approach for estimating catchment evapotranspiration: comparison of the combination equation and the complementary relationship approaches. Hydrological Processes, 17(8): 1509-1523.

Xu, Z.X., Takeuchi, K. and Ishidaira, H., 2003. Monotonic trend and step changes in Japanese precipitation. Journal of Hydrology, 279(1–4): 144-150.

Yang, J., Liu Q., Mei X., Yan C., Ju H., and Xu J., 2013. Spatiotemporal Characteristics of Reference Evapotranspiration and Its Sensitivity Coefficients to Climate Factors in Huang-Huai-Hai Plain,China. Journal of Integrative Agriculture, 12(12): 2280-2291.

Yang, J., Liu, Q., Yan, C. and Mei, X., 2011. Spatial and temporal variation of solar radition in recent 48 years in North China. Acta Ecologica Sinica, 31(10): 2748-2756.

Yang, J., Mei X., Huo Z., Yan C., Ju H., Zhao F., and Liu Q., 2015. Water Consumption in Winter Wheat and Summer Maize Cropping System Based on SEBAL Model in Huang-Huai-Hai Plain, China. Journal of Integrative Agriculture.

Yang, K., Wu H., Qin J., Lin C., Tang W., and Chen Y., 2014. Recent climate changes over the Tibetan Plateau and their impacts on energy and water cycle: a review. Global and Planetary Change, 112: 79-91.

Yu, P.S., Yang, T.C. and Chou, C.C., 2002. Effects of Climate Change on Evapotranspiration from Paddy Fields in Southern Taiwan. Climatic Change, 54(1-2): 165-179.

Yuan, B., Guo, J., Ye, M. and Zhao, J., 2012. Variety distribution pattern and climatic potential productivity of spring maize in Northeast China under climate change. Chinese Science Bulletin, 57(26): 3497-3508.

Yue, S., Pilon, P., Phinney, B. and Cavadias, G., 2002. The influence of autocorrelation on the ability to detect trend in hydrological series. Hydrological Processes, 16(9): 1807–1829.

Zamani, R., Mirabbasi, R., Abdollahi, S. and Jhajharia, D., 2016. Streamflow trend analysis by considering autocorrelation structure, long-term persistence, and Hurst coefficient in a semi-arid region of Iran. Theoretical and Applied Climatology.

Zeng, W. and Heilman, J., 1997. Sensitivity of evapotranspiration of cotton and sorghum in west Texas to changes in climate and CO2. Theoretical and applied climatology, 57(3-4): 245-254.

Zhai, P. and Pan, X., 2003. Change in extreme temperature and precipitation over northern China during the second half of the 20th century. Acta Ecologica Sinica, 58((S1)): 2-10.

Zhang, Q., Xu, C. and Chen, X., 2011. Reference evapotranspiration changes in China: natural processes or human influences. Theoretical and Applied Climatology, 103(3-4): 479-488.

Zhang, X., Kang, S., Zhang, L. and Liu, J., 2010. Spatial variation of climatology monthly crop reference evapotranspiration and sensitivity coefficients in Shiyang river basin of northwest China. Agricultural Water Management, 97(10): 1506-1516.

Zhao, R., Chen X., Zhang F., Zhang H., Schroder J. and Romheld V., 2006. Fertilization and nitrogen balance in a wheat–maize rotation system in North China. Agronomy Journal, 98(4): 938-945.

Zheng, C. and Wang, Q., 2014. Spatiotemporal variations of reference evapotranspiration in recent five decades in the arid land of Northwestern China. Hydrological Processes, 28(25): 6124–6134.

Zhou, T. and Hong, T., 2013. Projected changes of palmer drought severity index under an RCP 8.5 Scenario. Atmospheric and Oceanic Science Letters, 6(5): 273-278.

Zuo, D., Xu, Z., Yang, H. and Liu, X., 2012. Spatiotemporal variations and abrupt changes of potential evapotranspiration and its sensitivity to key meteorological variables in the Wei River basin, China. Hydrological Processes, 26(8): 1149-1160.

Chapter Ⅲ. Spatiotemporal variation of drought characteristics under the climate change scenario

Spatiotemporal variation of drought characteristics in the Huang-Huai-Hai Plain, China under the climate change scenario

Published in Journal of Integrative Agriculture, 9, March 2017 DOI: 10.1016/S2095- 3119(16)61545-9

LI Xiang-xiang, JU Hui, Sarah Garré, YAN Chang-rong, William D. Batchelor, **LIU Qin***

** Corresponding author*

outline

As drought negatively impact agricultural production in Huang-Huai-Hai Plain of China, the objective of this manuscript is to understand the variations of drought characteristics including drought event frequency, duration, magnitude and severity for both historical period and future scenario, utilizing climatic drought indices.

1. Abstract

Understanding the potential drought characteristics under climate change is essential to reduce vulnerability and establish adaptation strategies, especially in the Huang-Huai-Hai Plain (3H Plain), which is the grain production base in China. In this paper, we investigated the variations in drought characteristics (drought event frequency, duration, severity, and intensity) for the past 50 years (1961—2010) and under future scenarios (2010—2099), based on the observed meteorological data and the RCP 8.5 projection, respectively. First, we compared the applicability of three climatic drought indices: the Standardized Precipitation Index (SPI), the Standardized Precipitation Evapotranspiration Index based on the Penman–Monteith equation (SPEI-PM), and the Thornthwaite equation (SPEI-TH) to trace the recorded agricultural drought areas. Then, we analyzed the drought characteristics using "run theory" for both historical observations and future RCP 8.5 scenarios based on proper index. Correlation analyses between drought indices and agricultural drought areas showed that SPEI-PM performed better than SPI and SPEI-TH in the 3H Plain. Based on the results of SPEI-PM, the past 50 years have experienced reduced drought of shorter duration, and of weaker severity and intensity. However, under the future RCP 8.5 scenario, drought is expected to rise in frequency, duration, severity, and intensity from 2010—2099, although drought components during the 2010—2039 is predicted to be milder compared with the historical conditions. This study highlights that the estimations for atmospheric evaporative demand would bring in differences in the prediction of long-term drought trends by different drought indices. The results of this study can help inform researchers and local policy makers to establish drought management strategies.

Keywords： climate change, drought index, drought characteristics, Huang-Huai-Hai Plain

2. Introduction

Drought is one of the most damaging and widespread climate extremes that negatively affect the agricultural production, water resources, ecosystem function, and human lives around the world (Wilhite et al. 2007; Dai 2011b). Due to the interaction of monsoon climate with the complex topography in East Asia, China has suffered from long-lasting and severe droughts during the second half of twentieth century, which has caused significant socioeconomic and eco-environment damages to the country (Yong et al. 2013; Yang et al. 2015; Zhang et al. 2015a).With the projected temperature increase and change in the distribution of precipitation, the drought risk is expected to increase further (Sillmann et al. 2013; Wang and Chen 2014) and subsequently make crop production more uncertain. Thus, understanding the potential drought characteristics under climate change is of prime importance for reducing vulnerability and establishing drought adaptation strategies (Chen et al. 2014; Wilhite et al. 2014).

Several techniques have been developed to quantitatively analyze drought characteristics (Heim 2002). Some of these are the physically based indices, such as Palmer drought severity index(PDSI) and its derivative, and statistically based indices, such as Standardized Precipitation Index (SPI) and the Standardized Precipitation Evapotranspiration Index (SPEI) (Vicente-Serrano et al. 2011). These indices have been widely used in detecting long-term drought trends under climate change at several locations around the world. The general recognition is that drought has been intensifying around the world due to global warming in the past decades (Allen et al. 2010; Dai 2013). However, it has been difficult to understand how droughts have changed in China, because the findings based on the potential evapotranspiration (ET_0) equations vary among studies (Sheffield et al. 2012; Trenberth et al. 2014; Xu et al. 2015). For example, significant drying trends were found in northern and southwestern China during the past decades, when ET_0 was estimated by temperature only (Yu et al. 2014a; Wang et al. 2015a). However, when it was calculated by the Penman-Monteith equation, whose algorithm takes more climatic variables into account, no evidence of an increase in drought severity was found across China (Wang et al. 2015b), and even more wetting areas than drying areas were observed in the North China Plain and Northeast China Plain (Xu et al. 2015). Subsequently, such differences have led to confusion among scientists, policy makers, and the public (Vicente-Serrano et al. 2012). Thus, the applicability of an index should be verified prior to using it in drought analysis to obtain results that are more realistic. Substantial divergence of applicability exists between physically and statistically based drought indices, and difference exists even when using the same index with different ET_0 estimation methods, depending on the system and location. Dai (2011a) reported that PDSI performed better than other indices because of its physically based water balance model, but Vicente-Serrano et al. (2011) described the advantages of statistically based indices, including SPI and SPEI and provided a worldwide rating of the performance of PDSI, SPI, and SPEI on hydrological, agricultural, and ecological systems (Vicente-Serrano et al. 2012). Similar comparative studies have been conducted at different locations for different systems, such as river discharges (Zhai et al. 2010), tree-ring growth (Sun and Liu 2013), and crop production (Xu et al. 2013), resulting in site or system specific results.

The Huang-Huai-Hai Plain (3H Plain) is a major crop producing area in China that encompasses 19% of the total arable land in China. However, it has experienced serious droughts and water scarcity problems in recent years (Yong et al. 2013), which has been the limiting factor for agricultural production (Zhang et al. 2015a). Furthermore, water limitations is likely to be accentuated by increased food demand, soil quality deterioration and over-exploitation of groundwater resources (Yang et al. 2015). Climate variability, especially extreme climate events, such as drought, may cause fluctuation of crop yields (Lu and Fan 2013; Yu et al. 2014b).Thus, understanding the potential variations of drought characteristics under climate change is essential for reducing vulnerability and establishing drought adaptation strategies for agriculture in 3H Plain. Most previous studies have primarily reported the seasonal and spatial variability of water deficiency (Yong et al. 2013; Huang et al. 2014) and the long term drought evolutions, including dry/wet trends, spatial distribution of drought frequency, drought affected areas, and drought duration for historical periods (Yu et al. 2014a; Wang et al. 2015a; Wang et al. 2015b; Xu et al. 2015). However, few studies have evaluated the performance of multi-indices on estimating drought impact and assessed drought risk for future climate scenarios.

The objectives of this research are: (1) to evaluate the applicability of drought indices (SPI and two versions of SPEI) in describing historical agricultural drought areas in the Huang-Huai-Hai Plain; (2) to investigate the variations of drought characteristics, including duration, severity, and intensity for 1961—2010 and (3) evaluation of projected drought characteristics for 2010—2099 using the RCP 8.5 climate scenario. The results are expected to provide useful information on drought risk to decision makers and a wide range of stakeholders interested in the occurrence and consequences of recurrent droughts.

3. Materials and methods

Study region

The Huang-Huai-Hai Plain (3H Plain) is located in northern China, extending over 31°14′–40°25′ N and 112°33′–120°17′ E, with 23.3 million ha of arable land (19% of the total arable land in China), providing about 70% of national wheat production and 30% of national maize production with a dominant winter wheat-summer maize double cropping system (Yang et al. 2015). The 3H Plain belongs to the extratropical monsoon climatic region. The annual mean precipitation is 348.5mm with more than 70% rainfall in July to September and the atmospheric evaporative demand is about 1000mm/year (Zhang et al. 2011). For the wheat-maize rotation system, rainfall can only meet 65% of total agricultural water demand, and for winter wheat, only 25%—40% of water demand is satisfied by rainfall (Mei et al. 2013). The irrigation water is primarily pumped from groundwater. However, the groundwater level has decreased from a depth of 10m in the 1970s to 32m in 2001, and has continued to decrease at the rate of 1m per year (Zhang et al. 2005). Thus, drought in this region not only challenges food supplies, but also results in a series of environmental problems. The 3H Plain can be divided into six sub-regions (see Li et al., 2015 for detail

information) in terms of climate conditions and agricultural management practices (Figure 17).

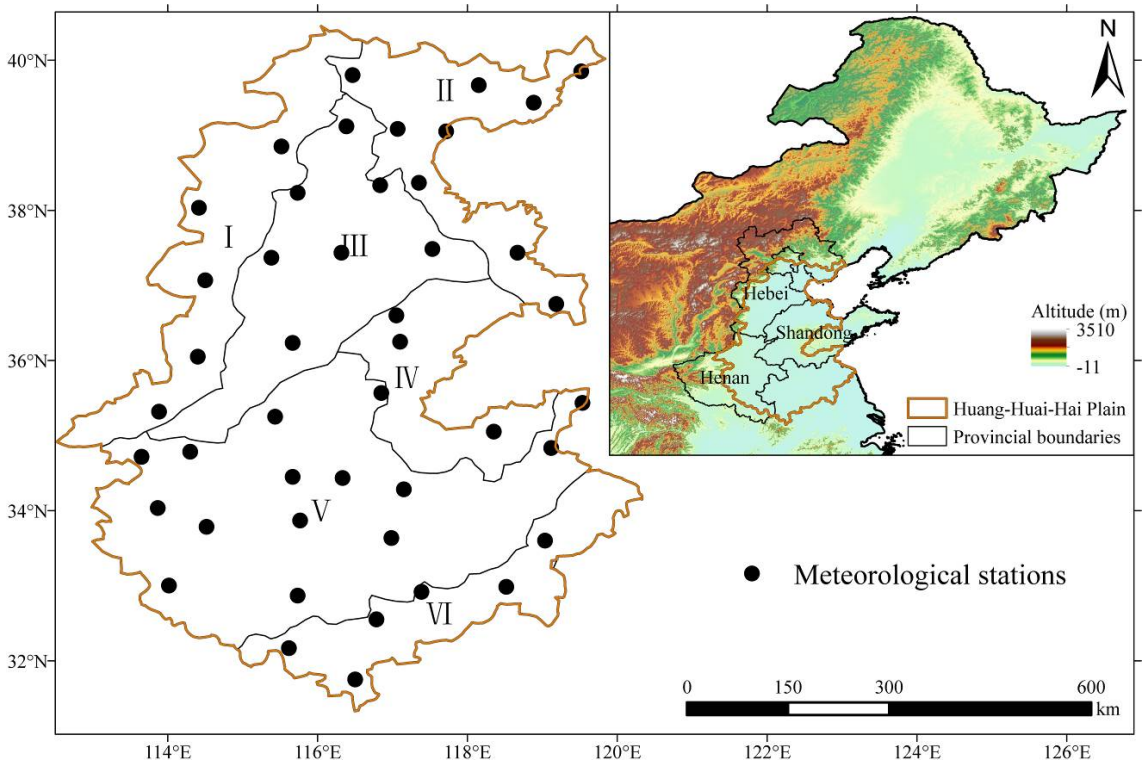

Figure 17 Location of the Huang-Huai-Hai Plain and the meteorological stations used in this study. (Ⅰ: Piedmont plain-irrigable land Zone; Ⅱ: Coastal land-farming-fishing area; Ⅲ: Low plain-hydropenia irrigable land and dry land; Ⅳ: Hill-irrigable land and dry land; Ⅴ: Basin-irrigable land and dry land; Ⅵ: Hill-wet hot paddy-paddy field). The map on the top right corner describes the location of Huang-Huai-Hai Plain in China. Climate data

Historical data covering a period of 50 years (1961—2010) and the interpolated future drought characteristics for the next 90 years (2010—2099) were used in this study. Historical meteorological data (maximum & minimum temperature, wind speed, relative humidity, and daily sunshine duration) for 45 weather stations (Figure 17) were obtained from the China Meteorological Administration (CMA). Future climate data was simulated using the RCP8.5 emission scenario of the HadGEM2-ES climate model, which assumes that the greenhouse gas emission continues to increase at the present rate. This dataset has been used for assessing potential effects of drought on winter wheat yield (Leng et al. 2015) and its vulnerability and adaptive capacity in the 3H Plain (Li et al. 2015).

Drought area data

Several previous studies have used crop yield data to verify the regional performance of drought indices (Vicente-Serrano et al. 2012; Ming et al. 2015; Potopova et al. 2015; Zhang et al. 2015b). However, in order to evaluate yield variability due to climate fluctuations alone, yield data should be detrended to remove the effect of agricultural technology improvements, such as better fertilizer application, new crop varieties, and better tillage practices (Yu et al. 2014b; Potopova et al. 2015). Similarly, it is difficult to

determine how much yield is affected by drought. Thus, in this study, we used drought area data to verify the performance of SPI, SPEI-TH, and SPEI-PM.

The drought area data, including the Drought-Induced Areas (DIA), Drought-Affected Areas (DAA), and Lost Harvest Areas (LHA) were obtained from the disaster database of Department of Plantation, Ministry of Agriculture (http://www.zzys.moa.gov.cn/). The DIA, DAA, and LHA represent the arable areas with yield losses caused according to the recorded data by drought at 10%, 30%, and 70%, respectively. Thus, they actually reflect the cumulative effect of drought on harvest yield for the whole growing season of winter wheat and summer maize (the agricultural pattern is winter wheat and summer maize rotation system in the 3H Plain), and not the conventional 'drought area' that measures the cover range of a certain drought event. The disaster database embodies provincial scale disaster data since 1949. However, considering the data's integrity and usability, data of DIA from 1971—2013, DAA from 1970—2012, LHA from 1982—2013 of Henan, Hebei, and Shandong provinces were considered.

Calculations of drought indices

The performances of SPI and the two versions of SPEI in describing historical agricultural drought areas were evaluated. The SPI (McKee et al. 1993) is the number of standard deviations of the standardized normal distribution transformed from the precipitation (P) series, while the SPEI (Vicente-Serrano et al. 2010) follows the same procedure but it is the difference of the precipitation (P) and the potential evapotranspiration (ET_0) series. To compute the indices, the probability density function of P sums series or P minus ET_0 sums series for a desired scale was estimated, which was then transformed to a normal distribution. As a result, the value of SPI or SPEI can be constructed as a split line that separates the standard normal distribution. The main strength of SPI and SPEI is that it can be calculated for any timescale (Heim 2002), which represent the cumulative impact of drought for different time periods (Hayes et al. 2011). The SPI depends only on precipitation data, which makes it popular and easy to implement around the world. The SPEI takes into account the atmospheric evaporation demand (i.e., ET_0), which makes it suitable for drought analysis under climate change (Vicente-Serrano et al. 2012). In the original version of SPEI, the evapotranspiration was estimated by the Thornthwaite equation, which only considers temperature. However, the Penman-Monteith method is widely accepted as the most physical and accurate estimation of ET_0 as it includes the effects of temperature, wind speed, relative humidity, and solar radiation (Chen et al. 2005; Sentelhas et al. 2010). Thus, we calculated the SPI and SPEI using the Thornthwaite (SPEI-TH) and FAO-PM equations (SPEI-PM) to compare their correlation with the observed agricultural drought areas.

The SPI and two versions of SPEI (SPEI-TH and SPEI-PM) were calculated utilizing the R package of SPEI, developed by Begueria et al. (2014). Since SPI and SPEI are both standardized, their values should have the same statistical meaning, and therefore should be comparable. Thus, the same threshold as shown in Table 8 was used to classify the drought conditions.

Table 8 Drought classifications based on Standardized precipitation index (SPI) and Standardized precipitation-evapotranspiration index (SPEI)

Drought classes	Probability (%)	Index value
Extreme wet	2.3	⩾2.0
Very wet	4.4	1.5—2.0
Moderate wet	9.2	1.0—1.5
Near normal	68.2	-1.0—1.0
Moderate dry	9.2	-1.5—-1.0
Severe dry	4.4	-2.0—-1.5
Extreme dry	2.3	⩽-2.0

Drought identification using run theory

The 'run theory' (Figure 18) proposed by Yevjevich (1967), which has been applied frequently to time series of anomalous hydrologic events, was used to identify drought components and investigate their statistical properties (Mishra and Desai 2005; Nam et al. 2015). A run or a drought event is defined as a consecutive sequence of months (t) with drought indices values, X_t, less than a chosen threshold, X_0. A drought event is characterized by the following components, which can be used for mathematical analysis of drought. Drought initiation time (T_s) is the onset month of a drought event. Drought termination time (T_e) represents the date when the water shortage becomes sufficiently small so that the drought no longer persists. Drought duration (D) is the time period between the initiation and termination of a drought. Drought severity (S) is obtained by the cumulative deficiency of the drought parameter below the critical level. Drought intensity (I) is calculated as the ratio of the drought deficit volume and the drought duration.

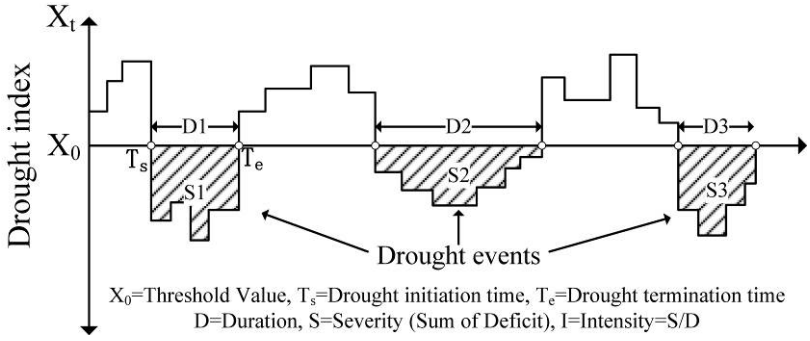

Figure 18 Drought characteristics identification using the run theory (According to Yevjevich 1967). In our study, three drought indexes were selected followed by Standardized Precipitation Index (SPI) and two versions of the Standardized Precipitation Evapotranspiration Index (SPEI), SPEI-TH and SPEI-PM.

4. Results

Selection of preferable drought index

As shown in Figure 19, drought areas have declined since the 1970s. Particularly, the DIA of all the provinces has decreased significantly (P<0.001). However, the DAA of the three provinces shows insignificant decline, but are still at lower levels after 2003. The LHA of Henan (Figure 19-A3) and Shandong (Figure 19-C3) decreased significantly (P<0.05), while it was not significant for the Hebei province (Figure 19-B3).

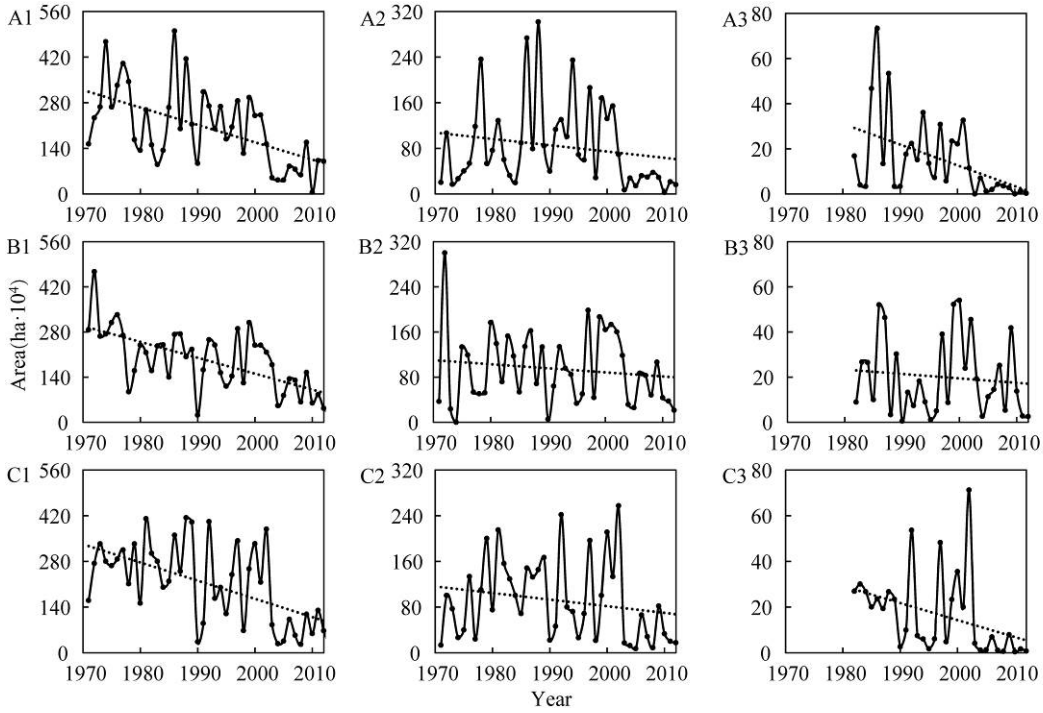

Figure 19 The series of drought area of Henan, Hebei, and Shandong Province. A, Henan province; B, Hebei province; C, Shandong province. 1, drought-induced areas (DIA); 2, drought-affected areas (DAA); 3, lost harvest areas (LHA). The dotted line is the linear trend line.

The Pearson correlation coefficients (r) between monthly drought index series at 1—12 timescales and the agricultural drought areas in Hebei (HB), Henan (HN), and Shandong (SD) provinces, obtained from the Ministry of Agriculture for historical years, are summarized in Figure 20. It shows that the absolute value of Pearson's r increased from January to December with the increase in timescale. Thus, a 12-month SPEI-PM at the end of December in the Huang-Huai-Hai Plain could capture the overall yearly dry conditions, which would reduce the crop yield. Table 9 compares the Pearson's *r* between SPI, SPEI-PM, and SPEI-TH in December at 12-month scale. The SPEI-PM gave higher Pearson's r values than the SPI and SPEI-TH, compared with the Ministry of Agriculture estimates of DIA, DAA, and LHA. For example, the median to high correlation between Lost Harvest Areas (LHA) and SPEI-PM in Hebei was -0.74, which was higher than that of SPI (-0.60) and SPEI-TH (-0.58) in 1981-2010. Thus, SPEI-PM was considered to be a proper index for drought analysis in the 3H Plain.

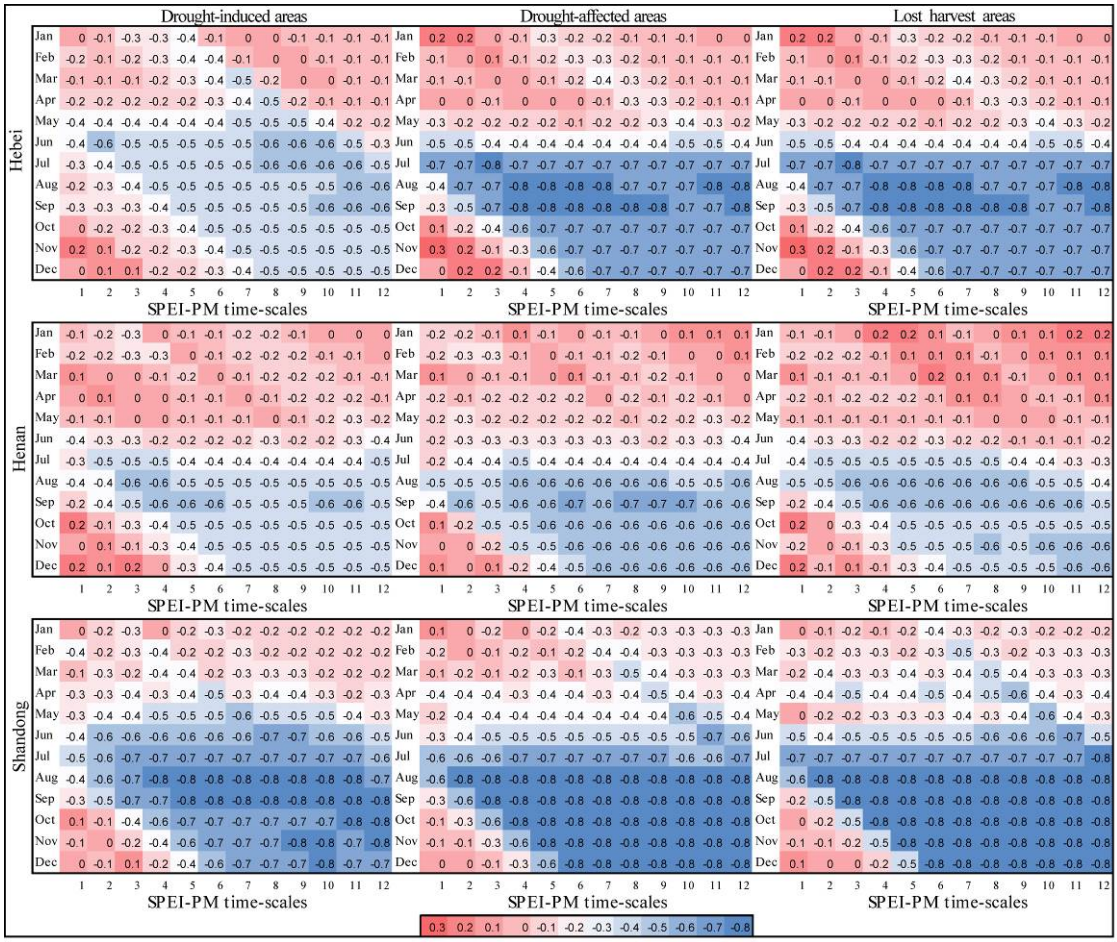

Figure 20 Pearson correlation coefficients between the monthly SPEI-PM series and the drought-induced areas, drought-affected areas, and lost harvest areas at 1-12month scales. Pearson correlation method comes from the literature reported by Ahlgren et al. (2003).

Table 9 Comparison of Pearson's r between SPEI-PM, SPEI-TH, and SPI at 12-month scale. Pearson correlation method comes from the literature reported by Ahlgren et al. (2003). (DIA, drought-induced areas; DAA, drought-affected areas; LHA, lost harvest areas; HB, Hebei province; HN, Henan province; SD, Shandong province)

Province	Classification	DIA	DAA	LHA
HB	SPEI-PM	-0.54	-0.73	-0.74
	SPEI-TH	-0.26	-0.65	-0.58
	SPI	-0.44	-0.73	-0.60
HN	SPEI-PM	-0.48	-0.64	-0.58
	SPEI-TH	-0.29	-0.58	-0.45
	SPI	-0.44	-0.64	-0.56
SD	SPEI-PM	-0.75	-0.81	-0.78
	SPEI-TH	-0.57	-0.70	-0.71
	SPI	-0.68	-0.76	-0.74

Drought characteristics over the past 50 years

Historical drought evolution

The drought/wet evolutions computed by SPEI-PM at 1—24-month scales is depicted for the six sub-regions of 3H Plain during 1961—2010 (Figure 21). The horizontal axis represents month series from January 1961 to December 2010, while the ordinate is the timescales from 1—24. By utilizing the single diagram, the temporal trends of the severity and duration of the drought indices and the development of the drought/wet stress conditions from 1 to 24 timescales over the past 50 years can be easily identified. Furthermore, the characteristics of drought occurrences in different regions can be compared. According to Figure 21, the moderate (≤-1.0) drought appeared broken in 1965—1970, 1980—1985, and 2000—2005 for all sub-regions. However, the severe drought s(≤-1.5) occurred primarily before the 1970s. Furthermore, after the severe to extreme wet period at around 1965, moderate-to-severe dry conditions occurred in all regions from 1965 to1970. Particularly, sub-regions five and six (Figure 21-E–F) experienced extreme dry conditions during this period.

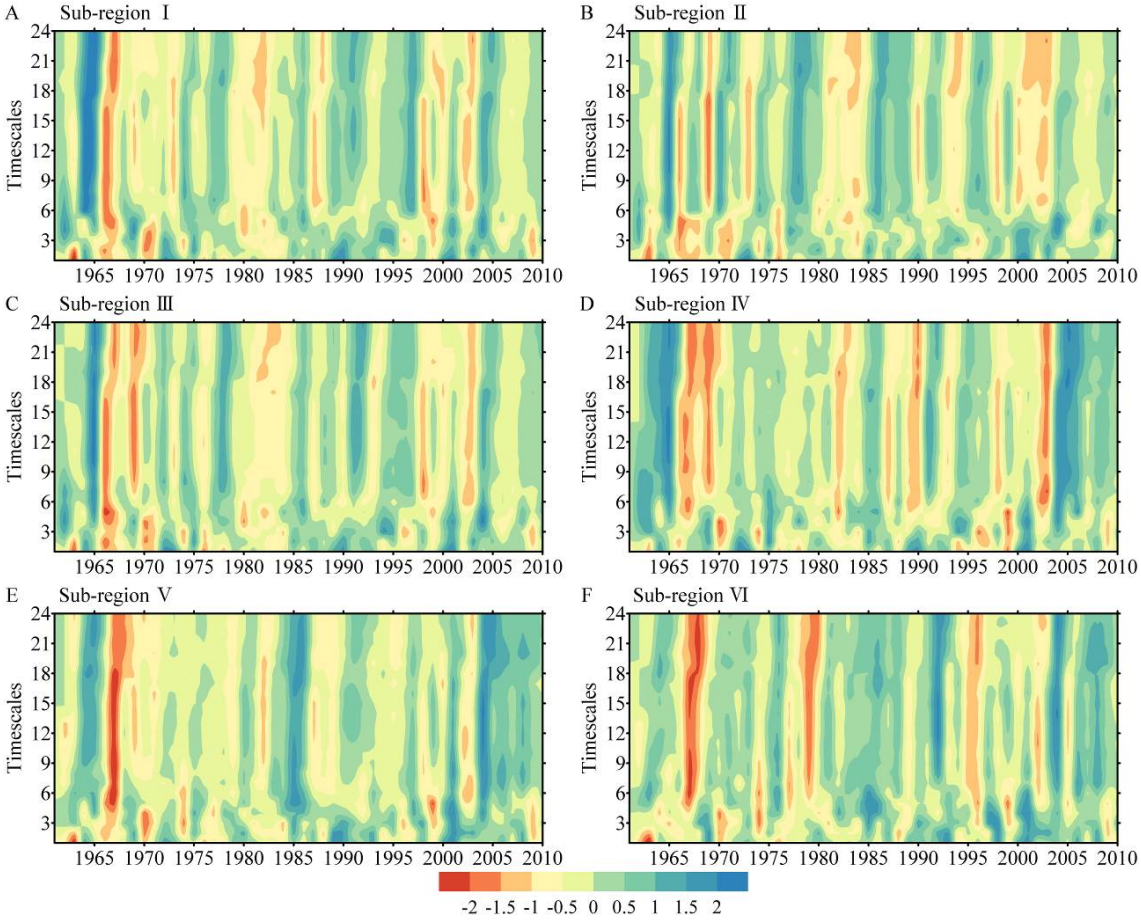

Figure 21 Spatio-temporal evolution of the SPEI-PM series indicating the development of drought from 1 to 24 month scales at 6 sub-regions during 1961—2010. These maps were obtained with the surfer software.

Temporal variation of historical drought characteristics

The changes in the number of total drought events was available for 45 meteorological stations at multiple timescales under historical periods and they were divided into the 1960s, 1970s, 1980s, 1990s, and 2000s (Table 10). A drought event was counted according to the 'run theory' (Figure 18). The threshold values are shown in Table 8. Drought events were categorized into two types: above-moderate drought events(hereinafter AM event) whose threshold was≤-1.0 and above-severe drought events(hereinafter AS event) whose threshold was≤-1.5. The ratio of AS events to AM events was also calculated to indicate changes in drought severity. An AM event includes all kinds of drought while an AS event includes more severe drought. In AM events, no significant trends were detected from 1960s to 2000s for all timescales (Table 10). AM events happened infrequently in the 1960s and 2000s. However, the AS/AM ratio in the 1960s was found to be the highest with a gradual decrease toward the 2000s for different timescales. In the case of SPEI-PM of 6-month, the ratio decreased from 72.8% in the 1960s, to 51.0% in the 1970s, to 37.8% in the 1980s, and then to 35.5% in the 2000s. Thus, total drought events showed no significant tendency over the historical period, but drought events with more severity decreased gradually from the 1960s to 2000s.

Table 10 Temporal variations in the number of drought events. AM events included all dry degree events, while AS events are for dry events more than severe degree. Numbers in parentheses are the ratio of AS events to AM

events in percentage.

Classification		1960s	1970s	1980s	1990s	2000s
1-month	AM event	610	741	628	717	560
	AS event	344(56.4)	298(40.2)	159(25.3)	270(37.7)	194(34.6)
3-month	AM event	380	456	425	407	361
	AS event	227(59.7)	202(44.3)	148(34.8)	189(46.4)	168(46.5)
6-month	AM event	224	296	328	315	262
	AS event	163(72.8)	151(51.0)	124(37.8)	165(52.4)	93(35.5)
12-month	AM event	122	142	188	187	148
	AS event	97(79.5)	65(45.8)	71(37.8)	102(54.5)	67(45.3)
24-month	AM event	77	108	151	101	111
	AS event	63(81.8)	48(44.4)	73(48.3)	50(49.5)	59(53.2)

Drought event changes might not represent the changes of other drought characteristics due to the association between drought duration, severity, and intensity. The average drought duration or severity was calculated as the average duration or severity for all drought events (SPEI-PM<-1.0). The average drought duration for almost all timescales decreased with fluctuations from the 1960s to the 2000s (Figure 22-A). Compared with the 1960s, the average drought duration in the 2000s decreased by 16.7% for the 1-month timescale, 25.7% for the 3-month timescale, 37.0% for the 6-month timescale, 37.2% for the 12-month timescale, and 33.5% for the 24-month timescale. Drought severity also decreased from the 1960s to 2000s (Figure 22-B). Compared with the 1960s, average drought severity in the 2000s decreased by 38.8% for the 1-month timescale, 44.5% for the 3-month timescale, 64.8% for the 6-month timescale, 66.2% for the 12-month timescale, and 54.9% for the 24-month timescale.

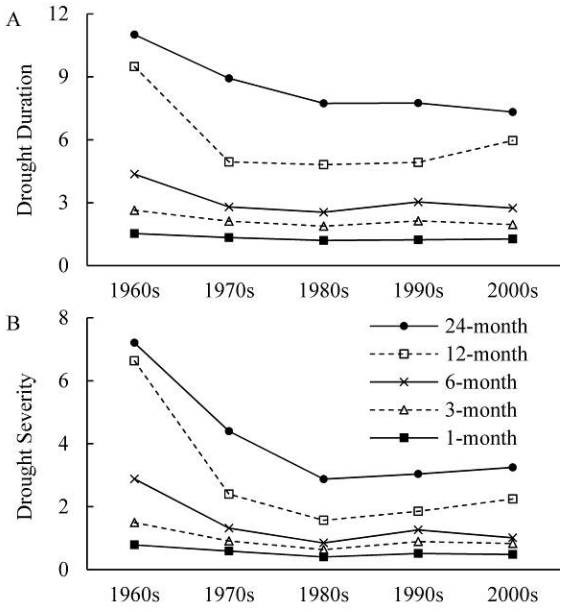

Figure 22 Temporal changes in average drought duration (A) and drought severity (B) for all drought events during

1961—2010.

The average drought intensity for all drought events for each decade shows decreased drought intensity from the 1960s to 2000s (Table 11). For all timescales, drought intensity in the 1960s was strongest during the past 50 years, while the weakest occurred during the 1980s. Compared with the 1960s, the drought intensity in the most recent 10 years was reduced by 23.4% for the 1-month timescale, 17.8% for the 3-month timescale, 37.5% for the 6-month timescale, 49.1% for the 12-month timescale, and 32.5% for the 24-month timescale.

Table 11 Temporal changes in average drought intensity for all drought events in 1961—2010

Timescales	1960s	1970s	1980s	1990s	2000s
1-month	0.47	0.43	0.34	0.41	0.36
3-month	0.45	0.36	0.3	0.35	0.37
6-month	0.48	0.37	0.28	0.36	0.3
12-month	0.53	0.29	0.23	0.28	0.27
24-month	0.4	0.26	0.22	0.27	0.27

Drought prediction for 2010—2099 under RCP 8.5 scenario

Drought evolution under future climate change

The drought evolution map of multi-scale SPEI-PM is shown in Figure 23 for six sub-regions during 2010—2099. Visual comparison of drought maps within each sub-region showed a tendency toward greater drought conditions through 2100. In the 2025s (2010—2040), particularly in the second half of 2020—2030, all regions were mainly characterized by longer wet events. The severe dry event (SPEI-PM<-1.5) during this period can only be found between 2030—2040 with a short dry event for sub-region Ⅰ to Ⅳ (Figure 23 -A-D). In the 2055s (i.e. 2040—2070), except for sub-region Ⅵ (Figure 23 -F) and the end of 2060—2070, longer drought event is predicted to occur frequently, particularly during 2050—2060. In the 2085s (i.e. 2070—2100), drought event is expected to occur persistently with higher frequency and longer duration during 2070—2080 for region Ⅳ to Ⅵ (Figure 23 -D-F) and the end of 2080—2090 for all regions. The main wet years were projected in the middle of 2070—2080 for sub-regions Ⅰ to Ⅲ (Figure 23 -A-C) and the last ten years for sub-regions Ⅰ to Ⅴ (Figure 23 -A-E).

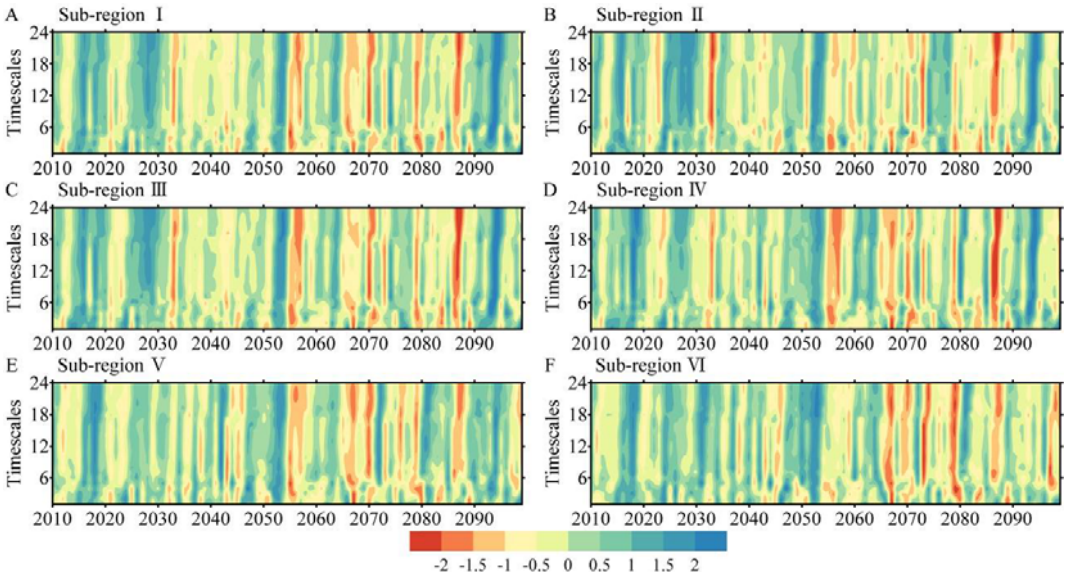

Figure 23 Spatio-temporal evolution of the SPEI-PM series indicating the development of drought from 1 to 24 month-scales at 6 sub-regions under the RCP 8.5 scenario. These maps were obtained with the surfer software.

Temporal variation of future drought characteristics

Table 12 Drought events changes for future weather scenario using the RCP 8.5 climate scenario. AM events represent all dry events while AS events are for severe dry events. Numbers in parentheses are the ratio of AS events to AM events in percentage.

Classification		1981—2010	RCP8.5		
			2025s	2055s	2085s
SPEI-PM1	AM event	1905	1321	2170	2242
	AS event	623(32.7)	360(27.3)	941(43.4)	1183(52.8)
SPEI-PM3	AM event	1193	832	1371	1430
	AS event	505(42.3)	227(27.3)	645(47.0)	825(57.7)
SPEI-PM6	AM event	905	605	981	1015
	AS event	382(42.2)	136(22.5)	483(49.2)	596(58.7)
SPEI-PM12	AM event	523	317	477	530
	AS event	240(45.9)	72(22.7)	251(52.6)	338(63.8)
SPEI-PM24	AM event	363	217	340	464
	AS event	182(50.1)	47(21.7)	198(58.2)	334(72.0)

Changes in the drought events were compared between the three 30-year periods centered on 2025, 2055, and 2085 under the RCP8.5 climate scenario and the recent (1981–2010) historical period (Table 12). Both the AM and AS events were predicted to be lower in the 2025s than in the historical period (1981–2010), indicating a lower drought frequency in the first 30 years in the future. Taking SPEI-PM3 as an example, the drought event in the 2025s was projected to be 30.3% (AM event) and 55.0% (AS event) lower compared with the historical standard. However, the frequency of drought events was predicted to continuously increase in the 2055s and 2085s for all time scales and surpasses that of the 1981—2010

periods. In the case of the SPEI-PM6, compared with the historical period (1981—2010), the results indicated an increase in moderate dry events in the 2055s and the 2085s at the rate of 8.4% and 12.2%, respectively. The ratio of AS events to AM events also showed an increasing trend in the RCP8.5 scenario. For example, the ratio increased from 50.1% in 1981—2010 to 72% in the 2085s for the 24-month timescale, indicating 72% of the drought events in the 2085s are expected to be intense than the severe drought.

Evolution of the duration and severity for all drought events under historical (1981—2010) and future RCP8.5 scenario periods (2010—2099) are shown in Figure 24. Compared with the historical period, the drought duration and severity are predicted to be shorter and weaker in the 2025s, which is similar to past drought events. However, drought duration and severity shows an increasing trend from 2025s to 2085s for all time scales (Figure 24). Compared with the 2025s, the highest increasing rate for drought duration and drought severity in the 2085s is 62.2% (12-timescale) and 188.1% (24-timescale), respectively.

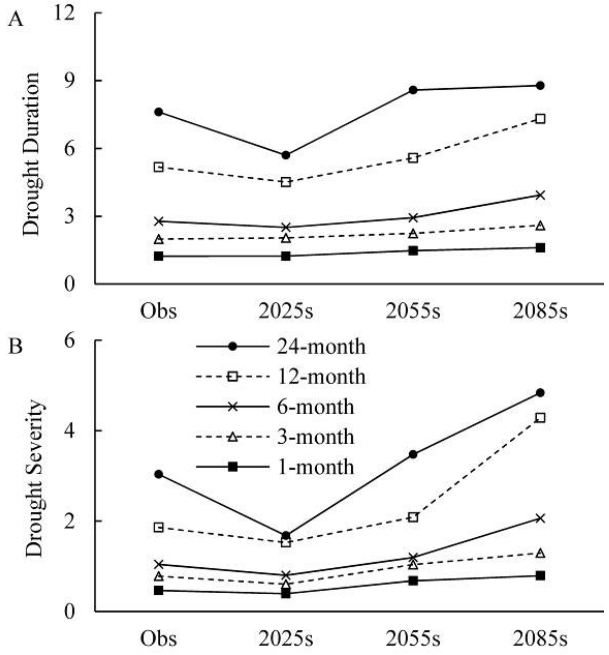

Figure 24 Temporal changes in average drought duration (A) and severity (B) for all drought events under RCP 8.5 scenario. The “obs” indicates the period of 1981—2010.

As shown in Table 13, drought is projected to become more severe in the 2085s. Compared with the 2025s, the intensity was found to be 43.3% (1-month), 61.5% (3-month), 62.5% (6-month), 86.3% (12-month), and 100% (24-month) higher in the 2085s. Similarly, the average drought intensity during the 2025s was projected to be lower than the historical period. Based on these results, while drought components, such as the number of event, duration, and severity tends to be lower in the 2025s, drought risk is predicted to intensify in the 2055s and 2085s, and will be severe in the 2055s and 2085s compared with the historical standards.

Table 13 Temporal changes in average drought intensity for all drought events in 2025s, 2055s, and 2085s under RCP 8.5 scenario

Timescales	1981—2010	RCP 8.5 scenario		
		2025s	2055s	2085s
1-month	0.37	0.32	0.42	0.46
3-month	0.34	0.26	0.39	0.42
6-month	0.31	0.24	0.33	0.39
12-month	0.26	0.22	0.27	0.41
24-month	0.25	0.17	0.24	0.34

5. Discussion

Trend variations between different drought indices

This work has shown that drought characteristics, including duration, intensity, and severity have become moderate over the past 50 years in the 3H Plain based on the verified SPEI-PM index. These results are inconsistent with the previous studies, where northern China was shown to have experienced a warm-drying trend (Yu et al. 2014a; Wang et al. 2015a). This inconsistency is likely due to the use of different indices in previous studies and especially due to the variation in estimating potential evapotranspiration (ET_0) for different indices. For example, PDSI_TH has detected global drying trends in the past decades (Dai 2013; Nam et al. 2015). However, some studies have evaluated the use of PM equation to calculate drought indices and concluded that drought has changed little globally (Sheffield et al. 2012) in China in the past decades (Wang et al. 2015b). To understand the variations between different drought indices in the 3H Plain, the Mann-Kendall trend test using the significant level of α=0.1 and α=0.05 was performed on annual mean SPI, SPEI-TH, and SPEI-PM of 3-month scale for the historical period (Figure 25) and the future RCP8.5 scenario (Figure 26). Stations marked with red inverted triangles in both Figure 25 and Figure 26 are significantly drying areas, and stations marked with blue triangles are significantly wetting areas.

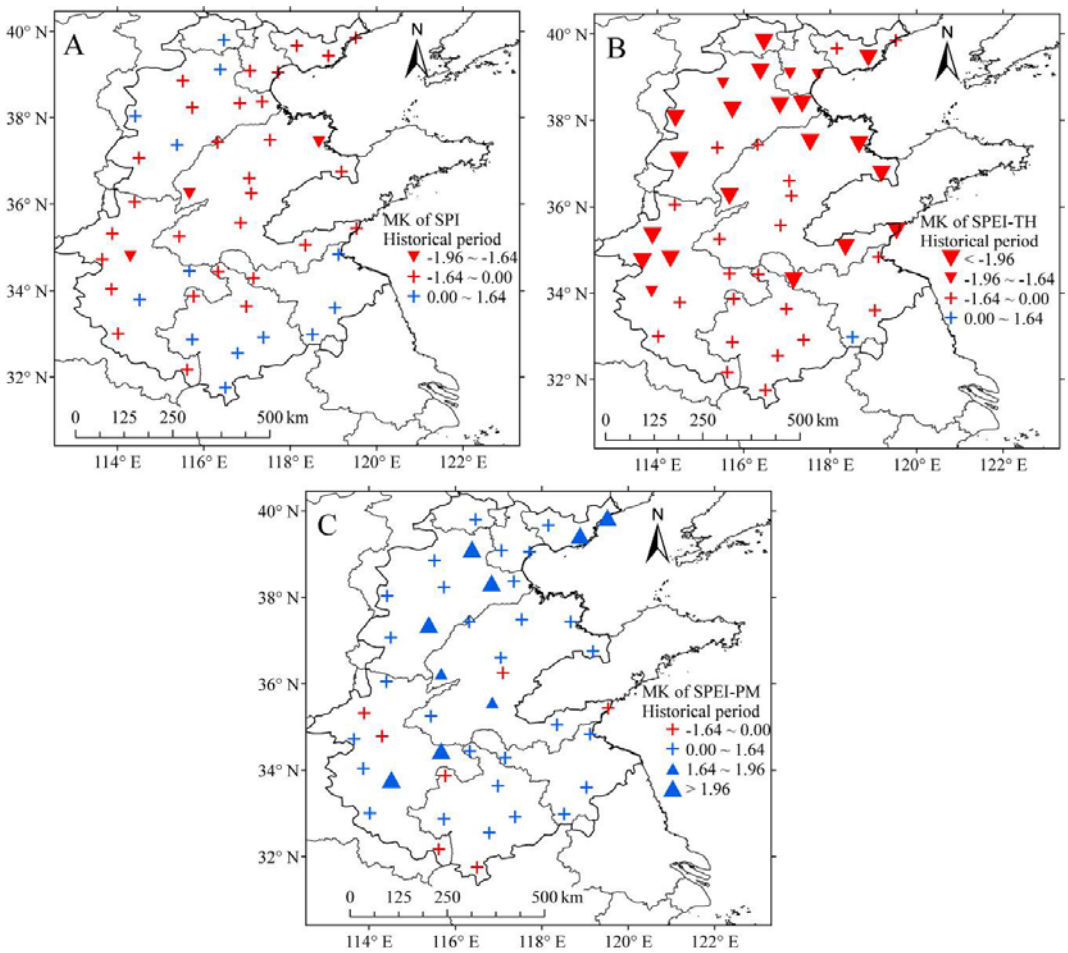

Figure 25 Trend variations of annual SPI-3 (A), SPEI-TH3 (B), and SPEI-PM3 (C) according to Mann-Kendall test and Theil–Sen's slope estimator.in the 3H Plain during 1961—2010. These maps were obtained with the Arcgis software.

In general, the drought trend detected by SPI was driven by precipitation (McKee et al. 1993), while SPEI depends on both precipitation and ET_0 (Vicente-Serrano et al. 2010). For the historical period, precipitation decreased insignificantly by 1.01mm·y^{-1} (Table 14). ET_0-TH gave an increase in ET_0 at 1.32mm·y^{-1}, which further increased water shortages. However, ET_0-PM decreased by 2.11mm·y^{-1}, which made up for decreasing precipitation. Thus, SPI and SPEI-TH showed a drying trend over the 3H Plain (Figure 25-A–B), while the SPEI-PM showed slightly wetter conditions (Figure 25-C). While precipitation is expected to increase by 1.88 mm·y^{-1} in the future period, the amplification of ET_0 by both TH and PM equations counteracted this positive increase in precipitation (Table 14). Thus, SPI predicted wetter conditions in the future period (Figure 26-A). However, SPEI-TH and SPEI-PM predicted that almost all meteorological stations would experience significant drying trends (Figure 26-B–C), except for the southwest regions where SPEI-PM showed an insignificant trend. Thus, for 3H Plain, even if the index takes an account of ET_0 (comparing SPI and SPEI) and how ET_0 is estimated (comparing SPEI-TH and SPEI-PM), it introduces differences in predicted drought trends. Drought hazard assessment should understand these differences and the index being chosen for drought studies should be explained and verified to justify the selected index.

Table 14 Annual trend of precipitation and potential evapotranspiration (ET_0_PM and ET_0_TH) and four major

climatic variables using Mann-Kendall test and Theil–Sen's slope estimator. *and ** represent significant level at P<0.05 and P<0.01, respectively.

Items	Historical period (1961—2010)	RCP8.5 scenario (2010—2099)
Precipitation (mm y^{-1})	-1.01	1.88*
ET_0_TH (mm y^{-1})	1.32**	6.84**
ET_0_PM (mm y^{-1})	-2.11**	3.58**
Daily temperature (℃ 10 y^{-1})	0.24**	0.77**
Relative humidity (% y^{-1})	-0.05*	-0.05*
Wind speed (m s^{-1} y^{-1})	-0.01**	-0.00**
Net solar radiation (MJ m^{-2} y^{-1})	-12.12**	5.19**

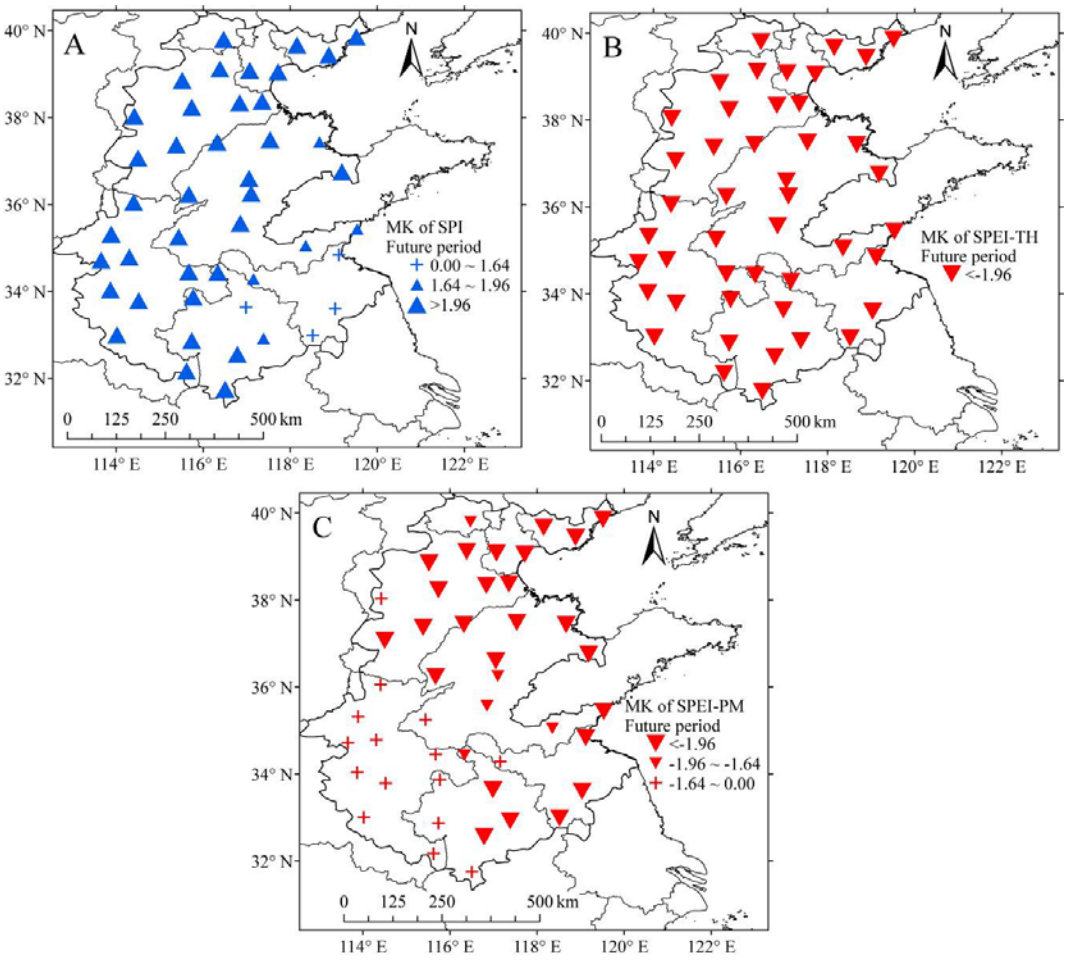

Figure 26 Trend variations of annual SPI-3 (A), SPEI-TH3 (B), and SPEI-PM3 (C) in the 3H Plain using Mann-Kendall test and Theil–Sen's slope estimator under future climate change (2010—2099). These maps were obtained with the Arcgis software.

Applicability of drought index

In this study, the applicability of SPI, SPEI-TH, and SPEI-PM was verified based on observed agricultural drought areas data in the 3H Plain. We found that SPEI-PM has higher correlation level with

historical drought area data. However, it does not mean that SPEI-PM would have the same applicability in other locations or systems. Remarkably, the best drought index for detecting impacts as a function of the analyzed system and the performance of the drought indices varied spatially (Vicente-Serrano *et al.* 2012). For example, the SPI is found to be well correlated with runoff anomaly in China (Zhai *et al.* 2010), while SPEI is better for hydrological application in western Canada.

For agricultural drought assessment, studies comparing the performance of several drought indices, like the ones evaluated in ours and previous studies, would be preferable to determine the best drought index for identifying a certain drought type and its impacts on agricultural systems. Nevertheless, the variable that could better reflect the drought impact for the analyzed system is of considerable importance. In this study, the observed drought area data was used to evaluate the applicability of drought index for agricultural application. Several previous studies (Vicente-Serrano et al. 2012; Potopova et al. 2015; Labudová et al. 2016) have used detrended yield (or climatic yield), by applying the first-difference or a linear regression model to eliminate the effects of technology change influence from actual crop yield, in order to assess the applicability of drought index. However, the reality of these studies were based on the hypothesis that yield fluctuations are mostly attributed to water stress, and agricultural technology is changed linearly (Yu et al. 2012).

Additionally, the comparison between SPEI-PM and SPEI-TH indicated that the way potential evapotranspiration is estimated would make differences in drought applicability and long-term drought trend. This difference has been found in other places of China (Wang et al. 2015b; Xu et al. 2015; Zhang et al. 2015b) and around the world (Sheffield *et al.* 2012; Begueria *et al.* 2014). The Thornthwaite (TH) and Penman-Monteith (PM) are widely used in drought index algorithm. The TH model used for computing potential evapotranspiration in drought assessment is popularly used due to its simplicity and less data requirements (only temperature), such as in original SPEI and PDSI indices. Chen et al. (2005) concluded that the TH method overestimates ET_0 in southeast China where ET_0 is low, and underestimates in the northern and northwest parts where ET_0 is high when compared to pan data, and it does not follow the temporal variation well. Instead, PM equation is the most reliable estimation and is recommended by the FAO to calculate crop water requirements(Allen *et al.* 2005). Thus, looking at the better applicability of SPEI-PM and estimation results, we recommend using Penman-Monteith equation to calculate drought index in 3H Plain.

6. Conclusion

The drought characteristics was investigated using “run theory” for both historical and future climate change under RCP 8.5 scenario in the 3H Plain based on the preferable drought index, i.e. SPEI-PM, selected among SPI and SPEI-TH. The results can be summarized as follows:

(1) In Huang-Huai-Hai Plain (3H Plain), SPEI based on FAO-56 Penman-Monteith (PM) formula, i.e. SPEI-PM, is more suitable for agricultural drought impact analysis as it has higher correlation coefficients with historical drought area data than SPI and traditional SPEI.

(2) Based on calculations using the SPEI-PM, although total drought events showed no significant tendency over the historical period, the decreasing potential evapotranspiration reduced the drought duration, severity, and intensity from the 1960s to the 2000s.

(3) Compared with the historical period, drought characteristics, including the frequency, duration, severity, and intensity tend to be lower in the first thirty years in the future RCP 8.5 scenario. However, it is predicted to be intensified in the 2055s and the 2085s, and will become very serious by historic standards after the 2055s.

Acknowledgements

This research was supported by the National Basic Research Program of China (973 Program) (2012CB955904), the 12th five-year plan of the National Key Technologies R&D Program (2012BAD09B01), and the National Science Foundation for Young Scientists of China (41401510). We thank the University of Liège-Gembloux Agro-Bio Tech and more specifically the research platform AgricultureIsLife for the funding of the scientific stay in Belgium that made this paper possible. We gratefully acknowledge the anonymous reviewers for their valuable comments on the manuscript.

7. References

Ahlgren, P., Bo, J. and Rousseau R.,2003. Requirements for a cocitation similarity measure, with special reference to Pearson's correlation coefficient. Journal of the Association for Information Science and Technology, 54(6): 550–560.

Allen C D, Macalady A K, Chenchouni H, Bachelet D, McDowell N, Vennetier M, Kitzberger T, Rigling A, Breshears D D, Hogg E H, Gonzalez P, Fensham R, Zhang Z, Castro J, Demidova N, Lim J-H, Allard G, Running S W, Semerci A, Cobb N. 2010. A global overview of drought and heat-induced tree mortality reveals emerging climate change risks for forests. Forest Ecology and Management, 259, 660-684.

Allen R G, Pereira L S, Smith M, Raes D, Wright J L. 2005.FAO-56 dual crop coefficient method for estimating evaporation from soil and application extensions.Journal of Irrigation and Drainage Engineering-Asce, 131, 2-13.

Begueria S, Vicente-Serrano S M, Reig F, Latorre B. 2014. Standardized precipitation evapotranspiration index (SPEI) revisited: parameter fitting, evapotranspiration models, tools, datasets and drought monitoring. International Journal of Climatology, 34, 3001-3023.

Chen D L, Gao G, Xu C Y, Guo J, Ren G Y. 2005. Comparison of the Thornthwaite method and pan data with the standard Penman-Monteith estimates of reference evapotranspiration in China. Climate Research, 28, 123-132.

Chen H, Wang J, Huang J. 2014. Policy support, social capital, and farmers' adaptation to drought in China.Global Environmental Change, 24, 193-202.

Dai A. 2011a. Characteristics and trends in various forms of the Palmer Drought Severity Index during 1900–2008.Journal of Geophysical Research: Atmospheres, 116, D12115.

Dai A. 2011b. Drought under global warming: a review.Interdisciplinary Reviews: Climate Change, 2, 45-65.

Dai A. 2013. Increasing drought under global warming in observations and models.Nature Climate Change, 3, 171-171.

Gurrapu S, Chipanshi A, Sauchyn D, Howard A. 2014. Comparison of the SPI and SPEI on predicting drought conditions and streamflow in the Canadian prairies.Proceedings of the 28th Conference of Hydrology-94th American Meteorological Society Annual Meeting, 10, 2-6.

Hayes M, Svoboda M, Wall N, Widhalm M. 2011. THE LINCOLN DECLARATION ON DROUGHT INDICES.Bulletin of the American Meteorological Society, 92, 485-488.

Heim R R. 2002. A Review of Twentieth-Century Drought Indices Used in the United States.Bulletin of the American Meteorological Society, 83, 1149-1165.

Huang Y, Wang J, Jiang D, Zhou K, Ding X, Fu J. 2014. Surface water deficiency zoning of China based on surface water deficit index (SWDI). Water Resources, 41, 372-378.

Labudová L, Labuda M, Takáč J. 2016. Comparison of SPI and SPEI applicability for drought impact assessment on crop production in the Danubian Lowland and the East Slovakian Lowland.Theoretical and Applied Climatology, DOI:10.1007/s00704-00016- 01870-00702.

Leng G, Tang Q, Rayburg S. 2015. Climate change impacts on meteorological, agricultural and hydrological droughts in China. Global and Planetary Change, 126, 23-34.

Li Y, Huang H, Ju H, Lin E, Xiong W, Han X, Wang H, Peng Z, Wang Y, Xu J, Cao Y, Hu W. 2015. Assessing vulnerability and adaptive capacity to potential drought for winter-wheat under the RCP 8.5 scenario in the Huang-Huai-Hai Plain.

Agriculture, Ecosystems & Environment, 209, 125-131.

Lu C, Fan L. 2013. Winter wheat yield potentials and yield gaps in the North China Plain. Field Crops Research, 143, 98-105.

McKee T B, Doesken N J, Kleist J. 1993. The relationship of drought frequency and duration to time scales.Proceedings of the 8th Conference on Applied Climatology, 17, 179-183.

Mei X, Kang S, Yu Q, Huang Y, Zhong X, Gong D, Huo Z, Liu E. 2013. Pathways to Synchronously Improving Crop Productivity and Field Water Use Efficiency in the North China Plain.Scientia AgriculturaSinica, 46, 1149-1157.

Ming B, Guo Y Q, Tao H B, Liu G Z, Li S K, Wang P. 2015. SPEIPM-based research on drought impact on maize yield in North China Plain.Journal of Integrative Agriculture, 14, 660-669.

Mishra A K, Desai V R. 2005. Drought forecasting using stochastic models.Stochastic Environmental Research and Risk Assessment, 19, 326-339.

Nam W-H, Hayes M J, Svoboda M D, Tadesse T, Wilhite D A. 2015. Drought hazard assessment in the context of climate change for South Korea.Agricultural Water Management, 160, 106-117.

Potopova V, Stepanek P, Mozny M, Tuerkott L, Soukup J. 2015. Performance of the standardised precipitation evapotranspiration index at various lags for agricultural drought risk assessment in the Czech Republic.Agricultural and Forest Meteorology, 202, 26-38.

Sentelhas P C, Gillespie T J, Santos E A. 2010. Evaluation of FAO Penman-Monteith and alternative methods for estimating reference evapotranspiration with missing data in Southern Ontario, Canada.Agricultural Water Management, 97, 635-644.

Sheffield J, Wood E F, Roderick M L. 2012.Little change in global drought over the past 60 years.Nature, 491, 435-438.

Sillmann J, Kharin V V, Zwiers F W, Zhang X, Bronaugh D. 2013. Climate extremes indices in the CMIP5 multimodel ensemble: Part 2.Future climate projections.Journal of Geophysical Research-Atmospheres, 118, 2473-2493.

Sun J, Liu Y. 2013. Responses of tree-ring growth and crop yield to drought indices in the Shanxi province, North China. International Journal of Biometeorology, 58, 1521-1530.

Trenberth K E, Dai A, van der Schrier G, Jones P D, Barichivich J, Briffa K R, Sheffield J. 2014. Global warming and changes in drought.Nature Climate Change, 4, 17-22.

Vicente-Serrano S M, Begueria S, Lopez-Moreno J I. 2010.A Multiscalar Drought Index Sensitive to Global Warming: The Standardized Precipitation Evapotranspiration Index.Journal of Climate, 23, 1696-1718.

Vicente-Serrano S M, Begueria S, Lopez-Moreno J I. 2011. Comment on "Characteristics and trends in various forms of the Palmer Drought Severity Index (PDSI) during 1900-2008" by Aiguo Dai. Journal of Geophysical Research-Atmospheres, 116, D19112.

Vicente-Serrano S M, Beguería S, Lorenzo-Lacruz J, Camarero J J, López-Moreno J I, Azorin-Molina C, Revuelto J, Morán-Tejeda E, Sanchez-Lorenzo A. 2012. Performance of Drought Indices for Ecological, Agricultural, and Hydrological Applications.Earth Interactions, 16, 1-27.

Wang H, Chen A, Wang Q, He B. 2015a.Drought dynamics and impacts on vegetation in China from 1982 to 2011.Ecological Engineering, 75, 303-307.

Wang L, Chen W. 2014. A CMIP5 multimodel projection of future temperature, precipitation, and climatological drought in China.International Journal of Climatology, 34, 2059-2078.

Wang W, Zhu Y, Xu R, Liu J. 2015b. Drought severity change in China during 1961–2012 Indicated by SPI and SPEI.Natural

Hazards, 75, 2437-2451.

Wilhite D A, Sivakumar M V K, Pulwarty R. 2014. Managing drought risk in a changing climate: The role of national drought policy.Weather and Climate Extremes, 3, 4-13.

Wilhite D A, Svoboda M D, Hayes M J. 2007. Understanding the complex impacts of drought: A key to enhancing drought mitigation and preparedness.Water Resources Management, 21, 763-774.

Xu K, Yang D, Yang H, Li Z, Qin Y, Shen Y. 2015. Spatio-temporal variation of drought in China during 1961–2012: A climatic perspective.Journal of Hydrology, 526, 253-264.

Xu L, Wang H, Duan Q, Ma J. 2013. The Temporal and Spatial Distribution of Droughts During Summer Corn Growth in Yunnan Province Based on SPEI. Resources Science, 35, 1024-1034.

Yang J, Mei X, Huo Z, Yan C, Ju H, Zhao F, Liu Q. 2015. Water consumption in summer maize and winter wheat cropping system based on SEBAL model in Huang-Huai-Hai Plain, China. Journal of Integrative Agriculture, 14, 2065-2076.

Yevjevich V. 1967.An objective approach to definitions and investigations of continental hydrologic droughts. Hydrology Paper 23, Colorado State University, Fort Collins, CO, 18pp.

Yong B, Ren L, Hong Y, Gourley J J, Chen X, Dong J, Wang W, Shen Y, Hardy J. 2013. Spatial–Temporal Changes of Water Resources in a Typical Semiarid Basin of North China over the Past 50 Years and Assessment of Possible Natural and Socioeconomic Causes. Journal of Hydrometeorology, 14, 1009-1034.

Yu M, Li Q, Hayes M J, Svoboda M D, Heim R R. 2014a. Are droughts becoming more frequent or severe in China based on the Standardized Precipitation Evapotranspiration Index: 1951-2010? International Journal of Climatology, 34, 545-558.

Yu Q, Li L, Luo Q, Eamus D, Xu S, Chen C, Wang E, Liu J, Nielsen D C. 2014b. Year patterns of climate impact on wheat yields. International Journal of Climatology, 34, 518-528.

Yu Y, Huang Y, Zhang W. 2012. Changes in rice yields in China since 1980 associated with cultivar improvement, climate and crop management. Field Crops Research, 136, 65-75.

Zhai J, Su B, Krysanova V, Vetter T, Gao C, Jiang T. 2010. Spatial Variation and Trends in PDSI and SPI Indices and Their Relation to Streamflow in 10 Large Regions of China.Journal of Climate, 23, 649-663.

Zhang H-L, Zhao X, Yin X-G, Liu S-L, Xue J-F, Wang M, Pu C, Lal R, Chen F. 2015a. Challenges and adaptations of farming to climate change in the North China Plain. Climatic Change, 129, 213-224.

Zhang J, Sun F, Xu J, Chen Y, Sang Y, Liu C. 2015b. Dependence of trends in and sensitivity of drought over China (1961-2013) on potential evaporation model.Geophysical Research Letters, 43, 206-213.

Zhang X, Chen S, Sun H, Shao L, Wang Y. 2011. Changes in evapotranspiration over irrigated winter wheat and maize in North China Plain over three decades. Agricultural Water Management, 98, 1097-1104.

Zhang X Y, Chen S Y, Liu M Y, Pei D, Sun H Y. 2005. Improved water use efficiency associated with cultivars and agronomic management in the North China Plain. Agronomy Journal, 97, 783-790.

Chapter IV. Potential effect of drought on winter wheat yield using CERES-Wheat model

Potential effect of drought on winter wheat yield using CERES-Wheat model over the Huang-Huai-Hai Plain

Submitted in Journal of Integrative Agriculture, 2017

Qin Liu, Sarah Garré*, Hui Ju, Xiangxiang Li

** Corresponding author*

outline

The following objectives will be addressed in this research: (1) an investigation of the trends of irrigation requirements over 12 selected locations during the last 35 years; (2) the evaluation of the potential impact of drought on the winter wheat yield using DSSAT; and (3) the establishment of the probability distribution of the yield reduction of 12 typical sites over the Huang-Huai-Hai Plain. The results are expected to provide basic information for drought management and the rational irrigation of winter wheat on the 3H Plain by focusing on the potential effects of drought in the critical growth stages of winter wheat.

1. Abstract

The Huang-Huai-Hai Plain (3H Plain) is recognized as a major crop-producing area that encompasses 19% of the total arable land in China and has experienced serious droughts and water scarcity problems in recent years. In this paper, the potential impacts of drought on wheat yield were determined at twelve stations representing different locations on the 3H Plain. The CERES-Wheat model is used to simulate the effects of a designed irrigation schedule on wheat yield. The cumulative probability of the yield reduction rate during the jointing to heading stage and the filling stage was investigated to determine the impacts of drought on the wheat yield during these two critical water demand periods. The results indicated that a significant gap between the actual and potential yields is seen, which can be attributed to the water stress and changes in the management inputs. The yield reduction rate for wheat was much larger during the jointing to heading stage than in the filling stage, with spatial variability due to the different meteorological conditions over the plain. The yield reduction rate under the same drought condition was much higher during the jointing to heading stage than in the filling stage. The cumulative probability of the yield reduction rate was higher during the jointing to heading stage in the north region than in the south region. The findings from this study provide basic information for drought management and the rational irrigation of winter wheat on the 3H Plain by focusing on the potential effects of drought during the critical growth stages of winter wheat.

Keywords:

Huang-Huai-Hai Plain; CERES-Wheat model; simulated yield; drought; critical grow periods

2. Introduction

Drought is one of the most damaging and widespread climate extremes, negatively affecting agricultural production, water resources, ecosystem function and human lives around the world (Dilley et al. 2005, Wilhite et al. 2007, Dai 2011). In China, drought has had large impacts on agricultural production, seriously challenging the sustainability of the food supply and security. Additionally, with projected increasing temperatures and changing precipitation distributions, the drought characteristics are expected to change (Sillmann et al. 2013, Wang et al. 2015, Liu et al. 2017) and subsequently make crop production levels more uncertain. The Intergovernmental Panel on Climate Change (IPCC) has reported that the period of 1980—2012 was the hottest period in the past 1400 years, with the global temperature increasing by approximately 0.85 °C totally (Gray 2010). Although the enhanced atmospheric CO_2 level will increase the rate of photosynthesis, the adverse impacts resulting from the increasing temperature and changing water availability will probably outweigh the advantages of the higher CO_2 concentration (Wassmann et al. 2009), especially if the average temperature increases by more than 3 °C (Attri and Rathore 2003). Researchers have already reported a decline in the productivity of wheat due to an increase in the temperature in China (Kouadio et al. 2015, Yang et al. 2014, Wilcox and Makowski 2014).

The Huang-Huai-Hai Plain (3H Plain) is a major crop producing area in China that encompasses 19% of the total arable land in China and has experienced serious droughts and water scarcity problems in recent years(Yong et al. 2013), representing the limiting factor for agricultural production (Zhang et al. 2015). Water limitations will likely be exacerbated in the future by increased food demand, soil quality deterioration and the over-exploitation of groundwater resources (Yang et al. 2015). Climate variability, especially extreme events such as drought, may result in a fluctuation of crop yields (Lu and Lan 2013, Yu et al. 2011). Thus, understanding the potential impact of drought on crop yields is necessary to reduce the vulnerability of the current food production and establish mitigation strategies for agriculture in the 3H Plain.

Conventionally, earlier studies have focused on the yield reduction for winter wheat due to water stress during the critical stage of water demand (Lv et al. 2007a, Wu et al. 2002). Furthermore, the impact of drought on the crop yield was evaluated in a manually controlled water supply field and using a computer simulation experiment at a single station to support the irrigation practice. However, less research has evaluated the DSSAT model's performance in estimating the drought risk and drought impact on crop yield at typical growth stages. Drought is widely accepted to be the most serious agricultural meteorological disaster in the Huang-Huai-Hai Plain (Wang et al. 2016). Accordingly, there is an urgent demand for conducting a study to analyze and evaluate the effects of drought that lead to crop yield reductions in areas of limited water resources.

DSSAT has been widely used for yield gap analysis, decision making and planning, strategic and tactical management decisions and climate change studies in Asia (Singh and Thornton 1992, Jalota et al. 2014, Pathak et al. 2003, He et al. 2013). The following objectives will be addressed in this research: (1) an investigation of the trends of irrigation requirements over 12 selected locations during the last 35 years; (2)

the evaluation of the potential impact of drought on the winter wheat yield using DSSAT; and (3) the establishment of the probability distribution of the yield reduction of 12 typical sites over the Huang-Huai-Hai Plain. The results are expected to provide basic information for drought management and the rational irrigation of winter wheat on the 3H Plain by focusing on the potential effects of drought in the critical growth stages of winter wheat.

3. Materials and methods

Study region and data description

Study region

The Huang-Huai-Hai Plain (3H Plain) is located in northern China, extending over 31°14′—40°25′N and 112°33′—120°17′E, with 23.3 million ha of arable land (19% of the total in China), providing approximately 70% of the national wheat production and 30% of the national maize production with a dominant winter wheat-summer maize double-cropping system (Yang et al. 2015). The 3H Plain belongs to the extratropical monsoon climatic region. The annual mean precipitation is 348.5 mm, with more than 70% falling in July to September, and the atmospheric evaporative demand is approximately 1000 mm/year (Zhang et al. 2011a). For the wheat-maize rotation system, rainfall can only meet 65% of the total agricultural water usage, and for winter wheat, only 25% – 40% of the water demand is satisfied by rainfall (Mei et al. 2013). Irrigation water is primarily pumped from groundwater, and the groundwater level has decreased from a depth of 10 m in the 1970s to 32 m in 2001 and has continued to decrease at a rate of 1 m per year (Zhang et al. 2015). Thus, drought in this region not only challenges food supplies, but it also results in a series of environmental problems.

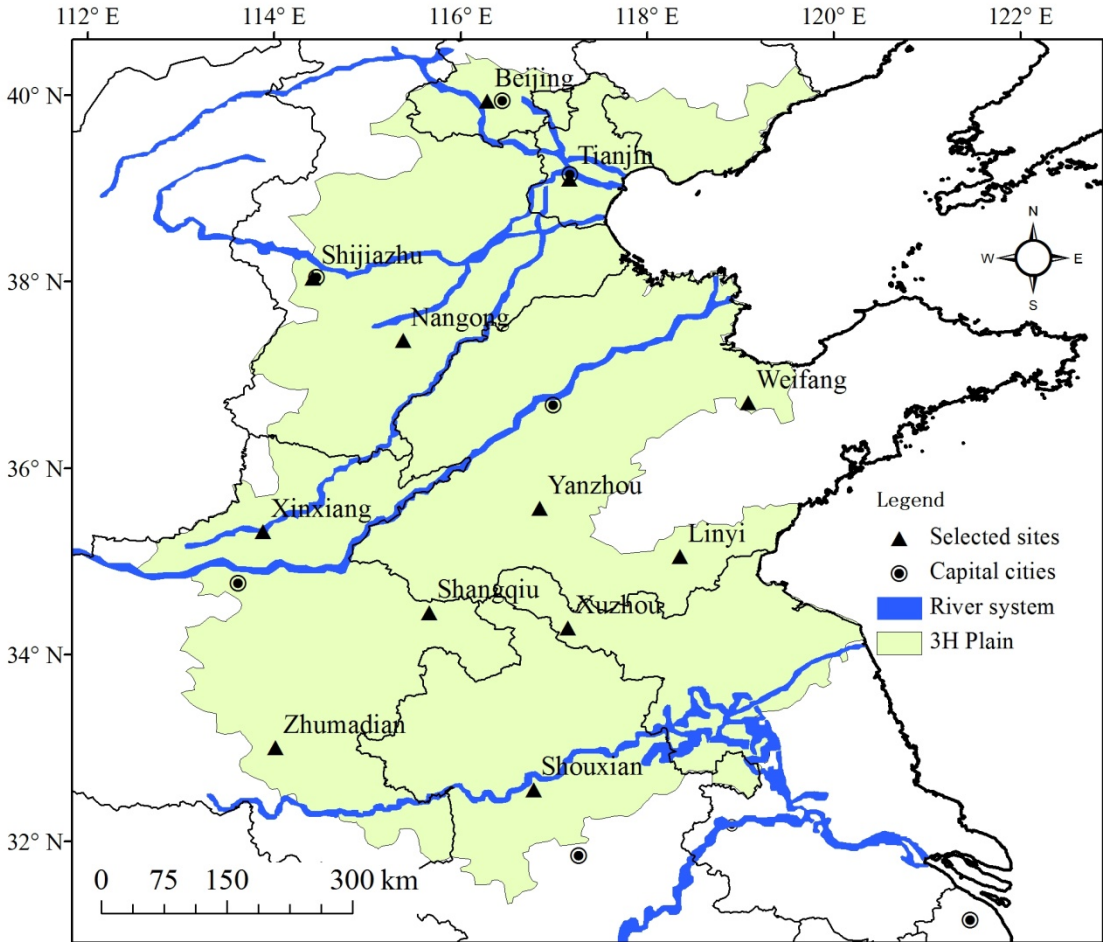

Figure 27 Location of the 12 agrometeorological stations in this study. The upper blue line is Hai River and the middle, below blue one is Yellow and Huai River, respectively. The meteorological stations were selected based on data accessibility and the principle of uniform distribution in six agricultural sub-regions over the Huang-Huai-Hai plain.

Table 15 Information of selected twelve stations in Huang-Huai-Hai Plain. The values described in this table were average data for precipitation, temperature and solar radiation during the winter wheat growing period in 1981-2010.

Station	Longitude	Latitude	Location	Precipitation (mm)	Temperature (℃)	Solar radiation ($MJ \cdot m^{-2}$)
Mi Yun	116°17	39°56′	North	213.2	7.9	3684.8
TianJin	117°43′	39°03′	North	192.6	9.5	3760.8
Luan Cheng	114°25′	38°02′	West	180.0	10.3	3748.7
Nan Gong	115°23′	37°22′	Central	178.2	10.5	3922.1
Yan Zhou	116°51′	35°34′	Central	270.9	10.6	3893.9
Wei Fang	119°11′	36°45′	East	233.8	9.6	3997.1
Lin Yi	118°21′	35°03′	East	324.1	10.9	3993.6
Xin Xiang	113°53′	35°19′	West	215.6	11.6	3769.3
Zhu Ma Dian	114°01′	33°	South	470.0	12.3	3606.3
ShangQiu	115°40′	34°27′	Central	315.1	11.5	3650.6
Xu Zhou	117°29′	34°17′	Central	369.7	11.8	3859.7
Shou Xian	116°47′	32°33′	South	509.6	12.3	3778.3

Meteorological data

The daily weather data, including precipitation (mm), maximum and minimum temperatures (℃), wind speed (m/s), relative humidity (%) and sunshine hours (h), recorded at meteorological observatories located in the region were collected from the China Meteorological Administration (CMA). The district wheat yield data were collected from the Directorate of Wheat during the study period.

Methodology

Calculation of precipitation deficit for winter wheat

In this study, the simulated irrigation amount was confirmed according to the practical situation and

the precipitation deficit (PD) during the jointing to heading stage and the anthesis to milk stage.

$$\mathrm{PD} = P_e - ET_c \quad \text{Formula 14}$$

where ET_c is the accumulative water requirement for winter wheat (mm) and P_e is the accumulative effective precipitation (mm).

Effective precipitation (P_e) is the amount of precipitation that is actually added and stored in the soil. During drier periods less than 5mm of daily rainfall would not be considered effective, as this amount of precipitation would likely evaporate from the surface before soaking into the ground (Smith 1992).

$$P_e = \begin{cases} P(4.17 - 0.2P)/4.17 & P < 8.3 \\ 4.17 + 0.1P & P \geq 8.3 \end{cases} \quad \text{Formula 15}$$

where P_e is the daily effective precipitation (mm/d), P is the daily precipitation.The crop coefficients vary between different crops and regions. In addition, they change based on the growing stage of the crop. In this study, the winter wheat coefficient was developed by the FAO, and a daily wheat coefficient can be obtained in relation to the climatic conditions for the phenological phases for winter wheat(Allen et al. 1998).

The irrigation schedule can be drawn through the investigation of the water consumption in different irrigation systems to make an appropriate irrigation programme under climate change (Cabelguenne et al. 1997, Santos et al. 2000). The simulated irrigation schedule was designed with four treatments in this study according to the practical situation on the basis of the same or other cultivation management measures. As shown in Table 16, CK is the treatment of full irrigation or no water stress and T1, T2, and T3 are the treatments with instead of no irrigation during the jointing and heading stage, filling stage and both stages, respectively.

Table 16 Simulated irrigation schedules based on fixed dates and precipitation deficit. PD1 indicates precipitation deficit at jointing to heading stage. PD2 indicates precipitation deficit at filling stage.

Treatment	Irrigation volume in winter (mm)	Irrigation volume at jointing stage (mm)	Irrigation volume at filling stage (mm)
CK	60	PD1	PD2
T1	60	0	PD2
T2	60	PD1	0
T3	60	0	0

Crop model description

Crop models can be used to analyse the effects of various climatic factors on crop growth and yield considering the interactions with edaphic, biotic and agronomic factors. DSSAT is an integrated software comprising different computer programs that can simulate crop growth and yield for research and decision-making. Its latest version DSSAT ver. 4.6.1.0 (http://dssat.net/downloads/dssat-v46) includes Cropping System Model (CSM), the primary modules of which are consisted by weather module, soil module,

soil-plant-atmosphere module, management operation module and 27 individual plant growth modules. Each plant growth is a separate module to simulate phenomenon, biomass and yield, based on the soil water and fertility supplement in response to weather and management (Jones et al. 2003). The model offers options to change the irrigation schedule to simulate plausible climatic drought effects on the crop. The DSSAT Crop Environment Resource Synthesis (CERES)-wheat model (He et al. 2013, He et al. 2012) was adopted here to simulate the wheat yield during 1981–2014 at all twelve locations. Much work has been done on the impacts of climate change, irrigation scheduling and water and fertilizer conditions on the crop yield using DSSAT in China (Hui et al. 2005, Jiang et al. 2016, Yang et al. 2013, Yang et al. 2010).

Statistical tests for trend analysis

Recent studies suggest that non-parametric tests are more suitable for non-normally distributed and censored data, which are frequently encountered in meteorological and hydrological time series. Among them, the non-parametric Mann-Kendall test (Mann 1945, Kendall 1975) is a widely accepted method for trend analysis in hydrological and meteorological series (Jhajharia *et al.* 2012, Zheng and Wang 2014), with little effect from the presence of outliers in the data. In addition, it is highly recommended for general use by the World Meteorological Organization (Zhang et al. 2011b). Therefore, we used the Mann-Kendall test for the trend analysis of our data. The magnitudes of the trends in the time series were estimated using the non-parametric Theil–Sen slope (Sen 1968, Theil 1992), which is robust because it is resistant to the effects of outlier values in the observations (Jhajharia et al. 2015, Su et al. 2015).

4. Results

DSSAT evaluation

The DSSAT model (CERES-Wheat) was calibrated and validated by changing the genetic coefficients (Table 17) to simulate the observed phenological growth and yield of wheat for approximately five years over the Huang-Huai-Hai Plain. The model simulates the crop duration, anthesis and maturity periods within 5 days' advance or delay compared to the observed data. Figure 28 presents a comparison of the observed and simulated wheat yields for the entire calibration and validation period . The model simulates the wheat yield with a coefficient of determination (R^2) value of 0.81 for wheat. The normalized root mean square error (NRMSE) is estimated to be, on average, 8.5 kg/ha for wheat. The overall results show an appropriate capability of the model to simulate the yield of winter wheat, and therefore it may be used to simulate the wheat yield to analyse the various aspects of climatic drought (Wen and Chen 2011).

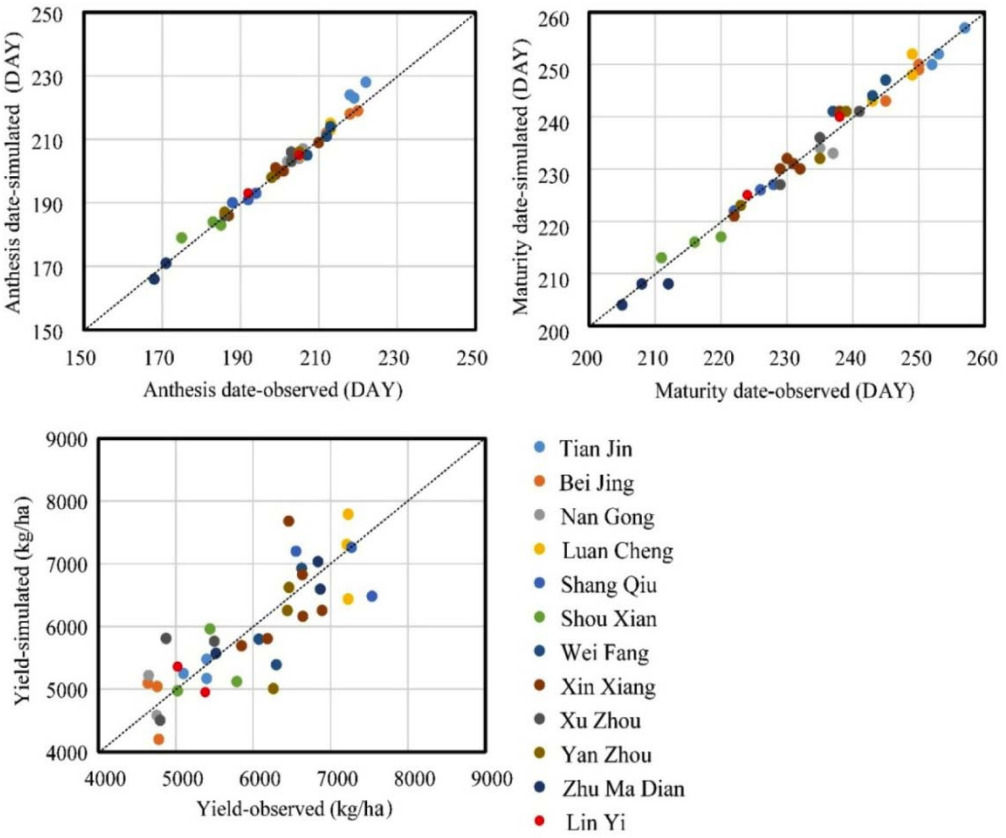

Figure 28 Comparison of observed and simulated dates of anthesis and maturity stage (d) and yields (kg/ha) for the entire calibration and validation period.

Table 17 Statistics of observed and simulated dates of flowering and maturity stage and yields. P1V is vernalization parameter (d). P1D is photoperiod parameter (%). P5 is grain filling duration parameter (°C d). G1 is grain parameter at anthesis (no g^{-1}). G2 is grain filling rate parameter (mg). G3 is dry weight of a single stem and spike (g). PHINT is interval between successive leaf tip appearances (°C d).

Station	Cultivar	P1V (d)	P1D (%)	P5 (°C d)	G1 (no g^{-1})	G2 (mg)	G3 (g)	PHINT (°C d)	NRMSE		
									Anthesis (d)	Maturity (d)	Yield (kg/ha)
Miyun	Jingdong8	58.34	31.65	536.30	25.75	24.80	1.18	95	0.27	0.52	9.64
Tianjin	Jing9428	44.23	72.63	513.20	23.86	20.46	1.91	95	2.47	0.51	3.08
Shijiazhuang	Shixin733	11.38	75.43	708.30	18.80	35.29	1.02	95	0.61	0.74	7.79
Nangong	Han6172	22.84	53.22	462.60	23.51	26.55	1.05	95	0.49	1.02	10.00
Yanzhou	Jining16	21.87	50.31	579.40	15.80	45.54	1.09	95	0.42	0.90	11.56
Weifang	Jimai22	6.42	61.77	559.30	27.19	56.80	1.01	95	0.67	1.09	9.08
Linyi	Linmai4	44.36	55.41	593.5	25.89	30.68	1.307	95	0.36	0.68	7.39
Xinxiang	Xinmai6	41.67	53.09	554.40	25.68	23.90	1.15	95	0.54	0.77	9.66
Zhumadian	Zhengmai9023	39.78	4.59	604.50	16.67	62.84	1.00	95	0.68	1.14	3.08
Shangqiu	Wenmai8	61.93	18.46	548.60	26.21	33.92	1.12	95	0.74	0.26	10.03
Xuzhou	Xuzhou25	36.44	59.54	614.90	24.23	28.86	1.01	95	0.88	0.55	11.57
Shouxian	Wanmai27	55.55	15.83	524.10	15.23	46.41	1.01	95	1.46	0.97	9.00

Trends and persistence of typical growth date and precipitation deficit

The annual magnitudes of the jointing date, heading date, anthesis date and milk ripe date for winter wheat for the selected twelve stations from 1981 to 2014 are described in Table 18. The linear regression is characterized by the fact that the jointing date had a declining trend for all the selected stations. The jointing date occurred earlier:-2.4 and -4.0d·decade^{-1} by the M–K test for the north and west stations, respectively, in the past 34 years. Similarly, for the central, east and south stations, significant shifts to earlier jointing of -3.4, -1.1 and -7.4 d·decade^{-1}, respectively, were detected. Consequently, the heading date also shifted by -3.0d·decade^{-1} for both the north and west stations, while the anthesis date shifted by -2.9 and -1.7d·decade^{-1}, respectively. Furthermore, for the central, east and south stations, significant decreases in magnitude of -3.3, -1.3 and -7.1 d·decade^{-1}, respectively, were found, and the values were 2.7, -0.3 and -5.9 d·decade^{-1} for anthesis. Finally, the milk ripe date also shifted by -1.9 and -1.8 d·decade^{-1} in the north and south stations, while it shifted to later dates in the west, central and east stations. The largest decrements were found for the jointing date, followed by the heading date and anthesis date.

As indicated in Table 18, the precipitation deficit (-66.5mm on average) during the jointing to heading stage was slightly greater than that (-42.1) during the anthesis to milk ripe stage. Smaller fluctuations were found during the anthesis to milk ripe stage for the 12 selected stations, with the range of 20—40mm. The precipitation deficit reached its smallest values in the north, east and central stations during the jointing to heading stage and in the west and central stations during the filling stage, and the largest values for both were in the two southern stations. The value of the precipitation deficit is the input of the DSSAT simulation. Santos et al. (2000) reported that the investigation of the water demand under different irrigation systems can serve the purpose of determining the optimal irrigation schedule.

Table 18 Variation of typical growth date for wheat and precipitation deficit (PD) during typical growth stages in 1981-2010. The slope (d·decade^{-1}) means the temporal trend in jointing, heading, anthesis and milk ripe date of winter wheat in 1981-2010 using Mann-Kendall test and Theil–Sen's slope estimator.

Station	Jointing date		Heading date		Anthesis date		Milk ripe date		PD during jointing to heading stage	PD during anthesis to milk ripe stage
	Mean (d)	Slope (d·decade^{-1})	Mean (d)	Slope (d·decade^{-1})	Mean (d)	Slope (d·decade^{-1})	Mean (d)	Slope (d·decade^{-1})	Mean (mm)	Mean (mm)
Miyun	113	-4.0**	132	-2.4**	137	-2.6**	154	-1.5**	-73.9	-48.1
Tianjin	108	-0.8**	128	-3.6**	133	-3.1**	148	-2.2**	-77.3	-26.7
Shijiazhuang	99	-2.4**	120	-2.6**	127	-1.8**	140	-1.2**	-78.2	-38.5
Nangong	94	0.5**	117	-2.9**	124	-2.2**	141	-0.3**	-91.0	-53.6
Yanzhou	90	-4.2**	114	-3.1**	121	-3.1**	142	1.4	-72.8	-43.6
Weifang	101	-0.7	122	-0.7**	128	1.2**	147	1.2**	-85.9	-36
Linyi	97	-1.4	120	-1.9**	127	-1.7**	147	0.7**	-77.3	-45.3
Xinxiang	87	-5.5**	113	-3.3**	120	-1.6**	138	1.3**	-53.7	-55.2
Zhumadian	79	-7.9**	105	-6.6**	112	-6.0**	134	-0.8**	-27.2	-41.4
Shangqiu	86	-3.5**	111	-3.6**	117	-2.5**	140	1.8*	-59	-39.6
Xuzhou	82	-6.4**	113	-3.4**	120	-3.1**	139	-1.1**	-72.1	-36
Shouxian	83	-6.8**	109	-7.5**	116	-5.8**	134	-2.7**	-29.3	-41.6

Variation of yield reduction rate

Using DSSAT, we determined the annual variation of potential yield reduction for wheat due to drought stress during the jointing to heading stage and filling stage was determined in the selected 12 stations in a recent 30-year period across the Huang-Huai-Hai Plain (Figure 29). Strong fluctuations were found for the yield reduction in Tianjin, with two periods of low values in the late 1980s and 1990s. For the Linyi station, the yield reduction rate declined in 1980—2000, while it increased in 2001—2010. It can be seen from Figure 30 that the largest yield reduction was found in the middle of the 1990s for Tianjian and Shijiazhuang stations and in the late 1990s for the other four stations, mainly due to drought events in 2000 over the Huang-Huai-Hai Plain. In the 1980s, the yield reduction rate declined significantly for all selected stations during the jointing to heading stage, and they declined except for Tianjin and Shijiazhuang during the filling stage. Furthermore, the yield reduction rate increased for the Tianjin and Linyi stations during the jointing to heading stage, while it decreased for Shangqiu station in the 1990s. For the filling stage, the yield reduction rate declined in only the Tianjin station, and it increased in the Zhumadian and Shangqiu stations. To summarize, the trends in the yield reduction rate without irrigation in both the jointing to heading stage and filling stage were similar to those of the yield reduction due to drought in the jointing to heading stage.

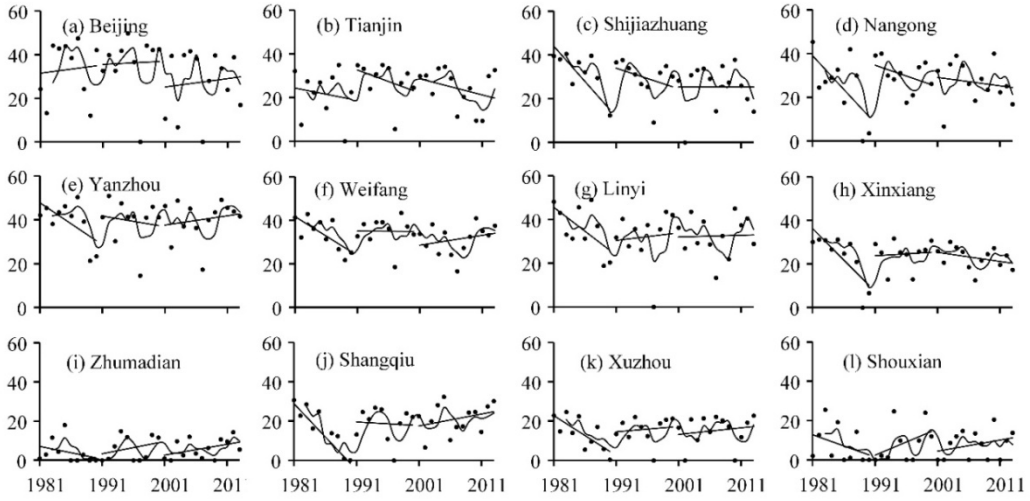

Figure 29 Variation of simulated yield reduction (%) for wheat under the treatment of no irrigation during the jointing and heading stage (T1 treatment).

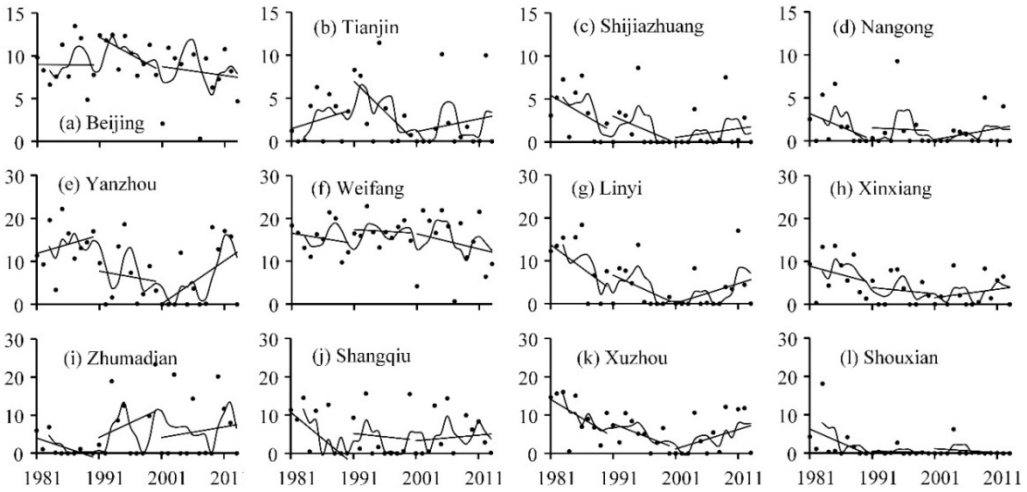

Figure 30 Variation of simulated yield reduction (%) for wheat under the treatment of no irrigation during the filling stage (T2 treatment).

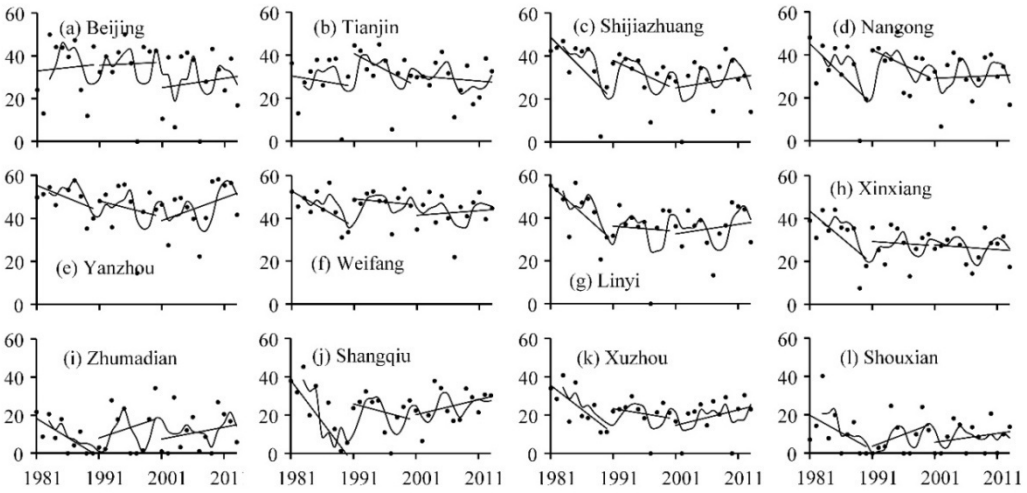

Figure 31 Variation of simulated yield reduction (%) for wheat under the treatment of no irrigation during both jointing - heading stage and filling stage (T3 treatment).

Cumulative probability of yield reduction rate

As described in Figure 32, the cumulative probability of the yield reduction rate during the jointing to heading stage and the filling stage was investigated to determine the impacts of drought on the wheat yield in these two typical water demand periods. It can be seen that the yield reduction rate under the same level was much higher during the jointing to heading stage than in the filling stage. The cumulative probability of the yield reduction rate, which is over 60% during the jointing to heading stage, was approximately 15% in the north and west stations and turned out to be around 65% in the north and east stations when the yield reduction rate was over 40%. The cumulative probability of the yield reduction rate was higher during the

jointing to heading stage in the north part than in the south region, while almost the same results were found during the filling stage.

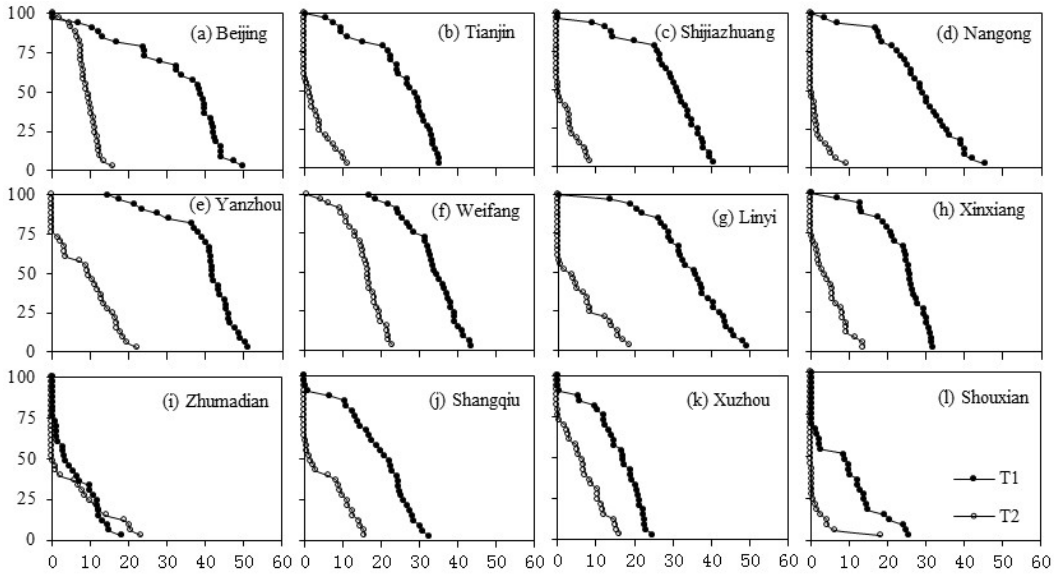

Figure 32 Cumulative probability of yield reduction rate (%) during jointing to heading stage (T1) and filling stage (T2) for winter wheat, respectively, in 12 typical sites

5. Discussion

Evapotranspiration is widely acknowledged as a factor that determines climatic drought in arid and semi-arid regions, where minor variations in precipitation or temperature easily induce significant changes in hydrological processes and crop water requirements (Ma et al. 2004, Temesgen et al. 2005). Over last decades, the aridity index is expected to have different trends in various regions (Su et al. 2015, Liu et al. 2013a, Wu et al. 2006). Droughts have become more frequent and intense during the last decades, which present a direct threat to crop growth in vast areas across China (Wang et al. 2016, Dalin et al. 2015, Wang et al. 2011). Liu et al. (2013b) identified an increasing trend of total water deficit of winter wheat in past three decades in Northern China, and therefore a negative influence on wheat production and water resources in the area can be expected in the future if no management changes, such as irrigation techniques, cropping pattern, mulching, etc. are adopted (Allen et al. 1998, Olesen and Bindi 2002). The present study gives a first hint of yield fluctuations based on CERES-Wheat model to be expected and regions to should be prioritized. The yield reduction rate for wheat was much larger during the jointing to heading stage than in the filling stage, which is in agreement with experimental results in Anhui province (Wang et al. 2001) and simulated findings by WOFOST model in Zhengzhou agro-meteorological station (Zhang et al. 2012). The drought reduced winter wheat yield by affecting grain-filling intensity due to soil water deficit. The reduction in yield was significantly different when drought occurred at different developmental stages. There was higher impact on winter wheat when drought occurred at several developmental stages than at a single

developmental stage. A study in North China revealed that under wheat production, mean daily soil evaporation from less and additional mulching was reduced by 16% and 37%, respectively (Chen et al. 2007). In Spain, Döll (2002) has predicted a declining in irrigation requirements by 2020 on account of the possibility of earlier sowing under more favourable higher temperatures. It will be necessary to develop feasible straw (film) mulching, regulated deficit irrigation, and soil water storage and preservation to reduce pressure on groundwater over-exploitation, especially for winter wheat in the 3H Plain.

Process-based crop models have been widely used to assess the impacts of future climate change on crop production, but using them to explore the impacts of past climate change are limited due to the model's capacity in reproducing the actual yield responses to environment largely dependent on a few important procedures such as calibration, validation and data aggregation. Furthermore, the simulation results often suffer from a number of models' uncertainties from pests, disease and some largely underestimated extreme events. Despite the uncertainties, our results are still in line with some previous statistical studies (Zhang et al. 2012, Lv et al. 2007b). The reduction of the grain number is due to water stress during the jointing to heading stage, while the reduction of the grain weight is mainly caused by water stress during the filling stage (Huang et al. 2013, Sun et al. 2004).

6. Conclusion

We have examined the impact of drought on the wheat yield at twelve different locations on the Huang-Huai-Hai Plain. The study provides insight into the impact of irrigation scheduling on the yield of winter wheat, the most important cereal crop on the 3H Plain. Through DSSAT simulations, we showed that the wheat yields vary spatially due to the same treatment all over the 3H Plain. A significant gap between the actual and potential yield is seen, which can be attributed to the water stress and changes in the management inputs. The yield reduction rate for wheat was much larger during the jointing to heading stage than in the filling stage, with spatial variability due to the climate conditions. A cumulative probability analysis indicated that the yield reduction rate under the same drought condition was much higher during the jointing to heading stage than in the filling stage. The cumulative probability of the yield reduction rate was higher during the jointing to heading stage in the north part than in the southern region.

Acknowledgements

This research was supported by the 12th Five-year Plan of the National Key Technologies R&D Program (2012BAD09B01), the National Basic Research Program of China (973 Program) (2012CB955904) and the National Science Foundation for Young Scientists of China (41401510). We thank the University of Liège-Gembloux Agro-Bio Tech and more specifically the research platform AgricultureIsLife for the funding of the scientific stay in Belgium that made this paper possible. We gratefully acknowledge the anonymous reviewers for their valuable comments on the manuscript.

7. References

Allen R G, Pereira L S, Raes D, Smith M. 1998. Crop evapotranspiration-Guidelines for computing crop water requirements-FAO Irrigation and drainage paper 56. FAO, Rome, 300, D05109.

Attri S D, Rathore L S. 2003. Simulation of impact of projected climate change on wheat in India. International Journal of Climatology, 23, 693–705.

Cabelguenne M, Debaeke P, Puech J, Bosc N. 1997. Real time irrigation management using the EPIC-PHASE model and weather forecasts. Agricultural Water Management, 96, 227-238.

Chen S Y, Zhang X Y, Pei D, Sun H Y, Chen S L. 2007. Effects of straw mulching on soil temperature, evaporation and yield of winter wheat: field experiments on the North China Plain. Annals of Applied Biology, 150, 261–268.

Dai A. 2011. Drought under global warming: a review. Wiley Interdisciplinary Reviews Climate Change, 2, 45-65.

Dalin C, Qiu H, Hanasaki N, Mauzerall D L, Rodrigueziturbe I. 2015. Balancing water resource conservation and food security in China. Proceedings of the National Academy of Sciences of the United States of America, 112, 4588-4593.

Dilley M, Chen R S, Deichmann U, Lerner Lam A L, Arnold M. 2005. Natural disaster hotspots: a global risk analysis. Uwe Deichmann, 1-145.

Döll P. 2002. Impact of Climate Change and Variability on Irrigation Requirements: A Global Perspective. Climatic Change, 54, 269-293.

Gray V. 2010. Climate Change 2013 - The Physical Science Basis. South African Geographical Journal Being A Record of the Proceedings of the South African Geographical Society, 92, 86-87.

He J, Cai H, Bai J. 2013. Irrigation scheduling based on CERES-Wheat model for spring wheat production in the Minqin Oasis in Northwest China. Agricultural Water Management, 128, 19-31.

He J, Dukes M D, Hochmuth G J, Jones J W, Graham W D. 2012. Identifying irrigation and nitrogen best management practices for sweet corn production on sandy soils using CERES-Maize model. Agricultural Water Management, 109, 61-70.

Huang L, Gao Y, Qiu X, Li X. 2013. Effects of irrigation amount and stage on yield and water consumption of different winter wheat cultivars. Transactions of the CSAE, 99-108.

Hui J U, Wei X, Long X Y, Lin E D. 2005. Impacts of Climate Change on Wheat Yield in China. Acta Agronomica Sinica.

Jalota S K, Vashisht B B, Kaur H, Kaur S, Kaur P. 2014. Location specific climate change scenario and its impact on rice and wheat in Central Indian Punjab. Agricultural Systems, 131, 77-86.

Jhajharia D, Dinpashoh Y, Kahya E, Singh V P, Fakheri-Fard A. 2012. Trends in reference evapotranspiration in the humid region of northeast India. Hydrological Processes, 26, 421–435.

Jhajharia D, Kumar R, Dabral P P, Singh V P, Choudhary R R, Dinpashoh Y. 2015. Reference evapotranspiration under changing climate overtheTharDesertinIndia. Meteorological Applications, 22, 425–435.

Jiang Y, Zhang L, Zhang B, He C, Jin X, Bai X. 2016. Modeling irrigation management for water conservation by DSSAT-maize model in arid northwestern China. Agricultural Water Management, 177, 37-45.

Jones J W, Hoogenboom G, Porter C H, Boote K J, Batchelor W D, Hunt L A, Wilkens P W, Singh U, Gijsman A J, Ritchie J T. 2003. DSSAT cropping system model. European Journal of Agronomy, 18, 235-265.

Kendall M. 1975. Rank Correlation Methods, Charles Griffin & Company Ltd.

Kouadio L, Newlands N, Potgieter A, McLean G, Hill H. 2015. Response of dryland spring wheat yield to elevated CO2 concentration and temperature by APSIM model. Agricultural Sciences, 6, 686-698.

Liu Q, Mei X R, Yan C, Ju H, Yang J. 2013b. Dybamic variation of water deficit of winter wheat and its possible climatic factors in Northern China. Acta Ecologica Sinica, 33, 6643-6651.

Liu Q, Yan C, Ju H, Garre S. 2017. Impact of climate change on potential evapotranspiration under a historical and future climate scenario in the Huang-Huai-Hai Plain, China. Theoretical and Applied Climatology.

Liu X, Zhang D, Luo Y, Liu C. 2013a. Spatial and temporal changes in aridity index in northwest China: 1960 to 2010. Theoretical and Applied Climatology, 112, 307-316.

Lu C, Lan F. 2013. Winter wheat yield potentials and yield gaps in the North China Plain. Field Crops Research, 143, 98-105.

Lv L, Hu Y, Li Y, Wang P. 2007a. Effect of irrigating treatments on water use efficiency and yield of different wheat cultivars. Journal of Triticeae Crops, 27, 88-92.

Lv L, Hu Y, Li Y, Wang P. 2007b. Effect of irrigating treatments on water use efficiency and yield of different wheat cultivars. Journal of Triticeae Crops, 27, 88-92.

Ma Z, Dan L, Hu Y. 2004. The extreme dry/wet events in northern China during recent 100 years. Journal of Geographical Sciences, 14, 275-281.

Mann H B. 1945. Nonparametric test against trend. Econometrica, 13, 245-259.

Mei X R, Kang S Z, Qiang Y U, Huang Y F, Zhong X L, Gong D Z, Huo Z L, Liu E K. 2013. Pathways to Synchronously Improving Crop Productivity and Field Water Use Efficiency in the North China Plain. Scientia Agricultura Sinica.

Olesen J E, Bindi M. 2002. Consequences of climate change for European agricultural productivity, land use and policy. European Journal of Agronomy, 16, 239–262.

Pathak H, Ladha J K, Aggarwal P K, Peng S, Das S, Singh Y, Singh B, Kamra S K, Mishra B, Sastri A S R A S. 2003. Trends of climatic potential and on-farm yields of rice and wheat in the Indo-Gangetic Plains. Field Crops Research, 80, 223-234.

Santos A M, Cabelguenne M, Santos F L, Oliveira M R, Serralheiro R P, Bica M A. 2000. EPIC-PHASE: a Model to explore Irrigation Strategies. Journal of Agricultural Engineering Research, 75, 409-416.

Sen P K. 1968. Estimates of the Regression Coefficient Based on Kendall's Tau. Journal of the American Statistical Association, 63(324), 1379-1389.

Sillmann J, Kharin V V, Zhang X, Zwiers F W, Bronaugh D. 2013. Climate extremes indices in the CMIP5 multimodel ensemble: Part 1. Model evaluation in the present climate. Journal of Geophysical Research Atmospheres, 118, 1716–1733.

Singh U, Thornton P K. 1992. Using crop models for sustainability and environmental quality assessment. Outlook on Agriculture, 21, 209-218.

Smith M. 1992. CROPWAT-A computer program for irrigation planning and management- irrigation and drainage paper. 46. Rome: Food and Agriculture Organization of the United, 20-21.

Su X, Singh V P, Niu J, Hao L. 2015. Spatiotemporal trends of aridity index in Shiyang River basin of northwest China. Stochastic Environmental Research and Risk Assessment, 29, 1571-1582.

Sun B, Wang Y, Li X, Liu F. 2004. The influence of climate and cultivation on the yield components of winter wheat in

different years. Journa l of T riticeae Crops, 24, 83-87.

Temesgen B, Eching S, Davidoff B, Frame K. 2005. Comparison of Some Reference Evapotranspiration Equations for California. Journal of Irrigation & Drainage Engineering, 131, 73-84.

Theil H. 1992. A Rank Invariant Method of Linear and Polynomial Regression Analysis. Springer Netherlands. 345-381.

Wang A, Lettenmaier D P, Sheffield J. 2011. Soil Moisture Drought in China, 1950–2006. Journal of Climate, 24, 3257-3271.

Wang H, Chen A, Wang Q, He B. 2015. Drought dynamics and impacts on vegetation in China from 1982 to 2011. Ecological Engineering, 75, 303-307.

Wang H, Vicente-Serrano S M, Tao F, Zhang X, Wang P, Zhang C, Chen Y, Zhu D, Kenawy A E. 2016. Monitoring winter wheat drought threat in Northern China using multiple climate-based drought indices and soil moisture during 2000–2013. Agricultural & Forest Meteorology, s 228–229, 1-12.

Wang M, Zhang C, Yao W, Wang X. 2001. Effects of drought stress in different development stages on wheat yield. Journal of Anhui Agricultural Sciences, 29, 605-607, 610.

Wassmann R, Jagadish S V K, Sumfleth K, Pathak H, Howell G, Ismail A, Serraj R, Redona E, Singh R K, Heuer S. 2009. Chapter 3 Regional Vulnerability of Climate Change Impacts on Asian Rice Production and Scope for Adaptation. Advances in Agronomy, 102, 91-133.

Wen X, Chen F. 2011. Simulation of climatic change impacts on yield potential of typical wheat varieties based on DSSAT model. Transactions of the CSAE, 74-79.

Wilcox J, Makowski D. 2014. A meta-analysis of the predicted effects of climate change on wheat yields using simulation studies. Field Crops Research, 156, 180-190.

Wilhite D A, Svoboda M D, Hayes M J. 2007. Understanding the complex impacts of drought: A key to enhancing drought mitigation and preparedness. Water Resources Management, 21, 763-774.

Wu S, Gao H, Wang S, Duan G. 2002. Analysis on the effect of drought on the grain weight grow and the character of the grain filling of winter wheat. Agricultural Research in the Arid Areas, 20, 49-51.

Wu S, Yin Y, Zheng D, Yang Q. 2006. Moisture conditions and climate trends in China during the period 1971–2000. International Journal of Climatology, 26, 193-206.

Yang J M, Yang J Y, Dou S, Yang X M, Hoogenboom G. 2013. Simulating the effect of long-term fertilization on maize yield and soil C/N dynamics in northeastern China using DSSAT and CENTURY-based soil model. Nutrient Cycling in Agroecosystems, 95, 287-303.

Yang J, Mei X, Huo Z, Yan C, Zhao F, Liu Q. 2015. Water consumption in summer maize and winter wheat cropping system based on SEBAL model in Huang-Huai-Hai Plain, China. Journal of Integrative Agriculture, 14, 2065-2076.

Yang P, Wu W, Li Z, Yu Q, Inatsu M, Liu Z, Tang P, Zha Y, Kimoto M, Tang H. 2014. Simulated impact of elevated CO2, temperature, and precipitation on the winter wheat yield in the North China Plain. Regional Environmental Change, 14, 61-74.

Yang Y, Yang Y, Moiwo J P, Hu Y. 2010. Estimation of irrigation requirement for sustainable water resources reallocation in North China. Agricultural Water Management, 97, 1711-1721.

Yong B, Ren L, Hong Y, Gourley J J, Chen X, Dong J, Wang W, Shen Y, Hardy J. 2013. Spatial–Temporal Changes of Water Resources in a Typical Semiarid Basin of North China over the Past 50 Years and Assessment of Possible Natural

and Socioeconomic Causes. Journal of Hydrometeorology, 14, 1009-1034.

Yu M, Hayes M J, Heim R R, Li Q. 2011. Are droughts becoming more frequent or severe in China? AGU Fall Meeting.

Zhang H L, Zhao X, Yin X G, Liu S L, Xue J F, Wang M, Pu C, Lal R, Chen F. 2015. Challenges and adaptations of farming to climate change in the North China Plain. Climatic Change, 129, 213-224.

Zhang J, Zhao Y, Wang C, Yang X. 2012. Impact simulation of drought disaster at different developmental stages on winter wheat grain-filling and yield. Chinese Journal of Eco-Agriculture, 20, 1158-1165.

Zhang Q, Xu C-Y, Chen X. 2011b. Reference evapotranspiration changes in China: natural processes or human influences? Theoretical and Applied Climatology, 103, 479-488.

Zhang X, Chen S, Sun H, Shao L, Wang Y. 2011a. Changes in evapotranspiration over irrigated winter wheat and maize in North China Plain over three decades. Agricultural Water Management, 98, 1097-1104.

Zheng C, Wang Q. 2014. Spatiotemporal variations of reference evapotranspiration in recent five decades in the arid land of Northwestern China. Hydrological Processes, 28, 6124–6134.

Chapter Ⅴ. Investigation of the impact of climate change on wheat yield using CERES-Wheat model

Investigation of the impact of climate change on wheat yield using CERES-Wheat model over the Huang-Huai-Hai Plain of China

Submitted in Theoretical and Applied Climatology, 2017

Qin Liu, Xiangxiang Li, Hui Ju, Changrong Yan, Sarah Garré*

** Corresponding author*

outline

This study aimed to understand the change in climate variables during the winter wheat growing season over the Huang-Huai-Hai Plain between the last 30 years (1985-2014) and the next 30 years (2021—2050) under the RCP4.5 and RCP8.5 pathways, and the relative impact of the change in each variable on winter wheat yield in isolation.

1. Abstract

Progress in understanding the impact of climate change on crop yields is essential for agricultural climate adaptation, especially for the Huang-Huai-Hai Plain (3H Plain), which is the grain production base of China. In this study, the effects of climate change (including solar radiation, maximum temperature, minimum temperature, and precipitation) between historical records (1985—2014) and future climate projections under the RCP4.5 and RCP8.5 pathways (2021—2050) on winter wheat yield, as well as the changes in each single climate variable alone, were analyzed using the CERES-Wheat crop model. The results show that solar radiation (SRAD), maximum temperature (TMAX), minimum temperature (TMIN), and precipitation (PRCP) during the winter wheat growing seasonal increased. The average SRAD received during the wheat growing seasons between 2021—2050 increased by 4.60% and 3.82% under the RCP4.5 and RCP8.5 scenarios, respectively, as compared to 1985—2014. The TMAX and TMIN of the wheat growing seasons during 2021—2050 were 1.30℃ and 1.07℃ higher under RCP4.5 and 1.28℃ and 1.09℃ higher under RCP8.5. Precipitation during this season also increased by 15.01% and 16.44% under the two pathways. According to our model simulations, these changes will have an overall positive impact on yield by increasing it by 17.34% and 15.76% under RCP4.5 and RCP8.5, respectively. We then isolated the impact of single weather variables. When we isolate the effect of each single weather variable on crop yield while keeping the other variables at the level of the historical data, we see different effects. Increases in temperature and precipitation result in positive evolutions: the changes in these variables raise simulated yield by 5.45% and 14.79%, respectively, under RCP4.5, and by 6.15% and 14.16%, respectively, under RCP8.5. Interestingly, the supposed positive impact of increasing solar radiation is visible in our simulations. Higher solar radiation also increases the evaporation amount and water stress and consequently causes the photosynthetically active radiation conversion to dry matter ratio (PARUE) to decrease. Logically, these negative impacts are lower at southern stations of the 3H Plain with less water stress. Thus, in conclusion, to take full advantage of increasing SRAD, TMAX, TMIN and PRCP, the optimized management of agricultural water resources and the improvement of water utilization efficiency (WUE) are essential, especially for the 3H Plain, which has already suffered from serious water shortages.

Keywords

Winter wheat; Grain yield; Climate change; RCP scenario; CERES-Wheat model; Huang-Huai-Hai Plain

2. Introduction

Agro-ecosystems are very sensitive to the effects of climate change, as they are directly exposed to changes in the atmosphere (Parry and Ruttan 1991; Piao et al. 2010). Global warming increases the thermal resources available in high-latitude areas so that the area of arable land has expanded (Ju et al. 2013); however, it worsens the severity of heat and drought stress for arid and semi-arid regions, which causes the food supply to fluctuate (Yuan et al. 2016). China is a large, densely populated country, so assuring food security is one of the priorities of the government. Thus, investigation in the impacts of climate change, and how to benefit from or mitigate its effects, is of great importance for agricultural adaptation and national food security (Ju et al. 2013; Piao et al. 2010).

Statistical models and numerical simulations are two popular approaches that have been widely used to investigate climate-crop relationships (Shi et al. 2013). Based on recorded yields and climate data, time-series regression models at the station level between time series of yield and several time series of climate variables can be established, and the signs of the regression coefficients represent the negative or positive impacts of climate change (David and Christopher 2007; Tao et al. 2008). In recent years, statistical models have been witnessed to be more performance in investigating crop responses to climatic warming than time series-based statistical models (Schlenker and Roberts 2009; Tao et al. 2014; Wolfram and David 2010). However, for these statistical models, the influences of non-climatic factors (such as cultivar and fertilizer change) on yield fluctuations need to be eliminated before establishing the statistical model. Although some simple elimination methods, such as the first-difference yield and the linear detrended yield, have been widely used in several studies, they are all based on certain hypotheses. For example, the linear detrended method is based on the concept that crop management and variety renewal change linearly with time, which does not match the practices of actual crop growth in the field (Xiong et al. 2014). Thus, the realism of these results remains questionable, and even opposite impacts of variables have been obtained using different elimination methods (Shi et al. 2013). In recognizing the complex interactions between crop growth and environmental factors, numerical simulations, or crop models, have become popular research tools for researchers in agro-meteorology in recent years. Dynamic crop models, such as the Erosion Productivity Impact Calculator (EPIC) model (Williams et al. 1983), APSIM (Keating et al. 2003), and DSSAT-CERES (Jones et al. 1998), have been tested and used in quantifying responses to water, nitrogen and weather at scales ranging from fields to regions around the world. Of these models, DSSAT is a software platform that includes multiple models for different crops, and it can quantitatively predict the growth and production of annual field crops given the interactions among the atmospheric and soil environments, cultivar factors and management (Ritchie et al. 1998). DSSAT has been used for climate change and climate extreme impact assessment for rice, wheat and maize for different zones in China in historical and future scenarios. Jabeen et al (2017) found that the rise in maximum and minimum temperature decreased the wheat yields using DSSAT and GIS across the Pothwar region of Pakistan. Araya et al (2015) observed that simulated maize yield under future climate scenarios may increase slightly compared to historical period by both 1.7% during the near future (2010–2039) for RCP4.5 and 8.5, subsequently 2.9% and 4.2%, and 3.5%

and 3.8% during the middle (2040–2069) and end of the 21st century (2070–2099) for RCP4.5 and 8.5 in southwestern Ethiopia. Wilcox and Makowski (2014) summarized from 90 studies that the effects of higher CO_2 concentrations (>640 ppm) outweighed that of increasing temperature (up to +2 ◦C) and moderate declines in precipitation (up to −20%), leading to augmenting yields. However, few studies have investigated the impact of single climate variables changing in isolation.

The Huang-Huai-Hai (3H) Plain, which is located in northern China, is the major grain-producing area in China (Yong et al. 2013). The conventional agricultural practice involves a rotation between winter wheat and summer maize, and this area provides approximately 70% and 30% of the wheat and maize produced in China, respectively (Yang et al. 2015). Due to the extratropical monsoon climate, more than 70% of annual precipitation falls during summer seasons (July to September) (Zhang et al. 2011). Thus, the winter wheat growing period has suffered from serious water deficits, of which only 25%—40% of water demand is satisfied by rainfall (Mei et al. 2013). To maintain high yield, the wheat is irrigated with pumped groundwater, which has led to environmental threats to society, such as groundwater lowering and surface subsidence (Zhang et al. 2005). Additionally, the warming temperatures and changing precipitation patterns caused by climate change have induced perturbations to regional crop production (Yu et al. 2014). Traditional climate-crop relationships based on statistical analyses have often produced conflicting conclusions because they use different elimination methods or consider different predictor variables (Shi et al. 2013). Thus, it is of concern to capture the impacts of climate change as estimated using physically based crop models.

The objectives of this study were to understand the changes in climate variables during the winter wheat growing season over the Huang-Huai-Hai Plain between the last 30 years (1985—2014) and the next 30 years (2021—2050) under the RCP4.5 and RCP8.5 pathways, as well as the combined and isolated impacts of these on winter wheat yield.

3. Materials and methods

Study region

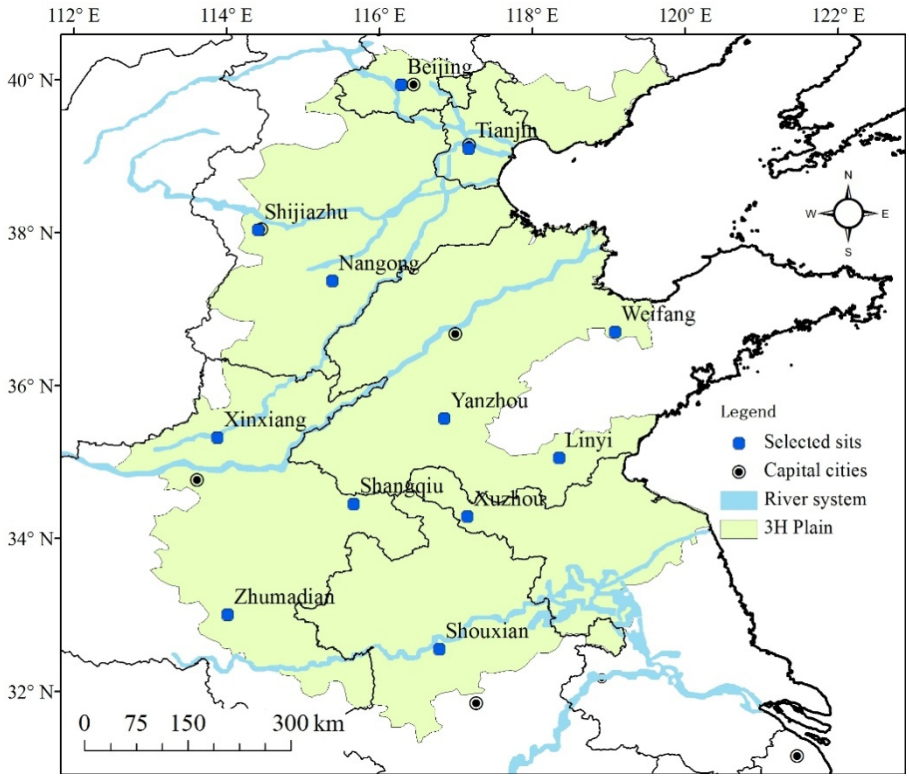

Figure 33 Geographical location of the wheat stations in Huang-Huai-Hai Plain. The upper blue line is Hai River and the middle, and below blue one is Yellow and Huai River, respectively.

Study stations in this study were selected from agro-meteorological experimental stations where observations on wheat growth and development information were available. The selected stations had a continuity in cultivar and disposed of detailed field management information for at least three years, and these stations were uniformly distributed. The 10 selected stations represent the general situation of the 3H Plain. The location of these stations, as well as general information about them, is shown in Figure 33 and Table 19. As we can see, annual mean precipitation and temperature values are systematically higher in the south than in the north, while solar radiation does not show obvious distribution patterns.

Table 19 General information on the ten selected stations in Huang-Huai-Hai Plain. The values described in this table were average data for precipitation, temperature and solar radiation during the winter wheat growing period in 1981-2010.

Station	Longitude	Latitude	Location	Precipitation (mm)	Temperature (℃)	Solar radiation ($MJ \cdot m^{-2}$)
Tian Jin	117°43′	39°03′	North	192.6	9.5	3760.8
Nan Gong	115°23′	37°22′	North	178.2	10.5	3922.1
Shang Qiu	115°40′	34°27′	Central	315.1	11.5	3650.6
Yan Zhou	116°51′	35°34′	Central	270.9	10.6	3893.9
Wei Fang	119°11′	36°45′	East	233.8	9.6	3997.1
Lin Yi	118°21′	35°03′	East	324.1	10.9	3993.6
Xin Xiang	113°53′	35°19′	West	215.6	11.6	3769.3
Zhu Ma Dian	114°01′	33°	West	470.0	12.3	3606.3
Xu Zhou	117°29′	34°17′	South	369.7	11.8	3859.7
Shou Xian	116°47′	32°33′	South	509.6	12.3	3778.3

CERES-Wheat crop model

The CERES-Wheat model is a simulation system that predicts daily wheat growth, development and yield based on input information on the atmospheric and soil environment, cultivar factors and management (Ritchie et al. 1998). CERES-Wheat, as well as models representing other cereal crops included in DSSAT (e.g., CERES-Maize and CERES-Rice), have been widely used in optimizing the use of resources and quantifying risks related to weather variations at scales ranging from fields to regions around the world (Timsina and Humphreys 2006). Additionally, the applicability of CERES-Wheat has been tested in a wide range of field trials (Xiong et al. 2014). Thus, the CERES-Wheat model was selected to evaluate the impact of climate change in this study.

Weather, soil and management information

The minimal data sets required for model operation include weather information (daily global solar radiation, maximum and minimum temperature, precipitation), soil information (classification and basic profile characteristics by soil layer) and management information (e.g., cultivar, planting, irrigation and

fertilization information). In this study, the daily weather data from 1985—2014 collected at the ten stations were obtained from the National Meteorological Information Center of China. As the daily solar radiation data were not available, it was calculated with the Angstrom formula, which relates solar radiation to extraterrestrial radiation and relative sunshine duration (Martínez-Lozano et al. 1984). The projected daily weather data for 2021—2050 under RCP4.5 and RCP8.5 were derived from the BCC_CSM1.1 model and downscaled to the ten stations using the bilinear interpolation method (Yuan et al. 2012). Soil classification and profile characteristics were collected from the China Soil Scientific Database. In this study, we focus on evaluating the impact of climate change on wheat yield and identifying the contributions of changes in each individual climate variable. Thus, during the simulations, nitrogen stress was turned off, to avoid the impact of variable fertilizer levels among stations on the final result. On the other hand, water stress was turned on, and no irrigation was applied, in order to fully capture the impact of climate change on water availability.

Model calibration and evaluation

In the CERES-Wheat model, there are seven main coefficients that control the development and growth of wheat (Ritchie et al. 1998). These coefficients must be calibrated and evaluated to meet the observed development and growth process under specific environmental conditions before being used for climate impact analyses (Hunt and Boote 1998). In this study, the observed dates of the major stages of wheat development (i.e., the anthesis date and the maturity date) and the final yield, which were obtained from the agro-meteorological stations of the China Meteorological Administration, were used to calibrate and then evaluate the model at each station. General information on the 12 stations with chosen seasons and representative cultivar names used in model calibration and evaluation, as well as averaged data on growth stages and yields, are shown in Table 20.

Table 20 The average planting date, anthesis days (days after planting, ADAP), maturity days (days after planting, MDAP) and yield (HWAM) of the seasons selected for model calibration and evaluation. The seasons marked with "*" were chosen for model evaluation.

Stations	Location	Seasons	Cultivar name	Planting dates (MM.DD)	ADAP	MDAP	HWAM (kg ha^{-1})
Tian Jin	North	2006, 2007*, 2008	Beijing 9428	10.03	220	254	5300
Nan Gong	North	2002, 2003, 2004*, 2005	Han 6172	10.12	201	234	4586
Shang Qiu	Central	2007, 2008, 2009*	Wenmai 6	10.15	191	225	5122
Yan Zhou	Central	2006*, 2007, 2008, 2009	Jining 6	10.15	197	234	6301
Wei Fang	East	2007*, 2008, 2009	Jimai 22	10.08	210	241	6285
Lin Yi	East	2007*, 2008, 2009	Linmai 4	10.12	205	236	5271
Xin Xiang	West	2004, 2005*, 2006, 2007	Xinmai 6	10.12	199	230	4285
Zhu Ma Dian	West	2006, 2007*, 2008, 2009	Zhengmai 9023	10.25	169	208	6299
Xu Zhou	South	2005, 2006, 2007*, 2008	Xuzhou 24	10.17	193	228	3853
Shou Xian	South	2006, 2007, 2008, 2009*	Xumai 27	10.21	180	214	5460

Simulated scenarios: past, future and isolated variables

During the wheat growing season, the average received solar radiation was 4.60% and 3.82% higher in 2021—2050 under the RCP4.5 and RCP8.5 pathways, respectively, when compared to 1985—2014 (Table **3**). Negative changes were only found in Shouxian, which is located in the west, and recorded reduction rates of 3.53% and 4.23%.

The average differences in the seasonal maximum temperature (TMAX) between 2021—2050 and 1985—2014 were 1.30℃ (RCP4.5) and 1.28℃ (RCP8.5), indicating that the maximum temperature during the wheat growing season becomes higher under the RCP4.5 scenario than inRCP8.5. Specifically, in Nangong (north), Shangqiu (central), Yanzhou (central), Linyi (east) and Xinxiang (West), changes in TMAX were higher under RCP4.5 than under RCP8.5. Additionally, in the northern locations (Tianjin and Nangong), the increasing amplitude of TMAX was higher than that of other regions, with the average increase of 1.48℃ and 1.45℃ under RCP4.5 and RCP8.5.

Increases in the minimum temperature (TMIN) during the wheat growing seasons are smaller than TMAX. The average changes in the TMIN are 1.07℃ and 1.09℃, which are higher under RCP8.5 than RCP4.5. Most stations experience greater increases under the RCP8.5 scenario than under RCP4.5, except for Shangqiu, Xinxiang and Xuzhou. Similarly, the changes in TMIN were also higher in the north than in other regions, with increases of 1.49℃ and 1.60℃. Precipitation (PRCP) increases by 15.01% under RCP4.5 and 16.44% under RCP8.5. The exceptions are Tianjin, Nangong and Shangqiu, for which PRCP shows a negative trend under RCP4.5 and/or RCP8.5.

To investigate the wheat yield response to climate change between the periods 1985—2014 and 2021—2050 and the relative contributions of changes in single climate variables, several simulation scenarios were set as shown in Table 21. The yield levels under historical climate conditions were simulated in SH using the observed daily maximum and minimum temperature (TMAX and TMIN), precipitation (RAIN) and solar radiation (SRAD, estimated using the Angstrom formula) for 1985-2014 to strip the effects of irrigation and fertilization which can be different in different stations, while the predicted yields for future projected climate conditions was simulated in SF using TMAX, TMIN, RAIN and SRAD values for 2021-2050 under RCP4.5 and RCP8.5 respectively. To study the impact of change in each climate variable individually, simulations SH-RAD, SF-TEMP and SF-RAIN were designed to simulate yields under historical climate conditions with only changes in SRAD, temperature (including TMAX and TMIN) and RAIN, respectively.

Table 21 Simulation scenarios established to characterize the impact of climate change on winter wheat yields.

Scenario	SRAD	TMAX	TMIN	RAIN	Purpose
SH	1985—2014	1985—2014	1985—2014	1985—2014	To simulate the yield level based on historical climate.
SF	2021—2050	2021—2050	2021—2050	2021—2050	To simulate the yield level based on projected climates for both RCP4.5 and RCP8.5.
SF-RAD	2021—2050	1985—2014	1985—2014	1985—2014	To simulate only the impact of radiation change on yield.
SF-TEMP	1985—2014	2021—2050	2021—2050	1985—2014	Same as SH, but for maximum and minimum temperature.
SF-RAIN	1985—2014	1985—2014	1985—2014	2021—2050	Same as SH, but for rainfall.

The impact of climate change on yield could be calculated by:

$$F_{ALL} = \frac{Y_{SF} - Y_{SH}}{Y_{SH}} \times 100\% \quad \text{Formula 16}$$

$$F_S = \frac{Y_{SF-RAD} - Y_{SH}}{Y_{SH}} \times 100\% \quad \text{Formula 17}$$

$$F_T = \frac{Y_{SF-TEMP} - Y_{SH}}{Y_{SH}} \times 100\% \quad \text{Formula 18}$$

$$F_R = \frac{Y_{SF-RAIN} - Y_{SH}}{Y_{SH}} \times 100\% \quad \text{Formula 19}$$

F_{ALL}, F_S, F_T and F_R represents the impacts of changes in all climate variables, only SRAD, only temperature and only RAIN, respectively. Y_{Si} represents the yield level for different simulated scenarios.

4. Results

Testing of CERES-Wheat model

The measured variables, specifically anthesis days after planting (ADAP), maturity days after planting (MDAP) and harvest weight at maturity (HWAM) of the selected agro-meteorological stations were used to calibrate and evaluate the performance of the CERES-Wheat model for each selected station. The scatter plots and the normalized root mean square errors (NRMSEs) between the measured and simulated variables are shown in Figure 34 and Table 22.

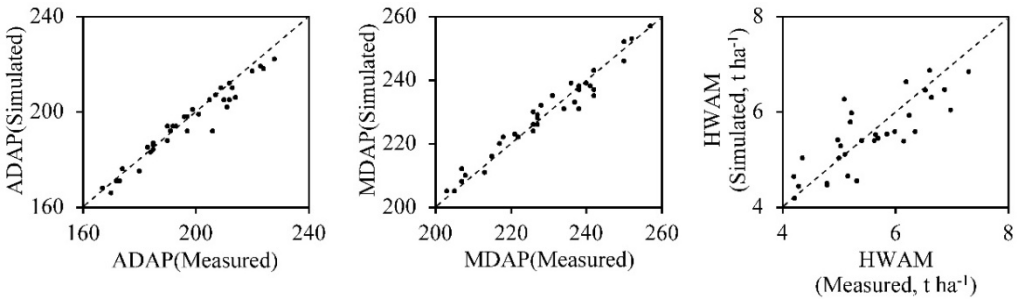

Figure 34 Comparison of simulated and measured anthesis days (ADAP, d), maturity days (MDAP, d) and yields (HWAM, kg/ha) for selected ten stations. The dotted line is the 1:1 reference line.

As Figure 34 and Table 22 shows, the output of the calibrated model correlate well with the measured variables, especially during the growth stages. The NRMSEs for ADAP, MDAP and HWAM range between 0.8%—4.9%, 0.4%—2.5% and 2.4%—12.4%, respectively, and these ranges lie within acceptable limits (10% for growth duration and 15% for measured yields) (Ritchie et al. 1998).

Table 22 The calibrated genetic coefficients and the normalized root mean square errors (NRMSEs, %) values for ADAP (Anthesis, d), MDAP (Maturity, d) and HWAM (Yield, kg/ha). P1V is vernalization parameter (d). P1D is photoperiod parameter (%). P5 is grain filling duration parameter (°C d). G1 is grain parameter at anthesis (no g^{-1}). G2 is grain filling rate parameter (mg). G3 is dry weight of a single stem and spike (g). PHINT is interval between successive leaf tip appearances (°C d).

Stations	Location	P1V (d)	P1D (%)	P5 (°C d)	G1 (no g^{-1})	G2 (mg)	G3 (g)	PHINT (°C d)	NRMSE (%)		
									ADAP (d)	MDAP (d)	HWAM (kg/ha)
Tianjin	North	34.2	52.3	652.5	28.6	22.6	1.6	95	2.5	0.5	2.4
Nangong	North	26.3	44.5	554.1	21.3	43.6	2.0	95	4.9	2.5	10.8
Shangqiu	Central	63.5	17.0	552.9	26.3	58.0	1.1	95	2.0	1.0	7.5
Yanzhou	Central	51.7	23.4	582.9	30.0	64.5	1.2	95	0.8	1.2	12.4
Weifang	East	6.8	66.6	473.0	26.2	38.2	2.0	95	0.8	0.4	5.9
Linyi	East	43.6	55.7	554.7	24.1	25.6	1.1	95	2.2	1.3	12.2
Xinxiang	West	42.0	48.3	498.2	29.8	62.9	1.9	95	0.8	1.3	8.6
Zhumadian	West	44.4	7.5	549.8	23.9	63.6	1.1	95	1.4	1.3	7.3
Xuzhou	South	64.5	27.6	642.7	20.0	56.1	1.1	95	1.3	1.3	11.4
Shouxian	South	46.5	23.9	504.3	28.1	58.4	1.9	95	1.6	1.0	9.2

Changes in growth duration and related climate variables

Changes in growth duration

In the model, the duration of growing stages was directly determined by temperature (Ritchie et al. 1998). In the context of global warming, a shortened growth period for wheat has been observed in both field observations and model predictions (Wang et al. 2008, Wei et al. 2012). In this study, based on the calibrated crop model, the ADAP (anthesis days after planting) and MDAP (maturity days after planting) were shortened in 2021—2050, compared with 1985—2014 (Figure 35). The dates of anthesis and maturity advance in all selected stations within the 3H Plain. The average decrease in duration for ADAP was 8 and 9 days under RCP4.5 and RCP8.5, respectively, while the decrease in MDAP was 9 days for both pathways. Additionally, as depicted in Figure 35, although the length of ADAP and MDAP are truncated, the duration between anthesis and maturity shows no significant change as the ADAP decreased by the same amount as MDAP.

This result is identical to findings based on long-term wheat phenology observations. Xiao et al. (2015) found that, while the phenology phases of winter wheat are shortening, the duration of the grain-filling stage even becomes slightly longer. They believed that this phenomenon was a self-adaptation strategy which, in turn, not only prolonged growth stages but also enhanced the productivity of winter wheat. Correspondingly, our results show that the self-adaptation mechanism would also be effective under future scenarios. Additionally, they found that temperature during the grain-filling stage decreases as the grain-filling date advances (Xiao et al. 2015, Xiao et al. 2014) which also benefits wheat production. In this study, we do not analyze the sensitivity of different wheat phenologies to temperature warming, as we are more concerned with the overall tendency of climate conditions from planting to maturity and the corresponding impact on wheat yields.

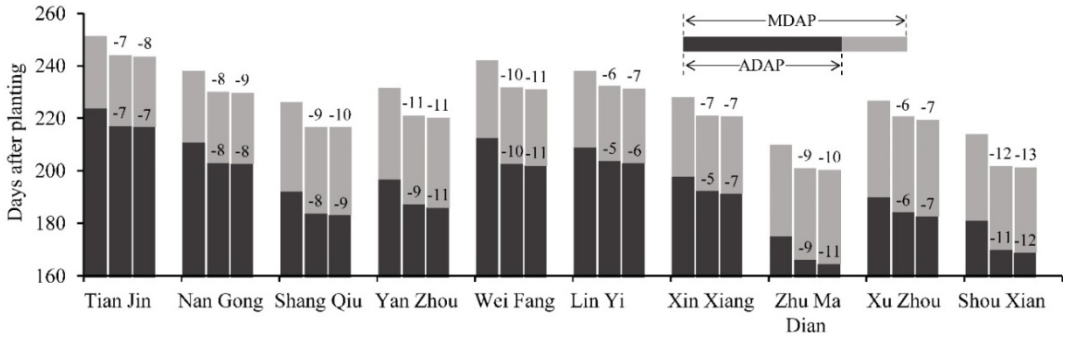

Figure 35 Changes in the number of days from planting to anthesis (ADAP, d) and from planting to maturity (MDAP, d). For each station, the columns from left to right represent the growing durations of 1985—2014 and 2021—2050 under the RCP4.5 scenario and 2021—2050 under the RCP8.5 scenario.

Changes in climate variables

During the wheat growing season, the average received solar radiation was 4.60% and 3.82% higher

in 2021—2050 under the RCP4.5 and RCP8.5 pathways, respectively, when compared to 1985—2014. Negative changes have been only found in Shou Xian, which is located in west, and recorded reduction rates of 3.53% and 4.23%.

The average differences in the seasonal maximum temperature (TMAX) between 2021—2050 and 1985—2014 were 1.30℃ (RCP4.5) and 1.28℃ (RCP8.5), indicating that the maximum temperature during wheat growing seasons becomes greater under the RCP4.5 pathway than in the RCP8.5 pathway. Specifically, in Nan Gong (north), Shang Qiu (central), Yan Zhou (central), Lin Yi (east) and Xin Xiang (West), changes in TMAX were found to be higher under RCP4.5 than RCP8.5. Additionally, in the northern locations (Tian Jin and Nan Gong), the increasing amplitude of TMAX was higher than that of other regions, with the average increase of 1.48℃ and 1.45℃ under RCP4.5 and RCP8.5.

Increases in the minimum temperature (Tmin) during the wheat growing seasons is resulted in a smaller effect than that of TMAX. The average changes in the TMIN are 1.07℃ and 1.09℃, which are higher under RCP8.5 than RCP4.5. Most stations experience greater increases under the RCP8.5 scenario than under RCP4.5, except for Shang Qiu, Xin Xiang and Xu Zhou. Similarly, the changes in TMIN were also higher in the north than in other regions, with increases of 1.49℃ and 1.60℃.

In terms of precipitation (PRCP), it increases by 15.01% under RCP4.5 and 16.44% under RCP8.5. The exceptions are Tian Jin, Nan Gong and Shang Qiu, for which PRCP shows a negative trend under RCP4.5 and/or RCP8.5. The increasing PRCP would inevitably ameliorate the water stress, which has been a serious problem in the study region.

Table 23 Changes in seasonal solar radiation (SRAD), maximum temperature (TMAX), minimum temperature (TMIN) and rainfall accumulation (RAIN) during the winter wheat growing season between 1985—2014 and 2021—2050 under RCP4.5 and RCP8.5 scenario.

Station	Change in SRDA (%)		Change in TMAX (℃)		Change in TMIN (℃)		Change in PRCP (%)	
	RCP4.5	RCP8.5	RCP4.5	RCP8.5	RCP4.5	RCP8.5	RCP4.5	RCP8.5
Tian Jin	7.73	6.56	1.47	1.49	1.34	1.48	-4.68	6.31
Nan Gong	5.57	4.67	1.49	1.41	1.64	1.73	-3.87	11.97
Shang Qiu	9.40	8.90	1.56	1.44	0.67	0.53	-0.90	-5.25
Yan Zhou	1.05	0.33	1.12	1.05	1.28	1.33	14.26	16.48
Wei Fang	1.32	0.66	1.12	1.16	1.63	1.76	5.10	6.03
Lin Yi	4.05	3.43	1.15	1.09	0.50	0.58	15.70	19.45
Xin Xiang	10.39	9.77	1.61	1.58	0.17	0.04	27.65	23.85
Zhu Ma Dian	4.80	3.59	1.08	1.10	1.07	1.11	33.97	29.13
Xu Zhou	5.22	4.51	1.27	1.32	0.55	0.50	41.44	38.77
Shou Xian	-3.53	-4.23	1.09	1.12	1.81	1.86	21.42	17.63
Average	4.60	3.82	1.30	1.28	1.07	1.09	15.01	16.44

Changes in yield and the contributions of single climate variables

Comparing the yield levels of simulation SF and SH (Figure 36a), the climate changes from 1958-2014 to 2021-2050 positively impact winter yields on the 3H Plain. The changes in SRAD, TMAX, TMIN and PRCP jointly increase winter wheat yield by 17.37% and 15.76% under RCP4.5 and RCP8.5 in terms of the regional average, respectively (Table 24, F_{ALL}). Additionally, the percent increase was higher at the southern stations (Xuzhou and Shouxian) than at the northern ones (Tianjin and Nangong).

Comparing the expected yield levels of simulation SF-RAD and SH (Figure 36b), changing solar radiation (SRAD) only, with the other climate variables kept the same as in historical observations, negatively impacts winter wheat yield in the study region. The change of SRAD in isolation reduced rainfed yields by 4.49% and 5.4% under RCP4.5 and RCP8.5, respectively (Table 24, F_S). In addition, the negative impact was lower at the southern stations. Nevertheless, it is typically assumed that increasing solar radiation is beneficial to photosynthesis and consequently yield. In this study, we assume that the expected benefit is reversed by the subsequent higher water stress, and this mechanism is explained in detail in Section 4.

Figure 36c depicts the changes in simulated yield caused by changes in temperature alone. It shows that warming temperatures have a positive impact on rainfed wheat yield in the 3H Plain. The overall rates of increase were 5.45% and 6.15% under RCP4.5 and RCP8.5, respectively (Table 24, F_T). Figure 36d depicts the changes in yield caused by changes in precipitation only. It shows that increasing precipitation during the wheat growing season is beneficial to wheat yields, except at Nangong and Shangqiu, where the precipitation decreases (Table 21). This positive impact tends to be higher at southern stations (Table 24, F_R) due to the larger increasein precipitation at these stations. In addition, the relative contributions of precipitation were 14.79% (RCP4.5) and 14.16% (RCP8.5) which were much higher than the positive contributions from warming temperatures. Thus, the change in precipitation was the dominant climate variable that contributed to the positive impact of climate changes on wheat yield in the 3H Plain.

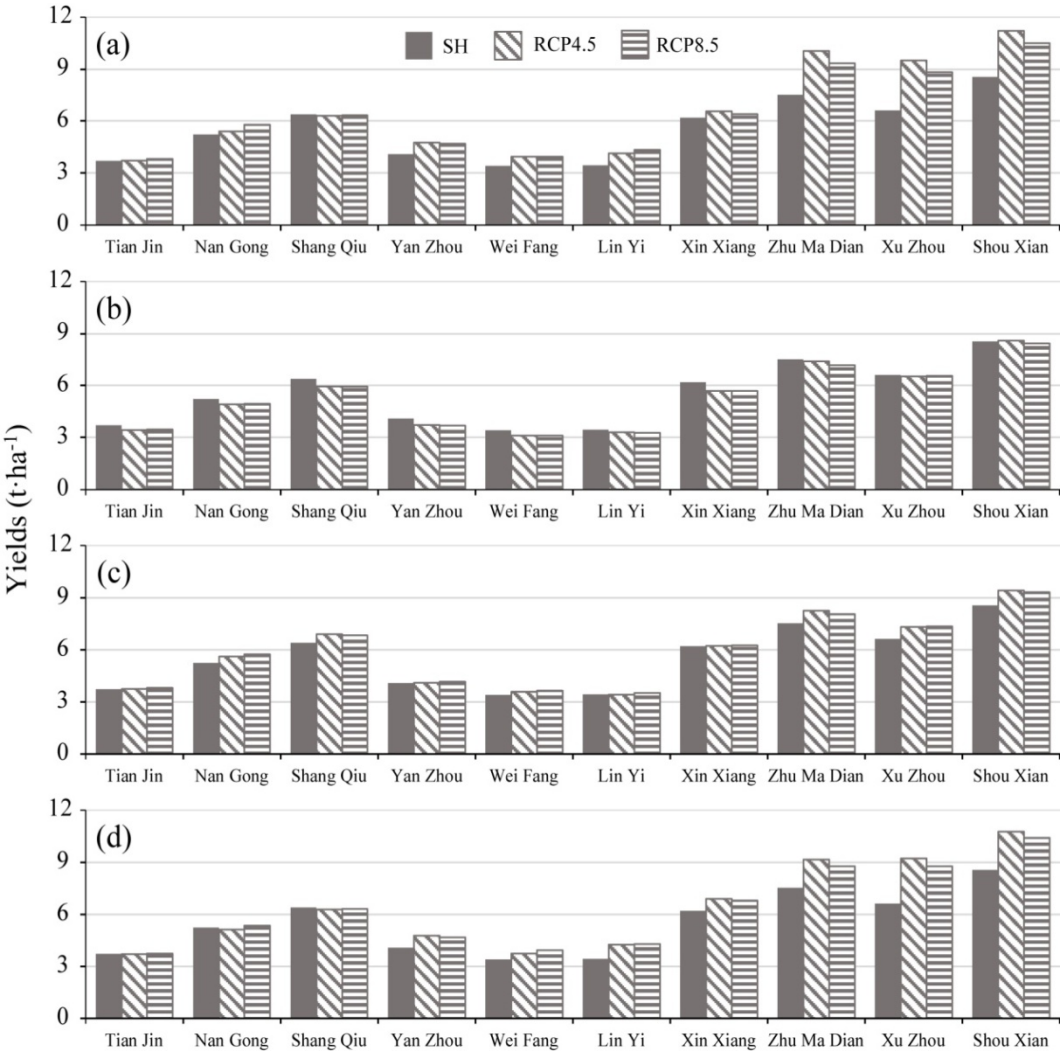

Figure 36 Comparisons of yields between simulation scenario SH and (a) SF; (b) SF-RAD; (c) SF-TEMP; and (d) SF-RAIN under RCP4.5 and RCP8.5 scenario.

Table 24 The relative contributions of changes in each climate variable individually to yield changes for 2021—2050 under the RCP4.5 and RCP8.5 scenarios compared to 1985—2014. The unit is percent in this table.

Station	F_{ALL}		F_S		F_T		F_R	
	RCP4.5	RCP8.5	RCP4.5	RCP8.5	RCP4.5	RCP8.5	RCP4.5	RCP8.5
Tian Jin	0.33	3.48	-6.98	-6.10	0.98	2.67	0.01	1.51
Nan Gong	3.81	10.98	-5.67	-5.15	7.35	9.83	-1.51	2.81
Shang Qiu	-1.01	-0.61	-6.53	-6.91	8.28	7.08	-1.53	-1.13
Yan Zhou	17.06	15.59	-8.72	-9.49	0.57	2.45	16.92	14.75
Wei Fang	16.14	16.10	-8.32	-8.02	5.57	7.87	10.29	16.24
Lin Yi	21.64	27.34	-3.44	-4.04	-0.10	2.62	24.50	25.40
Xin Xiang	6.52	3.87	-7.71	-7.90	0.88	1.48	11.56	10.15
Zhu Ma Dian	33.68	24.55	-1.41	-4.36	9.82	7.23	22.14	16.95
Xu Zhou	43.99	33.52	-1.01	-0.82	10.93	11.13	39.51	33.00
Shou Xian	31.27	22.77	0.40	-1.20	10.22	9.17	25.99	21.89
Average	17.34	15.76	-4.94	-5.40	5.45	6.15	14.79	14.16

5. Discussion

Negative impact of increasing solar radiation

In this study, the solar radiation during the winter growing seasons in 2021—2050 was 4.60% and 3.82% higher under the RCP4.5 and RCP8.5 scenarios than during 1985—2014. However, this increase had a negative impact on wheat yields (RECP 4.5: -4.49% and RCP8.5: -5.40%).The negative impacts were higher in the north than in the south. The result is inconsistent with previous studies, which suggest that crop yields are positively correlated with solar radiation, using both models (Wei et al. 2012) and statistical approaches (Tao et al. 2014).

It is generally recognized that increases in solar radiation would have a positive impact on wheat photosynthesis and would consequently increase yield(Tao et al. 2008). However, by comparing the photosynthetic active radiation (PAR) conversion to the dry matter ratio before last leaf stage (PARUE) between simulations SH and SF-RAD, the results show that the PARUE is higher under conditions of low radiation, indicating that there is a decrease in the conversion ratio from radiation to dry matter when the solar radiation increases to levels corresponding to the RCP4.5 and RCP8.5 (Table 25).

Table 25 Changes in photosynthetically active radiation (PAR) conversion to dry matter ratio before the last leaf stage (PARUE) between simulation scenarios SH and S SF-RAD under the RCP 4.5 and RCP 8.5 scenario.

Station	PARUE for SH	Changes in PARUE (SF-RAD-SH, %)	
	(g MJ^{-1})	RCP 4.5	RCP 8.5

Tian Jin	0.89	-12.79	-12.02
Nan Gong	1.05	-12.03	-11.08
Shang Qiu	1.16	-18.10	-18.10
Yan Zhou	0.92	-11.64	-11.27
Wei Fang	0.78	-11.54	-12.39
Lin Yi	0.95	-9.12	-9.82
Xin Xiang	1.06	-18.30	-16.72
Zhu Ma Dian	1.52	-9.19	-10.72
Xu Zhou	1.14	-9.06	-8.16
Shou Xian	1.48	-4.05	-4.50
Average	1.10	-11.58	-11.48

In the CERES-Wheat model, PARUE is affected by nitrogen, temperature and water (Ritchie et al. 1998). In this study, all simulation scenarios were free of nitrogen stress and the temperature and precipitation inputs were the same in simulations SH and SF-RAD. Thus, the nitrogen and temperature stress for photosynthesis were constant between simulations SH and SF-RAD. Therefore, the reduced PARUE is certainly caused by an increased water stress (increasing the soil evaporation in water balance). Comparing the relative moisture index (the ratio of total evapotranspiration minus precipitation to the total evapotranspiration) for SH and SF-RAD (Figure 37), we observe that the higher the relative moisture index is, the drier conditions are within a time period or a region. Figure 37 shows that the relative moisture index for SF-RAD was higher than that of SH. In other words, the increasing solar radiation has led to increased water stress, and consequently reduced PARUE and final yield. Additionally, as we can see, stations with lower relative moisture index values, such as Linyi, Zhumadian, Xuzhou, and Shouxian, display rates of decrease of PARUE (Table 25) and yield (Table 24) that are much smaller. Thus, the impact of increases in radiation on winter wheat yield is closely linked with regional water situations. For stations in the southern parts of the country, where precipitation is plentiful, the negative impact of increasing solar radiation is less apparent, whereas it is higher at the northern stations that experience serious precipitation shortages. As a conclusion, the supposed positive impact of increasing solar radiation is reversed by water deficiency, as it also induces higher atmospheric evapotranspiration demand.

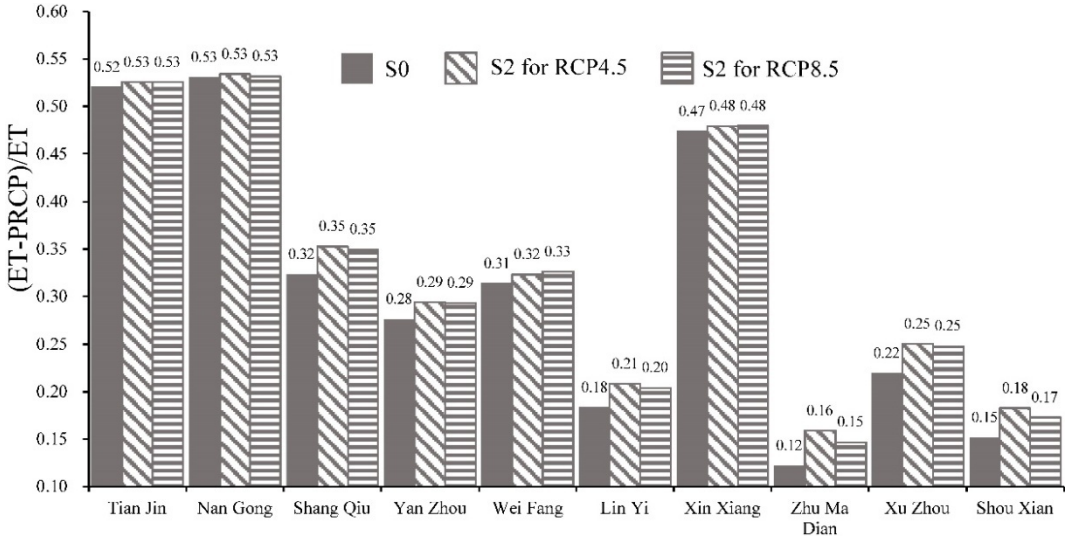

Figure 37 The charactertics in relative moisture index under historical period (S0), RCP 4.5 scenario (S1) and RCP 8.5 scenario (S2). The relative moisture index was estimated as the ratio of total evapotranspiration minus precipitation to the total evapotranspiration.

Positive impact of warming temperature and increasing precipitation

The impact of temperature (SF-TEMP) (or precipitation (SF-RAIN)) increase alone during the winter wheat growth period on wheat yield is positive. This positive impact of warming on wheat yield in the 3H Plain differed from the results of studies for China as a whole (Wang et al. 2008; You et al. 2009), Africa (Wolfram and David 2010), South Asia (Jerry et al. 2012), and the global average (David and Christopher 2007; Lobell et al. 2011). However, it is supported by the results of Tao (Tao et al. 2008; Tao et al. 2014) and Xiao (Xiao et al. 2008), who concluded that the wheat yield has benefited from climate warming in northern and northwest China. The impact of warming on crop yield is spatially variable in our study. Generally, a warming trend reduces crop productivity in areas at low latitudes where optimal temperatures already exist, while it may cause beneficial effects at high latitudes (Wei et al. 2012). Tao et al. (2014) concluded that increasing temperatures increased wheat yield in northern China but reduced wheat yield in south China, with the explanation that the temperature in northern China was less than the optimum temperature for wheat. Additionally, as shown in Fig. 34, although the period of vegetative growth (VGP) and the growing period as a whole tends to be shorter, the length of the reproductive growth stage (RGP, anthesis-maturity) shows no clear change, which indicates that the cultivated cultivar has a high thermal requirement during the RGP. Grain filling rates became higher as temperature increases below the optimum threshold and consequently increased grain yield. The self-adaptation ability of wheat cultivars in the last ten years (2001-2009) has compensated for the impact of climate change.

Rainfall has always been a limiting factor for agricultural production in China (Piao et al. 2010), especially in the Huang-Huai-Hai Plain, where only 25%-40% of water demand is satisfied by rainfall during the wheat growing seasons (Mei et al. 2013). Despite the uncertainty in precipitation amounts and the spatial patterns

simulated by climate models (Xin et al. 2013), our study showed that the increasing rainfall in the next 30 years could provide important benefits in terms of the wheat yield. Many other studies have investigated the relative contribution of changing rainfall in increasing wheat yield in China during the past several decades, based on long-term field observations or statistical datasets, and found that there was no significant influence of rainfall on yield (Tao et al. 2014; Wei et al. 2012; Xiao and Tao 2014). One reason for this result is that rainfall did not change substantially during the studied period (Wei et al. 2012). The other reason is that winter wheat in northern China is well irrigated, so that the deficit in water is compensated by pumped groundwater, and the impact of rainfall changes was smoothed over. However, in our study, to fully capture the rainfall changes to yield, the wheat growth and development was simulated under rainfed conditions. Thus, the contributions of increasing rainfall on wheat yield were higher than those in other studies.

6. Conclusion

Climate change during the next 30 years (2021—2050) was found to have a positive impact on simulated wheat yield for two Representative Concentration Pathways. The largest contribution is caused by increasing precipitation during the growing season, which is inconsistent with other statistical models of observed data. In these previous studies, the wheat is irrigated; thus, the impact of changes in precipitation is weakened. Interestingly, the increasing solar radiation shows a negative impact on wheat yield in our study. We further found that this reverse is caused by the higher evapotranspiration that results from increases in solar radiation, which consequently increases water stress. Most other studies have shown that crop yield is positively correlated with solar radiation, mainly because, in their simulations, the wheat was irrigated. Thus, the water stress remained at low levels, even though the evapotranspiration was increased by solar radiation.

Acknowledgements

This research was supported by the 12th five-year plan of the National Key Technologies R&D Program (2012BAD09B01), the National Basic Research Program of China (973 Program) (2012CB955904) and the National Science Foundation for Young Scientists of China (41401510). We thank the University of Liège-Gembloux Agro-Bio Tech and more specifically the research platform AgricultureIsLife for the funding of the scientific stay in Belgium that made this paper possible. We gratefully acknowledge the anonymous reviewers for their valuable comments on the manuscript.

7. Reference

David B L, Christopher B F. 2007. Global scale climate–crop yield relationships and the impacts of recent warming. Environmental Research Letters, 2, 014002.

Hunt L A, Boote K J. 1998. Data for model operation, calibration, and evaluation. In: Tsuji G Y, Hoogenboom G, Thornton P K (eds), Understanding Options for Agricultural Production. Springer Netherlands, Dordrecht. pp. 9-39.

Jerry K, Tim H, Andre D, Tim W. 2012. Climate change impacts on crop productivity in Africa and South Asia. Environmental Research Letters, 7, 034032.

Jones J W, Tsuji G Y, Hoogenboom G, Hunt L A, Thornton P K, Wilkens P W, Imamura D T, Bowen W T, Singh U. 1998. Decision support system for agrotechnology transfer: DSSAT v3. In: Tsuji G Y, Hoogenboom G, Thornton P K (eds), Understanding Options for Agricultural Production. Springer Netherlands, Dordrecht. pp. 157-177.

Ju H, van der Velde M, Lin E, Xiong W, Li Y. 2013. The impacts of climate change on agricultural production systems in China. Climatic Change, 120, 313-324. doi,10.1007/s10584-013-0803-7.

Keating B A, Carberry P S, Hammer G L, Probert M E, Robertson M J, Holzworth D, Huth N I, Hargreaves J N G, Meinke H, Hochman Z, McLean G, Verburg K, Snow V, Dimes J P, Silburn M, Wang E, Brown S, Bristow K L, Asseng S, Chapman S, McCown R L, Freebairn D M, Smith C J. 2003. An overview of APSIM, a model designed for farming systems simulation. European Journal of Agronomy, 18, 267-288. doi,http://dx.doi.org/ 10.1016/S1161-0301(02)00108-9.

Lobell D B, Schlenker W, Costa-Roberts J. 2011. Climate Trends and Global Crop Production Since 1980. Science, 333, 616-620. doi,10.1126/science.1204531.

Martínez-Lozano J A, Tena F, Onrubia J E, De La Rubia J. 1984. The historical evolution of the Ångström formula and its modifications: Review and bibliography. Agricultural and Forest Meteorology, 33, 109-128. doi, http://dx.doi.org/10.1016/0168-1923(84) 90064-9.

Mei X, Kang S, Yu Q, Huang Y, Zhong X, Gong D, Huo Z, Liu E. 2013. Pathways to Synchronously Improving Crop Productivity and Field Water Use Efficiency in the North China Plain. Scientia Agricultura Sinica, 46, 1149-1157.

Parry M L, Ruttan V W. 1991. Climate Change and World Agriculture. Environment: Science and Policy for Sustainable Development, 33, 25-29. doi,10.1080/ 00139157.1991.9931405.

Piao S, Ciais P, Huang Y, Shen Z, Peng S, Li J, Zhou L, Liu H, Ma Y, Ding Y, Friedlingstein P, Liu C, Tan K, Yu Y, Zhang T, Fang J. 2010. The impacts of climate change on water resources and agriculture in China. Nature, 467, 43-51.

Ritchie J T, Singh U, Godwin D C, Bowen W T. 1998. Cereal growth, development and yield. In: Tsuji G Y, Hoogenboom G, Thornton P K (eds), Understanding Options for Agricultural Production. Springer Netherlands, Dordrecht. pp. 79-98.

Schlenker W, Roberts M J. 2009. Nonlinear temperature effects indicate severe damages to US crop yields under climate change. Proceedings of the National Academy of Sciences of the United States of America, 106, 15594-15598. doi,10.1073/pnas.0906865106.

Shi W, Tao F, Zhang Z. 2013. A review on statistical models for identifying climate contributions to crop yields. Journal of Geographical Sciences, 23, 567-576. doi,10.1007/s11442-013-1029-3.

Tao F, Yokozawa M, Liu J, Zhang Z. 2008. Climate–crop yield relationships at provincial scales in China and the impacts of

recent climate trends. Climate Research, 38, 83-94.

Tao F, Zhang Z, Xiao D, Zhang S, Rötter R P, Shi W, Liu Y, Wang M, Liu F, Zhang H. 2014. Responses of wheat growth and yield to climate change in different climate zones of China, 1981–2009. Agricultural and Forest Meteorology, 189–190, 91-104. doi,http://dx.doi.org/10.1016/j.agrformet.2014.01.013.

Timsina J, Humphreys E. 2006. Performance of CERES-Rice and CERES-Wheat models in rice–wheat systems: A review. Agricultural Systems, 90, 5-31. doi,http://dx.doi.org/ 10.1016/j.agsy.2005.11.007.

Wang H L, Gan Y T, Wang R Y, Niu J Y, Zhao H, Yang Q G, Li G C. 2008. Phenological trends in winter wheat and spring cotton in response to climate changes in northwest China. Agricultural and Forest Meteorology, 148, 1242-1251. doi,http://dx.doi.org/ 10.1016/j.agrformet.2008.03.003.

Wei X, Ian H, Erda L, Declan C, Yue L, Wenbin W. 2012. Untangling relative contributions of recent climate and CO 2 trends to national cereal production in China. Environmental Research Letters, 7, 044014.

Williams J R, Renard K G, Dyke P T. 1983. EPIC: A new method for assessing erosion's effect on soil productivity. Journal of Soil and Water Conservation, 38, 381-383.

Wolfram S, David B L. 2010. Robust negative impacts of climate change on African agriculture. Environmental Research Letters, 5, 014010.

Xiao D, Moiwo J P, Tao F, Yang Y, Shen Y, Xu Q, Liu J, Zhang H, Liu F. 2015. Spatiotemporal variability of winter wheat phenology in response to weather and climate variability in China. Mitigation and Adaptation Strategies for Global Change, 20, 1191-1202. doi,10.1007/s11027-013-9531-6.

Xiao D, Tao F, Shen Y, Liu J, Wang R. 2014. Sensitivity of response of winter wheat to climate change in the North China Plain in the last three decades. Chinese Journal of Eco-Agriculture, 22, 430-438.

Xiao D, Tao F. 2014. Contributions of cultivars, management and climate change to winter wheat yield in the North China Plain in the past three decades. European Journal of Agronomy, 52, Part B, 112-122. doi,http://dx.doi.org/10.1016/j.eja.2013.09.020.

Xiao G, Zhang Q, Yao Y, Zhao H, Wang R, Bai H, Zhang F. 2008. Impact of recent climatic change on the yield of winter wheat at low and high altitudes in semi-arid northwestern China. Agriculture, Ecosystems & Environment, 127, 37-42. doi,http://dx.doi.org/ 10.1016/j.agee.2008.02.007.

Xin X G, Wu T W, Li J L, Zai Zhi W, Wei Ping L, Fang Hua W. 2013. How Well does BCC_CSM1.1 Reproduce the 20th Century Climate Change over China? Atmospheric and Oceanic Science Letters, 6, 21-26. doi,10.1080/16742834.2013.11447053.

Xiong W, van der Velde M, Holman I P, Balkovic J, Lin E, Skalský R, Porter C, Jones J, Khabarov N, Obersteiner M. 2014. Can climate-smart agriculture reverse the recent slowing of rice yield growth in China? Agriculture, Ecosystems & Environment, 196, 125-136. doi,http://dx.doi.org/10.1016/j.agee.2014.06.014.

Yang J-y, Mei X-r, Huo Z-g, Yan C-r, Ju H, Zhao F-h, Liu Q. 2015. Water consumption in summer maize and winter wheat cropping system based on SEBAL model in Huang-Huai-Hai Plain, China. Journal of Integrative Agriculture, 14, 2065-2076. doi,http://dx.doi.org/ 10.1016/S2095-3119(14)60951-5.

Yong B, Ren L, Hong Y, Gourley J J, Chen X, Dong J, Wang W, Shen Y, Hardy J. 2013. Spatial–Temporal Changes of Water Resources in a Typical Semiarid Basin of North China over the Past 50 Years and Assessment of Possible Natural and Socioeconomic Causes. Journal of Hydrometeorology, 14, 1009-1034. doi,10.1175/JHM-D-12-0116.1.

You L, Rosegrant M W, Wood S, Sun D. 2009. Impact of growing season temperature on wheat productivity in China.

Agricultural and Forest Meteorology, 149, 1009-1014. doi,http://dx.doi.org/10.1016/j.agrformet.2008.12.004.

Yu Q, Li L, Luo Q, Eamus D, Xu S, Chen C, Wang E, Liu J, Nielsen D C. 2014. Year patterns of climate impact on wheat yields. International Journal of Climatology, 34, 518-528. doi,10.1002/joc.3704.

Yuan B, Guo J, Ye M, Zhao J. 2012. Variety distribution pattern and climatic potential productivity of spring maize in Northeast China under climate change. Chinese Science Bulletin, 57, 3497-3508. doi,10.1007/s11434-012-5135-x.

Yuan W, Cai W, Chen Y, Liu S, Dong W, Zhang H, Yu G, Chen Z, He H, Guo W, Liu D, Liu S, Xiang W, Xie Z, Zhao Z, Zhou G. 2016. Severe summer heatwave and drought strongly reduced carbon uptake in Southern China. Scientific Reports, 6, 18813. doi,10.1038/srep18813.

Zhang X, Chen S, Liu M, Pei D, Sun H. 2005. Improved Water Use Efficiency Associated with Cultivars and Agronomic Management in the North China Plain. Agronomy Journal, 97, 783-790. doi,10.2134/agronj2004.0194.

Zhang X, Chen S, Sun H, Shao L, Wang Y. 2011. Changes in evapotranspiration over irrigated winter wheat and maize in North China Plain over three decades. Agricultural Water Management, 98, 1097-1104. doi,http://dx.doi.org/10.1016/j.agwat.2011.02.003.

Chapter VI. Water consumption in winter wheat and summer maize cropping system based on SEBAL model

Water consumption in winter wheat and summer maize cropping system based on SEBAL model in Huang-Huai-Hai Plain, China

Published in *Journal of Integrative Agriculture*, 2015, 14(10): 2065-2076

YANG Jianying, MEI Xurong, HUO Zhiguo, YAN Changrong, JU Hui, ZHAO Fenghua, **LIU Qin***

** Corresponding author*

outline

The purpose of this research is (1) to identify quantity of actual evapotranspiration for winter wheat and summer maize respectively, (2) to develop ETa spatial distribution of the two crops in 3H Plain; and (3) to find out its relationship between crop ETa and land surface parameters and geographic parameters. The results from this study would provide useful information for the development of sustainable agricultural water management practices for 3H Plain, China.

1. Abstract

Crop consumptive water use is recognized as a key element to understand regional water management performance. This study documents an attempt to apply a regional evapotranspiration model (SEBAL) and crop information for assessment of regional crop (winter wheat and summer maize) actual evapotranspiration (ET_a) in Huang-Huai-Hai (3H) Plain. The average seasonal ET_a of summer maize and winter wheat were 354.8and 521.5 mm respectively in 3H Plain. A high-ET a belt of summer maize occurs in piedmont plain, while a low ET_a area was found in the hill-irrigable land and dry land area. For winter wheat, a high ET_a area was located in the middle part of 3H Plain, including low plain-hydropenia irrigable land and dry land, hill-irrigable land and dry land, and basin-irrigable land and dry land. Spatial analysis demonstrated a linear relationship between crop ET_a, normalized difference vegetation index (NDVI), and the land surface temperature (LST). A stronger relationship between ET_a and NDVI was found in the metaphase and last phase than other crop growing phase, as indicated by higher correlation coefficient values. Additionally, higher correlation coefficients were detected between ET_a and LST than that between ET_a and NDVI, and this significant relationship ran through the entire crop growing season. ET_a in the summer maize growing season showed a significant relationship with longitude, while ET_a in the winter wheat growing season showed a significant relationship with latitude. The results of this study will serve as baseline information for water resources management of 3H Plain.

Keywords: ET_a, winter wheat, summer maize, SEBAL, crop information, Huang-Huai-Hai Plain

2. Introduction

Agriculture is the largest water-consuming sector (FAO 1994; Rosegrant et al. 2002) and irrigated agriculture has been expanding rapidly in many developing countries in recent decades, nearly doubling between 1962 and 1998 (Carruthers et al. 1997; Ali and Talukder 2008). During coming decades, water may become the most strategic resource, especially for agricultural production in arid and semi-arid regions of the world (Brewster et al. 2006), which could threaten the sustainability of world agriculture. Accordingly, understanding the quantity of agricultural water consumption is a high priority in areas in which water is currently scarce and over-exploited (Perry 2011). Evapotranspiration (ET) is a useful indicator of crop water consumption; therefore, accurate estimation of regional ET is essential to achieve large scale water resources management (Rwasoka et al. 2011). Current estimates of actual evapotranspiration in China are mainly based on plot-scale experiments (Zhang et al. 1999; Chen et al. 2002; Sun et al. 2003; Jiang and Zhang 2004), from the product of soil moisture and potential ET. However, such estimates are only useful for a specific area, and cannot be expanded to large-scale areas. The level of water consumption differs significantly across regions, farming systems, canal command areas, and farms (Molden et al. 2003). These differences come from many factors, including the source of irrigation water, farm management practices, the timing and efficiency of irrigation water in irrigated regions, and conservation tillage technologies, rainwater harvesting and cropping patterns in rainfed areas (Cai and Sharma 2010).

Development of remote sensing technology has made it possible to estimate land surface evapotranspiration at the regional or basin scale. Numerous remote sensing methods for modeling crop actual evapotranspiration (ET_a) have been improved (De Oliveira et al. 2009; Teixeira et al. 2009; Teixeira and Bassoi 2009; Jia et al. 2012). Bastiaanssen et al. (1998) were the first to use remote sensing data to estimate evapotranspiration in the Bhakra command area, India. And then, several studies demonstrated the strengths of remote sensing in estimating crop evapotranspiration (Courault et al. 2005; Allen et al. 2007). Accurate estimation of agricultural water consumption is based on two inputs, the model precision, which has been calibrated and validated by many studies, and the ground truth information, including crop dominance maps, phenological characteristics, and agriculture productivity. However, ground truth information is often scarce and difficult to obtain.

The Huang-Huai-Hai Plain (3H Plain) is the major crop producing region in China, with 3.5 million ha of highly intensive arable land, accounting for 19% of the country's crop production area. The recognized major limiting factor to crop production in the region is water shortage, which is expected to be exacerbated by increasing food demand in the region (Chen et al. 2005). Over exploitation of groundwater resources has resulted in water-table decrease at a rate of 1 m per year and severe groundwater depression in the past 20 years (Jia and Liu 2002; Wang et al. 2009). Moreover, climatic changes have intensified with an average decrease in rainfall of 2.92 mm per year (Liu et al. 2010). Thus, available agricultural water resources have become the most important factor influencing crop production in 3H Plain, with the regional water scarcity situation becoming aggravated each year. Considering the spatial variation, accurately identification and

region-wide water accounting are necessary in 3H Plain, to enable reasonable allocation of the limited available agricultural water resources.

In recent years, Li et al. (2008) estimated the ET_a for winter wheat using the SEBAL (Surface Energy Balance Algorithm for Land) model and NOAA (National Oceanic and Atmospheric Administration) data for Hebei Province in the North China Plain (NCP). Yang et al. (2013) analyzed the spatial and temporal variation of crop evapotranspiration (ET_c) and evapotranspiration of applied water (ET_{aw}) of summer maize during the growing season from 1960 to 2009 in the 3H farming region using the simulation of evapotranspiration of applied water (SIMETAW) model. However, observed phenological data was not considered in these investigations, and specific water consumption of winter wheat and summer maize has not yet been determined for larger areas, in 3H Plain. In this research, an approach to estimate the actual evapotranspiration for winter wheat and summer maize respectively based on the MODIS data and SEBAL model is proposed and applied in 347 counties of the 3H Plain in China, which is a farming region providing about 61 and 31% of the nation's wheat and maize production (Wang et al. 2009; Ma et al. 2013). The purpose of this study was: (1) to quantify actual evapotranspiration for winter wheat and summer maize, (2) to determine the spatial pattern of the ET_a of the two crops grown in 3H Plain; and (3) to identify the relationship between crop ET_a and land surface parameters and geographic parameters. The findings from this research will provide useful information for agricultural water management practices for 3H Plain, China.

3. Materials and methods

Study area

3H Plain in northern China is recognized as one of the largest plains in the country, extending from 31°14′ to 40°25′N and 112°33′ to 120°17′E (Figure 38), over an area of about 350000 km². The climate is characterized by a temperate, sub-humid, and continental monsoon climate with an average annual precipitation of 348.5 mm (Ren et al. 2008). Winter is characterized by insufficient water for winter wheat development and production (Nguyen et al. 2011). Nevertheless, 3H Plain is well accepted to be a major agricultural center, accounting for around 61% and 31% of China's wheat and maize production, respectively (Wang et al. 2009; Ma et al. 2013). Accordingly, the cropping system in the plain is well-known to be a winter wheat-summer maize rotation system (Zhao et al. 2006; Liang et al. 2011; Sun et al. 2011). Currently, it is widely recognized that winter wheat is sown in early October and harvested in June of the second year, and that summer maize is then sown immediately afterwards and harvested in later September. 3H Plain is divided into six agricultural sub-regions, coastal land, a farming-fishing area (including the northern part, Zone 1, and the southern part, Zone 7), piedmont plain-irrigable land (Zone 2), low plain-hydropenia irrigable land and dry land (Zone 3), hill-irrigable land and dry land (Zone 4), basin- irrigable land and dry land (Zone 5) and hill-wet hot paddy -paddy field (Zone 6).

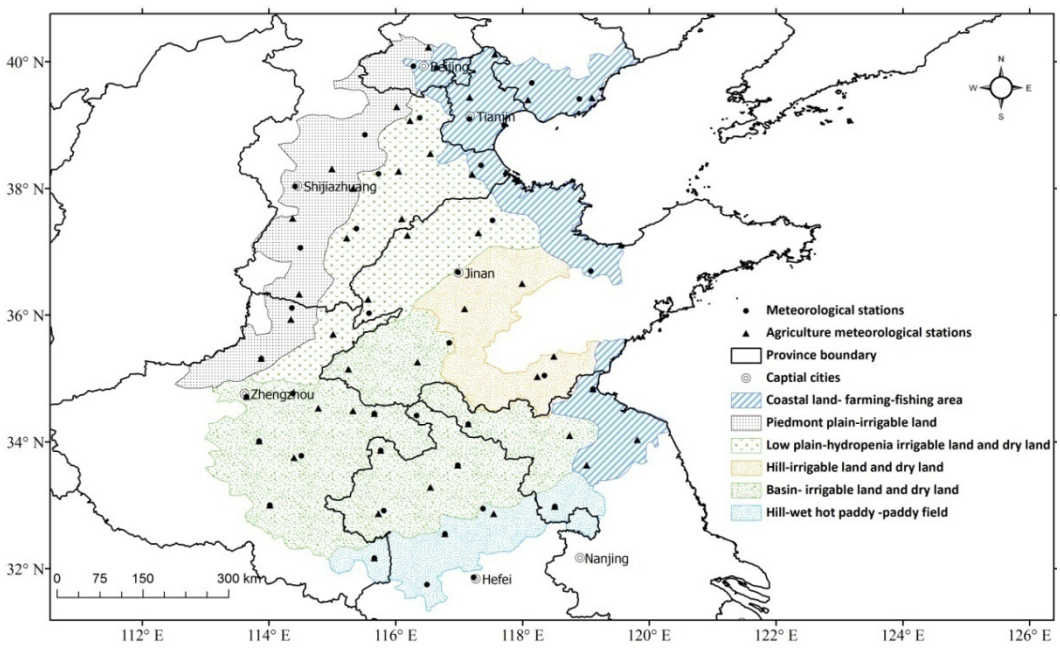

Figure 38 The inset map shows the location of the Huang-Huai-Hai Plain(3H Plain) and its six agricultural subregions. The six agricultural sub-regions of 3H plain include: Coastal land- farming-fishing area(including North part: Zone1 and South part: Zone7), Piedmont plain-irrigable land (Zone2), Low plain-hydropenia irrigable land and dry land (Zone3), Hill-irrigable land and dry land (Zone4), Basin- irrigable land and dry land(Zone5) and Hill-wet hot paddy field (Zone6). The triangles and round black spots mean agrometeorological stations and meteorological stations respectively. The round hollow spots mean the capital cities.

Crop dominance map

Ground truth missions were carried out in the 3H Plain in October 2011 and May 2012. The missions collected 175 samples from throughout the plain (Figure 39-A). Detailed crop patterns were recorded including a crop mixture percentage visual estimate, crop growth period and past crop types (Cai and Sharma 2010). The spectral signature curve of the summer maize-winter wheat rotation was extracted based on the sample points (Figure 39-B). ISODATA (Iterative Self-Organizing Data Analysis Technique) class identification technique and spectral matching technique (SMT) as proposed by Thenkabail et al. (2007b), were conducted to improve the summer maize-winter wheat rotation dominance map (Figure 39-C) using ground truth information as the input. The cultivated area data of 347 counties were used for validation, and the R square value was 0.719, suggesting that the generated summer maize-winter wheat rotation dominance map was reliable (Figure 39-D).

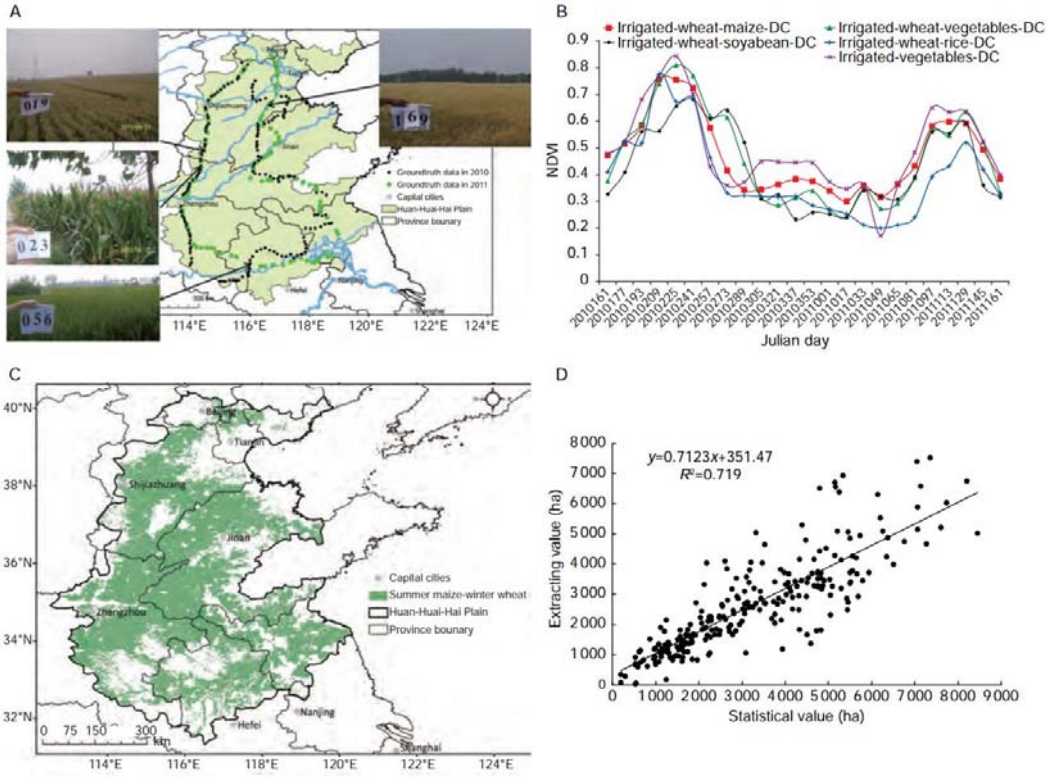

Figure 39 The crop dominance map extraction in the Huang-Huai-Hai Plain. A, samples distribution in 3H Plain. B, spectral signature of summer maize-winter wheat rotation. C, crop dominance map. D, accuracy analysis.

Phenology data

The phenology data for the six agricultural sub-regions of the 3H Plain from 2011 to 2012 were acquired from the China Meteorological Administration (CMA). The data included the date of sowing and maturity of winter wheat and summer maize provided by the 50 agricultural meteorological stations in 3H Plain. The average phenology date was calculated for the six agricultural sub-regions. Summer maize was sown from June 5 to June 20. Summer maize maturity was detected from the middle ten days to the last ten days of September. Winter wheat was sown during October, and harvested during the first ten days of June. Details regarding the phenology date of six agricultural zones are presented in Table 26.

Table 26 Average phenology data for winter wheat and summer maize in six sub region area of 3H Plain

agricultural zoning	Summer maize		Winter wheat	
	Sowing date	Maturity date	Sowing date	Maturity date
Coastal land- farming-fishing area(north)	6.15	9.25	10.1	6.15
Coastal land- farming-fishing area(sounth)	6.20	9.20	10.18	6.5

Piedmont plain-irrigable land	6.10	9.22	10.7	6.7
Low plain-hydropenia irrigable land and dry land	6.11	9.24	10.10	6.7
Hill-irrigable land and dry land	6.18	9.24	10.7	6.8
Basin- irrigable land and dry land	6.10	9.20	10.16	6.3
Hill-wet hot paddy -paddy field	6.5	9.16	10.27	5.25

MODIS products

MODIS products including MOD11A1 (land surface temperature/surface emissivity), MOD13A2 (NDVI) and MCD43B3 (surface albedo) were downloaded through NASA WIST for use in this study. The spatial accuracy of the three MODIS products is 1 km. The temporal accuracy of MOD11A1, MOD13A2 and MCD43B3 was 1-d, 16-d, and 8-d, respectively. For land surface temperature images, cloudy areas were eliminated by replacing the values with the average of two images in the nearest clear dates (Cai and Sharma 2010).

Meteorological data

Meteorological data is also needed for assessment of evapotranspiration. Datasets from 2011 to 2012 from 40 weather stations provided by the China Meteorological Administration (CMA) were used in this study (Figure 38). The obtained data consisted of the daily observed maximum and minimum air temperature and wind speed measured at 10 m. Wind speed at 2 m was calculated from the wind speed at 10 m according to Allen et al (2007) and interpolated with air temperature over the 3H Plain in pixels of 1000 m, which are needed for inputs in SEBAL.

SEBAL model

SEBAL model introduction

In this research, the SEBAL model based on remote sensing technology was applied to estimate the daily ET. The MODIS data were used to estimate the regional ET for the study area. The calculation of the main parameters by the SABEL model is described below (Cai and Sharma 2010).

The SEBAL model is based on the energy balance equation described by the following equation:

$$R_n = G + H + \lambda ET \quad (\text{W m}^{-2}) \qquad \text{Formula 20}$$

Where, R_n (W m^{-2}) is the net radiation; G (W m^{-2}) is the soil heat flux; H (W m^{-2}) is the sensible heat

flux; and λET (W m^{-2}) is the latent heat flux associated with evapotranspiration.

The net radiation flux on the land surface, R_n (W m^{-2}), was calculated using the following equation:

$$R_n = (1-\alpha)K_{in} + (L_{in} - L_{out}) - (1-\varepsilon)L_{in} \qquad \text{Formula 21}$$

Where α is the surface albedo, K_{in} is the incoming short wave radiation (W m^{-2}), L_{in} is the incoming long wave radiation (W m^{-2}), L_{out} is the outgoing long wave radiation (W m^{-2}) , and ε is the land surface emissivity.

The soil heat flux is known to primarily depend on land surface characteristics and soil water content. The soil heat flux was calculated for the SEBAL model by the following equation:

$$G = \frac{T - 273.16}{\alpha}\left[(0.0032\times\frac{\alpha}{0.9} + 0.0062\times(\frac{\alpha}{0.9})^2\right](1-0.98NDVI^4)R_n \qquad \text{Formula 22}$$

The sensible heat flux was calculated using the following equation:

$$H = \frac{\rho_{\text{air}} C_P dT}{r_{ah}} \qquad \text{Formula 23}$$

Where, H is the sensible heat flux (W·m^{-2}), ρ_{air} is the air density (kg·m^{-3}), and C_P is the air specific heat at constant pressure (J·kg^{-1}·K^{-1}).

Since the evaporative fraction Λ is constant during a day, the daily ET_{24} (mm) can be estimated using the following equations:

$$\Lambda = \frac{\lambda ET}{R_n - G} \qquad \text{Formula 24}$$

$$ET_{24} = \frac{\Lambda(R_{24} - G_{24})}{\lambda} \qquad \text{Formula 25}$$

Where, ET_{24} is the daily net radiation (W m^{-2}), G_{24} is the daily soil heat flux (W m^{-2}), and λ is the latent heat of vaporization (MJ kg^{-1}). The SEBAL model is described in detail in Bastiaanssen et al. (1998).

Model validation

In this study, it was difficult to validate the ET_a map because of its high variability and the low resolution produced by MODIS 1 km products. In recent years, the SEBAL model has been applied and

validated in the Americas (Morse et al. 2000; Allen et al. 2002; Trezza 2002), Europe (Jacob et al. 2002; Lagouarde et al. 2002), Africa (Bastiaanssen and Menenti 1990; Farah and Bastiaanssen 2001), and China (Li et al. 2008). Morse et al. (2000) reported that the error in daily ET was 15%, while that in monthly and quarterly ET estimation by SEBAL was 4% in Bear River Basin of Idaho. It was also reported that the error in the estimated daily ET was less than 7% in the Haihe basin (Xiong et al. 2006) and less than 8% in the middle region of Heihe basin(Wang et al. 2003). Taken together, these studies show that the SEBAL model has good efficiency and applicability for ET_a estimation. The model also works particularly well in the vegetative area including areas used for maize and wheat agriculture, which was the focus of the present study (Cai and Sharma 2010). Latent heat flux was extracted from the Yucheng station point, and Figure 40 shows the validation results with the field data for Yucheng station in Shandong Province. The correlation coefficient between the estimated and measured values was 0.888, with a $P<0.01$. Additionally, Table 27 compares the ranges of ET_a values from this study with those of previous studies. Taken together, these results show that SEBAL is suitable for estimating evapotranspiration in winter wheat and summer maize rotation in 3H Plain.

Table 27 Comparison on ET_a of maize and wheat growing season for 3H Plain from this study and literatures.

References	Crop	ET_a (mm)		References
		This study	Literature	
Yucheng, Shandong	Wheat	456	(400—500)450	Chen Bo et al.(2012)
Yucheng, Shandong	maize	349	(300—370)350	Chen Bo et al.(2012)
Xinxiang, Henan	wheat	521	(374.9—551.7)	Xiao J F et al(2009)
Piedmont plain	wheat	400—550	460	Ren H R(2004)
Piedmont plain	maize	300—500	390	Ren H R(2004)

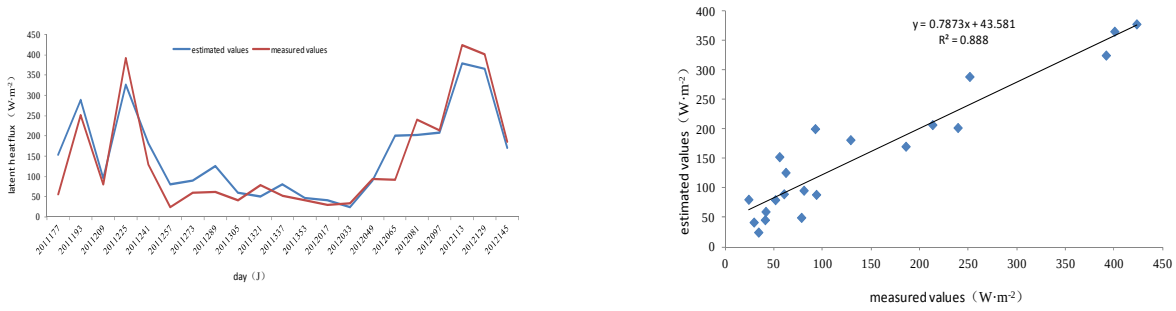

a. Comparation between estimated and measured values b. Scatter map of estimated and measured values

Figure 40 Validation results with the field data in Yucheng station, a: comparation between estimated and measured values; b: Scatter map of estimated and measured values

4. Results

Crop ET_a

Table 28 ET_a of winter wheat and summer maize in study area

	Average ET_a（mm）	Maximum ET_a（mm）	Minimum ET_a（mm）
Summer maize	354.8	552.3	239.4
Winter wheat	521.5	729.2	131.6

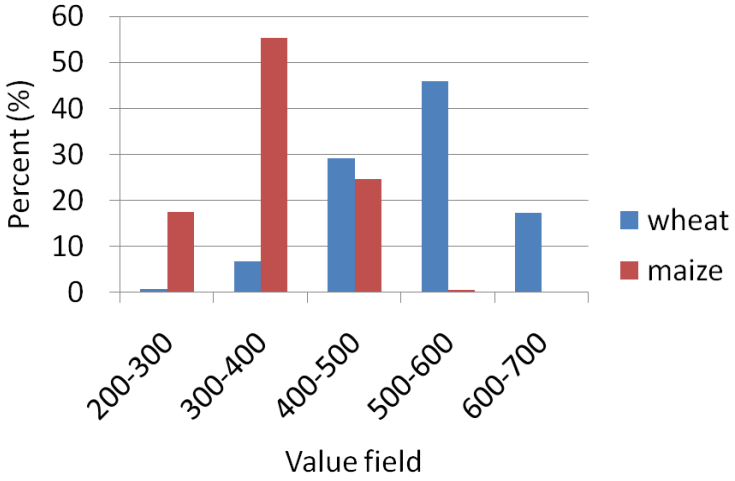

Figure 41 Value level distribution of ET_a in winter wheat and summer maize season in Huang-Huai-Hai Plain. The column chart was obtained based on the data at the size of 30 " ×30 " grid.

The ET_a of summer maize and winter wheat were calculated based on the crop dominant maps and phenology data. The ET_a map and histogram distribution, as well as its basic information are described in Table 28 and Figure 41. The seasonal average ET_a of summer maize was 354.8 mm at 3H Plain, with a minimum value of 239.4 mm and a maximum value of 552.3 mm. As shown in Figure 42-A, a high-ET belt occurs in the piedmont plain, from Beijing, Tianjin to the southern part of Hebei Province. The low ET_a area of summer maize was mainly found in the hill-irrigable land and dry land (Zone 4) area in Shandong Province. The total winter wheat ET_a was comparatively higher than the summer maize ET_a, with an average value of 521.5 mm. The maximum ET_a for winter wheat was 729.2 mm, which was found in the middle part of 3H Plain, while the minimum value was 131.6 mm in the southeast part of Hebei Province. An ET_a belt between 500 and 600 mm was detected in more than 40% of the winter wheat cover area, although significant variations in this value were observed. Difference from the summer maize ET_a map, higher ET_a area was mainly observed in the middle part of 3H Plain, including low plain-hydropenia irrigable land and dry land (Zone 3), hill-irrigable land and dry land (Zone 4), and basin-irrigable land and dry land (Zone 5). Overall, the ET_a between summer maize and winter wheat displayed different spatial distributions among levels.

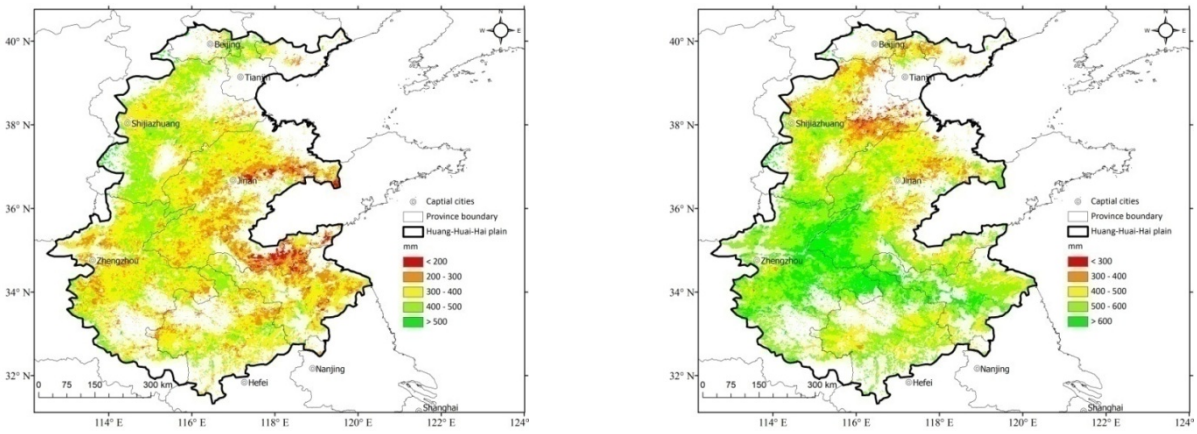

a summer maize　　b winter wheat

Figure 42 Spatial pattern of ET_a in winter wheat - summer maize rotation in 3H Plain, a: spatial pattern of ET_a in summer maize growing season; b: spatial pattern of ET_a in winter wheat growing season. These maps were obtained from the results based on SEBAL model.

Correlation among ET_a, NDVI, and land surface temperature

Investigation of the relationship between crop ET_a and the normalized difference vegetation index (NDVI) and the land surface temperature (LST) are helpful in understanding the effects of NDVI and LST changes on ET_a for winter wheat and summer maize in time series. Correlation coefficient analysis of the ET_a values of the two crops with NDVI and then LST for different Julian days. The ET_a value, NDVI and LST of the two crops were extracted from each raster in space. The relationships between ET_a and NDVI and ET_a and LST in the winter wheat and summer maize growing seasons are shown in Tables 29 and 30, respectively. NDVI is one of the most important parameters to the estimation of actual ET in many models. The results of this study showed that ET_a increased with NDVI. The linear relationship between ET_a and NDVI was consistent with as the results of a previous study by Wang *et al*. (2012). NDVI in the metaphase and last phase was more closed related to ET_a during the crop growing season, indicated by a higher positive correlation coefficient value. The positive relationship between ET_a and NDVI in the winter wheat growing season was stronger than in the summer maize growing season in the metaphase and last phase, as indicated by a correlation coefficient value of ET_a during the summer maize growing season of $\leqslant$0.4, but as high as 0.6 in the winter wheat growing season. This relationship appears to be stronger in Zone 3 (piedmont plain-irrigable land), where the correlation coefficient values reached 0.67. The NDVI index increased strongly in the metaphase and last phase, when crop activities intensified. These changes were expressed as a lower impedance of evapotranspiration and increased latent heat flux in each pixel. This crop physiological reaction may have led to an increase in the actual ET. These changes were more obvious in flat interior regions, such as piedmont plain-irrigable land, than in basins or hills. The relationship between ET_a and NDVI was greater during winter and spring, because there was less precipitation participating in the space hydrological cycle.

Table 29 Relationship between ET_a in summer maize growing season and NDVI, and then LST through multivariate regression analysis. *represents linear coefficients significant at $P<0.05$. **represents linear coefficients significant at $P<0.01$.

J day	Relationship between ET_a and NDVI							Relationship between ET_a and LST						
	1	2	3	4	5	6	7	1	2	3	4	5	6	7
2011193	0.22**	-0.04	0.11	-0.09	0.03	0.11	-0.05	-0.42**	-0.48**	-0.15*	-0.49**	-0.44**	-0.31**	-0.33**
2011209	0.32**	0.23**	0.24**	-0.11	0.00	-0.09	0.14	-0.31**	-0.25**	-0.10	-0.21**	-0.23**	-0.32**	-0.22**
2011225	0.14*	0.11	0.13	0.09	-0.08	0.19*	0.03	-0.28**	-0.48**	-0.18*	-0.45**	-0.31**	-0.41**	-0.34**
2011241	0.21**	0.30**	0.10	0.08	0.03	0.07	0.20**	-0.35**	-0.67**	-0.21**	-0.03	-0.19**	-0.17*	-0.28**
2011257	0.30**	0.26**	0.06	0.06	0.17*	0.21**	0.18*	-0.34**	-0.38**	0.16*	-0.47**	-0.28**	-0.08	-0.49**

Table 30 Relationship between ET_a in winter wheat growing season and NDVI, and then LST through multivariate regression analysis. *represents linear coefficients significant at $P<0.05$. **represents linear coefficients significant at $P<0.01$.

J day	Relationship between ET_a and NDVI							Relationship between ET_a and LST						
	1	2	3	4	5	6	7	1	2	3	4	5	6	7
2011289	0.01	0.12	-0.28**	0.02	-0.11	-0.14*	0.16*	-0.26**	-0.01	0.27**	-0.15*	0.06	-0.12	-0.26**
2011305	0.18*	0.17*	0.29**	0.12	-0.17*	-0.14*	-0.17*	-0.28**	-0.19**	-0.33**	-0.19**	-0.28**	-0.19**	-0.03
2011321	0.17*	0.06	0.35**	0.12	-0.04	-0.08	-0.01	-0.03	0.12	0.42**	0.14*	-0.45**	0.02	0.02
2011337	0.17*	0.11	0.43**	0.11	-0.08	-0.04	0.03	-0.38**	-0.25**	-0.70**	-0.30**	-0.36**	-0.07	0.05
2011353	0.19**	0.16*	0.44**	0.16*	-0.09	-0.01	0.05	-0.19**	0.20**	-0.24**	0.00	-0.42**	-0.16*	-0.45**
2012001	0.18*	0.15*	0.44**	0.16*	-0.07	-0.03	0.04	-0.24**	0.04	-0.36**	-0.16*	-0.45**	-0.40**	-0.30**
2012017	0.18	0.21	0.48	0.15	-0.12	0.06	0.07	-0.32**	-0.12	-0.22**	-0.17*	0.02	-0.19**	-0.10
2012033	0.15*	0.26**	0.56**	0.29**	-0.07	-0.06	0.19*	-0.45**	-0.02	0.09	-0.13	-0.29**	-0.27**	-0.05
2012049	0.18*	0.28**	0.54**	0.29**	-0.17*	-0.02	0.15*	-0.56**	-0.10	-0.15*	-0.48**	-0.15*	-0.22**	-0.15*
2012065	0.15	0.43**	0.55**	0.24**	-0.09	-0.02	0.32**	-0.52**	-0.38**	-0.35**	-0.45**	-0.13	-0.06	-0.29**
2012081	0.22**	0.36**	0.65**	0.19**	-0.05	0.02	0.09	-0.44**	-0.47**	-0.65**	-0.47**	-0.16*	-0.09	-0.26**
2012097	0.17	0.27**	0.67**	0.20**	0.07	-0.05	0.14*	-0.56**	-0.43**	-0.73**	-0.49**	0.05	-0.05	-0.36**
2012113	0.16	0.41**	0.66**	0.16	0.08	-0.03	0.11	-0.06	0.18*	-0.12	-0.32**	-0.27**	-0.18*	-0.28**
2012129	0.21	0.40**	0.57**	0.19**	0.14*	-0.13	0.12	-0.35**	-0.51**	-0.63**	-0.14	-0.30**	-0.47**	-0.50**
2012145	0.25**	0.31**	0.55**	0.14	0.32**	0.05	0.20*	-0.48**	-0.30**	-0.58**	-0.16*	-0.28**	-0.38**	-0.14*
2012161	0.23**	0.26**	0.03	0.21**	0.10	0.12	0.20**	-0.45**	-0.10	0.00	-0.14*	-0.07	-0.19**	0.06

As described above, a higher value of correlation coefficient was detected between ET_a and LST than between ET_a and NDVI, indicating a stronger relationship. The significant relationship between ET_a and LST ran through the entire crop growing season. Additionally, the correlation between ET_a and LST was negative, indicating that an increased LST may lead to a decreased ET_a. In the later portion of the winter wheat growing season in Zone 3 (piedmont plain-irrigable land), the correlation coefficient value was higher (R >0.7). Temperature is an important factor which is associated with stomatal conductance and transpiration (Yang et al. 2012). For maize, the effect of growth temperature on transpiration was obvious when maize was grown at low temperature (22/18°C) and measured at higher temperature (30°C). The 3H Plain is acknowledged as a water-stress area that primarily receives rainfall during summer. As results, serious drought always occurs in winter and spring, which may impact transpiration and canopy temperature. When crops are subjected to water stress, they close their leaf stomata, which reduces evapotranspiration, leading to increased crop canopy temperature.

Correlation between ET_a and geographic parameters

For a given region, reference evapotranspiration (ET_0) is only determined by weather parameters; however, several factors can affect actual evapotranspiration, such as soil types, current precipitation, crop types, soil moisture storage in the early stage, and field management. We attempted to identify the relationship between ET_a and geographic parameters in this study because they may reflect climate fluctuations, changes on soil characteristics, field management and irrigation schemes with geography transitions. ET_a in the summer maize period represented a significant relationship with longitude (P<0.01), which described an increasing trend from the eastern portion to the western part of 3H Plain (Figure 43-A). This spatial pattern of ET_a in the summer maize growing season is in accordance with that of precipitation. Usually, the growing season for summer maize in 3H Plain is from July to September, when there is concentrated precipitation and higher temperature. During this period, less than 20% of ET_a is from irrigation. When compared to temperature, crop physiology is more sensitive to water for summer maize owing to the sufficient heat resources in the summer maize growing season. Rainfall was considered as the main crop water resource in the eastern portion of 3H Plain, where more precipitation was detected in the past 40 years. Supplementary irrigation has always been used in the western part of the region, which is characterized by piedmont plain-irrigable land, low plain-hydropenia irrigable land and dry land.

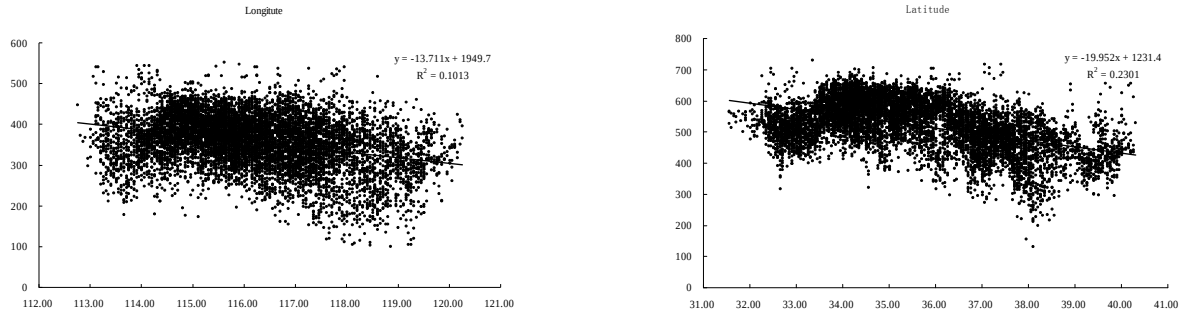

a Correlation analysis between ET_a in summer maize growing season and longitude

b Correlation analysis between ET_a in winter wheat growing season and latitude

Figure 43 Correlation analysis between crop ET_a and geographic parameters. a is correlation analysis between ET_a in summer maize growing season and longitude. X axes represents the longitude and Y axes represents ET_a (mm) for summer maize growing season. b is correlation analysis between ET_a in winter wheat growing season and latitude. X axes represents the latitude and Y axes represents ET_a (mm) for winter wheat growing season.

As shown in Figure 44-A, the ET_a for winter wheat had a significant relationship with latitude (with R^2=0.23, P<0.01), increasing as latitude increased. Winter wheat accounts for about 70% of the total agricultural water use in this area, and precipitation during the winter wheat growing season ranges from 100 to 180 mm (Li et al. 2010), which can only meet around 25%–40% of the water requirements for the season. Although it is an important area for winter wheat production, rainfall in the region is erratic and limited during the growing stage; accordingly, supplementary irrigation has been widely adopted to ensure maximum production (Sun et al. 2006; Li et al. 2008). For irrigated wheat, seasonal ET_a mostly ranges from 400 to 600 mm, 70% of which is derived from irrigation. Spatial differences have not only been found in precipitation, but also in irrigation practices. According to Yang et al. (2013), precipitation in the southeast part of 3H Plain can account for over 50% of the total water consumption for winter wheat. However, irrigation was identified as the dominant water resource in the northern part of 3H Plain, including piedmont plain-irrigable land (Zone 2) and low plain-hydropenia irrigable land and dry land (Zone 3), were irrigation accounts for more than 60% of the winter wheat water consumption.

5. Discussion

Assessment of regional crop evapotranspiration

The findings presented in this paper are the first region-wide, integrated remote sensing, SEBAL model, and ground truth and phenology data to estimate ET_a in 3H Plain. There are various ways to estimate crop water consumption, most of which are relatively precise at very small scales, but impractical over large

scales. Crop water consumption as the main water output in agricultural hydrological processes is necessary to identify not only experimental field points in a controlled environment, but also at regional scales. At regional scales, crop evapotranspiration is often more relevant to policy, agriculture input, soil types and available resources. However, water consumption by crops cannot be accurately identified without crop distribution information (Cai and Sharma 2010). This study is the first attempt to apply regional evapotranspiration model and crop information for assessment of crop (winter wheat and summer maize cropping system) evapotranspiration at a large regional scale, such as the Huang-Huai-Hai Plain. This addition marks the improvement of this research work over numerous previous studies (Zwart and Bastiaanssen 2007; Immerzeel et al. 2008; Cai and Sharma 2010; Zwart et al. 2010).

Separation of evapotranspiration of the two crops

A method was developed to extend daily evapotranspiration to the crop growing season in this study. The extrapolation of daily evapotranspiration to crop growing seasons in pixel level was conducted through spatial interpolation methods based on crop phenology data. Crop (winter wheat and summer maize) phenology data for the 3H Plain, as well as other essential information, was used to obtain pixel crop phenology data. Crop growth is more closely related to latitude and longitude, elevation, crop varieties and meteorological factors, such as air temperature, light and water (Yang et al. 2011). However, the method explained in this paper avoided complex factors and parameters above, and can be easily applied elsewhere. Additionally, evapotranspiration extracted from winter wheat and summer maize can be more accurately estimated than the aforementioned factors.

Possible uncertainty of results

The ET_a in this study was 354.8 and 521.5 mm for summer maize and winter wheat respectively, which is higher than previous studies (Chen et al. 2012; Xiao et al. 2009). It is not surprising that ET_a was lower at the research stations since they are operated under a controlled environment to achieve the maximum water use efficiency, and are less constrained than farmers with regards to resources availability (Yan and Wu 2014). In general, the ET_a of winter wheat was higher than that of summer maize in 3H Plain. These findings partially agreed with those of Ren and Luo (2004) and Chen et al. (2012) who pointed out that crop physiological characteristics, field management measures and irrigation programs are major factors influencing ET_a, even if reference evapotranspiration (ET_0) and crop water requirement (ET_c) occasionally showed different characteristics. However, spatial differences have made it possible for a target region to have contrary results. For example, in Hebei Province the ET_a of summer maize was a slightly higher than that during the winter wheat growing season. Spatial analysis demonstrated a linear relationship between crop ET_a and NDVI and land surface temperature, which is consistent with the result of a study conducted by Wang (2012). It should be noted that the raster pixel was upscaled to 1000 m$\times$1000 m for easier presentation, which may have caused the pixels to merge together, and decreased the relevance between

dependent and independent variables. As a result, the correlation coefficient between crop ET_a and NDVI and land surface temperature may actually be higher than the calculated value.

Need for refinement

It is important to note that there are some uncertainties associated with estimating crop evapotranspiration using remote sensing data and the SEBAL model over a large-scale region such as the 3H Plain. Gathering remote sensing data is a complicated process that must be followed by sensor calibration and atmospheric correction (Cai and Sharma 2010). The spatial distribution of evapotranspiration modeling from SEBAL is 1000 m×1000 m; however, mixed cropping patterns and fragmented farming are found common in crop planting extraction research, so sub-pixel area fraction estimation is well accepted (Thenkabail et al. 2007a; Hao et al. 2011). In some situations, one pixel contains several tapes except target crop, such as water body, residential areas, and forest land. Under the given conditions, the image element may be exaggerated or ignored, which can lead poor estimations and increased errors.

6. Conclusion

In this study, actual evapotranspiration for winter wheat and summer maize respectively and its spatial patterns were quantified in 3H Plain. The seasonal average ET_a of summer maize and winter wheat were 354.8 and 521.5 mm in 3H Plain. A high-ET belt of summer maize covers the piedmont plain, and low ET_a areas of summer maize are mainly found in the Hill-irrigable land and dry land area. For winter wheat, higher ET_a areas were located in the middle part of 3H Plain, including low plain-hydropenia irrigable land and dry land (Zone 3), hill-irrigable land and dry land (Zone 4), and basin-irrigable land and dry land (Zone 5). Spatial analysis demonstrated a linear relationship between crop ET_a and NDVI, as well as between ET_a and land surface temperature. During the crop growing season, ET_a was more closely related to NDVI in the metaphase and last phase.

We attempted to identify relationships between ET_a and crop growing season land surface parameters and geographic parameters. NDVI in the metaphase and last phase showed a closer correlation to ET_a in the crop growing season, and a significant relationship between ET_a and LST was observed throughout the crop growing season. ET_a in the summer maize growing season was correlated with longitude, while ET_a in the winter wheat growing season showed a significant relationship with latitude. Field management (supplemental irrigation) also showed a strong response to the ET_a pattern in 3H Plain.

Acknowledgements

This research was supported by the 12th five-year plan of the National Key Technologies R&D Program (2012BAD09B01), the National Basic Research Program of China (973 Program) (2012CB955904) and the Chinese National Scientific Foundation (41401510). We gratefully acknowledge Prof. Vinay Nangia, Agricultural Hydrologist, from the International Center for Agricultural Research in the Dry Areas (ICARDA) for his English editing.

7. References

Ali M H, Talukder M 2008. Increasing water productivity in crop production—a synthesis. Agricultural Water Management, 95, 1201–1213.

Allen R G, Morse A, Tasumi M, Trezza R, Bastiaanssen W, Wright J L, Kramber W. 2002. Evapotranspiration from a satellite-based surface energy balance for the Snake Plain Aquifer in Idaho. In: Proceedings of the USCID/EWRI Conference on Energy, Climate, Environment and Water Issues and opportunities for Irrigation and Drainage. San Luis Obispo, California, USA. pp. 167–178.

Allen R G, Tasumi M, Trezza R. 2007. Satellite-based energy balance for mapping evapotranspiration with internalized calibration (METRIC)—Model. Journal of Irrigation and Drainage Engineering, 133, 380–394.

Bastiaanssen W, Menenti M. 1990. Mapping groundwater losses in the western desert of Egypt with satellite measurements of surface reflectance and surface temperature. Proceedings and Information-TNO Committee on Hydrological Research,42, 61–90.

Bastiaanssen W, Menenti M, Feddes R A, Holtslag A. 1998. A remote sensing surface energy balance algorithm for land (SEBAL). 1. Formulation. Journal of Hydrology, 212, 198–212.

Brewster M, Herrmann T, Bleish B, Pearl R. 2006. A Gender Perspective on Water Resources and Sanitation. Spring, Wagadu. pp. 1–23.

Cai X L, Sharma B R. 2010. Integrating remote sensing, census and weather data for an assessment of rice yield, water consumption and water productivity in the Indo-Gangetic river basin. Agricultural Water Management, 97, 309–316.

Carruthers I, Rosegrant M W, Seckler D. 1997. Irrigation and food security in the 21st century. Irrigation and Drainage Systems, 11, 83–101.

Chen B, Ou Y, Chen W, Liu L. 2012. Water comsumption for winter wheat and summer maize in the North China plain in recent 50 years. Journal of Natural Resources, 27, 1186–1199. (in Chinese).

Chen J, Tang C, Sakura Y, Yu J, Fukushima Y. 2005. Nitrate pollution from agriculture in different hydrogeological zones of the regional groundwater flow system in the North China Plain. Hydrogeology Journal, 13, 481–492.

Chen S, Zhang X, Liu M. 2002. Soil temperature and soil water dynamics in wheat field mulched with maize straw. Chinese Journal of Agrometeorology, 23, 34–37. (in Chinese)

Courault D, Seguin B, Olioso A. 2005. Review on estimation of evapotranspiration from remote sensing data: From empirical to numerical modeling approaches. Irrigation and Drainage systems, 19, 223–249.

FAO (Food and Agriculture Organization). 1994. The state of food and agriculture 1993. Food and Agriculture Organization. Rome, Italy.

Farah H O, Bastiaanssen W. 2001. Spatial variations of surface parameters and related evaporation in the Lake Naivasha Basin estimated from remote sensing measurements. Hydrological Processes, 15, 1585–1607.

Hao W P, Mei X R, Cai X L, Du J T, Liu Q. 2011. Crop planting extraction based on muli-temporal remote sensing data in Northeast China. Transactions of the CSAE, 27, 201–207. (in Chinese).

Immerzeel W W, Gaur A, Zwart S J. 2008. Integrating remote sensing and a process-based hydrological model to evaluate water use and productivity in a south Indian catchment. Agricultural Water Management, 95, 11–24.

Jacob F, Olioso A, Gu X F, Su Z, Seguin B. 2002. Mapping surface fluxes using airborne visible, near infrared, thermal infrared remote sensing data and a spatialized surface energy balance model. Agronomie, 22, 669–680.

Jia J, Liu C. 2002. Groundwater dynamic drift and response to different exploitation in the North China Plain: A case study of Luancheng County, Hebei Province. Acta Geographica Sinica-Chinese Edition, 57, 201–209.

Jia Z, Liu S, Xu Z, Chen Y, Zhu M. 2012. Validation of remotely sensed evapotranspiration over the Hai River Basin, China. Journal of Geophysical Research (Atmospheres), 17, D13.

Jiang J, Zhang Y. 2004. Soil–water balance and water use efficiency on irrigated farmland in the North China Plain. Journal of Soil and Water Conservation, 18, 61–65. (in Chinese)

Lagouarde J, Jacob F, Gu X F, Olioso A, Bonnefond J, Kerr Y, Mcaneney K J, Irvine M. 2002. Spatialization of sensible heat flux over a heterogeneous landscape. Agronomie-Sciences des Productions Vegetales Environnement, 22, 627–634.

Li H, Zheng L, Lei Y, Li C, Liu Z, Zhang S. 2008. Estimation of water consumption and crop water productivity of winter wheat in North China Plain using remote sensing technology. Agricultural Water Management, 95, 1271–1278.

Li Q, Dong B, Qiao Y, Liu M, Zhang J. 2010. Root growth, available soil water, and water-use efficiency of winter wheat under different irrigation regimes applied at different growth stages in North China. Agricultural Water Management, 97, 1676–1682.

Liang W, Carberry P, Wang G, L R, L H, Xia A. 2011. Quantifying the yield gap in wheat-maize cropping systems of the Hebei Plain, China. Field Crop Research, 124, 180–185.

Liu S, Mo X, Lin Z, Xu Y, Ji J, Wen G, Richey J. 2010. Crop yield responses to climate change in the Huang-Huai-Hai Plain of China. Agricultural Water Management, 97, 1195–1209.

Ma Y, Feng S Y, Song X F. 2013. A root zone model for estimating soil water balance and crop yield response to deficit irrigation in the Northern China Plain. Agricultural Water Management, 127, 13–24.

Molden D, Murray-Rust H, Sakthivadivel R, Makin I. 2003. A water-productivity framework for understanding and action. In: Water Productivity in Agriculture: Limits and Opportunities for Improvement. CABI Publishing, Wallingford, UK. pp. 1–18.

Morse A, Tasumi M, Allen R G, Kramber W J. 2000. Application of The SEBAL Methodology for Estimating Consumptive Use of Water and Streamflow Depletion in the Bear River Basin of Idaho Through Remote Sensing. Idaho Department of Water Resources–University of Idaho, UAS.

Nguyen T T, Qiu J J, Ann V, Li H, Eric V R. 2011. Temperature and precipitation suitability evaluation for winter wheat and summer maize cropping system in the Huang-Huai-Hai plain of China. Journal of Integrative Agriculture, 10, 275–288.

De Oliveira A S, Trezza R, Holzapfel E A, Lorite I, Paz V P S . 2009. Irrigation water management in Latin America. Chilean Journal of Agricultural Research, 69, 7–16.

Perry C. 2011. Accounting for water use: Terminology and implications for saving water and increasing production. Agricultural Water Management, 98, 1840–1846.

Ren H, Luo Y. 2004. The experimental research on the water-consumpion of winter wheat and summer maize in the Northwest plain of Shandong province. Journal of Irrigation and Drainage, 23, 37–39. (in Chinese)

Ren J, Chen Z, Zhou Q, Tang H. 2008. Regional yield estimation for winter wheat with MODIS-NDVI data in Shandong, China. International Journal of Applied Earth Observation and Geoinformation, 10, 403–413.

Rosegrant M W, Cai X M, Cline S A, Cai X. 2002. Global water outlook to 2025: Averting an impending crisis. In: IFPRI-2020 Vision/ International Water Management Institute, Internat. Food Policy Institute, Washington, DC. pp. 26.

Rwasoka D T, Gumindoga W, Gwenzi J. 2011. Estimation of actual evapotranspiration using the Surface Energy Balance System (SEBS) algorithm in the Upper Manyame catchment in Zimbabwe. Physics and Chemistry of the Earth (Parts A/B/C), 36, 736–746.

Sun H, Liu C, Zhang X, Shen Y, Zhang Y. 2006. Effects of irrigation on water balance, yield and WUE of winter wheat in the North China Plain. Agricultural Water Management, 85, 211–218.

Sun H, Zhang Y, Zhang X, Mao X, Pei D, Gao L. 2003. Effects of water stress on growth and development of winter wheat in the North China Plain. Acta Agriculture Boreali-Sinica, 18, 23–26. (in Chinese)

Sun Q, Krbel R, Mller T, Rmheld V, Cui Z, Zhang F, Chen X. 2011. Optimization of yield and water-use of different cropping systems for sustainable groundwater use in North China Plain. Agricultural Water Management, 98, 808–814.

Teixeira A D C, Bassoi L H. 2009. Crop water productivity in semi-arid regions: From field to large scales. Annals of Arid Zone, 48, 1–13.

Teixeira A D C, Bastiaanssen W, Ahmad M D, Bos M G. 2009. Reviewing SEBAL input parameters for assessing evapotranspiration and water productivity for the Low-Middle Sao Francisco River basin, Brazil: Part A: Calibration and validation. Agricultural and Forest Meteorology, 149, 462–476.

Teixeira A H C, Bastiaanssen W G M, Ahmad M D, Bos M G. 2009. Reviewing SEBAL input parameters for assessing evapotranspiration and water productivity for the Low-Middle São Francisco River basin, Brazil: Part A: Calibration and validation. Agricultural and Forest Meteorology, 149, 462–476.

Thenkabail P S, Biradar C M, Noojipady P, Cai X L, Dheeravath V, Li Y J, Velpuri M, Gumma M K, Pandey S. 2007a. Sub-pixel area calculation methods for estimating irrigated areas. Sensors, 7, 2519–2538.

Thenkabail P S, GangadharaRao P, Biggs T, Krishna M, Turral H. 2007b. Spectral matching techniques to determine historical land-use/land-cover (LULC) and irrigated areas using time-series 0.1-degree AVHRR Pathfinder datasets. Photogrammetric Engineering & Remote Sensing, 73, 1029–1040.

Trezza R. 2002. Evapotranspiration using a satellite-based surface energy balance with standardized ground control. Ph D thesis, Utah State University, Logan, UT.

Wang E, Chen C, Yu Q. 2009. Modeling the response of wheat and maize productivity to climate variability and irrigation in the North China Plain. In: 18th World IM4CSIMODSIM Congress. Cairns, Australia. pp. 2742–2748.

Wang J, Gao F, Liu S. 2003. Remote sensing retrieval of evapotranspiration over the scale of drainage basin. Remote Sensing Technology and Application, 18, 332–338. (in Chinese)

Wang S, Song X, Wang Q, Xiao G, Liu C, Liu J. 2009. Shallow groundwater dynamics in North China Plain. Journal of Geographical Sciences, 19, 175–188.

Wang W T, Zhao Q L, Du J. 2012. Advances in the study of evapotranspiration of regional land surface based on remote sensing technology. Remote Sensing For Land and Resources, 24, 1–7. (in Chinese)

Xiao J, Liu Z, Duan A. 2009. Studies on water production function of winter wheat in Xinxiang district. Journal of Henan Agricultural, 1, 55–59. (in Chinese)

Xiong J, Wu B, Zhou Y, Li J. 2006. Estimating evapotranspiration using remote sensing in the Haihe basin. International

Geoscience and Remote Sensing Symposium. Denver, Colorado, USA,.pp. 1044–1047.

Yan N, Wu B. 2014. Integrated spatial–temporal analysis of crop water productivity of winter wheat in Hai Basin. Agricultural Water Management, 133, 24–33.

Yang J, Liu Q, Mei X, Yan C, Ju H, Xu J. 2013. Spatiotemporal characteristics of reference evapotranspiration and its sensitivity coefficients to climate factors in Huang-Huai-Hai plain, China. Journal of Integrative Agriculture, 12, 2280–2291.

Yang J, Mei X, Liu Q, Yan C, He W, Liu E, Liu S. 2011. Variations of winter wheat growth stages under climate changes in northern China. Chinese Journal of Plant Ecology, 35, 623–631. (in Chinese)

Yang X L, Gao W S, Shi Q H, Chen F, Chu Q Q. 2013. Impact of climate change on the water requirement of summer maize in the Huang-Huai-Hai farming region. Agricultural Water Management, 124, 20–27.

Yang Z, Sinclair T R, Zhu M, Messina C D, Cooper M, Hammer G L. 2012. Temperature effect on transpiration response of maize plants to vapour pressure deficit. Environmental and Experimental Botany, 78, 157–162.

Zhang H, Wang X, You M, Liu C. 1999. Water-yield relations and water-use efficiency of winter wheat in the North China Plain. Irrigation Science, 19, 37–45.

Zhao R F, Chen X P, Zhang F S, Zhang H, Schroder J, Rmheld V. 2006. Fertilization and nitrogen balance in a wheat - maize rotation system in North China. Agronomy Journal, 98, 938–945.

Zwart S J, Bastiaanssen W G. 2007. SEBAL for detecting spatial variation of water productivity and scope for improvement in eight irrigated wheat systems. Agricultural Water Management, 89, 287–296.

Zwart S J, Bastiaanssen W G, de Fraiture C, Molden D J. 2010. WATPRO: A remote sensing based model for mapping water productivity of wheat. Agricultural Water Management, 97, 1628–1636.

Chapter Ⅶ. An assessment of water consumption, grain yield and water productivity of winter wheat

An assessment of water consumption, grain yield and water productivity of winter wheat in agricultural sub-regions of Huang-Huai-Hai Plain, China
In preparation, to be submitted, 2017
Qin Liu, Bernard Tychon, Changrong Yan, Jianying Yang, Sarah Garré*,
* Corresponding author

Outline

Considering the above background, this research focuses on: (1) the crop productivity for wheat is estimated using satellite-based model, linear regression equation-integrated remotely sensed images, and census data; (2) the characteristics of the water productivity for wheat are investigated based on the relations among yield, CWP, and ET and results from spatial analysis; and (3) improvements of the water productivity for wheat are discussed in combination with water consumption structure and agronomical practice analysis across 3H Plain.

1. Abstract

Huang-Huai-Hai Plain (3H Plain), which is the wheat production base of China, is recognized to be one of the most water stressed areas of the world due to the excessive exploitation of groundwater combined with precipitation reduction. Identification of areas with a low crop water productivity (CWP) and achieving a higher grain yield per unit of consumed water are therefore of uttermost importance for the future agriculture in this region. In this paper, the crop water productivity of winter wheat (*Triticumaestivum L.)* was estimated and subsequently analyzed by combining remote sensing imagery and county-level census and meteorological data of six agricultural sub-regions of the 3H Plain. The average CWP of winter wheat in the plain is 0.95 $kg \cdot m^{-3}$, with CWP values across the plain ranging between 0.24 to 1.99 $kg \cdot m^{-3}$ for three periods, 2001, 2006, and 2011. The spatial analysis of the relationship among CWP, grain yield, and actual evapotranspiration (ET_a) describes a strong linear relationship between CWP, grain yield, and ET_a across the 3H Plain. The grain yield increases to a critical value of 520 mm and 480 mm for ET_a in the northern and southern zones, respectively, and then drops as the ET_a increases. The temporal analysis indicates an increase of the CWP and yield by an average of 0.25 $kg \cdot m^{-3}$ and 0.09 $t \cdot ha^{-1}$, respectively, and an average reduction of 82.1 mm for ET_a during two comparative periods of 2006 to 2001 and 2011 to 2006. It is concluded that the improvements of the CWP are due to the grain yield increment as a result of better cultivars, fertilizer improvement and other management practices rather than water consumption reductions. The results are expected to provide basic information for the agricultural water management, improvement of CWP, and choice of adaptive mechanisms in water-scarce regions.

Keywords

Crop water productivity, Winter wheat, Remote sensing, Agricultural sub-regions, Huang-Huai-Hai Plain

2. Introduction

The worldwide water demand has increased substantially over the past decades due to a rapid economic development, population growth, and increasing water scarcity in many parts of the world (Vrsmarty et al., 2000). The growing water scarcity in agriculture at the global scale has become a bottleneck of the ecological, environmental, and socioeconomic development and sustainability of agriculture (Immerzeel et al., 2010; Murray et al., 2012; Wolf et al., 2003; Yoffe et al., 2003). Agriculture is identified as the largest water-consuming sector and in sequence irrigated agriculture has expanded rapidly over recent decades in many developing countries (Ali and Talukder, 2008; Carruthers et al., 1997). Irrigated agriculture contributes between around 25% and 50% to global food production (Boutraa, 2010). A FAO analysis of 93 developing countries expects agricultural production to increase over the period 1998–2030 by 49% in rain fed systems and by 81% in irrigated systems (Playán and Mateos, 2006). To achieve a sustainable and higher grain yield, indispensable irrigation is needed, which makes the water shortage problem more serious (Quanqi et al., 2012). Understanding how the productivity of water can be increased is a high priority in regions with scarce and/or overexploited water resources (Perry, 2011).

The crop water productivity (CWP) is defined by the amount of produced output per unit of water consumption under a considered condition (Cai et al., 2011; Molden et al., 2010; Molden et al., 2007), and becomes a critical indicator for the quantification of the impact of irrigation scheduling concerning water management (Igbadun et al., 2006). Quantitative information on the CWP estimated from grain yield and water consumption is consequently essential for the irrigation water management strategies in a particular region. A number of researchers reported the CWP in China, with varied spatial and temporal resolutions based on model simulation, estimation from remote sensing data and calculation from collected irrigation district data (Cao et al., 2015; Huang and Li, 2010; Liu et al., 2007; Rosengrant et al., 2002; Yan and Wu, 2014).

Most of the above-mentioned studies reported the relationship between water consumption, grain yield, and CWP, which suggests that it is important to more generally consider the situation in the controlled environment and related decisions (Zwart and Bastiaanssen, 2004). Zhang et al. (2011) reported that winter wheat biomass has a more linear relationship with actual evapotranspiration (ET_a) than summer maize based on experimental research from 1979–2009. Perry et al. (2009) reported that the relationship between biomass and transpiration is essentially linear for given crops and climate conditions based on a literature review. However, other results suggest that the relationship between ET and yield is not always linear. Li et al. (2012) indicated the relationship between grain yields and seasonal ET was best described by a quadratic function obtained by regression analysis in Southwest China. Li et al. (2009) reported a relationship between ET and yield in the form of a parabola, however, which was not statistically significant.

The Huang-Huai-Hai Plain (3H Plain) is known as the largest agricultural production region in China, where the most important factor limiting agricultural production is water. This problem will most probably become more severe in the future due to the increasing food demand, soil quality deterioration, and diminishing

water quality (Chen et al., 2005). Hence, the 3H plain faces a serious threat of water scarcity due to excessive exploitation of groundwater combined with a precipitation reduction (Jia and Liu, 2002; Liu et al., 2010b). The key point to maintain high crop productivity and reduce the depletion of water resources is to improve the CWP in the 3H Plain. Nevertheless, the relationship between the water consumption and grain yield of the agricultural sub-regions in the 3H Plain and the critical ET_a value at which the grain yield begins to drop remain unknown up to now.

Therefore, this paper focuses on (1) a quantification of field scale productivity of wheat using a satellite-based model, linear regression equation-integrating remote sensing data, and census data; (2) a spatially differentiated characterisation of the water productivity of wheat; and (3) a discussion of potential improvements of the water productivity for wheat using the structure of water consumption and an analysis of agronomical practice across the 3H Plain.

3. Materials and methods

Study region description

The Huang-Huai-Hai Plain is generally acknowledged as one of the largest plains in China, located in the temperate, subhumid, and continental monsoon climate zone with a cumulative temperature (>0°C) of 4200°C to 5500°C and average annual precipitation of 348.5 mm (Ren et al., 2008). Although the precipitation is insufficient for cultivation, 3H plain remains one of the main Chinese crop production centres, providing 31% and 61% of the nation's maize and wheat production respectively (Wang et al., 2009).Typically, the main crop system is characterized by maize–wheat rotation with two harvests per year.(Liang et al., 2011; Sun et al., 2011; Zhao et al., 2006).

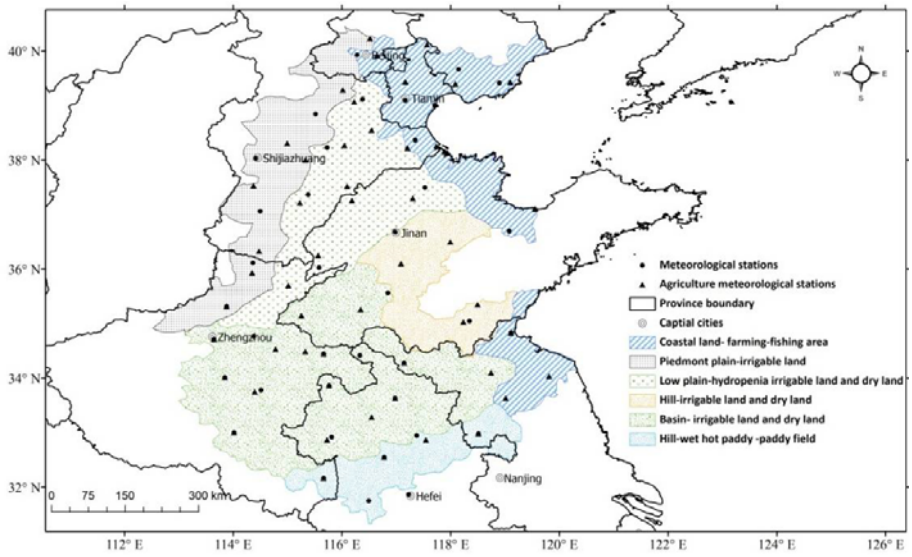

Figure 44 The The inset map shows the location of the Huang-Huai-Hai Plain(3H Plain) and its six agricultural

sub-regions. The six agricultural sub-regions of 3H plain include: Coastal land- farming-fishing area (including North part: Zone1 and South part: Zone7), Piedmont plain-irrigable land (Zone2), Low plain-hydropenia irrigable land and dry land (Zone3), Hill-irrigable land and dry land (Zone4), Basin- irrigable land and dry land (Zone5) and Hill-wet hot paddy field (Zone6). The triangles and round black spots mean agrometeorological stations and meteorological stations respectively. The round hollow spots mean the capital cities.

Data collection

The China Meteorological Administration (CMA) provided us with a historical dataset acquired between 2001 and 2015, composed of climatic variables from 40 meteorological stations (Figure. 44): daily observed maximum and minimum air temperature and wind speed. Three kinds of MODIS (Moderate-resolution imaging spectroradiometer) products were used as the inputs for the SEBAL (the Surface Energy Balance Algorithm for Land model) model which is used to estimate the actual evapotranspiration (ETa) of winter wheat: (i) MOD11A1 (land surface temperature/surface emissivity), (ii) MOD13A2 (NDVI), and (iii) MCD43B3 (surface albedo). For land surface temperature images, cloudy areas were eliminated by replacing the values with the average of two images in the nearest clear dates (Cai and Sharma, 2010; Yang et al., 2015)

.CWP estimation

The crop water productivity is defined as the output of crops per unit of water consumption (Perry et al., 2009), as determined in the following equation (Yan and Wu, 2014):

$$CWP = \frac{Y}{ET_a}, \quad \text{Formula 26}$$

where Y is the wheat yield ($t \cdot ha^{-1}$), ET_a is the corresponding water consumption (mm), and CWP is the winter productivity ($kg\ m^{-3}$).

It differs from water efficiency, which is the ratio of crop yield to the actual amount of water applied to the field (losses included).

The physical location of winter wheat planting has to be known for crop-specific water consumption and water productivity analysis in this study (Cai and Sharma, 2010; Yang et al., 2015). To improve the wheat dominance map, ISODATA class identification and spectral matching proposed by Thenkabail et al. (2007) and widely used in China (Hao et al., 2011) were performed using the ground truth information as the input (Figure. 45).

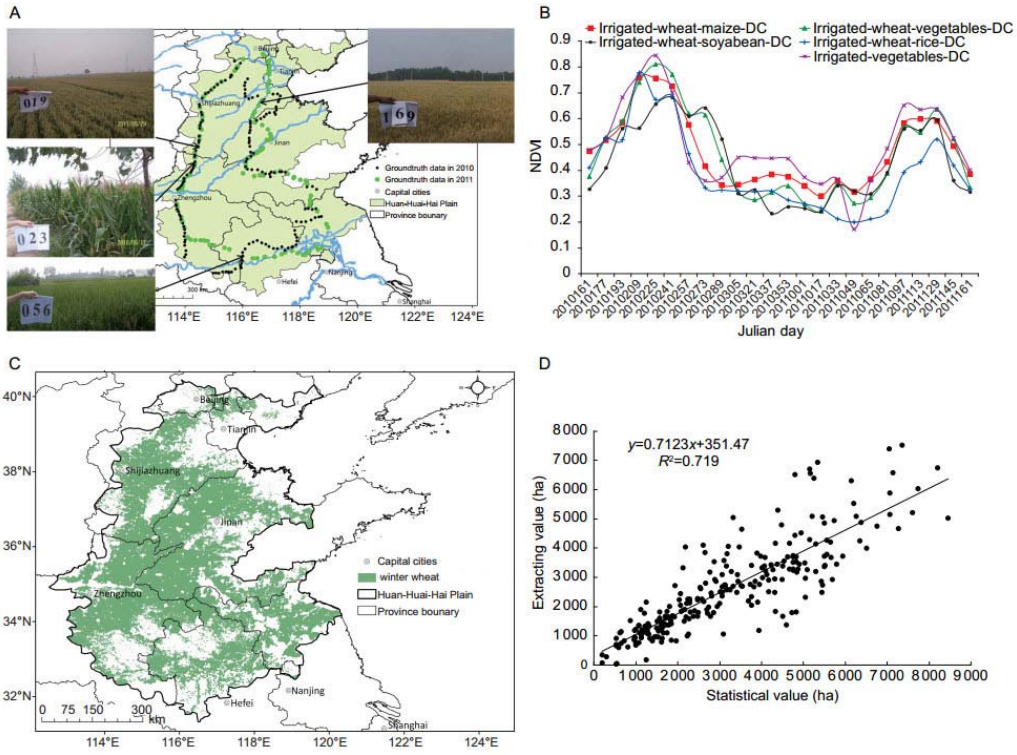

Figure 45 The map shows the distribution of winter wheat planting information over the Huang-Huai-Hai Plain. A: ground truth points distribution. B: spectral signature of wheat-other crops (maize, soybean, rice and vegetables) rotation. C: winter wheat dominance map. D: accuracy analysis based on extracting and statistical value of wheat planting area.

With the development of remote sensing technology, the SEBAL model for ET_a estimation has been applied in the Americas (Allen et al., 2002; Paul et al., 2013; Trezza, 2002), Europe(A et al., 2007; Jacob et al., 2002), Africa (Dzikiti et al., 2016; Kongo et al., 2011), and China (Li et al., 2013; Tang et al., 2013; Yang et al., 2015). These studies demonstrate that the SEBAL model is proved to be with a good efficiency and applicability for water consumption estimations in vegetative area, which is the focus of our study (Cai and Sharma, 2010).

In our study, the SEBAL model based on MODIS data was applied to estimate the daily ET. The SEBAL model is based on the energy balance equation described by the following equation:

$$R_n = G + H + \lambda ET \qquad \text{Formula 27}$$

where R_n (W·m^{-2}) is the net radiation; G (W·m^{-2}) is the soil heat flux; H (W·m^{-2}) is the sensible heat flux; and λET (W·m^{-2}) is the latent heat flux associated with evapotranspiration. The main parameters such as the net radiation flux on the land surface (R_n) , the soil heat flux (G) and the sensible heat flux (H) can be calculated according to literatures reported by Bastiaanssen et al. (1998), Yang et al. (2015) and Ju et al. (Ju et al., 2016)

Since the evaporative fraction Λ is constant during a day, the daily ET_{24} (mm) can be estimated using the following equations:

$$\Lambda = \frac{\lambda ET}{R_n - G} \quad \text{Formula 28}$$

$$ET_{24} = \frac{\Lambda(R_{24} - G_{24})}{\lambda} \quad \text{Formula 29}$$

where ET_{24} is the daily evapotranspiration (mm), G_{24} is the daily soil heat flux ($W \cdot m^{-2}$), and λ is the latent heat of vaporization ($MJ \cdot kg^{-1}$).

Hence, the SEBAL was validated to be suitable for estimating evapotranspiration of winter wheat in 3H Plain with correlation coefficient of 0.88 between the estimated and measured values from the field data for Yucheng station in Shandong Province (Yang et al., 2015).

In this study, the county district-level wheat yield map from census data with vectors of administrative county was resolved to the pixels size of the MODIS NDVI data with a stepwise multiple regression equation (Ju et al., 2016). The county-level census data included wheat area and grain yield for 347 counties in 3H Plain and were obtained from the Ministry of Agriculture of China. Areas where wheat was not the dominant crop were masked out using the wheat planting map. The stepwise multiple regression equation was obtained from county district average NDVI values for wheat from the MODIS images and the related district average wheat yield. As such, we obtained the following the linear regression equation was obtained, as shown in (Eq.5):

$$Yield_p = Yield_{avg} \times \frac{NDVI_p}{NDVI_{avg}} \quad \text{Formula 30}$$

Where $Yield_p$ and $Yield_{avg}$ are the average yields of the individual pixel and of the county; $NDVI_{avg}$ is the county-level averaged NDVI; and $NDVI_p$ is the NDVI of individual pixel during the wheat growth stage. The equation was then applied to each pixel on the NDVI wheat subset, leading to a yield map of wheat with 250 m × 250 m resolution. This downscaled method is described in detail in Cai and Sharma (2010).

4. Results

ET map

The ET_a of winter wheat was calculated based on wheat-dominant planting map and wheat phenological data in different agricultural sub-regions. The wheat ET_a map and histogram are shown in Figures 46 and 47. The seasonal average wheat ET_a is 630mm, 550mm, and 538mm, ranging from 169 mm to

729 mm, 203 mm to 729mm, and 164mm to 727mm with a standard deviation of 49.2 mm, 66.2mm, and 84.7mm, respectively (1% of the points were filtered), from October to the following June of 2001, 2006, and 2011. The average value is detected to be pronouncedly less than the wheat potential ET (680 mm) (Yang et al., 2013a). Figure. 46 shows the histogram of the average wheat ET_a with a sharp peak at 641, 574, and 559mm, respectively, in 2001, 2006, and 2011.The histogram shows that the ET_a range is 320–700 mm, accounting for 99% of the total pixels. The pixels with ET_a values below 320mm are probably at the margin of the winter wheat production area.

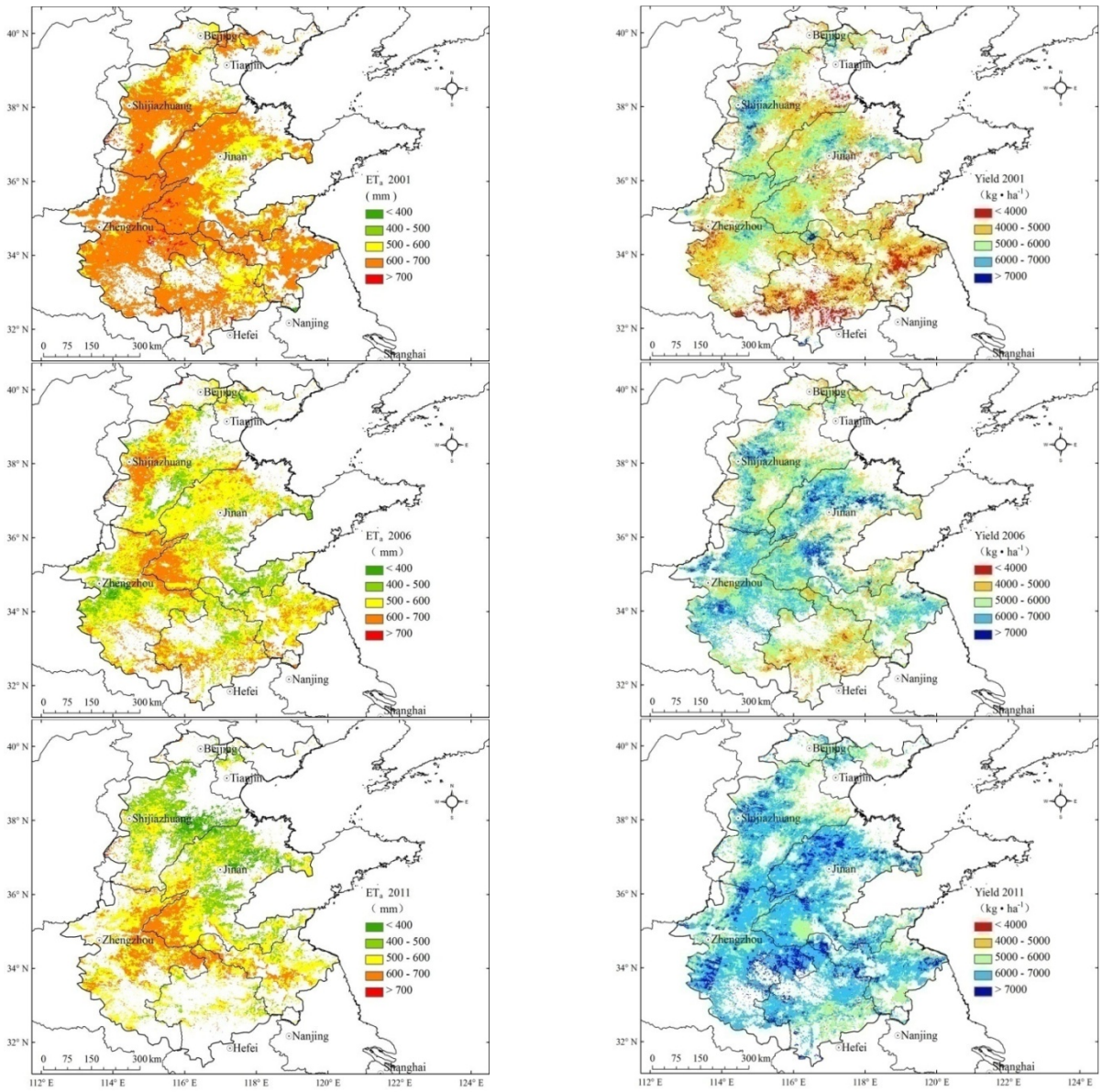

Figure 46 Actual evapotranspiration (ET_a, unit: mm) and average yield (Y, unit: ton ha^{-1}) of winter wheat in the Huang-Huai-Hai Plain (2001, 2006 and 2011). The left maps were obtained from the results based on SEBAL model. The right maps were obtained from grid-level yield with Arcgis software.

In 2001 and 2006, the maximum ET_a for winter wheat in the basin irrigable land and dry land (zone 5) and hill-wet hot paddy field (zone 6) of the 3H Plain was 729 mm, while the minimum value was 169 mm and 203 mm in the coastal land–farming–fishing area (zone 1) and low plain-hydropenia irrigable land and dry land (zone 2), respectively. A higher ET_a belt between 600 and 700 mm and 500 and 600mm was detected in more than 78% and 54.8% of the winter wheat area for these two periods, respectively, although significant variations were observed. Furthermore, the maximum ET_a in 2011 was 727mm in zone 5, while the minimum value of 164 mm was determined mainly in zones1 and 2. We conclude that, compared with 2001, the decreasing areas with an average reduction of 88.4mm are the southern Hebei Province, Henan Province, and northern Jiangsu Province in 2006. Similarly, the decreasing areas with an average reduction of 75.8mm are the Hebei and northern Shandong provinces in 2011 compared with 2006.

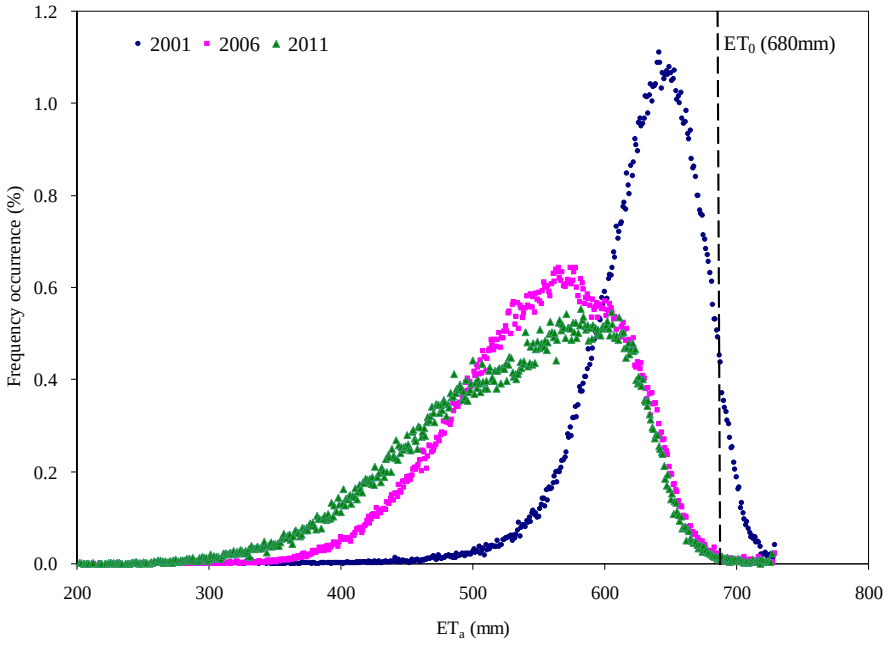

Figure 47 The histogram distribution of wheat cropland ET_a in 3H Plain for the period from October to following June in 2001, 2006 and 2011. X axes represents ET_a (mm) for winter wheat growing season and Y axes represents frequnency occurance (%) for ET_a for winter wheat growing season across the Huang-Huai-Hai Plain. The vertical dashed line repreasents area-averaged value of ET_0 for winter wheat growing season across the Huang-Huai-Hai Plain according to Yang et al. (2013).

Wheat yield map

The wheat yield was sequently rasterized based on the wheat-dominant planting map and MODIS NDVI products. The wheat yield map is shown in Figure. 47. The average wheat yield is 5.0 $t{\cdot}ha^{-1}$, 5.7$t{\cdot}ha^{-1}$, and 6.3$t{\cdot}ha^{-1}$, ranging from 1.9 $t{\cdot}ha^{-1}$to 7.8 $t{\cdot}ha^{-1}$, 3.4 $t{\cdot}ha^{-1}$to 7.9 $t{\cdot}ha^{-1}$, and 3.9 $t{\cdot}ha^{-1}$to 8.1 $t{\cdot}ha^{-1}$with a

standard deviation of 0.08 t·ha^{-1}, 0.07 t·ha^{-1}, and 0.05 t·ha^{-1}respectively (1% of the points were sieved), from October to the following June in 2001, 2006, and 2011.

In 2001 and 2006, the highest wheat yield in zone 2 and the piedmont plain-irrigable land (zone 3) of the 3H Plain was more than 7 t·ha^{-1}, while the lowest value was less 1.9 t·ha^{-1}and 3.4 t·ha^{-1}in zone 6, respectively. A yield belt between 5 t·ha^{-1}and 7 t·ha^{-1}was detected in more than 48.2% and 77.9% of the winter wheat area during these two periods, although significant variations of this value were observed. Furthermore, the highest yield in 2011 was detected in zones 3 and 5 (more than 8 t·ha^{-1}), while the minimum value of less 3.9 t·ha^{-1}was mainly determined in zone 1. The pixels with wheat yield values below 1.9 t·ha^{-1}, 3.4 t·ha^{-1}, and 3.9 t·ha^{-1}are probably associated with areas in which the wheat failed due to drought disasters, pest attacks, or other causes. Compared with 2001, the 2006 yield increase (average increment of 0.10 t·ha^{-1}), mainly took place in the Shandong, Henan, and northern Jiangsu provinces. Similarly, the increasing area, with an average increment of 0.08 t·ha^{-1}, includes the Henan and northern Anhui provinces in 2011 compared with 2006.

CWP map

Based on Equation (2), the ET and yield data estimated based on remote sensing were used to calculate the annual CWP of winter wheat for 2001, 2006, and 2011 for each pixel in the study area. The wheat WP map and the histogram distribution are shown in Figures 48 and 49. The results indicate that the average CWP of the basin was 0.79 kg·m^{-3}, 0.99 kg·m^{-3}, and 1.08 kg·m^{-3}, ranging from 0.24 kg·m^{-3} to 1.92 kg·m^{-3}, 0.40 kg·m^{-3} to 1.78 kg·m^{-3}, and 0.50 kg·m^{-3} to 1.99 kg·m^{-3} with a standard deviation of 0.48 kg·m^{-3}, 0.52 kg·m^{-3}, and 0.43 kg·m^{-3} (1% of the points were sieved), respectively, from October to the following June in 2001, 2006, and 2011. The average value in 2001 and 2006 is smaller than the wheat WP (1.05) reported for the Hai Basin (Yan and Wu, 2014). Figure. 48 shows the histogram of the average wheat WP with a sharp peak of 0.75 kg·m^{-3}, 1.05 kg·m^{-3}, and 1.0 kg·m^{-3}, respectively in 2001, 2006, and 2011.The histogram indicates that the CWP range is 0.4–1.9 kg·m^{-3}, accounting for 99% of the total pixels. The pixels with WP values below 0.4 kg·m^{-3}are probably at the margin of the winter wheat production area, in misclassified winter wheat areas, or in areas in which the crop failed due to drought disasters, pest attacks, or other causes.

The highest WP in 2001 was > 1.0 kg·m^{-3}, which was detected in zones 2 and 3 of the 3H Plain, while the lowest value was determined to be 0.5kg·m^{-3}in zone 6. The highest value in 2006 and 2011 was > 1.2 kg·m^{-3}in zones4 and 5, while the lowest value was < 0.9kg·m^{-3}, mainly in the eastern part of zones 5, 2, and 6. Furthermore, a higher WP belt between 1.1kg·m^{-3} and 1.2kg·m^{-3} was detected in more than 13.8% and 18.7% of the winter wheat area of zone 4 during these two periods, respectively, although significant variations of this value were observed. Accordingly, compared with 2001, the increasing area with an average increment of 0.24kg·m^{-3} was detected mainly in the Shandong, Henan, and northern Jiangsu provinces in 2006. Similarly, the increasing area with an average increment of 0.11kg·m^{-3} includes zones 2 and 5 in 2011 compared with 2006.

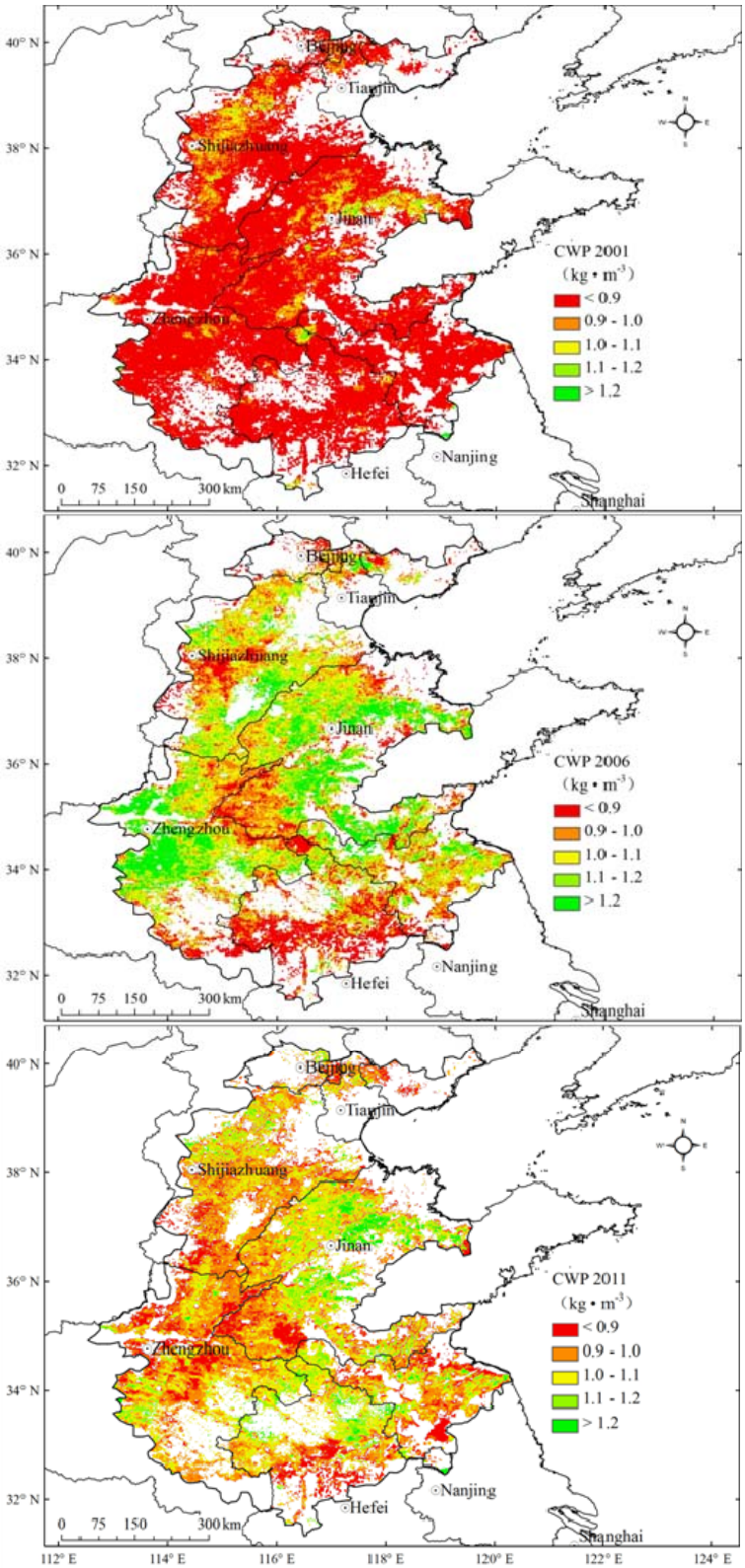

Figure 48 Water productivity (WP, unit: kg m^{-3}) of winter wheat in the Huang-Huai-Hai Plain (2001, 2006 and 2011). These maps were obtained from the results of ET_a and grid-level yield of winter wheat according to the method described as Formula **30** with Arcgis software.

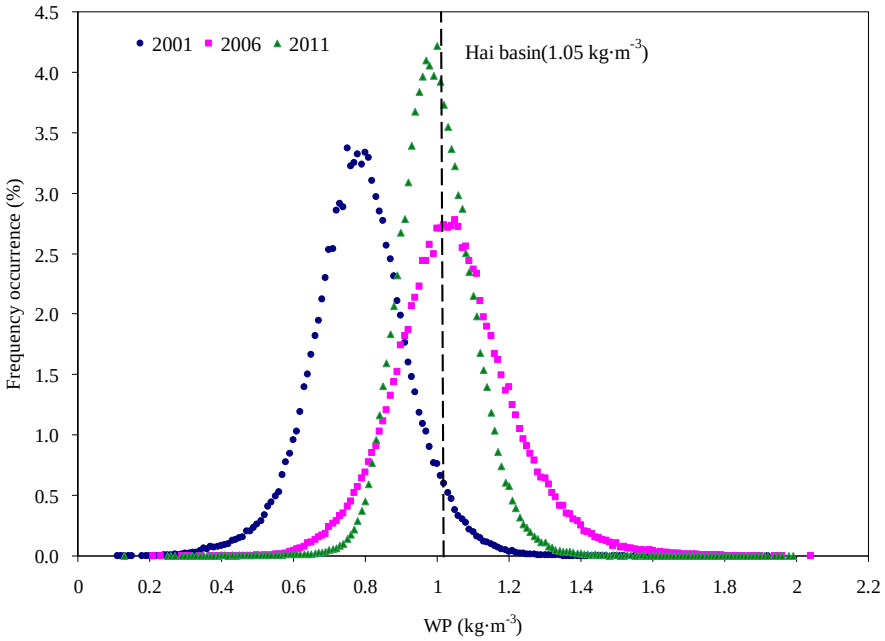

Figure 49 The histogram distribution of wheat water productivity in 3H Plain for the period of from October to following June, 2001, 2006 and 2011. X axes represents crop water productivity (kg·m^{-3}) for winter wheat growing season and Y axes represents frequnency occurance (%) for crop water productivity for winter wheat growing season across the Huang-Huai-Hai Plain. The vertical dashed line represents area-averaged value of crop water productivity for winter wheat growing season across the Hai Basin according to Yan and Wu (2014) which is part of Huang-Huai-Hai Plain.

Relations among yield, ET_a and CWP

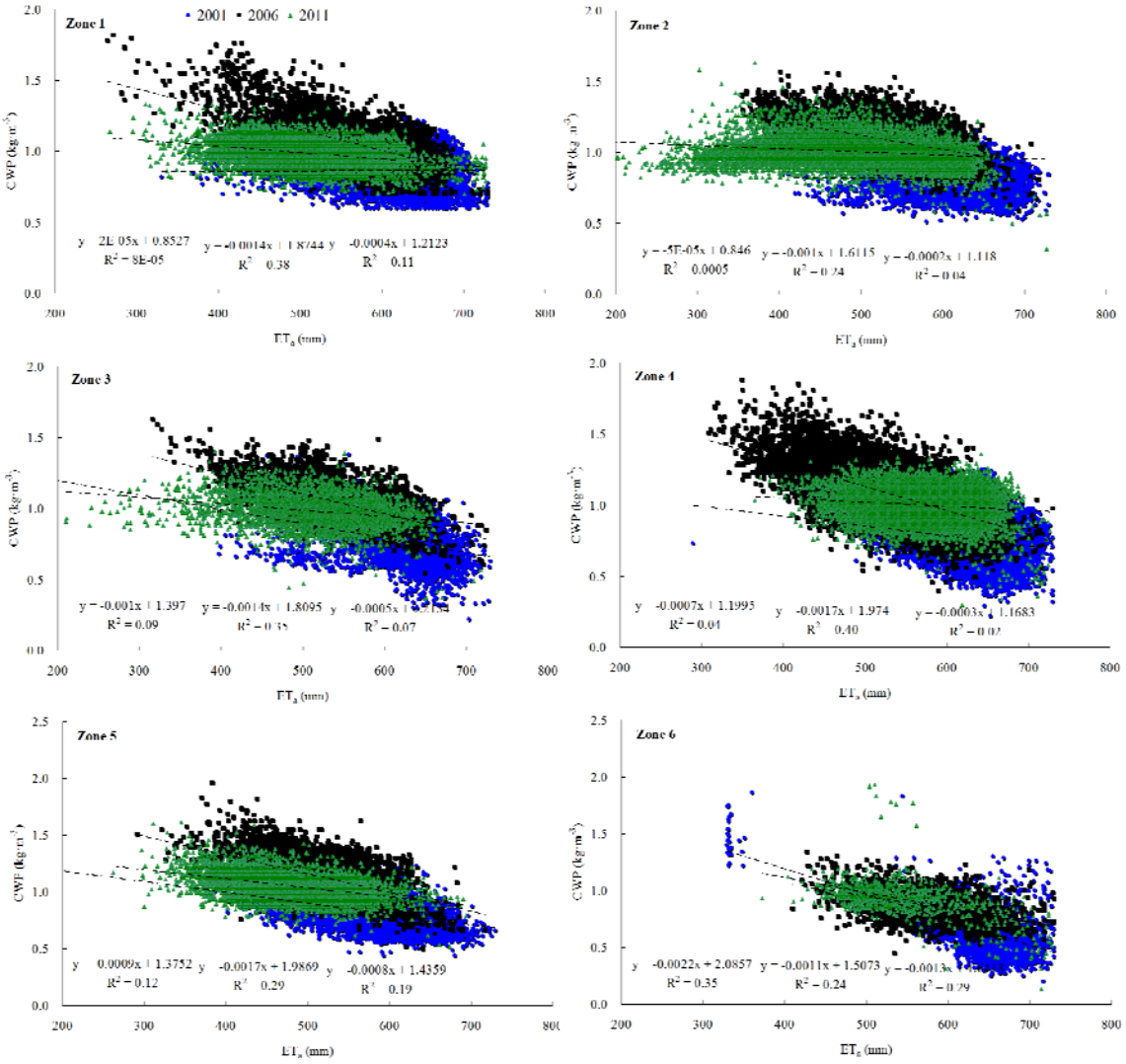

Figure 50 Relationships between actual evapotranspiration (ET_a) and crop water productivity for winter wheat in 3H Plain, using average values for ET_a and crop water productivity for 2001, 2006 and 2011 across the plain. X-axis is area-averaged ET_a value with the unit of mm and the left Y-axis is area-averaged crop water productivity of winter wheat with the unit of $kg \cdot m^{-3}$.

To determine the relations among yield, ET_a, and CWP in the 3H Plain, correlation analysis was conducted on 0.01°×0.01° pixels in three study periods. Figures 51 and 52 illustrate the change in the CWP with cumulative ET_a and yield for winter wheat using average values for ET_a and CWP from 2001, 2006, and 2011 across the 3H Plain. It is noteworthy that the ET_a data below 200mm and yield values below 2.0 $t \cdot ha^{-1}$ are not included in the graph.

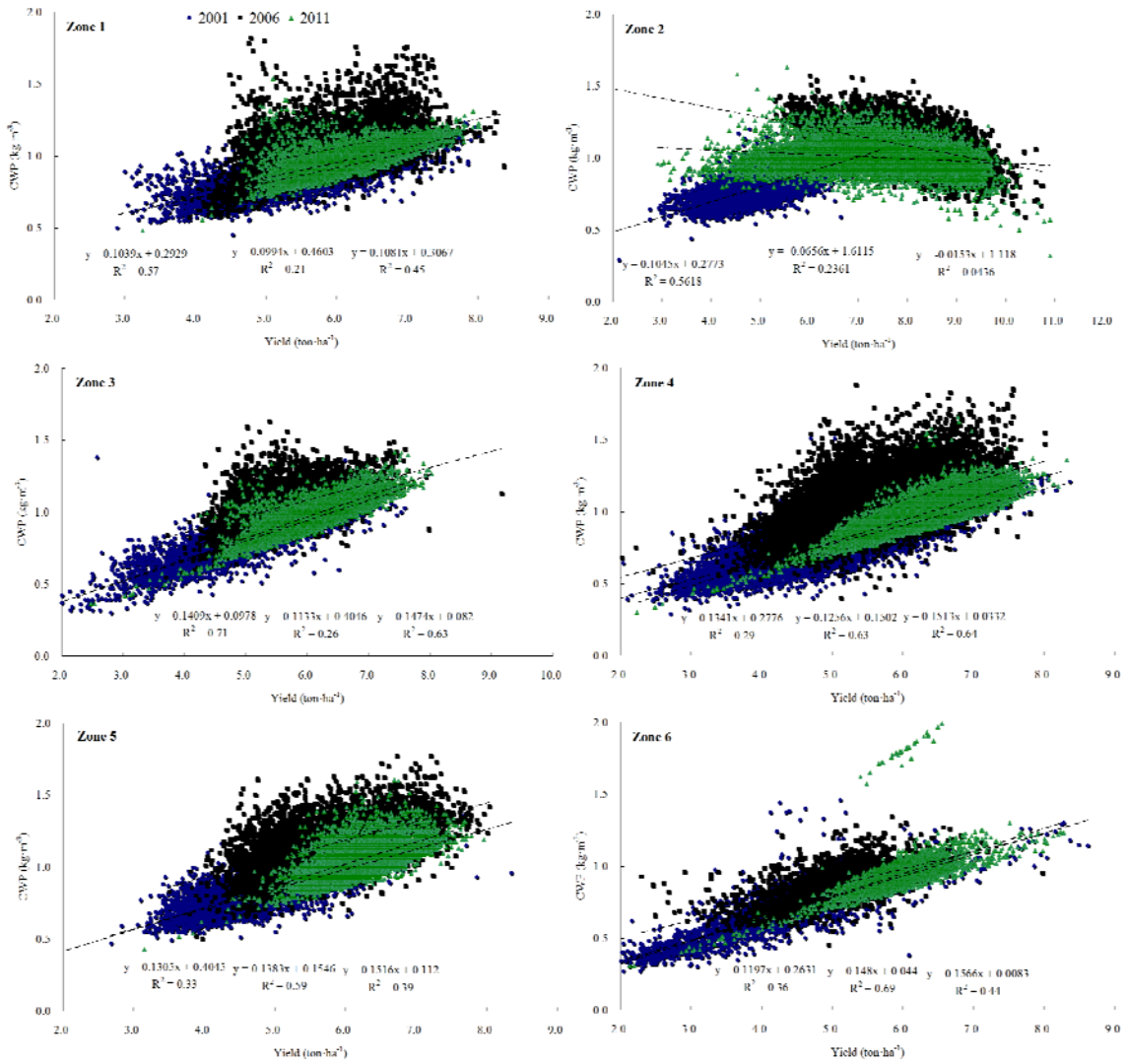

Figure 51 Relationships between yield and crop water productivity (CWP) for winter wheat in 3H Plain, using average values for yield and crop water productivity for 2001, 2006 and 2011 across the plain. X-axis is area-averaged yield of winter wheat with the unit of ton·ha^{-1} and the left Y-axis is area-averaged crop water productivity of winter wheat with the unit of kg·m^{-3}.

Figure.51 indicates that the CWP decreases with increasing ET_a from 200–750mm. The relation between the CWP and ET_a has a significance level of 0.05 (R^2> 0.12, n = 4600, 890) for the three studied periods in zones5 and 6 of the 3H Plain. Furthermore, the correlation coefficient between CWP and ET_a is bigger in 2006 than in 2011. However, the relation between CWP and ET_a of the other four zones in 2006 has a significance level of 0.05. The correlation coefficient between CWP and ET_a is bigger in 2006 than in 2011. Figure. 51 indicates that the CWP increases with increasing yield from 2.0–9.0 t·ha^{-1}. The relation between the CWP and yield is pronounced, with a significance level of 0.05 (R^2> 0.21, n >4600, 890) in the three periods in the six agricultural sub-regions, except for zone 2. The correlation coefficient between the CWP and yield is bigger in 2011 than in 2006. Hence, the wheat yield has a stronger linear relationship with CWP than with ET_a in the 3H Plain.

Based on the combined correlation analysis described in Figures 50 and 51, we conclude that the spatial increase of the yield principally controls the increase of the water productivity in zones 1 and 4; the spatial increase of the water productivity is governed more by the increment of the yield than by the reduction of ETa in the other four agricultural sub-regions.

5. Discussion

The range of the CWP of winter wheat in the 3H Plain (0.24 to 1.99 $kg \cdot m^{-3}$) for three periods, 2001, 2006, and 2011, is in accordance with results simulated for the Northern Plain, China (Chao et al., 2009), and results estimated from remote sensing data (Liu et al., 2010a) but lower compared with experimental data from the Luancheng Station (Zhang et al., 2011). It is not unexpected that the CWP is higher at the research stations because researchers perform studies in a given conditions to achieve the higher potential yield per hectare and have more resources at disposal than regular farmers (Yan and Wu, 2014; Zhang et al., 2011). The relatively low values for the CWP in the 3H Plain suggest that there is room for improvement for the agricultural practices in the 3H Plain.

The spatial analysis demonstrates the linear relation between the CWP, ET_a, and grain yield across the 3H Plain. As a whole, the CWP values are more affected by grain yield in the given range described in Figures 50 and 51. The increasing CWP values is identified as the increment of the grain yield rather than the reduction of ET in accordance with reported results in the Indo–Gangetic River Basin (Cai and Sharma, 2010) and HaiBasin (Yan and Wu, 2014). Dong et al. (2007) reported a stronger linear relationship between the CWP with grain yield under different irrigation treatments, despite of much differences of the CWP among 19 wheat species in the North China Plain. Zhang et al. (2005) also observed that the wheat yield was increased by 50% and consequently resulted in significant CWP improvements in the past 20 years in the North China Plain. On the other hand, the temporal analysis shows an increase by an average of 0.24 $kg \cdot m^{-3}$ and 0.11 $kg \cdot m^{-3}$ and 0.10 $t \cdot ha^{-1}$ and 0.08 $t \cdot ha^{-1}$of the CWP and yield, respectively, and an average reduction of 88.4 mm and 75.8 mm for ET during the two comparative periods. The yield increase is due to the fertilizer and pesticide use in the North China Plain (Wang et al., 2010). The relationship between the grain yield and ET in the six agricultural subregions of the 3H Plain in 2011 is described by a shape of typical parabola. The wheat yield increases before reaching the parabola peak (the yield is 5.8 $t \cdot ha^{-1}$and ET_a is 522 mm in the northern zones; the yield is 5.9 $t \cdot ha^{-1}$and ET_a is 460 mm in the southern zones) and then drops as the ET_a increases. This can be concluded that a higher irrigation amount does not inevitably achieve higher grain yield, which is similar to results of field experiments from other researchers (Li et al., 2005; Sun et al., 2006).

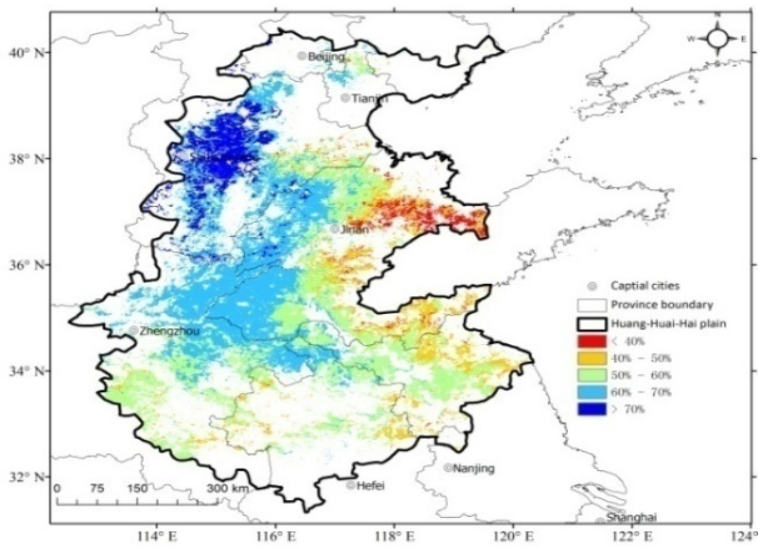

Figure 52 Spatial pattern of effective irrigation proportion in winter wheat in 3H Plain, irrigation proportion in total water consumption. These maps were obtained from ET_a and effective precipitation of winter wheat growing season with the Arcgis software.

The Huang-Huai-Hai Plain faces a serious water shortage threat due to the excessive exploitation of groundwater and precipitation reductions at an average rate of 2.92 mm·year^{-1}(Liu et al., 2010b). In recent years, many studies have focused on the crop water use in the 3H Plain(Li et al., 2008; Yang et al., 2013b). In this study, a method based on the water balance was used to quantify the effective irrigation volume and characteristics of crop water use patterns for winter wheat in the 3H Plain in 2011. Figure.52 shows the spatial distribution of the effective precipitation and irrigation proportions with respect to total winter wheat water consumption. The precipitation in the eastern part of the 3H Plain accounts for more than 50% of the total water consumption. However, irrigation was widely accepted to be the dominant water resource in the Hebei and Henan provinces in which it accounts for more than 60% of total water consumption. The winter wheat production in the 3H Plain strongly depends on supplementary irrigation (Li et al., 2008; Sun et al., 2006). According to Yang et al. (2013a), field management is a more important factor with respect to ET_a of winter wheat compared with climate transitions and geography. Although the water saving method is promoted in the 3H Plain, traditional surface-flooding irrigation is still common in the irrigation district. The irrigation efficiency in Northern China was 0.42 in 2010, which is much lower than the world average (Bai et al., 2011). Liu et al. (2011) hold the view that the relative higher grain yield and CWP of winter wheat are gained through using a coefficient of 0.63 to multiply the ET_a with a guidance for the sprinkler irrigation in winter wheat production area.

It is widely accepted that the improvement of the CWP is more complicated on the plain scale than in field experiments due to factors such as crop cultivar, soil type, drought disaster, and pest attacks. China has a good extension system to promote suitable technology to farmers. Deng et al.(2006) found that mulching with crop residues can increase the CWP by 10%–20% due to reducing soil evaporation together with increasing plant transpiration. Straw mulching can easily be implemented and extended in the 3H Plain. In

addition to droughts, the soil infertility is a factor constraining the productivity. A 15-year field experiment depicted that nitrogen fertilizer is important for the improvement of the CWP, while phosphate fertilizer is highly effective in increasing the total soil water use at the Changwu Ecological Station (Dang, 1999). Furthermore, the winter wheat cultivars have been changed five times in past 20 years, with the average yield increasing due to the increase of the average kernel numbers per spike (Zhou et al., 2007). Other land and crop interventions, such as crop variety, drought adaption, insects control, are also indispensable indicators to be accepted in addition to water management.

6. Conclusion

The average CWP of winter wheat in the 3H Plain is in the range of 0.24 to 1.99 $kg \cdot m^{-3}$ in 2001, 2006 and 2011. The spatial analysis demonstrates that the CWP values are more affected by the grain yield based on the linear relation between CWP with ET_a and the grain yield across the 3H Plain. Furthermore, the grain yield increases to a critical value of 522 mm and 460 mm in the northern and southern zones, respectively, and then drops as the ET_a increases. The temporal analysis shows an average increase of 0.25$kg \cdot m^{-3}$ and 0.09 $t \cdot ha^{-1}$ of CWP and yield, respectively, and an average reduction of 82.1 mm for ET_a during the two comparative periods.

The relatively low CWP across the plain suggests that it is possible to achieve a higher yield for the same amount of water consumption in the plain, which should be a goal for agricultural investments in water-scarce regions. In general, the findings presented in this paper suggest that the basic equation describing the relationship between CWP, ET_a, and grain yield implies that improving CWP depends on the ET_a reduction and, more specifically, on E. However, the analysis results show that this measure did not play a substantial role in improving the CWP so far. Consequently, adaptive measures, such as cultivar alternatives, disaster and pest control, compensatory irrigation scheduling, and residue mulching, are expected to be adapted by farmers to achieve a CWP improvement in the six agricultural sub-regions of the 3H Plain.

Acknowledgements

This research was supported by the National Science Foundation for Young Scientists of China (41401510). We thank the University of Liège-Gembloux Agro-Bio Tech and more specifically the research platform AgricultureIsLife for the funding of the scientific stay in Belgium that made this paper possible. We gratefully acknowledge the anonymous reviewers for their valuable comments on the manuscript.

7. Reference

Wallensten, A., Munster, V.J., Latorre-Margalef, N., Brytting, M., Elmberg, J., Fouchier, R.A., Fransson, T., Haemig, P.D., Karlsson, M., Lundkvist, A. and Osterhaus, A.D.,, 2007. Surveillance of influenza A virus in migratory waterfowl in northern Europe. Emerging Infectious Diseases, 13(3): 404-11.

Ali, M.H. and Talukder, M.S.U., 2008. Increasing water productivity in crop production—A synthesis. Agricultural Water Management, 95(11): 1201-1213.

Allen, R.G., Morse, A., Tasumi, M., Trezza, R., Bastiaanssen, W., Wright, J.L. and Kramber, W., 2002. Evapotranspiration from a satellite-based surface energy balance for the Snake Plain Aquifer in Idaho, 167-178 pp.

Gangshuan, B., Rui, Z., Guijun, G., Zhi-hong, R.E.N., Pei-qi, Z.H.A.N.G. and Ji-gang, S.H.I., 2011. Integrating agricultural water-saving technologies in Hetao Irrigation District. Bulletin of Soil and Water Conservation, 31(1): 149-154.

Bastiaanssen, W.G.M., Menenti, M., Feddes, R.A. and Holtslag, A.A.M., 1998. The Surface Energy Balance Algorithm for Land (SEBAL): Part 1 formulation. Journal of Hydrology, 212(98): 801-811.

Boutraa, T., 2010. Improvement of Water Use Efficiency in Irrigated Agriculture: A Review. Journal of Agronomy, 9(1): 1-8.

Cai, X., Molden, D., Mainuddin, M., Sharma, B., Ahmad, M.U.D. and Karimi, P., 2011. Producing more food with less water in a changing world: assessment of water productivity in 10 major river basins. Water International, 36(1): 42-62.

Cai, X.L. and Sharma, B.R., 2010. Integrating remote sensing, census and weather data for an assessment of rice yield, water consumption and water productivity in the Indo-Gangetic river basin. Agricultural Water Management, 97(2): 309-316.

Cao, X., Wang, Y., Wu, P. and Zhao, X., 2015. Water productivity evaluation for grain crops in irrigated regions of China. Ecological Indicators, 55: 107-117.

Carruthers, I., Rosegrant, M.W. and Seckler, D., 1997. Irrigation and food security in the 21st century. Irrigation & Drainage Systems, 11(2): 83-101.

Chao, C., Qiang, Y., En-li, W. and Jun, X., 2009. Modeling the spatial distribution of crop water productivity in the North China Plain. Resources Science, 31(9): 1477-1485.

Dang, T., 1999. Effects of fertilization on water use efficiency of winter wheat in arid highland. Eco-Agricultural Research, 7(2): 28-31.

Deng, X., Shan, L., Zhang, H. and Turner, N.C., 2006. Improving agricultural water use efficiency in arid and semiarid areas of China. Agricultural water management, 80(1): 23-40.

Baodi, D., Zhengbin, Z., Mengyu, L., Yizhang, Z., Quanqi, L., Lei, S. and Yongtian, Z., 2007. Water use characteristics of different wheat varieties and their responses to different irrigation schedulings. Transactions of the Chinese Society of Agricultural Engineering, 2007(9).

Dzikiti, S., Gush, M.B., Le Maitre, D.C., Maherry, A., Jovanovic, N.Z., Ramoelo, A. and Cho, M.A., 2016. Quantifying potential water savings from clearing invasive alien Eucalyptus camaldulensis using in situ and high resolution remote sensing data in the Berg River Catchment, Western Cape, South Africa. Forest Ecology & Management, 361: 69-80.

Hao, W., Mei, X., Cai, X., Du, J. and Liu, Q., 2011. Crop planting extraction based on multi-temporal remote sensing data in Northeast China. Nongye Gongcheng Xuebao/transactions of the Chinese Society of Agricultural Engineering, 27(1): 201-207.

Huang, F. and Li, B., 2010. Assessing grain crop water productivity of China using a hydro-model-coupled-statistics approach. Part II: Application in breadbasket basins of China. Agricultural water management, 97(9): 1259-1268.

Igbadun, H.E., Mahoo, H.F., Tarimo, A.K. and Salim, B.A., 2006. Crop water productivity of an irrigated maize crop in Mkoji sub-catchment of the Great Ruaha River Basin, Tanzania. Agricultural Water Management, 85(1): 141-150.

Immerzeel, W.W., Van Beek, L.P. and Bierkens, M.F., 2010. Climate change will affect the Asian water towers. Science, 328(5984): 1382-1385.

Jacob, F., Olioso, A., Gu, X.F., Su, Z. and Seguin, B., 2002. Mapping surface fluxes using airborne visible, near infrared, thermal infrared remote sensing data and a spatialized surface energy balance model. Agronomie, 22(6): 669-680.

Jia, J. and Liu, C., 2002. Groundwater dynamic drift and response to different exploitation in the North China Plain: A case study of Luancheng County, Hebei Province. Acta Geographica Sinica-Chinese Edition, 57(2): 201-209.

Ju, H., Liu, Q., Yang, J.Y. and Yan, C., 2016. Potential effect of climate drought on the yield and water productivity of winter wheat over the Huang-Huai-Hai Plain. Science Press.

Kongo, M.V., Jewitt, G.W.P. and Lorentz, S.A., 2011. Evaporative water use of different land uses in the upper-Thukela river basin assessed from satellite imagery. Agricultural Water Management, 98(11): 1727-1739.

Li, F., Li, Q. and Wang, Z., 2009. Analysis of Agricultural Water Saving in Hai Basin Based on Remote Sensing Water Productivity, Proceedings of International symposium of Hai Basin Integrated Water and environment management. Beijing: Orient academic forum, pp. 413-418.

Li, H., Zheng, L., Lei, Y., Li, C., Liu, Z. and Zhang, S., 2008. Estimation of water consumption and crop water productivity of winter wheat in North China Plain using remote sensing technology. Agricultural Water Management, 95(11): 1271-1278.

Li, J., Inanaga, S., Li, Z. and Eneji, A.E., 2005. Optimizing irrigation scheduling for winter wheat in the North China Plain. Agricultural water management, 76(1): 8-23.

Li, Q., Zhou, X., Chen, Y. and Yu, S., 2012. Water consumption characteristics of winter wheat grown using different planting patterns and deficit irrigation regime. Agricultural Water Management, 105(1): 8-12.

Li, Z., Liu, X., Ma, T., Kejia, D., Zhou, Q., Yao, B. and Niu, T., 2013. Retrieval of the surface evapotranspiration patterns in the alpine grassland–wetland ecosystem applying SEBAL model in the source region of the Yellow River, China. Ecological Modelling, 270: 64-75.

Liang, W.L., Carberry, P., Wang, G.Y., Lü, R.H., Lü, H.Z. and Xia, A.P. , 2011. Quantifying the yield gap in wheat–maize cropping systems of the Hebei Plain, China. Field Crops Research, 124(2): 180-185.

Liu, C., Sshi, R., Gao, W. and Gao, Z., 2010a. Analyze the Regional Water Budget in Shandong Province by Applying the Evapotranspiration Remote Sensing Method. Journal of Natural Resources, 11: 013.

Liu, H., Yu, L., Luo, Y., Wang, X. and Huang, G., 2011. Responses of winter wheat (Triticum aestivum L.) evapotranspiration and yield to sprinkler irrigation regimes. Agricultural Water Management, 98(4): 483-492.

Liu, J., Wiberg, D., Zehnder, A.J. and Yang, H., 2007. Modeling the role of irrigation in winter wheat yield, crop water productivity, and production in China. Irrigation Science, 26(1): 21-33.

Liu, S., Mo, X., Lin, Z., Xu, Y., Ji, J., Wen, G. and Richey, J., 2010b. Crop yield responses to climate change in the Huang-Huai-Hai Plain of China. Agricultural water management, 97(8): 1195-1209.

Molden, D., Oweis, T., Steduto, P., Bindraban, P., Hanjra, M.A. and Kijne, J. , 2010. Improving agricultural water productivity: between optimism and caution. Agricultural Water Management, 97(4): 528-535.

Molden, D., Oweis, T.Y., Pasquale, S., Kijne, J.W., Hanjra, M.A., Bindraban, P.S., Bouman, B.A., Cook, S., Erenstein, O., Farahani, H. and Hachum, A. , 2007. Pathways for increasing agricultural water productivity, International Water Management Institute.

Murray, S., Foster, P. and Prentice, I., 2012. Future global water resources with respect to climate change and water withdrawals as estimated by a dynamic global vegetation model. Journal of Hydrology, 448: 14-29.

Paul, G., Gowda, P.H., Prasad, P.V., Howell, T.A., Aiken, R.M. and Neale, C.M. , 2013. Investigating the influence of roughness length for heat transport (z oh) on the performance of SEBAL in semi-arid irrigated and dryland agricultural systems. Journal of Hydrology, 509(4): 231-244.

Perry, C., 2011. Accounting for water use: Terminology and implications for saving water and increasing production. Agricultural Water Management, 98(12): 1840-1846.

Perry, C., Steduto, P., Allen, R.G. and Burt, C.M., 2009. Increasing productivity in irrigated agriculture: Agronomic constraints and hydrological realities. Agricultural Water Management, 96(11): 1517-1524.

Playán, E. and Mateos, L., 2006. Modernization and optimization of irrigation systems to increase water productivity. Agricultural Water Management, 80(1–3): 100-116.

Quanqi, L., Xunbo, Z., Yuhai, C. and Songlie, Y., 2012. Water consumption characteristics of winter wheat grown using different planting patterns and deficit irrigation regime. Agricultural Water Management, 105: 8-12.

Ren, J., Chen, Z., Zhou, Q. and Tang, H., 2008. Regional yield estimation for winter wheat with MODIS-NDVI data in Shandong, China. International Journal of Applied Earth Observation and Geoinformation, 10(4): 403-413.

Rosengrant, M., Cai, X. and Cline, S.A., 2002. World water and food to 2025. International Food Policy Research Institute, Washington, DC.

Sun, H., Liu, C., Zhang, X., Shen, Y. and Zhang, Y., 2006. Effects of irrigation on water balance, yield and WUE of winter wheat in the North China Plain. Agricultural water management, 85(1): 211-218.

Sun, Q., Kröbel, R., Müller, T., Römheld, V., Cui, Z., Zhang, F. and Chen, X., 2011. Optimization of yield and water-use of different cropping systems for sustainable groundwater use in North China Plain. Agricultural water management, 98(5): 808-814.

Tang, R., Li, Z.L., Chen, K.S., Jia, Y., Li, C. and Sun, X. , 2013. Spatial-scale effect on the SEBAL model for evapotranspiration estimation using remote sensing data. Agricultural & Forest Meteorology, s 174–175(s 174–175): 28-42.

Thenkabail, P.S., Gangadhararao, P., Biggs, T.W., Krishna, M. and Turral, H., 2007. Spectral Matching Techniques to Determine Historical Land-use/Land-cover (LULC) and Irrigated Areas Using Time-series 0.1-degree AVHRR Pathfinder …. Photogrammetric Engineering & Remote Sensing, 73(9): 1029-1040.

Trezza, R., 2002. Evapotranspiration using a satellite-based surface energy balance with standardized ground control.

Vrsmarty, C.J., Green, P., Salisbury, J. and Lammers, R.B., 2000. Global water resources: vulnerability from climate change and population growth. science, 289(5477): 284-288.

Wang, S., Song, X., Wang, Q., Xiao, G., Liu, C. and Liu, J., 2009. Shallow groundwater dynamics in North China Plain.

Journal of Geographical Sciences, 19(2): 175-188.

Wang, X., Li, Z., Ma, W. and Zhang, F.-s., 2010. Effects of fertilization on yield increase of wheat in different agro-ecological regions of China. Scientia Agricultura Sinica, 43(12): 2469-2476.

Wolf, A.T., Yoffe, S.B. and Giordano, M., 2003. International waters: identifying basins at risk. Water policy, 5(1): 29-60.

Yan, N. and Wu, B., 2014. Integrated spatial–temporal analysis of crop water productivity of winter wheat in Hai Basin. Agricultural Water Management, 133: 24-33.

Yang, J.Y., Qin, L., Mei, X.R., Yan, C.R., Hui, J.U. and Xu, J.W., 2013a. Spatiotemporal characteristics of reference evapotranspiration and its sensitivity coefficients to climate factors in Huang-Huai-Hai Plain, China. Journal of Integrative Agriculture, 12(12): 2280-2291.

YANG, J.Y., MEI, X.R., HUO, Z.G., YAN, C.R., Hui, J.U., ZHAO, F.H. and Qin, L., 2015. Water consumption in summer maize and winter wheat cropping system based on SEBAL model in Huang-Huai-Hai Plain, China. Journal of Integrative Agriculture, 14(10): 2065-2076.

Yang, X., Gao, W., Shi, Q., Chen, F. and Chu, Q., 2013b. Impact of climate change on the water requirement of summer maize in the Huang-Huai-Hai farming region. Agricultural water management, 124: 20-27.

Yoffe, S., Wolf, A.T. and Giordano, M., 2003. Conflict and cooperation over international freshwater resources: indicators of basins at RISR1. Wiley Online Library.

Zhang, X., Chen, S., Liu, M., Pei, D. and Sun, H., 2005. Improved water use efficiency associated with cultivars and agronomic management in the North China Plain. Agronomy Journal, 97(3): 783-790.

Zhang, X., Chen, S., Sun, H., Shao, L. and Wang, Y., 2011. Changes in evapotranspiration over irrigated winter wheat and maize in North China Plain over three decades. Agricultural Water Management, 98(6): 1097-1104.

Zhao, R.F., Chen, X.P., Zhang, F.S., Zhang, H., Schroder, J. and Römheld, V. , 2006. Fertilization and nitrogen balance in a wheat–maize rotation system in North China. Agronomy Journal, 98(4): 938-945.

Zhou, Y., He, Z.H., Sui, X.X., Xia, X.C., Zhang, X.K. and Zhang, G.S. , 2007. Genetic improvement of grain yield and associated traits in the northern China winter wheat region from 1960 to 2000. Crop Science, 47(1): 245-253.

Zwart, S.J. and Bastiaanssen, W.G., 2004. Review of measured crop water productivity values for irrigated wheat, rice, cotton and maize. Agricultural Water Management, 69(2): 115-133.

Chapter Ⅷ. General discussion, conclusions, and prospects

1. Overview of results and hypotheses

Droughts and water shortage are generally accepted to be one of the most critical problems faced by worldwide agriculture, and it is so especially in China where agricultural production are largely dependent on the timely, adequate, and proper distribution of rainfall. The overall ambition of this thesis was to investigate to what extent the grain yield and crop water productivity for winter wheat can respond to climate change and drought across the Huang-Huai-Hai Plain, which is the wheat production base of China. This chapter first summarizes the main results and how they support the hypotheses raised throughout this thesis, and then provides a discussion of the main findings. Finally, I conclude with implications of this research followed by an outlook for future research and a broader perspective about the role of scientific knowledge in informing policy and decision making.

ET_0 and drought characteristics

In our study, the temporal characteristics in ET_0 and response to climatic variables was witnessed using Mann-Kennall test and a partial derivative method based on a combined dataset composed of a historical 54-year time series and the RCP 8.5 scenario. In subsequence, the drought characteristics was investigated for 1961—2010 and future 2010—2099 of RCP 8.5 climate scenario based on the evaluation of drought indices over the Huang-Huai-Hai Plain, China.

SPEI based on FAO-56 Penman-Monteith formula is recognized as be more suitable for agricultural drought impact analysis over the 3H Plain due to its higher correlation coefficients with historical drought data. However, it does not mean that SPEI-PM would have the same applicability in other locations or systems. Remarkably, the best drought index for detecting impacts as a function of the analyzed system and the performance of the drought indices varied spatially (Vicente-Serrano et al. 2012). For example, the SPI is found to be well correlated with runoff anomaly in 10 Large Regions of China (Zhai et al. 2010), while SPEI is better for hydrological application in western Canada. Additionally, the comparison between SPEI-PM and SPEI-TH indicated that the way ET_0 is estimated would make differences in drought applicability and long-term drought trend. This difference has been also found in other places of China (Wang et al. 2015b; Xu et al. 2015; Zhang et al. 2015) and around the world (Begueria et al. 2014; Sheffield et al. 2012). Both Thornthwaite (TH) and Penman-Monteith (PM) are widely used in drought index algorithm, while the TH model used for computing ET_0 in drought assessment is popularly used due to its simplicity and less data requirements (only temperature), such as in original SPEI and PDSI indices. Chen et al. (2005) concluded that the TH method overestimates ET_0 in southeast China where ET_0 is low, and underestimates in the northern and northwest parts where ET_0 is high when compared to pan data, and it does not follow the temporal variation well. Instead, PM equation is the most reliable estimation and recommended by the FAO to calculate crop water requirements (Allen et al. 2005).

Total drought events in 3H Plain were described as no significant tendency over the historical period due to

the drought duration, severity, and intensity reduced by the decreasing ET_0. In contrast with the historical period, drought characteristics tended to be lower in the first thirty years in the future RCP 8.5 scenario, nevertheless it is predicted to be intensified in the 2055s and the 2085s. The precipitation is expected to increase by 1.88 $mm \cdot y^{-1}$ in the future period, the amplification of ET_0 by PM equations counteracted this positive increase in precipitation. Thus, SPEI-PM predicted that almost all meteorological stations would experience significant drying trends, except for the southwest regions where SPEI-PM described an insignificant trend. Whereas ET_0 was detected to slightly decrease in past 54 years, the projected scenario RCP 8.5 describes an bigger increment of 1.36 mm y^{-1} in summer and 3.37 mm y^{-1} in the entire year. **Results from this chapter confirm the hypothesis that drought conditions will aggravate due to climate change by increasing ET_0 and will augment crop water consumption in studied region.**

Effects of climate change and drought on wheat yield

The issue of climate change is one of the most discussed topics among individuals and organizations, especially within the scientific community. The effect of future scenario on crop production has been widely investigated using DSSAT-CERES model(Challinor and Wheeler 2008; Guo et al. 2010; Tao et al. 2008a). The relative impact of the change in solar radiation, maximum temperature, minimum temperature and precipitation on wheat yield was investigated using CERES-Wheat model during the last 30 years (1985—2014) and the next 30 years (2021—2050) under the RCP4.5 and RCP8.5 pathways. As a matter of prime importance, the potential impact of drought related to climate change on wheat yield and the probability distribution of yield reduction were witnessed over 12 selected locations of Huang-Huai-Hai Plain during the last 1981—2015 years.

This chapter aimed to resolve the hypothesis that the response of winter wheat yield to climate change and drought is available throughout the 3H Plain. Increases in temperature and precipitation result in positive evolutions: the changes in these variables raise simulated yield by 6.2% and 14.2%, respectively, under RCP8.5 in 3H Plain. The results is supported by the results of Tao (2008b; 2014) and Xiao (2008), who concluded that the wheat yield has benefited from climate warming in northern and northwest China.

Rainfall has always been a limiting factor for agricultural production in China (Piao et al. 2010), especially in the Huang-Huai-Hai Plain, where only 25%—40% of water demand is satisfied by rainfall during the wheat growing seasons (Mei et al. 2013). Despite the uncertainty in precipitation amounts and the spatial patterns simulated by climate models (Xin et al. 2013), our study showed that the increasing rainfall in the next 30 years could provide important benefits in terms of the wheat yield production to reduce the pressure of groundwater resource. Whereas many other studies have found that there was no significant influence of rainfall on yield based on long-term field observations or statistical datasets (Tao et al. 2014; Wei et al. 2012; Xiao and Tao 2014). The main reason is that the water deficit is compensated by pumped groundwater, and the impact of rainfall changes was smoothed over. However, in our study, to fully capture the rainfall changes to yield, the wheat growth and development was simulated under rainfed conditions (no irrigation). Thus,

the contributions of increasing rainfall on wheat yield were higher than those in other studies. Nevertheless, the supposed positive impact of increasing solar radiation is visible in our simulations. The result is inconsistent with previous studies, which suggest that crop yields are positively correlated with solar radiation, using both processed- crop models (Wei et al. 2012) and statistical approaches (Tao et al. 2014). Higher solar radiation also increases the evaporation amount and water stress and consequently causes the photosynthetically active radiation conversion to dry matter ratio (PARUE) to decrease. Logically, these negative impacts are lower at southern stations of the 3H Plain with less water stress.

The results from the analysis of cumulative probability for grain yield reduction described a significant gap between the observed and potential yields, which can be resulted by water stress and management inputs' variations. Furthermore, the grain yield reduction was found to be larger during jointing to heading stage compared to the filling stage, which is in agreement with experimental results in Anhui province (Wang et al. 2001) and simulated findings by WOFOST model in Zhengzhou agro-meteorological station (Zhang et al. 2012). The drought reduced wheat yield by affecting grain-filling intensity due to soil water deficit. The reduction in yield was significantly different when drought occurred at different developmental stages. There was higher impact on winter wheat when drought occurred at several developmental stages than at a single developmental stage.

Spatial variability in crop water productivity

In our study, an attempt has been made to partition the regional actual evapotranspiration for wheat from the double crop rotation system using SEBAL and crop dominance information. On this basis, the characteristic of water productivity for the wheat were investigated by the lights of relations among yield, CWP, and ET in 3H Plain.

The grid-level wheat yield was generated from the county-level yield using estimated multiple regression equation based on MODIS NDVI and crop dominance map. In subsequence, the averaged water productivity was estimated for 0.95 kg m^{-3} with CWP values across the Plain ranging between 0.24 to 1.99 kg m^{-3} for three periods of 2001, 2006 and 2011 for winter across the Plain. From the correlation analysis, we can conclude that the spatial increment of yield principally controlled increase of water productivity in north agricultural sub-regions and the spatial increase of water productivity was more governed by increment of yield than the reduction of ET_a in other agricultural sub-regions. **Results from this chapter confirm the hypothesis that the relationship between water productivity & ET and yield of winter wheat should be defined at the level of the sub-agricultural regions in the 3H Plain.**

The averaged seasonal ET_a of winter wheat was 572.7 mm and detected to be a significant relationship with latitude from October to following June, 2001, 2006 and 2011 over the Huang-Huai-Hai Plain. Our study is the first attempt to apply SEBAL model and crop information for estimating wheat ET_a from double crop rotation at a large regional scale, such as the Huang-Huai-Hai Plain, which manifests performance in our research over diverse previous studies (Zwart and Bastiaanssen 2007; Immerzeel et al. 2008; Cai and Sharma

2010; Zwart et al. 2010).

Sustainable irrigation practices and adequate water allocation strategies at the right spatial scale are crucial to avoid over-exploitation of various resources (Condon and Maxwell 2014; Esnault et al. 2014). Details of crop water use patterns is needed to water management including irrigation practices and agriculture water use strategies in water short areas at the spatial level of a particular irrigation region because it is at this level that sustainable water supply for agriculture can meaningfully be improved by active management. Estimating the water balance and especially the total amount of irrigation water applied is a complex task in researches of crop water consumption structure. Current estimates of irrigation water applied in regional scale are mainly based on plot-scale experiments (Chen et al. 2002; Jie and Zhang 2004), water balance methods (Cheema et al. 2014; Ruud et al. 2004), or surveys, which in costly and often associated with practical and legal difficulties. Additionally, such estimates and surveys are only useful for a specific area, and cannot be expanded to large-scale areas, because of difference in farming systems, canal command areas, and especially irrigation schemes (Molden et al. 2003).

2. General discussion

Agricultural adaptations for CWP improvements

Over-irrigation analysis from water consumption of winter wheat

In this section, we estimated the effective precipitation deficit (PD_ET_a) by subtracting the cumulative precipitation (P) from the cumulative ET_a. This approach has been used previously by De Pauw (2002) in an agroecological study of the Arabian Peninsula and in Northern China (Liu et al. 2013). A positive value indicates water in excess of crop water requirements (ET_c) and a negative value indicates a deficit in terms of ET_c. Crop water requirement (ET_c) is calculated from ET_0 as suggested, usually, by Food and Agriculture Organization of the United Nations (FAO). The guidelines suggested methods to derive ET_c and discussed the application of data on crop water requirements in irrigation project planning, design and operation (Liu et al. 2015). In subsequence, the water requirement deficit (ED) was estimated by subtracting the cumulative ET_c from ET_a. A positive value indicates water consumption in excess of crop water requirements and a negative value indicates a deficit in terms of crop water requirements. In our study, a correlation of the precipitation deficit (PD_ET_a) and water requirement deficit (ED) with crop water productivity for winter wheat was conducted (as an instance) in 2011—2012 over 3H Plain. As described in Figure 53, supplement irrigation was needed to get higher yield for winter wheat due to irregular and concentrated precipitation. The value of correlation coefficient demonstrated higher potential for crop water productivity of winter wheat under alleviated water stress. In the same way, the negative correlation of water productivity and ED indicated that crop water productivity of winter wheat deceased in light of increasing ED. The positive value from water consumption in excess of crop water requirements was resulted in unreasonable supplement irrigation mode. Consequently, adapted irrigation schedules could be defined and strategies could be developed optimizing

water use as well as yield. The present study gives a first hint of trends to be expected and regions to should be prioritized. Furthermore, results indicated that the grain yield increased before critical value of 522mm in north zones and 460mm in south zones and then dropped as the ET_a increased. A study in North China revealed that under wheat production, mean daily soil evaporation from additional mulching was reduced by 16% and 37%, respectively (Chen et al. 2007). In Spain, Döll (2002) has predicted a declining in irrigation requirements by 2020 on account of the possibility of earlier sowing under more favorable higher temperatures.

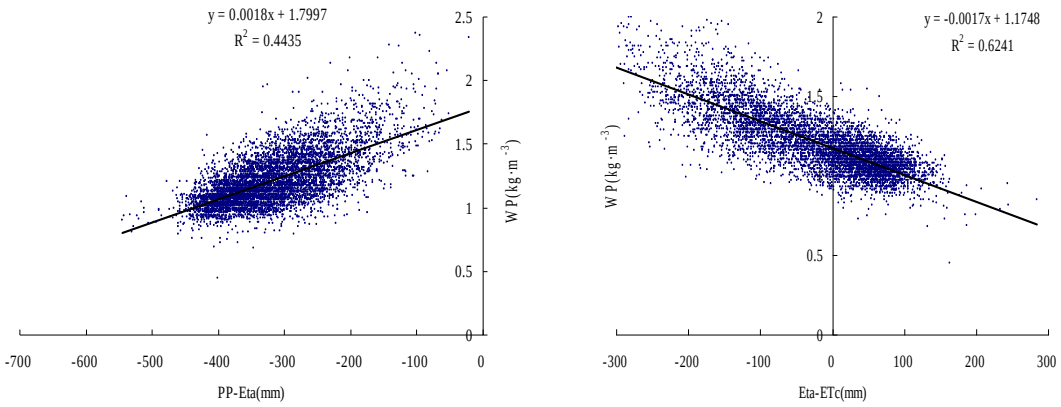

Figure 53 The correlation of crop water productivity and the precipitation deficit ($PP-ET_a$), the water requirement deficit (ET_a-ET_c) for winter wheat in 2011—2012 over the Huang-Huai-Hai Plain

Adaptive capacity to potential drought

The grain yield damage of winter wheat due to drought is inclined to accelerate in the future, described by a significantly increasing of drought events under RCP 8.5. Li et al (2015) documented a modeling approach by using crop model DSSAT and hydrological indices to assess the vulnerability of winter wheat to future potential drought, based on an integrated assessment of exposure, sensitivity and adaptive capacity in 3H Plain.

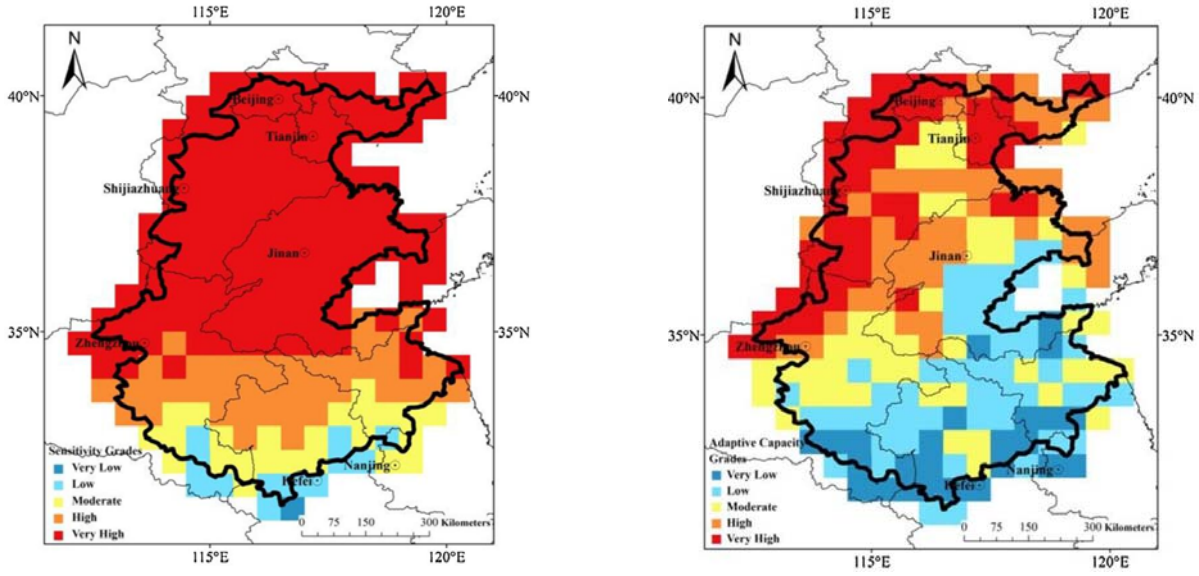

Figure 54 Geographic distribution of sensitivity of winter-wheat to drought and its adaptive capacity of irrigation using DSSAT-CERES-Wheat model for the 2040s in 3H Plain (Li et al. 2015). Sensitivity is defined as the degree of the impact of the potential drought on winter wheat yield, which is the difference between yield levels under no irrigation and full irrigation management scenarios. Adaptive capacity of winter wheat to potential drought is the ability to adapt to potential drought to reduce the potential damages, which represents crop yields losses under no irrigation compared with traditional irrigation.

As presented in Figure 54, areas with very high and high grades of adaptive capacity of irrigation are mainly located in Beijing, Tianjin and Hebei, which indicates that the irrigation is more advanced in these regions than in other regions. The beneficial effect of irrigation is more evident in the north 3H Plain than in the south. Crop yields under no irrigation condition are relative high in southern 3H region since the southern part generally receives more rainfall than in the north and therefore is less exposed to potential drought. Consequently, under RCP 8.5 emission scenario and the period of 2010–2050, the worst drought effect is projected to occur around 2030. With increasing drought risks, we suggest immediate and appropriate adaptation actions to be taken before 2030s, especially in Shandong and Hebei province, the most vulnerable provinces of 3H Plain. Consequently, adaptive measures such as straw mulching, soil water preservation, irrigation scheduling are encourage to be developed in agriculture practice to cope with the decline level of groundwater especially in winter wheat growing stage over the 3H Plain.

Alternative tillage to increase water storage in the soil profile

Increasing CWP and drought tolerance for winter wheat in virtue of genetic improvements and physiological regulation is supposed be alternatives to achieve efficient water application. Ali and Talukder (2008) witnessed a synthesis of the factors affecting crop yield and water productivity, and the possible techniques to improve water productivity. Increasing water storage within the soil profile is necessary to increase plant available soil water. Conventionally, tillage can roughen the soil surface and break any soil crust, which in subsequence bring about water storage increased. Li (2007) already reported that, change in

bulk density depends on the intensity of tillage systems. Different tillage systems produce different results like No tillage (NT) promotes SOC sequestration (Dick et al. 1991; Liu et al. 2014a) and improved soil aggregates (Lal et al. 1994), while conventional tillage (CT) usually increases available water capacity and infiltration rate and decreases runoff (Wright et al. 1999). A meta-analysis of the yield based on 807 experiments and water productivity based on 501 experiments was conducted for winter wheat under different tillage in China. From the Figure 55, it can be seen that NT and deep tillage increased yield of winter wheat by 6% and 9.5% and subsequently water productivity by 4.5% and 9.0% compared with CT in China. Adopting a better tillage system not only improves the soil properties and crop productivity but also improves water productivity. For 3H Plain, deep tillage should be chosen to increase the soil water storage in south part due to shortage precipitation, while NT turns to be a good alternative to promotes SOC sequestration and reduce soil evaporation.

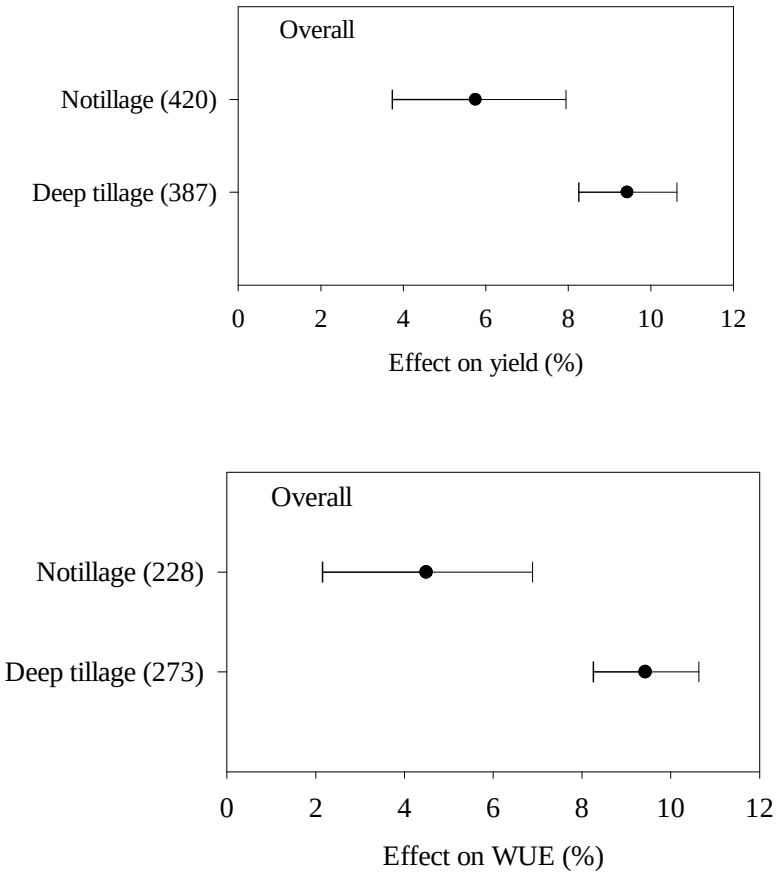

Figure 55 A meta-analysis of the yield and crop water productivity for winter wheat under different tillage in China. The top map was obtained from 807 literatures 420 of which are about no tillage and 387 of which are about deep tillage. The below map was obtained from 501 literatures 228 of which are about no tillage and 273 of which are about deep tillage.

Adaptive measures for farmers

Improvement of CWP is widely accepted to be more complicated at plain scale than in field

experiment as a result of the involved factors such as crop cultivar, soil type, drought disaster, pest attacks, etc. There is a good extension services in China to promote the suitable technology to farmers to increase. Deng et al (2006) found that mulching with crop residues can improve CWP by 10%—20% through reduced soil evaporation and increased plant transpiration. Straw mulching can be easily implemented and extended in 3H Plain. Soil infertility besides drought is accepted to be another factor constraining productivity. The relatively low CWP across the plain suggests that achieving higher yield for the same amount of water consumption is possible for the plain and should be a goal for agricultural investments in water scare region. However, the analysis of the results showed that this measure did not play a substantial role in improving CWP thus far. Consequently, adaptive measures such as cultivar alternatives, disaster and pest control, compensatory irrigation scheduling, residue mulching, etc are expected to be adapted for farmers to achieve CWP improvement with concentration of six agricultural sub-regions in 3H Plain.

The uncertainties

Many studies have shown that drought, mainly agricultural drought, may become more severe and widespread under greenhouse gas (GHG)-induced global warming in the 21st century based on model projections (Burke et al. 2006; Cook et al. 2014; Sheffield and Wood 2008; Zhao and Dai 2016). There are still large uncertainties in recent and projected future drought changes, especially regarding the extent to which the drought trends will be forced by changes in precipitation versus evaporative demand (Sheffield et al. 2012; Taylor et al. 2013; Trenberth et al. 2014). Total drought events (based on SPEI-PM index) were described as no significant tendency over the historical period due to the drought duration, severity, and intensity reduced by the decreasing potential evapotranspiration. While, these results in our study are inconsistent with the previous studies, where northern China was shown to have experienced a warm-drying trend (Wang et al. 2015a; Yu et al. 2014). This inconsistency is likely due to the use of different indices in previous studies and especially due to the variation in estimating potential evapotranspiration for different indices. Some studies have evaluated the use of PM equation to calculate drought indices and concluded that drought has changed little globally (Sheffield et al. 2012) and in China in the past decades (Wang et al. 2015b). Mcvicar et al. (2012) reported a global declining rate of evaporative demand of 1.31mm y^{-1} by reviewing papers reporting trends in estimated ET_0 (n = 26), whereas Thomas (2000) come to a declining rate of 2.3 mm y^{-1} over China on basis of a time series from 1954 to 1993). In our study, the annual averaged ET_0 across the entire 3H Plain revealed a pronounced decreasing trend of -1.29 mm y^{-1}, which was higher than that of the Yellow River Basin (Liu et al. 2014b; Ma et al. 2012), the Yangtze River catchment (Gong et al. 2006; Xu et al. 2006), and Haihe River Basin (Bo et al. 2011; Wang et al. 2010). These differences in declining magnitude were mainly due to higher decrement of RH over the entire 3H Plain (as the governing climatic variable for ET_0).

Uncertainties in projections of climate change impacts on future crop yields derive from different sources in modeling. The relative impact of the change in each variable on wheat yield in isolation was conducted in this study using DSSAT-CERES-Wheat model under historical and RCP scenarios with the findings of positive

impact of warming temperature and increasing precipitation on wheat yield in this study. Process-based crop models include the highest level of detail in simulating biophysical crop responses to multiple drivers of climate change and diverse farming management practices, however these models need to be calibrated to a specific location and their aggregation for global scale climate impacts assessments, as done by Parry et al. (2004) and Nelson et al. (2009). Yet, these crop models present some important uncertainties that need to be clearly identified and quantified as much as possible for robust impact assessments and sound decision making. First of all, some uncertainties in crop modeling results arise from uncertainties in the input data. Furthermore, unknown future socio-economic development and radiative concentration pathways (RCPs) necessitate comparison of different assumptions and scenarios of future GHG emissions, that directly infer with the climate system. In addition, uncertainties within soil and farming management data (e.g. crop calendar dataset, irrigated cropping areas and fertilizer application) required to drive crop models, and also within crop yield data used for model calibration and/or validation, will propagate to crop simulations (Falloon et al., 2014; Lobell, 2013).

Referable value from dataset and methodology of this thesis

Some main findings were found out with the emphasis on investigating to what extent the yield and crop water productivity for winter wheat in response to climatic warming and drought condition across the 3H Plain. Hence, the referable value is expected for other study and somewhere else from building-related dataset and developed methodology of this thesis.

The increased frequency of extreme climatic events has started breaking balances in hydrological cycle and is resulting in large fluctuations in crop yields and water productivity in the recent years. In addition, expected changes in soil moisture may alter the amount of water available to plant roots for transpiration (Goyal 2004). Under elevated CO_2 conditions, the stomatal conductance in most species decreases, which may result in lower transpiration per unit leaf area (Kruijt et al. 2008). The potential impacts of climate change are expected to reshape the water demand and supply patterns, therefore it is essential to evaluate the impacts of climate change on water consumption and crop water productivity. Hence, the built dataset consisted of meteorological variables with daily time step under both historical 54 years and a high CO_2 emission scenario RCP 8.5 can be applied to conduct the regional response of crop water productivity to climate change using process-based crop models.

And furthermore, this thesis documented an early plain-wide method integrated spatial and temporal assessment of CWP, ET_a, and grain yield with concentration of six agricultural sub-regions in 3H Plain. This study is the first attempt to apply regional evapotranspiration model and crop information for estimating wheat actual evapotranspiration from double crop rotation system at a large regional scale. Besides, the county-level wheat yield map was further disaggregated to the pixel level using MODIS NDVI data during crucial growth stages as a bridge. The methodology can be easily replicated in other areas regardless of one single crop or one crop from double crop rotation system due to the simplicity of the process and the popularity of the data set required.

3. Conclusions

Droughts and water shortage are generally accepted to be one of the most critical problems faced by the agricultural production of Huang-Huai-Hai Plain. The overall ambition of this thesis was to investigate to what extent the yield and crop water productivity for winter wheat could respond to climate change and drought using SPEI-PM method, DSSAT-CERES-Wheat model, SEBAL model and remote sensing data across the Huang-Huai-Hai Plain, which is the wheat production base of China.

Among our main findings, we highlighted the fact that an increase of ET_0 were predicted leading to subsequent drought rise in frequency, duration, severity and intensity under the RCP 8.5 scenario and that the cumulative probability of the simulated yield reduction was higher during jointing to heading stage in northern than southern region due to water stress and changes in the management inputs, and that the spatial increment of yield principally controlled increase of water productivity in north agricultural sub-regions and the spatial increase of water productivity was more governed by increment of yield than the reduction of ET_a in other agricultural sub-regions.

Our results can have major agronomic consequences regarding the reform of the common agricultural policy in Huang-Huai-Hai Plain, China. Despite insufficient precipitation for cultivation in 3H Plain, it is one of the main Chinese crop production centers, providing about 61% of the nation's wheat production. Furthermore, the farmers in 3H Plain apply unplanned times, through flood irrigation during the winter wheat growing season to get high wheat yield. Consequently, 3H Plain faced the double threat of both making contributions of high and stable yield to government and improving the crop water productivity of winter wheat through reducing water consumption. It will be adopted to develop feasible straw (film) mulching, regulated deficit irrigation, and soil water storage and preservation to reduce pressure on groundwater over-exploitation, especially for winter wheat in the 3H Plain. The results is expected to provide a basis information for agricultural water management, improvement of crop water productivity and choice of adaptive mechanism under climate change in Huang-Huai-Hai Plain. Finally, it is worth mentioning that our results have some uncertainties due to lack of collection of deficit irrigation and fertilizer practices for CERES-Wheat calibration and observed crop water productivity in agro-meteorological stations for temporal analysis and also from the uncertainties in the input data of CERES-Wheat modeling. It is clear that further studies are needed to better understand how to implement these practices with emphasis of improving the sustainability of these agroecosystems.

4. Prospects and improvements

Increasing RCP scenarios alternatives

In our study, only RCP 8.5 scenario was selected to estimate SPEI-PM associated with ET_0 and in subsequence investigation of the impact of climate shifts on wheat yield using CERES-Wheat model. The

RCP8.5 scenario describes the hypotheses about highest population and relatively slow income growth with modest rates of technological change and energy intensity improvements (Riahi et al. 2011). A set of scenarios known as RCPs including RCP 2.6, 4.5, 6.0 and 8.5 with different level of radiative forcing (Figure 56) has been adopted to conduct related research based on a range of possible futures for the evolution of atmospheric composition (Moss et al. 2008; Moss et al. 2010). Projections of climate change impacts on drought and crop yields are accepted in our subsequent study with consideration of four RCP scenarios.

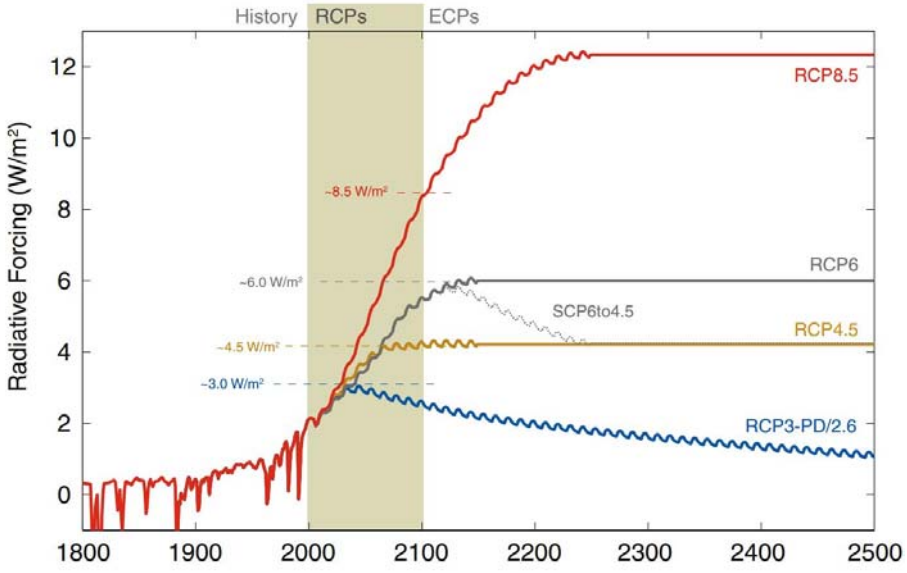

Figure 56 Total radiative forcing for RCPs,—supporting the original names of the four pathways as there is a close match between peaking, stabilization and 2100 levels for RCP2.6, RCP4.5 & RCP6, as well as RCP8.5, respectively (Meinshausen et al. 2011).

Increasing collection of irrigation and fertilizer management for DSSAT simulation

In this thesis, the potential impacts of drought on wheat yield were determined under a designed irrigation schedule from the estimation of precipitation deficit during growth stages at twelve stations representing different locations on the 3H Plain. Some uncertainties will come from simulated results due to lack of deficit irrigation practices. Attia et al (2016) found that a single irrigation of 100 mm at jointing or booting had 35% higher grain yield than dryland while 140 mm at anthesis or grain filling produced 68% higher grain yield compared to dryland in the Texas High Plains. Zahe et al (2014) observed that increases of the water and salinity stresses lead to the shrinkage in seed yield and WUE and more usage of N fertilizer leads to better WUE in west Azerbaijan, Iran. Chen et al (2015) also observed that the nitrogen and phosphorus fertilizers treatment after the jointing stage increased the grain yield (112%) and WUE (96%) of winter wheat but resulted in soil water storage reduced by 12% and that with the nitrogen and phosphorus fertilizers +plastic film treatment compared to the NP treatment, the grain yield has increased by 53% associated with WUE increased of 46% and soil water storage increased by 21% after jointing stage. Consequently, a long history irrigation station together with deficit irrigation and fertilizer practice and

variety alternative is required for crop modeling in our study.

Increasing collection of observed CWP in agro-meteorological stations

The relationship between water productivity & ET_a and yield of winter wheat was conducted after partitioning the regional ET_a for wheat from the double crop rotation system at the level of the sub-agricultural zone in the 3H Plain. The ET_a was validated by latent heat flux estimated by SEBAL model and measured by eddy covariance during growing period of winter wheat during 2011—2012 in Yucheng station located in Northwest of 3H Plain. As mentioned in above chapter, the 3H Plain encompasses around 18 million hectares of farmland for wheat and maize double rotation production (Jin et al. 2009). More indispensable agro-meteorological stations need to be collected to validate the ET_a in our study. Despite the crop water productivity of winter wheat was estimated for three periods of 2001—2002, 2005—2006 and 2011—2012, the combination with a temporal analysis of water productivity at agro-meteorological stations can help to present a comprehensive picture of the relationships among CWP, ET, and yield in the 3H Plain in recent years.

5. Closing words

Over the last four years of the project, our perception of crop yield and water productivity in relation to climate shift has profoundly changed. In the context of agricultural production found in Huang-Huai-Hai Plain, our study was a pioneer in getting insights into water productivity at station and regional level. In Gembloux Agro-Bio Tech, before the start of the AgricultureIsLife project in 2013, for an over-exploitation of groundwater region where future warmer and drought conditions will heighten crop water demand, the questions about what are the characteristics of ET and drought in various climate scenarios and how is winter wheat yield affected by climate shift and drought are kept unclear. With our study, we have acknowledged that drought conditions will aggravate due to climate change by increasing ET_0 and augmenting ET_c and that the relationship between water productivity & ET and yield of winter wheat can be defined at the level of the sub-agricultural zone in the 3H Plain. Finally, more indispensable agro-meteorological stations need to be collected to capture a comprehensive picture of the relationships among CWP, ET and yield. The results based on above prospects is expected to provide a basis information for agricultural water management, improvements of crop water productivity and choice of adaptive mechanism under climate change in Huang-Huai-Hai Plain.

Our study has led us to ‘play’ with various disciplines to answer our different questions: agronomy, microbial ecology, molecular biology, bioinformatics, and statistics. We point out that more holistic and multidisciplinary approaches are now required to increase our understanding of agroecosystem functioning with a view to achieving sustainability.

6. Reference

Ali MH, Talukder MSU (2008) Increasing water productivity in crop production—A synthesis. Agricultural Water Management 95:1201-1213

Allen RG, Pereira LS, Smith M, Raes D, Wright JL (2005) FAO-56 dual crop coefficient method for estimating evaporation from soil and application extensions. Journal of Irrigation and Drainage Engineering-Asce 131:2-13

Attia A, Rajan N, Xue Q, Nair S, Ibrahim A, Hays D (2016) Application of DSSAT-CERES-Wheat model to simulate winter wheat response to irrigation management in the Texas High Plains. Agricultural Water Management 165:50-60

Begueria S, Vicente-Serrano SM, Reig F, Latorre B (2014) Standardized precipitation evapotranspiration index (SPEI) revisited: parameter fitting, evapotranspiration models, tools, datasets and drought monitoring. International Journal of Climatology 34:3001-3023

Bo T, Ling T, Shaozhong K, Lu Z (2011) Impacts of climate variability on reference evapotranspiration over 58 years in the Haihe river basin of north China. Agricultural Water Management 98:1660-1670

Burke EJ, Brown SJ, Christidis N (2006) Modeling the recent evolution of global drought and projections for the twenty-first century with the Hadley Centre climate model. Journal of Hydrometeorology 7:1113-1125

Challinor A, Wheeler T (2008) Crop yield reduction in the tropics under climate change: processes and uncertainties. Agricultural and Forest Meteorology 148:343-356

Cheema M, Immerzeel W, Bastiaanssen W (2014) Spatial quantification of groundwater abstraction in the irrigated Indus basin. Groundwater 52:25-36

Chen D, Gao G, Xu C, Guo J, Ren G (2005) Comparison of the Thornthwaite method and pan data with the standard Penman-Monteith estimates of reference evapotranspiration in China. Climate Research 28:123-132

Chen S, Zhang X, Liu M (2002) Soil temperature and soil water dynamics in wheat field mulched with maize straw. Chin J Agrometeorol 23:34-37

Chen S, Zhang X, Pei D, Sun H, Chen S (2007) Effects of straw mulching on soil temperature, evaporation and yield of winter wheat: field experiments on the North China Plain. Annals of Applied Biology 150:261-268

Chen Y, Liu T, Tian X, Wang X, Chen H, Li M, Wang S, Wang Z (2015) Improving Winter Wheat Grain Yield and Water Use Efficiency through Fertilization and Mulch in the Loess Plateau. Agronomy Journal 107:2059-2068

Condon LE, Maxwell RM (2014) Feedbacks between managed irrigation and water availability: Diagnosing temporal and spatial patterns using an integrated hydrologic model. Water Resources Research 50:2600-2616

Cook BI, Smerdon JE, Seager R, Coats S (2014) Global warming and 21st century drying. Climate Dynamics 43:2607-2627

Döll P (2002) Impact of climate change and variability on irrigation requirements: a global perspective. Climatic change 54:269-293

Deng X, Shan L, Zhang H, Turner NC (2006) Improving agricultural water use efficiency in arid and semiarid areas of China. Agricultural water management 80:23-40

Dick WA, Mccoy EL, Edwards WM, Lal R (1991) Continuous Application of No-Tillage to Ohio Soils. Agronomy Journal 83:65-73

Esnault C, Stewart A, Gualdrini F, East P, Horswell S, Matthews N, Treisman R (2014) Rho-actin signaling to the MRTF coactivators dominates the immediate transcriptional response to serum in fibroblasts. Genes & development

28:943-958

Gong L, Xu C, Chen D, Halldin S, Chen YD (2006) Sensitivity of the Penman–Monteith reference evapotranspiration to key climatic variables in the Changjiang (Yangtze River) basin. Journal of Hydrology 329:620-629

Goyal R (2004) Sensitivity of evapotranspiration to global warming: a case study of arid zone of Rajasthan (India). Agricultural Water Management 69:1-11

Guo R, Lin Z, Mo X, Yang C (2010) Responses of crop yield and water use efficiency to climate change in the North China Plain. Agricultural Water Management 97:1185-1194

Jie J, Zhang YQ (2004) Soil-Water Balance and Water Use Efficiency on Irrigated Farmland in the North China Plain. Journal of Soil Water Conservation

Jin H, Qingjie W, Hongwen L, Lijin L, Huanwen G (2009) Effect of alternative tillage and residue cover on yield and water use efficiency in annual double cropping system in North China Plain. Soil and Tillage Research 104:198-205

Kruijt B, Witte JPM, Jacobs CM, Kroon T (2008) Effects of rising atmospheric CO 2 on evapotranspiration and soil moisture: a practical approach for the Netherlands. Journal of Hydrology 349:257-267

Lal R, Mahboubi AA, Fausey NR (1994) Long-Term Tillage and Rotation Effects on Properties of a Central Ohio Soil. Soil Science Society of America Journal 58:37-46

Li H, Gao H, Wu H, Li W, Wang X, He J (2007) Effects of 15 years of conservation tillage on soil structure and productivity of wheat cultivation in northern China. Australian Journal of Soil Research 45:344-350

Li Y, Huang H, Ju H, Lin E, Xiong W, Han X, Wang H, Peng Z, Wang Y, Xu J (2015) Assessing vulnerability and adaptive capacity to potential drought for winter-wheat under the RCP 8.5 scenario in the Huang-Huai-Hai Plain. Agriculture, Ecosystems & Environment 209:125-131

Liu E, Teclemariam SG, Yan C, Yu J, Gu R, Liu S, He W, Liu Q (2014a) Long-term effects of no-tillage management practice on soil organic carbon and its fractions in the northern China. Geoderma 213:379-384

Liu Q, Mei XR, Yan CR, Ju H, Yang JY (2013) Dynamic variation of water deficit of winter wheat and its possible climatic factors in Northern China. Acta Ecologica Sinica 33:6643-6651

Liu Q, Yan C, Yang J, Mei X-r, Hao W, Ju H (2015) Impacts of Climate Change on Crop Water Requirements in Huang-Huai-Hai Plain, China. Climate Change and Agricultural Water Management in Developing Countries 8:48

Liu Q, Yan C, Zhao C, Yang J, Zhen W (2014b) Changes of daily potential evapotranspiration and analysis of its sensitivity coefficients to key climatic variables in Yellow River basin. Transactions of Chinese Society of Agricultural Engineering 30:157-166

Ma X, Zhang M, Li Y, Wang S, Ma Q, Liu W (2012) Decreasing potential evapotranspiration in the Huanghe River Watershed in climate warming during 1960–2010. Journal of Geographical Sciences 22:977-988

Mcvicar TR, Roderick ML, Donohue RJ, Li LT, Niel TGV, Thomas A, Grieser J, Jhajharia D, Himri Y, Mahowald NM (2012) Global review and synthesis of trends in observed terrestrial near-surface wind speeds: Implications for evaporation. Journal of Hydrology s 416–417:182-205

Mei X, Kang S, Yu Q, Huang Y, Zhong X, Gong D, Huo Z, Liu E (2013) Pathways to Synchronously Improving Crop Productivity and Field Water Use Efficiency in the North China Plain. Scientia Agricultura Sinica 46:1149-1157

Meinshausen M, Smith SJ, Calvin K, Daniel JS, Kainuma MLT, Lamarque J, Matsumoto K, Montzka SA, Raper SCB, Riahi K (2011) The RCP greenhouse gas concentrations and their extensions from 1765 to 2300. Climatic Change 109:213-241

Molden D, Murray-Rust H, Sakthivadivel R, Makin I (2003) A water-productivity framework for understanding and action. Water productivity in agriculture: Limits and opportunities for improvement

Moss R, Babiker W, Brinkman S, Calvo E, Carter T, Edmonds J, Elgizouli I, Emori S, Erda L, Hibbard K (2008) Towards New Scenarios for the Analysis of Emissions: Climate Change, Impacts and Response Strategies. Intergovernmental Panel on Climate Change Secretariat (IPCC)

Moss RH, Edmonds JA, Hibbard KA, Manning MR, Rose SK, Van Vuuren DP, Carter TR, Emori S, Kainuma M, Kram T (2010) The next generation of scenarios for climate change research and assessment. Nature 463:747-756

Nelson GC, Rosegrant MW, Koo J, Robertson R, Sulser T, Zhu T, Ringler C, Msangi S, Palazzo A, Batka M (2009) Climate change: Impact on agriculture and costs of adaptation. Intl Food Policy Res Inst

Parry ML, Rosenzweig C, Iglesias A, Livermore M, Fischer G (2004) Effects of climate change on global food production under SRES emissions and socio-economic scenarios. Global Environmental Change 14:53-67

Pauw ED, Pauw WD (2002) An agroecological exploration of the Arabian Peninsula. An Agroecological Exploration of the Arabian Peninsula

Piao S, Ciais P, Huang Y, Shen Z, Peng S, Li J, Zhou L, Liu H, Ma Y, Ding Y, Friedlingstein P, Liu C, Tan K, Yu Y, Zhang T, Fang J (2010) The impacts of climate change on water resources and agriculture in China. Nature 467:43-51

Riahi K, Rao S, Krey V, Cho C, Chirkov V, Fischer G, Kindermann G, Nakicenovic N, Rafaj P (2011) RCP 8.5—A scenario of comparatively high greenhouse gas emissions. Climatic Change 109:33

Ruud N, Harter T, Naugle A (2004) Estimation of groundwater pumping as closure to the water balance of a semi-arid, irrigated agricultural basin. Journal of hydrology 297:51-73

Sheffield J, Wood EF (2008) Projected changes in drought occurrence under future global warming from multi-model, multi-scenario, IPCC AR4 simulations. Climate dynamics 31:79-105

Sheffield J, Wood EF, Roderick ML (2012) Little change in global drought over the past 60 years. Nature 491:435-438

Tao F, Hayashi Y, Zhao Z, Sakamoto T, Yokozawa M (2008a) Global warming, rice production, and water use in China: Developing a probabilistic assessment. Agricultural & Forest Meteorology 148:94-110

Tao F, Yokozawa M, Liu J, Zhang Z (2008b) Climate–crop yield relationships at provincial scales in China and the impacts of recent climate trends. Climate Research 38:83-94

Tao F, Zhang Z, Xiao D, Zhang S, Rötter RP, Shi W, Liu Y, Wang M, Liu F, Zhang H (2014) Responses of wheat growth and yield to climate change in different climate zones of China, 1981–2009. Agricultural and Forest Meteorology 189–190:91-104

Taylor I, Burke E, McColl L, Falloon P, Harris G, McNeall D (2013) The impact of climate mitigation on projections of future drought. Hydrology and Earth System Sciences 17:2339

Thomas A (2000) Spatial and temporal characteristics of potential evapotranspiration trends over China. International Journal of Climatology 20:381-396

Trenberth KE, Dai A, Van Der Schrier G, Jones PD, Barichivich J, Briffa KR, Sheffield J (2014) Global warming and changes in drought. Nature Climate Change 4:17-22

Vicente-Serrano SM, Beguería S, Lorenzo-Lacruz J, Camarero JJ, López-Moreno JI, Azorin-Molina C, Revuelto J, Morán-Tejeda E, Sanchez-Lorenzo A (2012) Performance of Drought Indices for Ecological, Agricultural, and Hydrological Applications. Earth Interactions 16:1-27

Wang H, Chen A, Wang Q, He B (2015a) Drought dynamics and impacts on vegetation in China from 1982 to 2011.

Ecological Engineering 75:303-307

Wang M, Zhang C, Yao W, Wang X (2001) Effects of drought stress in different development stages on wheat yield. Journal of Anhui Agricultural Sciences 29:605-607, 610

Wang W, Peng S, Yang T, Shao Q, Xu J, Xing W (2010) Spatial and temporal characteristics of reference evapotranspiration trends in the Haihe River basin, China. Journal of Hydrologic Engineering 16:239-252

Wang W, Zhu Y, Xu R, Liu J (2015b) Drought severity change in China during 1961–2012 indicated by SPI and SPEI. Natural Hazards 75:2437-2451

Wei X, Ian H, Erda L, Declan C, Yue L, Wenbin W (2012) Untangling relative contributions of recent climate and CO 2 trends to national cereal production in China. Environmental Research Letters 7:044014

Wright SF, Starr JL, Paltineanu IC (1999) Changes in Aggregate Stability and Concentration of Glomalin during Tillage Management Transition. Soil Science Society of America Journal 63:1825-1829

Xiao D, Tao F (2014) Contributions of cultivars, management and climate change to winter wheat yield in the North China Plain in the past three decades. European Journal of Agronomy 52, Part B:112-122

Xiao G, Zhang Q, Yao Y, Zhao H, Wang R, Bai H, Zhang F (2008) Impact of recent climatic change on the yield of winter wheat at low and high altitudes in semi-arid northwestern China. Agriculture, Ecosystems & Environment 127:37-42

Xin XG, Wu TW, Li JL, Zai Zhi W, Wei Ping L, Fang Hua W (2013) How Well does BCC_CSM1.1 Reproduce the 20th Century Climate Change over China? Atmospheric and Oceanic Science Letters 6:21-26

Xu C, Gong L, Jiang T, Chen D, Singh VP (2006) Analysis of spatial distribution and temporal trend of reference evapotranspiration and pan evaporation in Changjiang (Yangtze River) catchment. Journal of Hydrology 327:81-93

Xu K, Yang D, Yang H, Li Z, Qin Y, Shen Y (2015) Spatio-temporal variation of drought in China during 1961–2012: A climatic perspective. Journal of Hydrology 526:253-264

Yu M, Li Q, Hayes MJ, Svoboda MD, Heim RR (2014) Are droughts becoming more frequent or severe in China based on the Standardized Precipitation Evapotranspiration Index: 1951-2010? International Journal of Climatology 34:545-558

Zahe FK, Rad MN, Besharat S, Majnooni-Heris A, Jabbari A (2014) Developing Regression Models between Water Use Efficiency (WUE) and Winter Canola Yield, Under Water and Salinity Stresses and Different Nitrogen Fertilizer Levels. International Journal of Basic Sciences and Applied Research 3:680-687

Zhai J, Su B, Krysanova V, Vetter T, Gao C, Jiang T (2010) Spatial Variation and Trends in PDSI and SPI Indices and Their Relation to Streamflow in 10 Large Regions of China. Journal of Climate 23:649-663

Zhang J, Sun F, Xu J, Chen Y, Sang Y, Liu C (2015) Dependence of trends in and sensitivity of drought over China (1961-2013) on potential evaporation model. Geophysical Research Letters 43:206-213

Zhang J, Zhao Y, Wang C, Yang X (2012) Impact simulation of drought disaster at different developmental stages on winter wheat grain-filling and yield. Chinese Journal of Eco-Agriculture 20:1158-1165

Zhao T, Dai A (2016) Uncertainties in historical changes and future projections of drought. Part II: model-simulated historical and future drought changes. Climatic Change:1-14